

Circulation and Sediment Transport at Headlands with Implications for Littoral Cell Boundaries

By

DOUGLAS ADAM GEORGE

B.S. (Humboldt State University, Arcata) 1999

M.S. (Columbia University, New York City) 2001

M.Sc. (Dalhousie University, Halifax) 2003

DISSERTATION

Submitted in partial satisfaction of the requirements for the degree of

DOCTOR OF PHILOSOPHY

in

Hydrologic Sciences

in the

OFFICE OF GRADUATE STUDIES

of the

UNIVERSITY OF CALIFORNIA

DAVIS

Approved:

John L. Largier, PhD, Chair

Brian P. Gaylord, PhD

Gregory B. Pasternack, PhD

Committee in Charge

2016

Copyright © Douglas Adam George 2016

All rights reserved.

Douglas Adam George

September 2016

Hydrologic Sciences

Circulation and Sediment Transport at Headlands with Implications for Littoral Cell Boundaries

Abstract

Coastal communities face the highest base sea level elevations in human history as the uncontrolled experiment of anthropogenic-driven climate change continues. Coastal engineering is expected to greatly expand as protection of infrastructure, property, and habitats becomes increasingly necessary. One of the most basic approaches in the protection toolbox is beach nourishment – the practice of placing large volumes of sand on existing beaches to shore up dunes and create a wider buffer from the ocean. The underlying assumption to beach nourishment projects is that they are temporary and will be repeated as the sand washes away over time. The clash between the natural coastal processes of littoral drift and the human efforts to build beaches leads to the framing question of this dissertation – where should sand be or not be placed to maximize the efficacy of a climate change adaptation strategy? The most exemplary coastal engineering projects dovetail with natural features to positively exploit fluid dynamic processes that are self-perpetuating and universal. For example, using a rocky headland as a protective anchor against erosion is prudent to optimize the longevity of a sand placement – yet most research has been conducted on beaches that are somewhat removed from the effects of

headlands. Further, not all headlands are equal, though, and some may not provide any benefits to a nourishment project.

This dissertation focuses on the knowledge gap about how sediment moves around headlands. Historically, studies on the hydrodynamics of headlands have emphasized tide-dominated systems through observations and numerical modeling. This yielded an opportunity to explore circulation and sediment transport around headlands located on wave-dominated coasts. Three studies were undertaken to conduct a deeper investigation on the geomorphic, oceanographic, and sedimentologic influences on sediment flux. The first used a GIS-based classification of headlands to identify morphological features common among 78 California headlands that may or may not perform as littoral cell boundaries. The second executed a field observation study at a large headland in southern California with the goal of understanding sediment pathways and patterns under different forcing conditions. The last study was a numerical modeling effort using Delft-3D and SWAN to identify how variable oceanographic and sedimentologic conditions affect sediment transport around four idealized headlands that were designed based on the first study. Through these three studies, headland size and shape coupled with incident wave angle emerged as the dominant factors influencing sediment pathways and sediment grain size determined the volume of sediment flux. The findings in each study were interpreted in the context of littoral cell boundaries, in particular to assess the “openness” of a headland-defined boundary. Assigning gradations of boundaries instead of the more commonly used “boundary” or “no boundary” monikers became apparent from the results that revealed sediment pathways varied by sediment grain size. The overarching conclusion from this dissertation is that a new set of parameters should be utilized to define littoral cell boundaries at headlands that take into account size, shape, and sediment. The headlands most

likely to be candidates for absolute boundaries are large, pointed ones for most common beach-sized sand while large, broad-faced ones are barriers for coarser sand but not finer sand; smaller headlands are less likely to be absolute boundaries in general but can be barriers for coarser sand under certain conditions. The discoveries presented herein expand knowledge of headland dynamics as it relates to particle transport and delineation of dynamic littoral cell boundaries, both of which lead to the prospect of improved coastal management decisions in an era of profound coastal change.

Acknowledgements

My dissertation is the product of the support and guidance from a slew of people including my advisor, John Largier, my UCD committee, Greg Pasternack and Brian Gaylord, and my USGS committee, Curt Storlazzi and Patrick Barnard. John was open to me being a part-time student trying to sustain my career and myriad of challenges associated with conducting my research from afar; this product came about from his collegial style with me that respected my background and prompted growth in new areas. Greg also greatly assisted me in navigating the UCD realm and battled on my behalf many times, including unexpectedly providing student funding more than once. Curt and Patrick were stalwarts who encouraged me to grow and keep my eye on the prize. Numerous others provided intelligent conversations, tutoring, and thoughtful discourse during these past four years: Rocko Brown, Justin Vandever, Matt Robart, my sugar mama Phyllis Grifman, members of the Coastal Sediment Management Workgroup, colleagues at the USGS including Li Erikson, Guy Gelfenbaum, Andrew Stevens, and Jon Warrick, and my labmate Kate Hewett. The backing of my friends through this experience was grounding and invaluable and so I thank Liz Pittinos, Joe Toland, Lori Kelly, Amy East, Steve Grimes, Nena Vandebroek, Ken and Laura Krueger, Conor and Joél Flannery, Amy Foxgrover, Paul Melvin, Sean Corcoran, Kathi Koontz, my ETC family, and many others. Covering the geography from Bodega Marine Laboratory to Davis to Santa Cruz was only possible with the generosity of guest rooms and couch space from more than a dozen friends and family, and my trusty set of wheels, Digdoug. I was also fortunate to garner the support of my employers at ESA and AMS who allowed me the space to balance two worlds.

I thank my siblings, Amber and Peter, my cousin Danielle, my Aunt Georgette and Uncle Joe, and my nephews, Daniel and Gabriel, for celebrating the highs and enduring the lows with me. Finally, I thank my parents who have stood behind me for more than a decade to help me realize this dream – there's no doubt in my mind that without their love and encouragement from this earthly place (Mom) and from beyond (Dad), I would not have accomplished this PhD.

*To understand the heart and mind of a person, look not at what he
has already achieved, but at what he aspires to.*

-Khalil Gibran

Chapter Specific Acknowledgments

In addition to the individuals named above, the following provided further assistance that was greatly appreciated for the three studies.

Chapter 2

Elena Vandebroek, Dennis Hall (NOAA), and Joshua Novac and Erin Musgrave (Dewberry) provided geospatial technical assistance and data and Li Erikson (USGS) provided wave data. Discussions regarding geomorphology with Rocko Brown and cluster analysis with Christie Hegermiller helped guide this research. The published manuscript from Chapter 2, which was co-authored with John, Curt, and Patrick, was improved upon by review from Bruce Jaffe (USGS), Edward Thornton (NPS), and an anonymous review. The methodological appendix, published under a co-authorship with Elena, benefitted from review by Clif Davenport (CGS), John Dingler (USACE), and Nancy Ferris (BAAMA). The Hydrologic Sciences Graduate Group at the University of California Davis and the US Geological Survey's Coastal and Marine Geology program supported this work.

Chapter 3

The field observational component of this dissertation was completed in Malibu with extensive assistance from the following individuals: Matt Robart, David Dann, and Brian Gaylord (all BML), Tom Ford (The Bay Foundation), and Dan Hoover, Tim Elfers, Andrew Stevens, and Jackson Curry (all USGS). Instruments came from John, Brian, Curt, and Patrick. Jon Warrick (USGS) provided guidance for sediment photogrammetry. This work was produced with support from the USC Sea Grant Program, National Oceanic and Atmospheric

Administration, U.S. Department of Commerce, under grant number NA14OAR4170089, and the USGS Coastal and Marine Geology program. Unpublished work off Bodega Head utilized the assistance of Matt Robart and David Dann (both BML), and Sam Johnson (USGS), with funding from the PADI Foundation and the UC Natural Reserve System.

Chapter 4

The monumental modeling task could not have been attempted nor completed without the deep involvement of Edwin Elias, Andrew Stevens, Li Erikson, and Andrea O'Neill (all USGS). Patrick provided a much-needed modern computer that accelerated the process many times over. The USC Sea Grant Program, National Oceanic and Atmospheric Administration, U.S. Department of Commerce, financially supported the modeling under grant number NA14OAR4170089, with substantial computer and software support from the USGS Coastal and Marine Geology program.

Table of Contents

Chapter 1 – Context and Scope of Dissertation	1
1.1 Introduction	2
1.2 General Scientific Literature	3
1.3 Rocky Headlands and Coastal Management	4
1.4 Headlands as Boundaries of Littoral Cells	7
1.5 Approach to Problem – Classifying, Field Observations, and Modeling	9
1.6 Outline of Dissertation	11
Chapter 2 – Classification of Rocky Headlands in California with Relevance to Littoral Cell Boundary Delineation	11
Chapter 3 – Sediment Flux around Rocky Headlands: An Example of Sand Transport at Pt. Dume, California	12
Chapter 4 – Modeling Sediment Flux across Rocky Headlands	13
1.7 References	15
Chapter 2 – Classification of Rocky Headlands in California with Relevance to Littoral Cell Boundary Delineation	17
2.1 Introduction	18
2.2 Background	19
2.2.1 Headlands as Littoral Cell Boundaries	21
2.3 Study Area	23

2.4	Data Collection and Analysis.....	27
2.4.1	Geomorphology: Shoreline and Bathymetry	27
2.4.2	Wave Climate.....	34
2.4.3	Database Pre-processing.....	35
2.4.4	Cluster Analysis	36
2.5	Results.....	41
2.5.1	Single-Parameter Distributions.....	41
2.5.2	Morphological Classification.....	43
2.6	Discussion	48
2.6.1	Classes of Headlands and Key Parameters.....	48
2.6.2	Wave-Driven Transport Past Headlands.....	52
2.6.3	Littoral Cell Boundaries in California	55
2.7	Conclusion.....	59
2.8	References	60
2.9	Appendix 1	63
2.10	Appendix 2: Making Headland Classes From A Geospatial Mash-Up	66
2.10.1	A Headland-sized Knowledge Gap.....	66
2.10.2	Headlands Along the Ocean, Headlands in the Bay	67
2.10.3	GIS for Geometry and Bathymetry.....	68

2.10.4	Conclusion	70
2.10.5	References.....	70
2.10.6	Appendix 2 Figures.....	72

Chapter 3 – Sediment Flux around Rocky Headlands: An Example of Sand Transport at Pt.

Dume, California.....		76
3.1	Introduction and Background.....	77
3.1.1	Hydrodynamics at Headlands	77
3.1.2	Conceptual Sediment Transport Pathways	79
3.1.3	Study Motivation	81
3.2	Study Site	83
3.3	Methods.....	87
3.3.1	Field Data Collection	87
3.3.2	Data Processing.....	90
3.3.3	Data Analysis	94
3.4	Results	95
3.4.1	Tide and Wave Event Determination.....	95
3.4.2	Wind.....	98
3.4.3	Wave Climate.....	99
3.4.4	Near-bottom Currents	102
3.4.5	Sediment: Bed Distribution and Suspension.....	104

3.4.6	Synthesis of Results: Sediment Flux around Pt. Dume	114
3.5	Discussion	116
3.5.1	Near-bottom Flow and Sediment Flux.....	116
3.5.2	Headland as a Barrier to Littoral Drift.....	123
3.6	Conclusion.....	125
3.7	References	126
Chapter 4 – Modeling Sediment Bypassing around Idealized Rocky Headlands		133
4.1	Introduction	134
4.2	Background	135
4.2.1	Modeling Flow and Flux around Headlands.....	135
4.2.2	Headlands as Barriers to Sediment Flux.....	136
4.2.3	Factors That Affect Sediment Bypassing a Headland	139
4.3	Methods.....	142
4.3.1	Headland Morphology	142
4.3.2	Numerical Models.....	142
4.3.3	Model Input.....	144
4.3.4	Modeling Approach	153
4.3.5	Analysis Approach.....	155
4.4	Results	163
4.4.1	General Current and Deposition Patterns	163

4.4.2	Analysis of Key Factors.....	167
4.4.3	Forcing Terms and Sediment Response.....	176
4.5	Discussion	186
4.5.1	Factors Affecting Sediment Bypassing.....	186
4.5.2	Specifying Sediment Bypassing Potential	187
4.5.3	Mechanisms for Sediment Bypassing.....	190
4.5.4	Generalized Sediment Bypassing	194
4.5.5	Model Improvements	196
4.6	Conclusion.....	197
4.7	References	198
4.8	Appendices.....	207

Chapter 1 – Context and Scope of Dissertation

1.1 Introduction

Picture a sandy beach tucked between two rocky headlands. The straight line of the shoreline curves gently at first as it approaches small outcrops of rock nestled in the shadow of the headland itself. The beach ends abruptly and towering above are layers of wave-beaten pockmarked rock. Strata formed beneath ancient seafloors and tilted backwards toward the land show themselves as streaks of black, gray, brown, or mottled white. With every passing wave that swallows parts of the headland, a surge of sea rises up in a frothy mass. The water drops as the wave dissipates and the lower layers of the headland are revealed, quartz veins shimmering in the sun. The foaming water sighs as bubbles are released and the blue tint of the ocean gives way to bright turquoise, cerulean, and the unmistakable burst of golden pyrite flakes boiling in the brown of sand plumes. The water has no chance to clear itself of sand before another wave ricochets in from a distant storm, churning the bed with a rolling – and roiling – current. Again and again, for days, months, and decades, this continues without pause, driving sand like leaves in a breeze.

While easy to describe in a poetic, literary manner, the transport of sediment around a headland is far from understood. Yet the movement of sand may prove to be one of humanity's greatest tools this century as climate change adaptation to higher sea levels will necessitate the largest mobilization for beach nourishment in human history. Despite extensive study of waves and currents along sandy beaches, there is a paucity of studies along rocky shores and thus in locations where alongshore transport may be perturbed or interrupted by headlands. Understanding transport around headlands (termed headland transport for this dissertation) is important for both biological and physical transport,

underpinning coastal ecosystems and human uses. Hence, this dissertation focuses on the transport of suspended particles past headlands – a phenomenon that is directly relevant to issues such as larval dispersal and population connectivity, sediment management for beaches, pollution patterns, and climate change adaptation. The sections below present the general background for this topic, the relationship between rocky headlands and coastal management, how littoral cell boundaries and headlands interact, the approach to the research questions, and finally an overview of each dissertation section, including the abstracts of the chapters.

1.2 General Scientific Literature

The gap in headland transport research is quite prevalent. Literature searches reveal an absence of quantified headland transport rates as well as more generalized explorations of how promontories affect alongshore sediment movement. Several studies deduce transport from analysis of bed characteristics (grain size, morphology, etc.), but mechanistic studies that explicitly connect oceanographic and morphologic processes to transport rates are lacking. This geological approach of observations of deposition and erosion has been used in many environments, such as southern United Kingdom (Bastos et al., 2002), New Zealand (Hume et al., 2000), or Western Australia (Stul et al., 2012). Some biologically-driven research has explored larval dispersal dynamics in the lee of a headland (Roughan, Mace, et al., 2005), which by proxy can indicate part of the circulation patterns in the water column. From a numerical modeling perspective, Signell and Geyer (1991), Davies et al. (1995), and Guillou and Chapalain (2011) explored headland transport with generic idealized headland designs. These studies focused on the hydrodynamics and posited the influence on sediment movement but field measurements

were not included. Another gap in the research is the treatment of geometric asymmetry that most headlands exhibit; this is particularly evident in numerical modeling studies. Any headland that is non-symmetrical should be viewed as two partially independent transport scenarios. For example, Denniss et al. (1995) identified different spectral energies of currents on either side of Bass Point, Australia, and attributed additional variation in the circulation to the complexity of the headland geometry. Many modeling studies however design equilateral triangle-shaped headlands that cannot reproduce the eddy wakes observed in the ocean around asymmetrical promontories.

1.3 Rocky Headlands and Coastal Management

Rocky headlands are a common feature of cliff-backed shorelines, which Emery and Kuhn (1982) observed to comprise approximately 80% of coasts globally. California has a varied and diverse coastline composed of several types of beaches and geological features: approximately 28.4% of the coastline consists of pocket beaches, 32.3% is sandy beach, and 39.3% is rocky shoreline (Scholar and Griggs, 1997). Headlands are found in all three coastline types with particular prominence in creating pocket beaches and defining rocky shorelines. As a result, two challenges California, and truly the world, must face will directly benefit from this effort to improve knowledge of how headlands affect alongshore transport: (i) sediment and pollution management at the local scale, e.g., beach nourishment decisions; and (ii) regional scale planning, e.g., marine protected area networks or statewide sediment management.

Local Beach Nourishment. The beach communities throughout California are facing sea-level rise of 0.42-1.67 m (OPC, 2013), threatening coastal infrastructure, tourist- and recreation-based economies, and beach habitats. Amongst the “softer”

adaptation measures (ones that do not involve heavy construction of seawalls and revetments) is beach nourishment – placement of sand on the shoreline with the intent of widening beaches that are naturally narrow or where the natural supply of sand has been significantly reduced through human activities (Patsch and Griggs, 2006). The 2012 draft AdaptLA report identified the Venice-Marina Peninsula-Playa del Rey-LAX stretch of coast for nourishment to combat beach retreat from sea level rise (Grifman et al., 2012). The San Diego Coastal Regional Sediment Management Plan called for beach nourishment along many portions of the San Diego County coastline (SANDAG, 2009), while in northern California, Ocean Beach, San Francisco, is the target of extensive nourishment projects by municipal, State and Federal agencies. Despite historic nourishment activities, 55 beaches in San Francisco, Alameda, San Mateo, Monterey, Santa Barbara, Ventura, Los Angeles, Orange, and San Diego counties were identified in the 2010 California Beach Erosion Assessment Survey as in severe need of erosion mitigation (CSMW, 2010). The combination of the value of coastal land, beach erosion and climate-change adaptation ensures that widespread beach nourishment will continue throughout California.

One of the challenges in assessing the economics of beach nourishment is determining the residence time of the placed sand. Many factors may influence sediment transport – wave energy and direction, sediment grain size, alongshore and cross-shore currents, and equilibrium shoreline position. In the vicinity of a headland, currents and waves are directly affected. The impact of a headland on sediment transport has been inferred in modeling studies, but not quantified. Broadly applicable empirical relationships have also remained elusive. Equations that explicitly connect headland and

flow/wave parameters to sediment transport downstream of the headland would be invaluable to local, regional, state and federal agencies interested in maximizing the efficacy of beach nourishment activities. Here we take necessary steps towards developing that tool.

Statewide Coastal Management. The appeal of demarcating zones for marine conservation and coastal management has increased as our understanding of the nearshore environment has grown. California's first littoral cell boundaries were published by Habel and Armstrong (1978). Originally called "coastal compartments" by Inman and Frautschy (1966), the idea of a littoral cell forms around the concept that a geographic region can be defined with negligible alongshore import/export of sediment and within which other imports and exports are based on specific physical processes and geomorphology (Rosati, 2005). Formalized coastal management was still in its infancy at the time California's littoral cells were postulated and conservation zones were yet to be created. Over subsequent decades, "protection areas" for water quality and ecosystems were established in nearshore State waters. However, littoral cells have not always been recognized in setting conservation areas, such as the recently defined California Marine Protected Areas. The Coastal Sediment Management Workgroup, founded in 1999 as a joint federal-state multi-agency body, has sought to better incorporate coastal processes and the littoral cells into all types of coastal management, including the new ecological reserves, commonly referred to as "marine protected areas". Successful examples of combining littoral cells with coastal management and conservation efforts can be found around the world, including Western Australia (Stul et al., 2012), the United Kingdom (Cooper and Pontee, 2006), and Pacific island atolls (Collen et al., 2009).

1.4 Headlands as Boundaries of Littoral Cells

While recognition of littoral cells is an important foundation for coastal planning, it is not clear for which sediment sizes and particles these littoral cells are effective – nor how effective. In reality, some leakage is expected across boundaries, but there is little insight as to when that occurs and for which grain sizes. As a result, there is little ability to effectively link littoral cells to downstream beach changes or to project future conditions under climate change scenarios. Davies (1974) introduced the concept of ‘closed’ and ‘open’ cell circulation and questioned the validity of boundaries by suggesting that most boundaries are drawn arbitrarily. He also noted that littoral cells have varying degrees of exclusivity, which is a measure of the amount of connectedness to other cells.

Patsch and Griggs (2007) attempted to improve estimates of sediment budgets within 10 of 25 of California’s littoral cells. Their refinements advanced understanding of the volumes of sediment circulating along portions of the coast. Questions still remained about certain headland boundaries, such as Point San Pedro in Pacifica, and prominent headlands inside a cell, such as Point Dume in Malibu. While Habel and Armstrong (1978) categorized the Santa Monica Littoral Cell as bounded by Point Dume and Redondo Canyon, Patsch and Griggs (2007) described the cell as stretching from Mugu Canyon to Palos Verdes Peninsula, with Point Dume dividing two sub-cells. Against the uncertainties about littoral cell boundaries, conservation areas were created throughout State waters with the goal of protecting water quality and preserving coastal ecosystems. For example, California created the Laguna Point to Latigo Point Area of Special Biological Significance (1974), the Point Dume State Marine Conservation Area (2012)

and the Point Dume State Marine Reserve (2012) in the vicinity of Point Dume, one of my two study sites. Adjacent to my other study site at Bodega Head, the Bodega Head State Marine Reserve (2010) and Bodega Head State Marine Conservation Area (2010) were established. Due to the gap in understanding fundamental coastal processes and sediment transport in the vicinity of headlands, these considerations had no influence in establishing these conservation areas. The opportunity to inform coastal management with littoral cell knowledge remains to be realized. A case in point is the South Coast Marine Protected Area Monitoring Plan, which identifies understanding sediment behavior from beach nourishment and dredging activities as a priority to assess progress towards the goals of the Marine Life Protection Act (OST, 2011).

This dissertation seeks to improve understanding of littoral cell boundaries by identifying how much sediment is transported around headlands or exported offshore under different oceanographic conditions and for different sediment grain sizes. The research addresses the sediment-specific openness of a boundary. Although hinted at by other researchers (e.g., Davies, 1974), the seasonality of transport around a headland could play a large role in determining the hardness of the boundary. Conceptually, the hardness of a boundary is related to energy and sediment load, both of which fluctuate throughout the year. For example, there may be thresholds of wave energy that convert a “closed” boundary to an “open” one by increasing the amount of sediment bypassing the boundary-defining headland. Meanwhile, some “open” boundaries may not have the capacity to block sediment bypassing, regardless of wave energy, indicating they are not littoral cell boundaries. To date, few explicit investigations have addressed this question despite interest from coastal resource managers. The results of my research will be useful

in re-examining littoral cells and considering revisions to how they are used in coastal resource management, here in California and around the world.

1.5 Approach to Problem – Classifying, Field Observations, and Modeling

The primary goals of this dissertation were to use field observations and modeling to (i) quantify transport past headlands and (ii) identify the primary controls on the proportion of material that passes a headland versus that which is either blocked or exported offshore. A three-pronged investigatory approach was employed to meet the primary goals: (1) classification of headland types, (2) field observations at a large rocky headland, and (3) numerical modeling of idealized headlands. Each step of the work is unique while drawing upon established relationships, techniques, and concepts related to beach morphodynamics, numerical modeling, oceanographic and coastal processes, and fluid mechanics. The three studies target different but overlapping scientific groups. The classification study adds to our constantly expanding knowledge base for coastal processes by contributing to specific designations of coastal morphology. The field observation study directly assists characterization of processes at headlands and demonstrates methods to expand time-series data from existing observation nodes – those methods could be duplicated by other researchers conducting experiments in similar wave-dominated, cliff-backed rocky shoreline environments. The numerical modeling study advances headland modeling from the generic realm to broadly applicable classes of headlands and specifically identifies the relevant control factors on alongshore transport. The objectives for the three studies are listed here:

Classification of California Headlands

- Use readily available information to characterize the geomorphology, bathymetry and oceanography associated with headlands of varying sizes in California.
- Develop groupings of headlands based on advanced clustering and statistical analysis techniques to classify headland types.
- Compare headland types to traditional littoral cell boundaries as a crosscheck on the littoral cells and the headland classifications.

Field Observations of Flow at a California Headland

- Use boat-borne and moored instruments to identify patterns of near-bed localized circulation and estimate sediment movement around a headland of significant size.
- Determine the mechanism of sediment flux at the headland according to a general conceptual model.

Numerical Modeling of Flow past Idealized Headlands

- Develop idealized headland models based on the headland classifications to identify the controlling factors on sediment transport, including the relative importance of those factors with respect to:

Headland geomorphology

Oceanographic processes

Sediment size and availability

- Explore role of extreme events as compared to normal background conditions on sediment transport for headland classes.

1.6 Outline of Dissertation

This dissertation presents:

- In Chapter 2 – a GIS-based study on the development and application of a classification scheme based on geomorphology and bathymetry for 78 California headlands. A short communication detailing the GIS techniques used in Chapter 2 is provided as a technical appendix.
- In Chapter 3 – a field-based test case exploring sediment flux around Point Dume, a headland in Malibu, California, to comment broadly on the mechanisms for such flux.
- In Chapter 4 – a numerical model study using Delft-3D of four headland types subjected to various hydrodynamic forcings for three typical beach-sized sand classes to investigate the behavior of sediment flux and comment on littoral cell boundaries.

Abstracts for the chapters are provided below.

Chapter 2 – Classification of Rocky Headlands in California with Relevance to Littoral Cell Boundary Delineation

Despite extensive studies of hydrodynamics and sediment flux along beaches, there is little information on the processes, pathways and timing of water and sediment transport around rocky headlands. In this study, headlands along the California coast are

classified to advance understanding of headland dynamics and littoral cell boundaries in support of improved coastal management decisions. Geomorphological parameters for 78 headlands were quantified from geological maps, remote-sensing imagery, navigational charts, and shoreline geospatial databases. *K*-means cluster analysis grouped the headlands into eight distinct classes based on headland perimeter, bathymetric slope ratio, and the headland apex angle. Wave data were used to investigate the potential for sediment transport around the headland types and determine the efficacy of the headland as a littoral cell boundary. Four classes of headland appear to function well as littoral cell boundaries, with headland size (e.g., perimeter or area) and a marked change in nearshore bathymetry across the headland being relevant attributes. About half of the traditional California littoral cell boundaries align with headland classes that are expected to perform poorly in blocking alongshore sediment transport, calling into question these boundaries. Better definition of these littoral cell boundaries is important for regional sediment management decisions.

Chapter 3 – Sediment Flux around Rocky Headlands: An Example of Sand Transport at Pt. Dume, California

Sediment transport past rocky headlands is relatively poorly studied compared to transport along beaches. Here we identify six possible pathways for sediment movement and test them via a field-based study conducted adjacent to the Point Dume headland within Santa Monica Bay, near Los Angeles, California. This prominent shoreline feature is a nearly symmetrical, triangular-shaped promontory interior to the Santa Monica Littoral Cell. We collected current, wave, and turbidity data for 74 days during which

several moderate-scale (larger than 4 m) wave events occurred, including one associated with a remote hurricane and another generated by the first winter storm of 2014; we also acquired sediment grabs to quantify seabed grain-size distributions. Near-bottom current patterns showed consistent flow towards the headland apex from both sides, with wave-driven longshore currents faster on the exposed side. Bed shear stresses and resultant sediment fluxes were dominated by the waves compared to currents. Three sediment regimes are proposed based on different transport behavior around the apex: resuspension on the exposed side, minimal sediment movement (transition) at the apex, and advection on the protected side. It is unlikely that sediment transits across the apex itself although transit of finer sand fractions could be possible in deep water. These findings enhance our understanding about transport around headlands in other hydrodynamic regimes, regional sediment management, and littoral cell boundaries by developing potential mechanisms that describe sediment pathways.

Chapter 4 – Modeling Sediment Flux across Rocky Headlands

Sediment bypassing rocky headlands remains understudied despite the importance of characterizing littoral processes for erosion abatement, climate change adaptation, and beach management. To address this gap, a numerical model sediment transport study was developed to identify controlling factors on sediment bypassing potential and the mechanisms supporting bypassing. Four idealized rocky headlands were designed based on recent classification efforts, and then sediment flux around the headlands was investigated using the process-based hydrodynamic model Delft-3D and spectral wave model SWAN. The experimental design involved 120 simulations to explore a range of

possibilities by varying the morphology, substrate composition, sediment grain size, and physical forcings. The four headlands represented sizes and shapes found in natural settings, grain sizes ranged from fine to medium sand similar to beach sand, and substrates adjacent to the headland were either a sandy bed or offshore reef. Options to force the model included a constructed representative tide, an alongshore background current, and four wave conditions derived from observational records in the eastern Pacific Ocean. An analytical framework based on flow disruption and sediment volume was used to refine which factors and conditions were more useful to address sediment bypassing. A ratio was developed for alongshore flux between upstream and downstream cross-shore transects to determine the degree of blockage by a headland. Results showed oblique large waves ($\theta_{dom} = 345^\circ$, $H_s = 7$ m, $T_p = 16$ s) generated the most flux around headlands while direct waves (270°) blocked flux across a headland apex. However, the shape of the headland heavily influenced the fate of the sediment by changing the relative angle between the shore and the incident waves. The bypassing ratio was useful in characterizing each headland's capacity to allow alongshore flux under different wave conditions. All headlands may allow flux although larger ones blocked sediment more effectively, promoting their ability to be littoral cell boundaries over smaller headlands. The controlling factors on sediment bypassing were determined to be wave angle, morphology of the headland (shape and size), and sediment grain size. This novel numerical modeling study advances headland modeling from the generic realm to broadly applicable classes of headlands and encourages further investigation into the mechanics of sediment bypassing.

1.7 References

- Bastos, A.C., Kenyon, N.H., Collins, M., 2002. Sedimentary processes, bedforms and facies, associated with a coastal, headland: Portland Bill, Southern UK. *Marine Geology* 187, 235-258.
- Collen, J.D., Gardner, J.P.A., Garton, D.W., 2009. Application of the littoral cell concept to managing a protected atoll: Palmyra Atoll National Wildlife Refuge. *Ocean & Coastal Management* 52, 628-635.
- Cooper, N.J., Pontee, N.I., 2006. Appraisal and evolution of the littoral 'sediment cell' concept in applied coastal management: Experiences from England and Wales. *Ocean & Coastal Management* 49, 498-510.
- CSMW, 2010. California Beach Erosion Assessment Survey. Coastal Sediment Management Workgroup, Sacramento, CA, p. 72.
- Davies, J.L., 1974. The coastal sediment compartment. *Australian Geographical Studies* 12, 139-151.
- Davies, P.A., Dakin, J.M., Falconer, R.A., 1995. Eddy Formation Behind a Coastal Headland. *Journal of Coastal Research* 11, 154-167.
- Denniss, T., Middleton, J.H., Manasseh, R., 1995. Recirculation in the Lee of Complicated Headlands - A Case-Study of Bass-Point. *Journal of Geophysical Research-Oceans* 100, 16087-16101.
- Emery, K.O., Kuhn, G.G., 1982. Sea cliffs: Their processes, profiles, and classification. *Geological Society of America Bulletin* 93, 644-654.
- Grifman, P., Hart, J., Ladwig, J., Schulhof, M., 2012. DRAFT Sea Level Rise Vulnerability Study for the City of Los Angeles. University of Southern California Sea Grant Program, Los Angeles, CA, p. 87.
- Guillou, N., Chapalain, G., 2011. Effects of waves on the initiation of headland-associated sandbanks. *Continental Shelf Research* 31, 1202-1213.
- Habel, J.S., Armstrong, G.A., 1978. Assessment and Atlas of Shoreline Erosion Along the California Coast. State of California, Department of Navigation and Ocean Development, Sacramento, CA, p. 277.
- Hume, T.M., Oldman, J.W., Black, K.P., 2000. Sediment facies and pathways of sand transport about a large deep water headland, Cape Rodney, New Zealand. *New Zealand Journal of Marine and Freshwater Research* 34, 695-717.
- Inman, D.L., Frautschy, J.D., 1966. Littoral processes and the development of shorelines, Coastal Engineering Special Conference. ASCE, pp. 511-536.
- OPC, 2013. State Of California Sea-Level Rise Guidance Ocean Protection Council, Sacramento, CA, p. 13.
- OST, 2011. South Coast California MPA Monitoring Plan. MPA Monitoring Enterprise, California Ocean Science Trust, Oakland, CA.
- Patsch, K., Griggs, G., 2006. Littoral Cells, Sand Budgets, and Beaches: Understanding California's Shoreline, Institute of Marine Sciences, University of California, Santa Cruz, p. 40.
- Patsch, K., Griggs, G., 2007. Development of Sand Budgets for California's Major Littoral Cells. Institute of Marine Sciences, University of California, Santa Cruz, p. 115.
- Rosati, J.D., 2005. Concepts in sediment budgets. *Journal of Coastal Research* 21, 307-322.

Roughan, M., Mace, A.J., Largier, J.L., Morgan, S.G., Fisher, J.L., Carter, M.L., 2005. Subsurface recirculation and larval retention in the lee of a small headland: A variation on the upwelling shadow theme. *Journal of Geophysical Research-Oceans* 110.

SANDAG, 2009. Coastal Regional Sediment Management Plan for the San Diego Region. Prepared by Moffatt and Nichol, Everest International Consultants and SIAC. San Diego Association of Governments, p. 220.

Scholar, D.C., Griggs, G.B., 1997. Pocket Beaches of California: Sediment Transport Along a Rocky Coastline, *Proceedings of California's Coastal Natural Hazards*. University of Southern California Sea Grant Program, Santa Barbara, pp. 65-75.

Signell, R.P., Geyer, W.R., 1991. Transient Eddy Formation around Headlands. *Journal of Geophysical Research-Oceans* 96, 2561-2575.

Stul, T., Gozzard, J., Eliot, I., Eliot, M., 2012. Coastal Sediment Cells between Cape Naturaliste and the Moore River, Western Australia in: *Transport*, W.A.D.o. (Ed.). Damara WA Pty Ltd and Geological Survey of Western Australia, Fremantle, WA, Australia, p. 44.

**Chapter 2 – Classification of Rocky Headlands in
California with Relevance to Littoral Cell Boundary
Delineation**

2.1 Introduction

Rocky headlands are prominent morphological features that can deflect or block alongshore currents and sediment transport, focus wave energy, shed eddies, and/or create sediment retention zones (Alaee et al., 2004; Davies et al., 1995; Winant, 2006). Headlands are frequently associated with cliff-backed shorelines, which Emery and Kuhn (1982) observed to comprise approximately 80% of coasts globally. The geological and oceanographic parameters that form and evolve headlands include the balance of wave attenuation vs. refraction, base lithology, the presence of a shore platform, and the strike of the most resistant formation with respect to wave direction (Stuiver, 2013). Presently, many assumptions must be made to characterize relationships between sediment flux, sediment deposits, and morphodynamics around headlands. Despite extensive study offshore of embayed beaches (Loureiro et al., 2012; Sallenger et al., 2002), flow and sediment transport along rocky shores and around headlands remains poorly understood. Some studies have deduced transport from analysis of bed characteristics such as grain size, grain composition, and morphology (Storlazzi and Field, 2000) while geologically-based studies have reported deposition and erosion patterns in the vicinity of headlands in the United Kingdom (Bastos et al., 2002), New Zealand (Hume et al., 2000) and Western Australia (Stul et al., 2012). Other ecological studies have explored the transport of planktonic larvae in the lee of a headland (Roughan, Mace, et al., 2005). However, mechanistic studies that connect oceanographic processes to sediment transport rates and morphological change are still lacking.

These research gaps and societal needs argue for new research to better understand how headlands affect circulation and transport rates of sediment or biota. A

first step is to categorize different types of headlands, based on shape, size, complexity and nearshore bathymetry. Many approaches to grouping environmental phenomena are found in the oceanographic, hydrologic, and geologic disciplines. Examples of classification methods for marine features come from beaches (Scott et al., 2011; Wright and Short, 1984), coral reefs (Freeman et al., 2012), wave climates (Camus et al., 2011), and submarine canyons (Harris and Whiteway, 2011). Developing a classification for headlands would open new avenues for research, both in explaining these headland types (e.g., geological framework or rock types) and in determining the effect of different headland types on flow, sediment transport and associated geomorphology and ecology. The primary aim of this paper is to develop a classification of headlands by identifying key factors that differentiate types of headlands. The secondary goal is to investigate littoral cell boundaries associated with each headland type.

2.2 Background

Several numerical modeling studies have explored transport around headlands with generic idealized headland designs (Davies et al., 1995; Guillou and Chapalain, 2011; Signell and Geyer, 1991). These studies focused on the hydrodynamics and posited the influence on sediment movement; field measurements were not included. Further, the geometric asymmetry of headlands has also been ignored in numerical modeling studies. Most headlands are not symmetrical, so that two different flow-topography scenarios occur for alongshore flow in two different directions. Denniss et al. (1995) identified different spectral energies of currents on either side of Bass Point, Australia, and attributed circulation variability to the complexity of the headland geometry. Asymmetric development of sandbanks on either side of a headland has also been explored through

analysis of the Coriolis effect and seabed slope (Jones et al., 2006; Neill and Scourse, 2009).

Extensive research on beach dynamics connects the physical oceanography of water transport (jets, eddies and wakes) to sediment transport. Prior investigations most relevant to this paper focused on headland embayed beaches where the influence of headlands on beach morphology is addressed. The seminal work in this area is by Short (1999), who used observations of Australian beaches to establish a conceptual model of sand bypassing and a non-dimensional embayment scaling parameter. The parameter categorizes beach circulation as ‘normal’, ‘transitional’, or ‘cellular’, with ‘cellular’ referring to headland-dominated circulation. The relationship informs a conceptual model of sand bypassing by suggesting sediment migrates along a beach toward a headland before conditions are favorable for transport around the apex of the promontory. Loureiro et al. (2012) explored the ideas of Short (1999) at six relatively ‘small’ embayed beaches in Portugal. They suggest that there may be bounds to the upstream length of beaches influenced by headlands. Other headland/embayed beach examples span the globe: Australia (Goodwin et al., 2013), China (Dai et al., 2010), Mexico (Silva et al., 2010), Brazil (de Castilhos and Gre, 2006) and Ireland (Backstrom et al., 2009). More generally, van Rijn (2010) suggests that the most important characteristics of headlands are: 1) convergence points for wave energy; 2) obstruction to alongshore tide- and wind-induced currents and convergence of currents; 3) large-scale circulation zones downstream of headlands; 4) obstruction to littoral drift; 5) fixation points for seaward rip currents promoting offshore transport; and, 6) fixation points for spit formation and shoals originating from headland erosion.

2.2.1 Headlands as Littoral Cell Boundaries

In California, 22 of the 25 littoral cells, originally called “coastal compartments” by Inman and Frautschy (1966) in southern California and extended statewide by Habel and Armstrong (1978), are either fully or partially defined by headlands, but done so purely qualitatively. Improving knowledge of how headlands affect alongshore transport can impact how society faces two coastal challenges: 1) sediment and pollution management at the local scale, e.g., beach nourishment decisions; and 2) regional scale planning, e.g., marine protected area networks or sediment management. Beach communities throughout the world are facing varying amounts of sea-level rise that threaten coastal infrastructure, tourist- and recreation-based economies, and coastal habitats. Beach nourishment (placement of sand on the shoreline) is used to widen beaches that are naturally narrow or where the natural supply of sand has been significantly reduced through human activities (Patsch and Griggs, 2007). It is a tool that can be used for climate change adaptation as well as sustaining recreational resources. One of the challenges for beach nourishment is estimating the residence time of the sand placed on the beach with many factors influencing sediment transport – wave energy and direction, sediment grain size, alongshore and cross-shore currents. Waves and currents are affected by headlands and the headlands’ potential to be a boundary to sediment transport. The second challenge, regional coastal management, connects the littoral cell concept and its application to conservation efforts. Littoral cells have frequently been set between headlands, although other features such as rivers, inlets, and submarine canyons are also used as boundaries. Successful examples of combining littoral cells with coastal management can be found around the world, including Western Australia (Stul et al.,

2012), the United Kingdom (Cooper and Pontee, 2006), and Pacific Ocean island atolls (Collen et al., 2009).

Whereas recognition of littoral cells is an important foundation for coastal planning, it is not clear for which sediment sizes these littoral cells are effective nor how effective. Limber et al. (2008) note the importance of sediment size in accounting for sediment budgets in a littoral cell and Sanderson and Eliot (1999) used cluster analysis of grain sizes to define littoral cells along the west coast of Australia. In reality, some leakage is expected across boundaries, but there is little insight as to when that occurs and thus little ability to project future conditions under climate change scenarios. Davies (1974) questioned the validity of boundaries by suggesting that most boundaries are drawn arbitrarily and noted that littoral cells have varying degrees of connectedness to other cells. van Rijn (2010) proposed three types of alongshore cell boundaries, including both natural and constructed features:

Fixed absolute boundaries – barriers to all sediment (hard rock headlands, long jetties, deep inlets, canyons, navigation channels; long harbor breakwaters);

Fixed partial boundaries – bypassing or periodic (often storm-related) throughput of sediment take place (soft rock/compound cliff type headlands and shallow inlets);

Transient partial boundaries – generally, have a more diffusive character and have limited stability (spits, sand banks, shallow channels, short headlands, short breakwaters).

2.3 Study Area

The 1,800-km coastline of California is extremely diverse, ranging from steep coastal cliffs, marine terraces, and coastal plains to coastal lagoons and sandy beaches. The coastline is composed of different types of beaches and geological features: approximately 28.4% is pocket beaches, 32.3% is sandy beach, and 39.3% is rocky shoreline (Scholar and Griggs, 1997). Headlands are found in all three coastline types, with particular prominence in creating pocket beaches and defining rocky shorelines. Approximately two-thirds of the coast is oriented north-south from the Oregon border to Point Conception, where it turns east and forms the Southern California Bight as the shoreline curves south to Mexico. The largest interruption to the coast is the entrance to San Francisco Bay, but other large inlets include Humboldt Bay, Tomales Bay, the ports of Los Angeles and Long Beach, and San Diego Bay (Figure 2.1). Major peninsulas are Monterey Peninsula, Palos Verdes and Point Reyes, while Cape Mendocino, Point Arena and Point Conception represent even larger scale promontories or coastal curvature that exert a first-order effect on shelf-scale circulation (Largier et al., 1993).

The geology of California's headlands is related to the underlying structure and tectonic processes along the coast. Inman and Nordstrom (1971) described the coastline as a transform-fault with attributes of formerly being a collision coast including a narrow shelf, offshore trenches, coastal mountains and hills, and uplifted coastal terraces. The three geomorphic provinces that comprise the coast (Coast Ranges, Transverse Ranges, and Peninsular Ranges) are primarily continental and marine Mesozoic and Cenozoic sedimentary rock, some of which has been folded and faulted (CGS, 2002, 2006). The vertically and longitudinally variable rock type along the coastline helps support the models

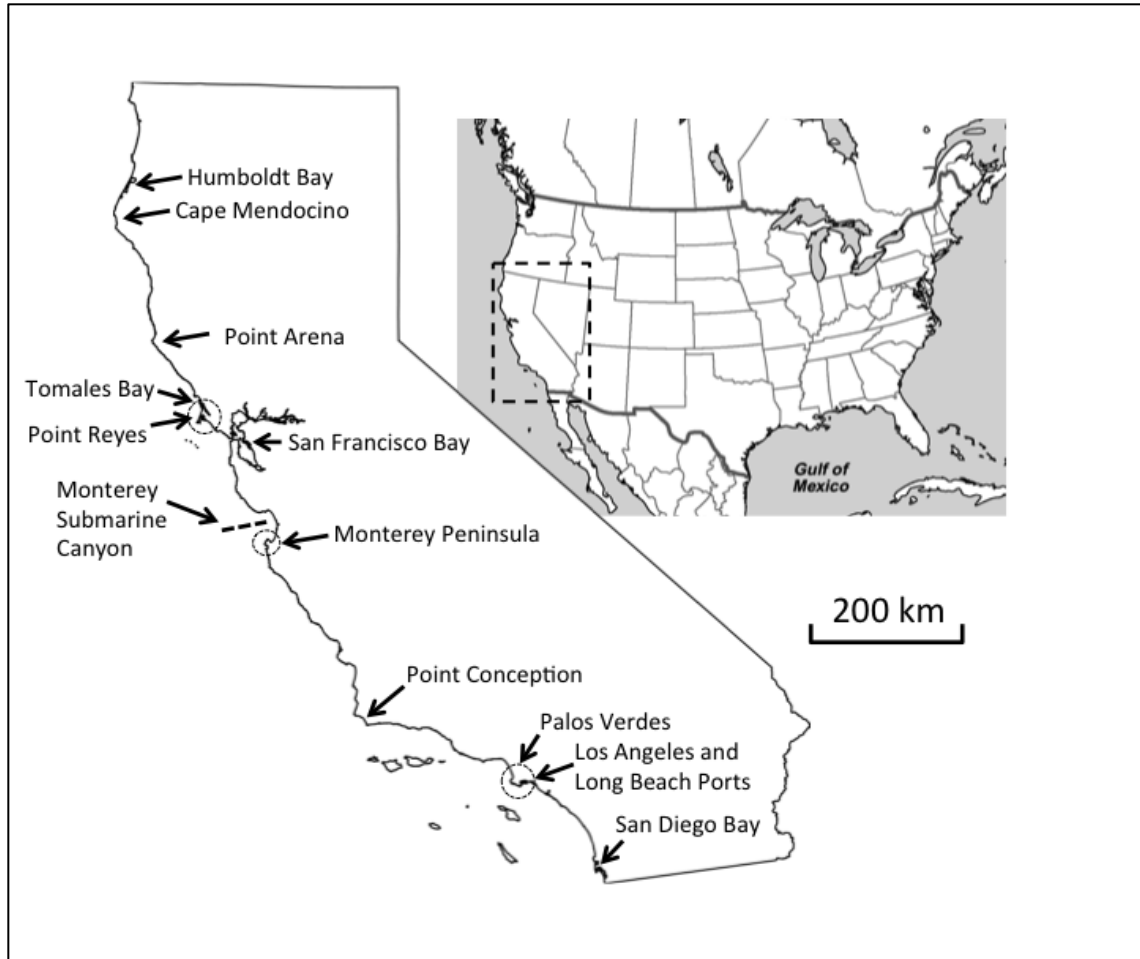


Figure 2.1. Overview of California study area with major bays, peninsulas, and promontories noted.

of headland formation and evolution described by Stuiver (2013) and Limber and Murray (2015). Both include wave activity as a key parameter of headland development, which will be addressed below.

The supply of gravel, sand, and mud that characterize the sediment type offshore of California comes primarily from rivers, with cliff erosion as a secondary source (Milliman and Farnsworth, 2011; Slagel and Griggs, 2008). The largest river systems in either annual water or sediment delivery directly to the Pacific Ocean (as opposed to San Francisco Bay) include the Smith, Klamath, Mad, Eel, Russian, Salinas, Santa Clara, Santa Ana, and Tijuana (Milliman and Farnsworth, 2011). The Sacramento and San Joaquin Rivers, which drain 40% of California, empty into San Francisco Bay. Numerical modeling estimates 1,200,000 t/yr of suspended sediment migrates to the outer coast through the Golden Gate (Erikson et al., 2013). Slagel and Griggs (2008) estimated that approximately 10,000,000 m³/yr of sand and gravel would be delivered by the 21 major river systems of the state (excluding the Sacramento-San Joaquin) if it were not for the 66 dams that impound 2,300,000 m³/yr of sediment. Best and Griggs (1991) estimated that statewide, 70-85% of sand delivered to the coast originates from rivers although recent work has suggested otherwise. For example, Perg et al. (2003) found a 50:50 ratio of fluvial vs. terrace contribution in Santa Cruz, whereas Young and Ashford (2006) found 67% of littoral sediment originated from seacliffs in the San Diego area. Comparable values for gravel and fine-grained sediment have yet to be compiled statewide. On the opposite side of littoral transport, submarine canyons are the primary sink for sediment that flows around headlands along California. More than 25 submarine canyons can be identified along the California coast that incise the shelf and extend across the continental

slope. The largest and most complex is the Monterey Submarine Canyon in Monterey Bay. Canyons with their heads close to the shoreline are most relevant to alongshore sediment transport. Everts and Eldon (2000) identified five southern California canyons as likely to be actively removing sand from littoral cells by funneling sediment down through the continental rise, such as Mugu, Hueneme, and La Jolla. Building on this work, Covault et al. (2007) found that different canyon-channel systems intercept the littoral cells depending on the shelf width between the canyon head and the littoral zone. On the northern end of the state, Mullenbach et al. (2004) found that the Eel Canyon removed approximately 12% of Eel River sediment delivered to the shelf.

The sediment that reaches the ocean enters a wave-dominated environment. Wingfield and Storlazzi (2007) described the wave climate for central California, but all of California experiences relatively similar patterns with wave energy decreasing from north to south. Three types of wave conditions characterize the nearshore processes over the course of a typical year: northern hemisphere swell, southern hemisphere swell, and local wind-driven seas. The winter months (November-March) are dominated by northern hemisphere swell with maximum significant wave heights that can be larger than 7 m in the northern part of the state but closer to 4 m in the southern section. Summer months are more quiescent, with southern hemisphere swell on the order of 2-3 m significant wave height and peak wave periods greater than 12 s. Winds and local sea are stronger north of Point Conception, where local wind-driven waves may dominate swell energy.

Currents due to tides and wind forcing are also important for sediment motion along the California coast, particularly the fine grain size classes. The range of the mixed, semi-diurnal tides along the coast increases from south to north, with an average diurnal

range of 1.6 m along the open coast in San Diego, up to 2.1 m in Crescent City (NOAA, 2014). With a micro-tidal range, tidal currents are not strong in general, although tidal jets may be observed at the mouth of the larger bays (e.g., San Francisco Bay, Barnard et al. (2012), and San Diego Bay, Chadwick and Largier (1999)). Weaker tidal jets may also occur at headlands, but few observations exist. In central and northern California, subtidal currents outside of the wave-dominated nearshore are primarily wind-driven (e.g., Largier et al. (1993)). Strong northerly winds drive upwelling and a southward shelf jet during much of the year, although exhibiting marked synoptic variability. At times, offshore eddies associated with the California Current may enhance these flows (Kaplan et al., 2009). However, strong shelf currents are slowed by bottom drag in shallow waters near the coast (typically inshore of 30 m) described as a “coastal boundary layer” by Nickols et al. (2012). In winter, strong southerly wind events can lead to fast northward flow with downwelling and significant speeds nearshore (Drake et al., 2005). Typically, the general circulation and wind-driven coastal currents are weaker south of Point Conception in the Southern California Bight.

2.4 Data Collection and Analysis

Data on geomorphology, including shoreline and bathymetric features, and wave processes were collected, prepared and analyzed as summarized in Figure 2.2.

2.4.1 Geomorphology: Shoreline and Bathymetry

A total of 78 headlands were defined using USGS geological maps, remote-sensing imagery, NOAA navigational charts, and shoreline characterization geospatial databases from the California Coastal Sediment Management Workgroup (CSMW) (<http://www.dbw.ca.gov/csmw/SpatialData.aspx>, accessed 2013). The selection process

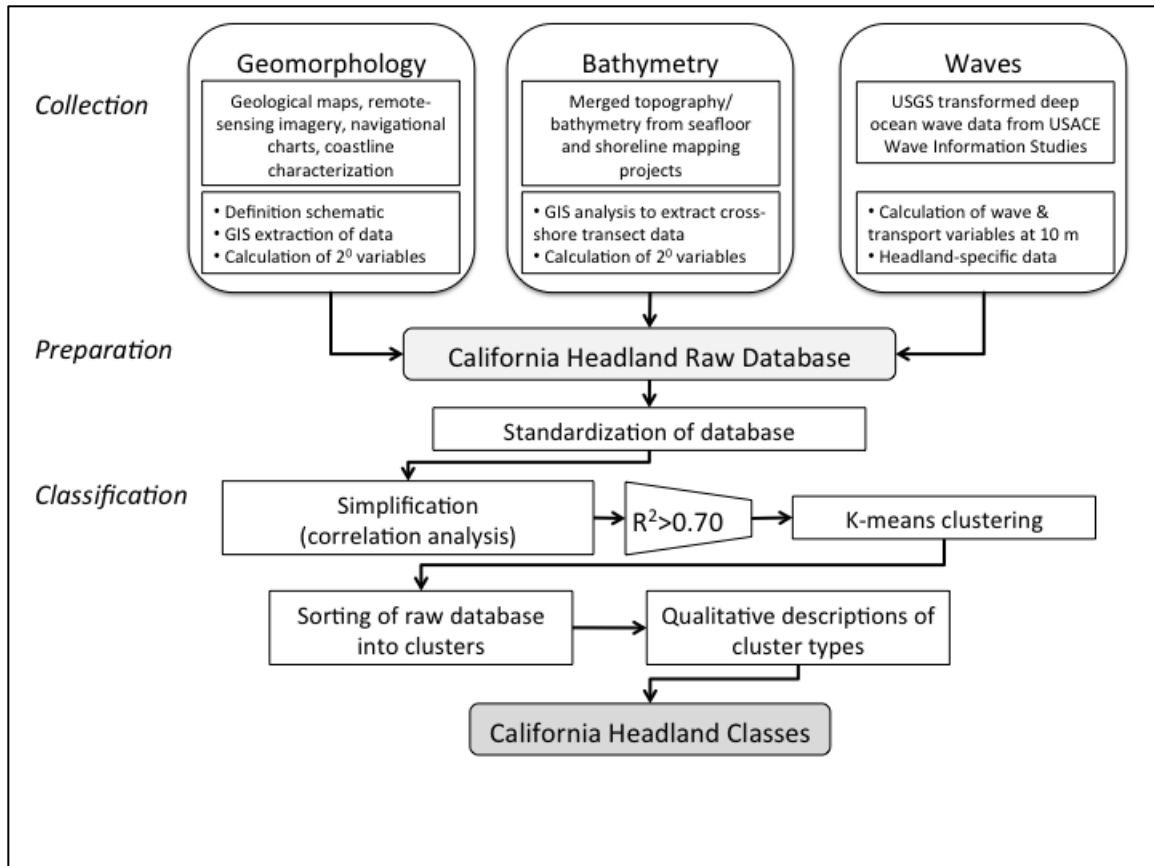


Figure 2.2. Flow diagram illustrating the process for assembly and analysis of morphological and wave data to produce a headland classification scheme.

for inclusion of a headland is as follows: 1) identification of a perturbation in the coastline in the remote-sensing imagery; 2) confirmation of a named headland in the navigational charts; 3) cross-confirmation as a distinct unit in the geological maps; and 4) identification of a change in shoreline characterization in the CSMW geospatial database. Criterion #2 preferentially selects headlands that are substantial in relative size because of their importance to navigation. At the base of each headland, a baseline was obtained by projecting a straight coastline that would exist in the absence of that headland (similar to low-pass filtering that separates the slowly curving coastline from the local perturbation due to the headland feature). Because of the asymmetrical nature of headlands, the 78 headlands represent 156 case studies for flow-topography interaction as flow patterns and sediment transport may be completely different for flow approaching the headland from one side versus the other.

A set of geometric parameters was extracted in ArcGIS (ESRI, 2013) based on the schematic displayed in Figure 2.3. These parameters were selected to quantify the size, symmetry, and complexity of each headland and its relationship to the general trend of the coastline. If appropriate for a parameter, an “upstream” (‘up’) and “downstream” (‘down’) measurement was taken with upstream on the northerly or westerly side of a headland (i.e., on the right-hand side if looking out to sea) and downstream on the southerly or easterly side (i.e., left-hand side), based on the dominant direction of sediment transport in Southern California (Sallenger et al., 2002). For example, the angle of intersection between the shoreline of the headland and the baseline (ϕ) is expected to differ from one side to the other. Thus, measurements were obtained for both intersection points (ϕ_{up} , ϕ_{down}). Additional parameters were calculated from these measured

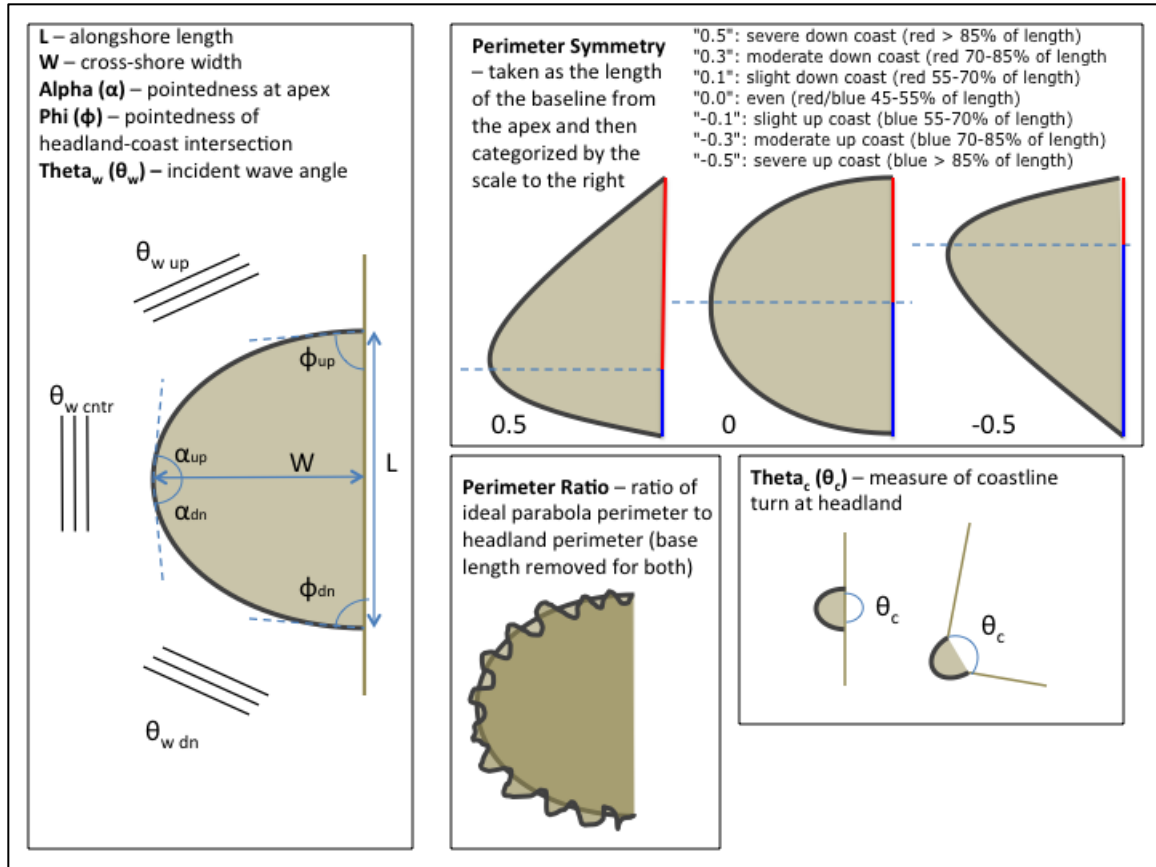


Figure 2.3. Schematics of geometric and geomorphic parameters used in analysis of California headlands.

parameters, including aspect ratio (width/length of headland), rugosity (baseline length/perimeter length), and combination of upstream and downstream angles at the apex of the headland. A summary of the measured and derived parameters is found in Table 2.1.

The underwater expression of a headland was determined by extracting bathymetry from merged data of the California Seafloor Mapping Program and California Shoreline Mapping Project (<http://walrus.wr.usgs.gov/mapping/csmp/index.html>). Five transects were plotted: three radiating transects locally normal to the shoreline of the headland and a shore-normal reference transect either side of the headland, where the shoreline is approximately straight and aligns with the baseline of the headland (Figure 2.4). The headland transects include upstream, center, and downstream transects (B, C, D) while the reference transects are only upstream and downstream (A, E). Bathymetry between 0 and 10 m was linearly interpolated and deeper depths were measured with advanced bathymetric acoustic surveying. The distance from the shoreline to the 5, 10, 15, 20, 25, 30, 40, 50, and 75 m contours was tabulated along each of the five transects. Ratios were calculated between distances on a headland transect (e.g., X_{C10} where C denotes the center transect and 10 denotes distance to the 10 m isobath) and distances on a reference transect (e.g., X_{A10} referring to the distance to the 10 m isobath on the reference transect A); in this case the ratio $\chi_{10up} = X_{C10} / X_{A10}$. The downstream ratio would be $\chi_{10down} = X_{C10} / X_{E10}$. The median of χ along each transect was determined to yield simpler indicators of the bathymetric expression of the headland. Four ratios involving bathymetry were used to indicate whether an offshore ridge accompanies a headland. A ratio of one indicates that isobaths run parallel to the shoreline, curving

Table 2.1. Measured and Derived Parameters and Exploratory Ratios for Headlands Classification

Category	Measured Parameters	Derived Parameters	Exploratory Ratios
Geomorphology	Width (W)		Aspect Ratio (W/L)
	Length (L)		Rugosity (Perimeter/ L)
	Perimeter	Perimeter Symmetry	
	Area		
	Curvature of Coast (θ)		
	Inside Angle of Headland-Coast	Difference in Upstream-Downstream Angle ($\Delta\phi$)	
Bathymetry	Intersection (ϕ_{up}, ϕ_{down})		
	Angle of Headland	Apex Sharpness (α_{total})	
	Apex ($\alpha_{up}, \alpha_{down}$)		
	Cross-shore Distance to Contours* for 3 Radiating Headland Normal Transects ($x_{hdlnd_up/ctr/dn}$)	Median of Distance for Each Headland Transect ($x_{hdlnd_up/ctr/dn}$) Mean of Median Distances for the Headland Transects (x_{hdlnd_ave})	Ratio of Means ($\chi_{ave} = x_{hdlnd_ave}/x_{reference_ave}$) Ratio of Upstream Transects ($\chi_{up} = x_{hdlnd_ctr}/x_{normal_up}$) Ratio of Downstream Transects ($\chi_{down} = x_{hdlnd_ctr}/x_{normal_down}$) Bathymetric Slope Ratio ($\chi_m = \text{Upstream/Downstream}$)
	Cross-shore Distance to Contours* for 2 Shore Normal Transects ($x_{normal_up/dn}$)	Median of Distance for Each Reference Transect ($x_{reference_up/dn}$) Mean of Median Distances for the Reference Transects ($x_{reference_ave}$)	
Oceanography	Wave Climate at 3 Points per Headland (seasonal, mean and top 5% extreme events)	Wave-driven Transport at 3 Points per Headland and Mean per Headland	Ratio of Wave and Transport Parameters between Upstream and Downstream Points by Season and Event (e.g., Winter Mean $H_{sig_upWM}/H_{sig_downWM}$)
	<ul style="list-style-type: none"> • Significant Wave Height (H_{sig}) • Peak Period (T_p) • Dominant Direction (θ_d) 	<ul style="list-style-type: none"> • Wave power (P) • Bottom orbital velocities (U_w) • Bottom shear stress (τ) 	
		Mean H_{sig}, P, U_w, τ for Headland in Winter and Summer Mean and Top 5% Conditions	

* - Contour depths: 5, 10, 15, 20, 25, 30, 40, 50, and 75 m

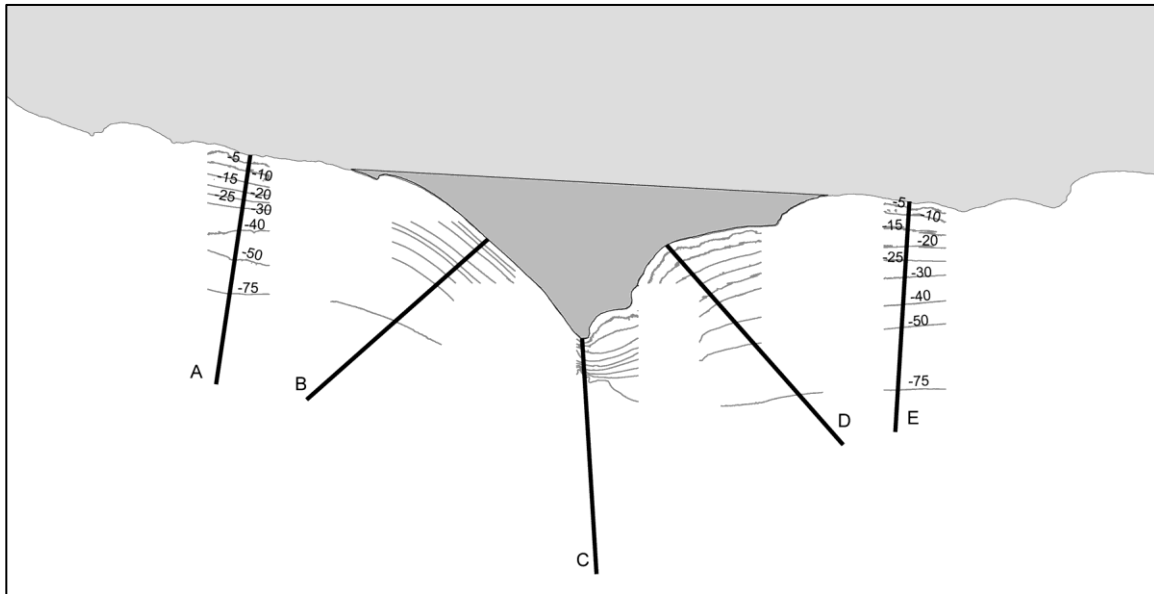


Figure 2.4. Schematic of bathymetry used to characterize the underwater expression of a headland. Relevant bathymetric blocks were extracted from merged data of the California Seafloor Mapping Program and California Shoreline Mapping Project. The darker gray shaded portion is the defined headland. Bathymetric contours for depths of 5, 10, 15, 20, 25, 30, 40, 50, and 75 m are shown. Lines B, C and D are the “headland” transects and lines A and E are the “reference” transects. The distance from shore to the contours was tabulated along the five transects for all headlands.

offshore the same distance as the shoreline around the headland. If a ratio is greater than one, then the headland is more pronounced than the ridge (muted ridge), and vice versa – if the ratio is less than one, the ridge is amplified. The first ratio is the average for similar transect types (χ_{ave} = headland:reference). Ratios between the median of A and C (χ_{up}) and E and C (χ_{down}) were calculated to differentiate the upstream and downstream expression of the headland. Also, the ratio of the upstream to downstream median was calculated as an indicator of the bathymetric slope ratio (χ_m) between the two sides of the headland. In this ratio, the bathymetry off the headland is common, so it is comprised of ratios between X_A and X_E and the same measures for other isobaths – thus it represents the difference in offshore extent of shallow water (or nearshore bathymetric slope) from one side of the headland to the other.

2.4.2 Wave Climate

Waves are expected to dominate transport of sand past headlands. Storlazzi and Reid (2010) summarize the literature regarding wave-driven circulation and transport off central California. Modeled wave data were generated using the SWAN numerical model (Simulating WAVes Nearshore, Holthuijsen et al. (1993); Booij et al. (1999); Ris et al. (1999)) to transform data on waves at outer shelf moorings to produce wave data for inner shelf locations (Erikson et al., 2014). Outer shelf wave data were obtained from the USACE Wave Information Studies (<http://wis.usace.army.mil>), based on 32 years of hourly hind-cast wave data (1984-2011). The same refraction-diffraction wave model was used to hindcast wave conditions for each headland in this study, yielding data for the 10 m isobath on the three headland transects (Figure 2.4). Monthly and seasonal means and 95-percentile values (high-energy events) were calculated for significant wave

height (H_{sig}), peak period (T_p), and dominant direction (θ_d). Further, wave power (P), near-bed wave-orbital velocity (U_w), and wave-induced bed shear stress (τ) were calculated at the points according to methods of Soulsby (1997). Ratios of H_{sig} were also calculated to index the asymmetry of waves between upstream and downstream sides of each headland.

2.4.3 Database Pre-processing

The database consists of 50 parameters for each headland, yielding an extensive catalogue for data-mining techniques. Prior to analysis, the database was pre-processed to allow for direct comparison of the varied data types (discrete, continuous, and parameterized). In general, and specifically when using Euclidean distance as a clustering tool, parameters require the same scale for an unbiased comparison. Thus data were standardized to rescale each parameter, which assumes the data exhibit a Gaussian distribution with representative mean and standard deviation values. Standardization produces a zero-mean and unit-variance for each parameter whereas normalization tends to overweight outliers and skew the remaining data toward low values.

The large multivariate database was reduced in size through correlation analysis using a threshold of $R^2 > 0.70$ to identify and remove parameters that are largely redundant with another parameter. The correlation analysis is key to simplify the extensive geomorphic and oceanographic parameters that were measured or derived. To aid interpretation, correlation analysis was chosen to retain selected measurable “real-world” variables instead of the orthogonal functions or principle components that would be generated using an EOF approach. For example, headland perimeter correlated with width ($R^2=0.92, p<0.005$), length ($R^2=0.79, p<0.005$), and area ($R^2=0.90, p<0.005$),

allowing perimeter to represent all four parameters of “size”. A correlation threshold value of 0.70 was selected as it achieves a high level of parameter reduction while maximizing the types of variables (i.e., size, shape, shoreline complexity, wave processes). The number of variables was reduced from 50 to 14 for the next stage of analysis. The initial 14 representative and 36 eliminated parameters are shown in Table 2.2.

2.4.4 Cluster Analysis

K-means clustering was selected for classification of headlands. *K*-means clustering is a simple, unsupervised learning algorithm that solves clustering problems (MacQueen, 1967). The procedure classifies a given data set into a certain number of clusters (selected by user) and defines *K* centroids, one for each cluster. Through iteration, the centroids migrate to 1) minimize variability within clusters and 2) maximize variability between clusters. The minimization of the total intra-cluster variance, or the squared error function, *J* is

$$J = \sum_{j=1}^k \sum_{i=1}^n \|x_i^{(j)} - c_j\|^2 \quad (2.1)$$

where *k* is the number of clusters, *n* is the number of data point, $x_i^{(j)}$ is a data point at *i* for cluster *j* and c_j is the cluster center. In *K*-means clustering, the process moves objects (e.g., cases) in and out of clusters to get the most significant ANOVA (analysis of variance) results. Once the process is complete, the *F*-score for each parameter quantifies how much that parameter assists in defining a cluster. This data mining technique has been used in the oceanographic and coastal morphology sciences on wave climates

Table 2.2. Correlated Parameters for Variable Reduction

Representative Parameter	Eliminated Parameters	R ² (all p<0.005)
Perimeter	Width	0.92
	Length	0.79
	Area	0.90
Aspect Ratio	Rugosity	-0.70
Perimeter Symmetry	None	-
Curvature of Coast (θ)	None	-
Difference in Upstream- Downstream Angle ($\Delta\phi$)	ϕ_{up}	0.73
	ϕ_{down}	-0.72
Apex Sharpness (α_{total})	α_{up}	0.85
	α_{down}	0.77
Ratio of Means (χ_{ave})	None	-
Ratio of Upstream Transects (χ_{up})	None	-
Ratio of Downstream Transects (χ_{down})	None	-
Bathymetric Slope Ratio (χ_m)	None	-
Mean H_{sig} in Winter Mean Conditions	Top 5% Winter H_{sig}	0.91
	Top 5% Winter P	0.85
	Top 5% Winter U_w	0.90
	Top 5% Winter τ	0.90
	Mean Winter P	0.95
	Mean Winter U_w	0.83
	Mean Winter τ	0.77
Ratio of H_{sig} between Upstream and Downstream Points in Winter Mean Conditions ($H_{sig_upWM}/H_{sig_downWM}$)	Top 5% Winter H_{sig} Ratio	0.85
	Top 5% Winter P Ratio	0.70
	Top 5% Winter U_w Ratio	0.74
	Top 5% Winter τ Ratio	0.72
	Mean Winter P Ratio	0.78
	Mean Winter U_w Ratio	0.70
	Mean Winter τ Ratio	0.70
Mean H_{sig} in Summer Mean Conditions	Top 5% Summer H_{sig}	0.98
	Top 5% Summer P	0.91
	Top 5% Summer U_w	0.86
	Top 5% Summer τ	0.80
	Mean Summer P	0.94
	Mean Summer U_w	0.77
	Mean Summer τ	0.70
Ratio of H_{sig} between Upstream and Downstream Points in Summer Mean Conditions ($H_{sig_upSM}/H_{sig_downSM}$)	Top 5% Summer H_{sig} Ratio	0.98
	Top 5% Summer P Ratio	0.82
	Top 5% Summer U_w Ratio	0.74
	Top 5% Summer τ Ratio	0.76
	Mean Summer P Ratio	0.90
	Mean Summer U_w Ratio	0.70
	Mean Summer τ Ratio	0.71

(Camus et al., 2011), Pacific Ocean coral reefs (Freeman et al., 2012), and beaches (Scott et al., 2011).

The clustering process involved two rounds of iterations to refine the number of clusters and the types of parameters used. First, the subset of 14 parameters identified from the correlation analysis was used to perform clustering of 6-10 groups. As the wave climate variation along the coast from north to south was dominating over the geomorphic and bathymetric characteristics, the analyses were repeated with the four wave parameters removed to allow the 10 morphological parameters to drive the clustering. The wave parameters were not used for any further clustering analyses. The F -scores of parameters were reviewed to select the consistently highly rated parameters (Figure 2.5). The members of the clusters were cross-checked for sensible groupings (i.e., how similar were the mean values and variance for the parameter? Is the combination of the shoreline and bathymetric data appropriate?). Eight clusters presented the preferred grouping. Second, the strength of each of the 10 parameters was tested by removing each one and re-running the eight clusters using the remaining nine parameters. In addition, cluster analysis was done using only parameters with $F > 5.0$ and using only the three parameters with the highest F -scores. The mean of each cluster in these 12 additional cluster analyses was plotted using multi-dimensional scaling (MDS) to determine the similarity of the eight groups (Figure 2.6). The purpose of MDS is to provide a visual representation of the pattern of proximities (i.e., similarities or distances) among a set of objects (Kruskal, 1964; Kruskal and Wish, 1978). To assess the goodness-of-fit numerically and measure how well the visual configuration matches the data, a key evaluation factor is the stress test given as

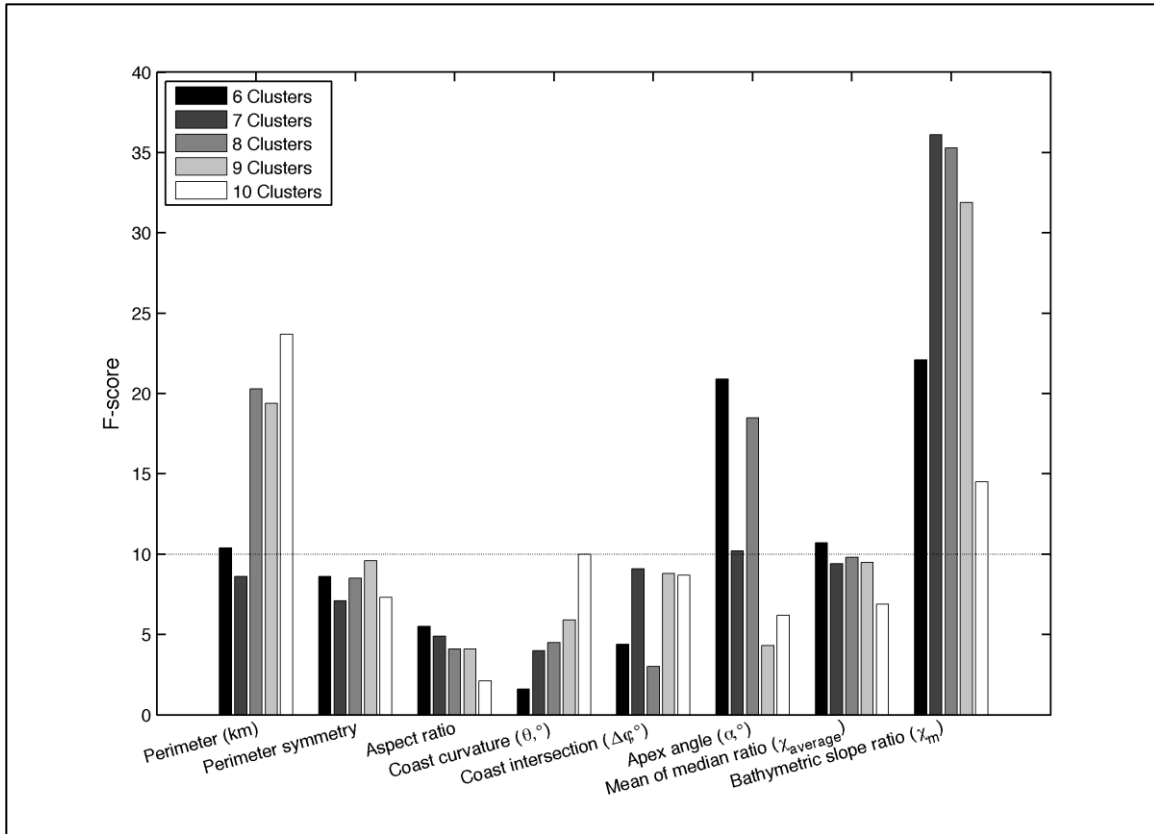


Figure 2.5. *F*-values for the morphological parameters evaluated for analyses producing different numbers of clusters: perimeter, perimeter symmetry of headland, aspect ratio of width/length, curvature of coast at the headland, difference between the upstream and downstream intersection of the headland and coastline, apex angle, mean of median transects ratio, and the bathymetric slope ratio between the upstream and downstream underwater expression of the headland. Perimeter, apex angle, and bathymetric slope ratio scored consistently higher than the other parameters in influencing the clustering.

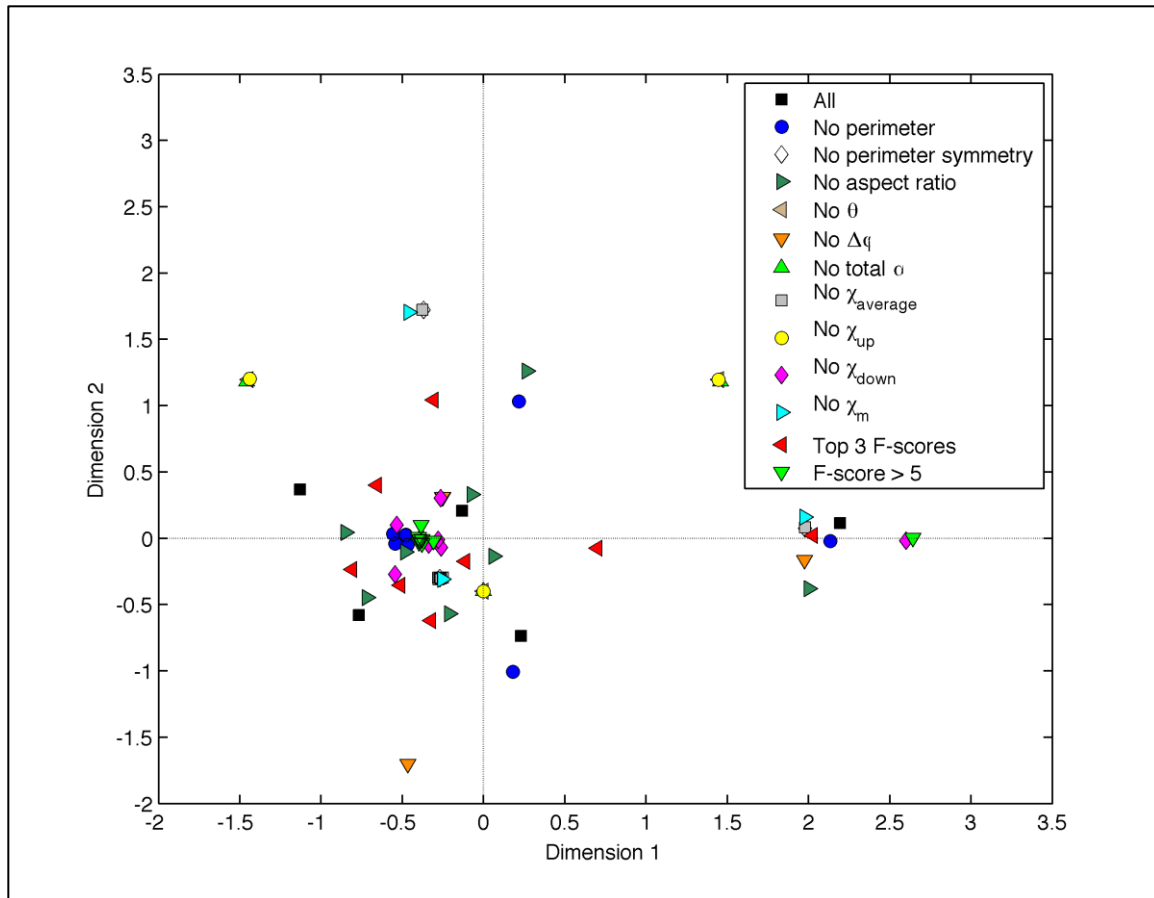


Figure 2.6. Investigation of the influence of each parameter on the clustering algorithm for eight clusters using multi-dimensional scaling (MDS) analysis. Each parameter was removed from the K-means clustering process and the mean of the eight clusters was plotted. Two other cluster analyses were also used: the top three F-scoring parameters and any parameter with $F > 5.0$. Based on the MDS plot, the top three F-scoring parameters of perimeter, bathymetric slope ratio, and sharpness of headland apex produce the most distinct eight clusters.

$$S = \sqrt{\frac{\sum \sum (f(x_{ij}) - d_{ij})^2}{scale}} \quad (2.2)$$

where $f(x_{ij})$ is a function of the input data, d_{ij} is the Euclidean distance between i and j , and $scale$ is a factor to maintain S ranging from 0 to 1. A stress of 0 shows perfect ordination. Scott et al. (2011) and Camus et al. (2011) used MDS to accompany the usage of K -means clustering in their classifications of beaches and wave climate, respectively. As seen in Figure 2.6, the “Top 3 F-scores” assortment of clusters produces the best spatial distribution in the MDS analysis; this assortment also produced a highly acceptable stress test value of $S = 0.057$. The final step to create the classes was to reverse the standardization and recover the actual values and units used for each parameter (i.e., return to a measured parameter with dimensions).

2.5 Results

2.5.1 Single-Parameter Distributions

The parameters could have been used individually to classify headlands (e.g., clustering exclusively based on aspect ratio). The distributions of the geomorphic-based 10 parameters across all headlands show variable structure (Figure 2.7). Most are unimodal (perimeter, aspect ratio, χ_{ave} , χ_{up} , χ_{down} , and χ_m); the remaining four are more evenly distributed (perimeter symmetry, coast curvature, coast intersection, and apex sharpness). The majority of the headlands are less than 5 km around, have lengths approximately twice the width (or amplitude), and have clear underwater expressions. The size distribution in particular shows the emphasis in this research on headlands that

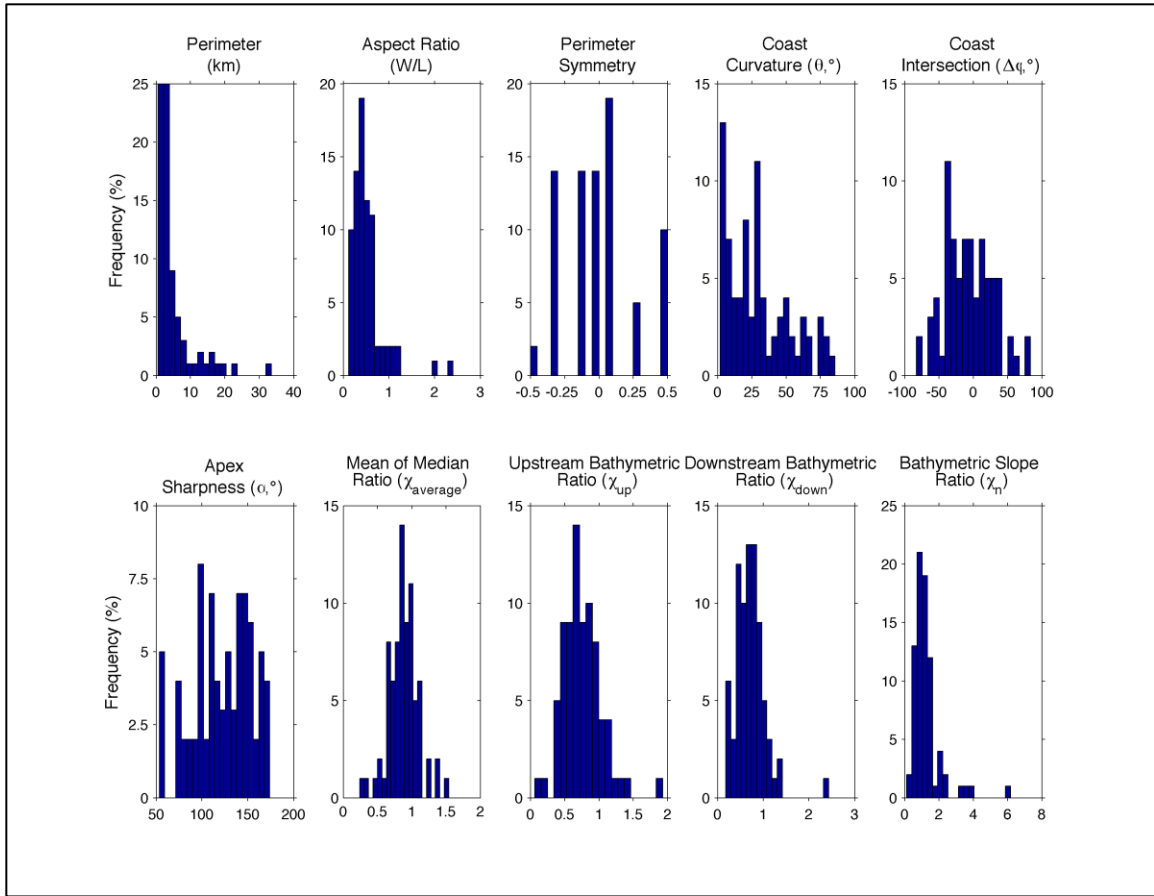


Figure 2.7. Histograms for the distribution of values for the 10 geomorphic parameters used in the cluster analysis.

interrupt the nearshore flow and transport, not the shelf-scale circulation. The headlands' shorelines are also generally skewed upcoast although the largest category is the slight downcoast skewness. The shape of the headlands in terms of intersection with the coast and sharpness of the apex angle are less conclusive as individual clustering parameters. A multivariate approach to clustering was used instead to classify the headlands because multiple properties of headland shape are expected to influence flow and transport processes.

2.5.2 Morphological Classification

The three most important parameters in distinguishing the classes using morphological parameters are bathymetric slope ratio, size, and the sharpness of the headland's apex (α_{total}). If each parameter had three descriptive categories (e.g, small, medium, large or acute, balanced, obtuse), 27 hypothetical groups are possible. Classification allowed identification of just eight clusters as preferred groupings after iterations, cross-checking and the 16 test analyses. These eight classes exhibit maximum similarity within each cluster and minimum similarity between clusters. The classes contain varying number of members (Table 2.3). For each class, the mean and standard deviation of distance from the center of the class are given as measures of the distribution of members within that class. Histograms of the three parameters show how the values distribute across the classes and for all classes combined (Figure 2.8). The following are summary descriptions of the eight classes, with individual headland details found in Appendix 1.

Table 2.3. Headland Classes after Clustering and California Littoral Cell Comparison

Headland Class	Number of Members	Percent of Database (%)	Distance from Cluster Center	Perimeter (mean km) (description)	Bathymetric Slope Ratio (mean) (description)	Apex Sharpness (mean °) (description)	Littoral Cell Boundary ¹
1	22	28.2	0.31±0.15	3.46±2.02 Small	0.97±0.37 Upstream	107±8.7 Mildly obtuse	4 (18%)
2	3	3.8	0.26±0.14	2.49±0.66 Small	3.55±0.23 Downstream	141±17 Obtuse	3 (100%)
3	12	15.4	0.39±0.12	5.21±2.30 Small-medium	1.56±0.40 Downstream	142±13 Obtuse	3 (25%)
4	1	1.3	--	5.41 Small-medium	6.17 Extreme downstream	116 Obtuse	1 (100%)
5	10	12.8	0.32±0.14	3.99±1.87 Small	1.13±0.37 Downstream	108±8.0 Mildly obtuse	1 (10%)
6	20	25.6	0.26±0.10	1.74±1.16 Small	0.97±0.23 Upstream	151±12 Obtuse	6 (30%)
7	5	6.4	0.49±0.14	13.77±2.20 Large-medium	1.03±0.56 Balanced	77±20 Acute	3 (60%)
8	5	6.4	0.73±0.35	23.35±6.87 Large	1.23±0.80 Downstream	162±13 Very obtuse	4 (80%)
All	78	100	0.35±0.21	7.30±7.13	2.08±1.87	128±28	25

44 1 – Percent of class members defined as a littoral cell boundary by Habel and Armstrong (1978)

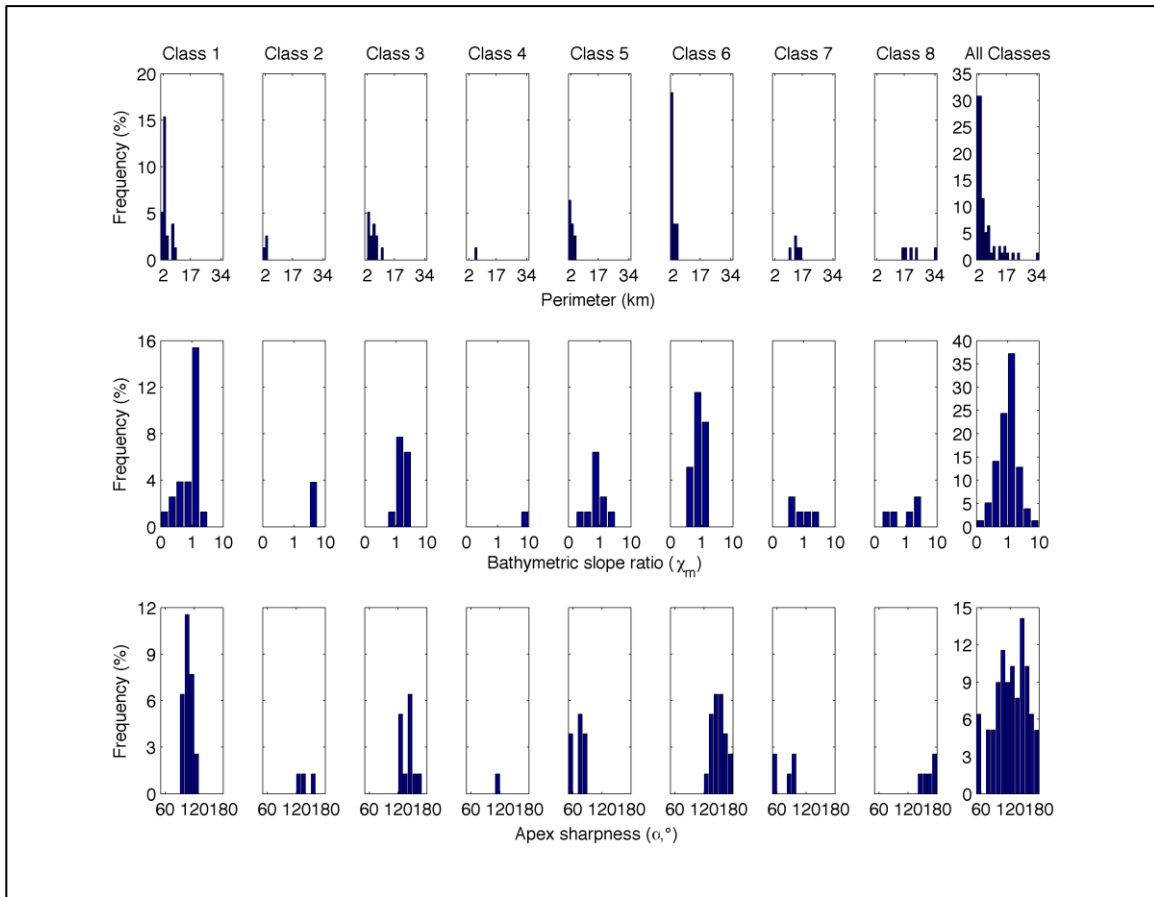


Figure 2.8. Histograms for the distribution of values for the top three parameters responsible for cluster generation by class (first 8 columns) and for all classes combined (last column). Top row: Perimeter (km). Middle row: Bathymetric slope ratio. Bottom row: Apex angle α (degrees). Vertical axis scale expands for the last column. Horizontal scales for perimeter and angle are linear, and logarithmic for ratio.

Type #1. Small size, mildly obtuse angle at apex, bathymetric symmetry; twenty-two headlands, constituting 28% of the database. This class is characterized by a mean perimeter size of $3.46 \text{ km} \pm 2.02$ tightly grouped around the mean, a bathymetric slope ratio mean of 0.97 ± 0.37 , and an apex angle mean of $107^\circ \pm 8.7$. These headlands show slightly more underwater expression in the downstream direction (broader shallow region downstream). The range of apex angle is $90\text{-}120^\circ$, suggesting the headlands are neither strongly acute nor obtuse on the ocean-facing front. The headland closest to the cluster mean is El Jarro Point (Figure 2.9).

Type #2. Small size, slightly obtuse, strong downstream bathymetric expression; three headlands, constituting 4% of the database. This class is characterized by a mean perimeter size of $2.49 \text{ km} \pm 0.66$, a bathymetric slope ratio mean of 3.55 ± 0.23 , and an apex angle mean of $141^\circ \pm 17$. These headlands are slightly obtuse on the ocean-facing front. The most distinguishing feature of this class is the strong downstream bathymetric expression (deep nearshore waters downstream of headland), which is the second highest of all the classes. The three headlands are in Southern California, with Point La Jolla most representative (Figure 2.9).

Type #3. Mid-sized, obtuse, more downstream than upstream bathymetric expression; twelve headlands, constituting 15% of the database. This class is characterized by a mean perimeter size of $5.21 \text{ km} \pm 2.3$, a bathymetric slope ratio mean of 1.56 ± 0.4 , and an apex angle mean of $142^\circ \pm 13$. These headlands are fairly obtuse and have more of a downstream underwater expression than upstream. Horseshoe Point is closest to the mean of the class (Figure 2.9).

Type #4. Mid-sized, obtuse, extreme downstream bathymetric expression; a single headland, Point Loma, constituting 1% of the database (Figure 2.9). This headland has a perimeter size of 5.41 km, a bathymetric slope ratio of 6.17, and an apex angle of 116° . The extreme imbalance of the bathymetric slope ratio is due to the geography of Point Loma at the entrance to San Diego Bay to the east of the headland. For the other two parameters, this class is very similar to Type #3 and would be included in that group if not for the bathymetric slope ratio.

Type #5. Small sized, acute, upstream bathymetric expression; ten headlands, constituting 13% of the database. This class is characterized by a mean perimeter size of $3.99 \text{ km} \pm 1.87$, a bathymetric slope ratio mean of 1.13 ± 0.37 , and an apex angle mean of $108^\circ \pm 8.0$. Point Sierra Nevada is representative of this class (Figure 2.9).

Type #6. Small size, obtuse, upstream bathymetric expression; twenty headlands, constituting 26% of the database. This class is characterized by a mean perimeter size of $1.74 \text{ km} \pm 1.16$, a bathymetric slope ratio mean of 0.97 ± 0.23 , and an apex angle mean of $151^\circ \pm 12$. This large group contains the two tombolos in the database – Goat Rock and Morro Rock. Despite the appearance of very different headlands, the overall mean distance for the group is 0.26 ± 0.10 (tighter than most clusters). Bolsa Point is a good representative (Figure 2.9).

Type #7. Large size, acute, balanced bathymetric expression; five headlands, constituting 6% of the database. This class is characterized by a mean perimeter size of $13.77 \text{ km} \pm 2.2$, a bathymetric slope ratio mean of 1.03 ± 0.56 , and an apex angle mean of $77^\circ \pm 20$. These headlands are sharply acute and have a balanced underwater expression. Picking a representative for this class is more challenging than the others because they

are large enough to contain small, unidentified headlands. Point Arena shows several characteristics of a large headland with sharp points protruding well past the width of the surf zone but generally represents this class well (Figure 2.9).

Type #8. Largest size, obtuse, balanced bathymetric expression; five headlands, constituting 6% of the database. This class is characterized by a mean perimeter size of $23.35 \text{ km} \pm 6.87$, a bathymetric slope ratio mean of 1.23 ± 0.8 , and an apex angle mean of $162^\circ \pm 13$. These headlands are the largest in the database, broad faced, and have a balanced underwater expression. This group includes the mega-headland of Monterey Peninsula. They show complex shorelines with several smaller headlands, some of which have been identified in the other headland types. The representative for this class is Patrick's Point/Trinidad Head, which has a compound shoreline (Figure 2.9).

The eight types of headland classes described above create the best possible arrangement using the three most important parameters based on the clustering analysis. The morphologically-based headland classes provide a sorting of California headlands to perform analysis of flow regimes, wave interactions, and littoral cell boundaries specific to each class.

2.6 Discussion

2.6.1 Classes of Headlands and Key Parameters

The process used to classify the 78 California headlands sought to merge easily measured shoreline and bathymetric parameters into a large database for cluster analysis. Several of the basic parameters (size, shape, shoreline complexity) suggested clusters, but

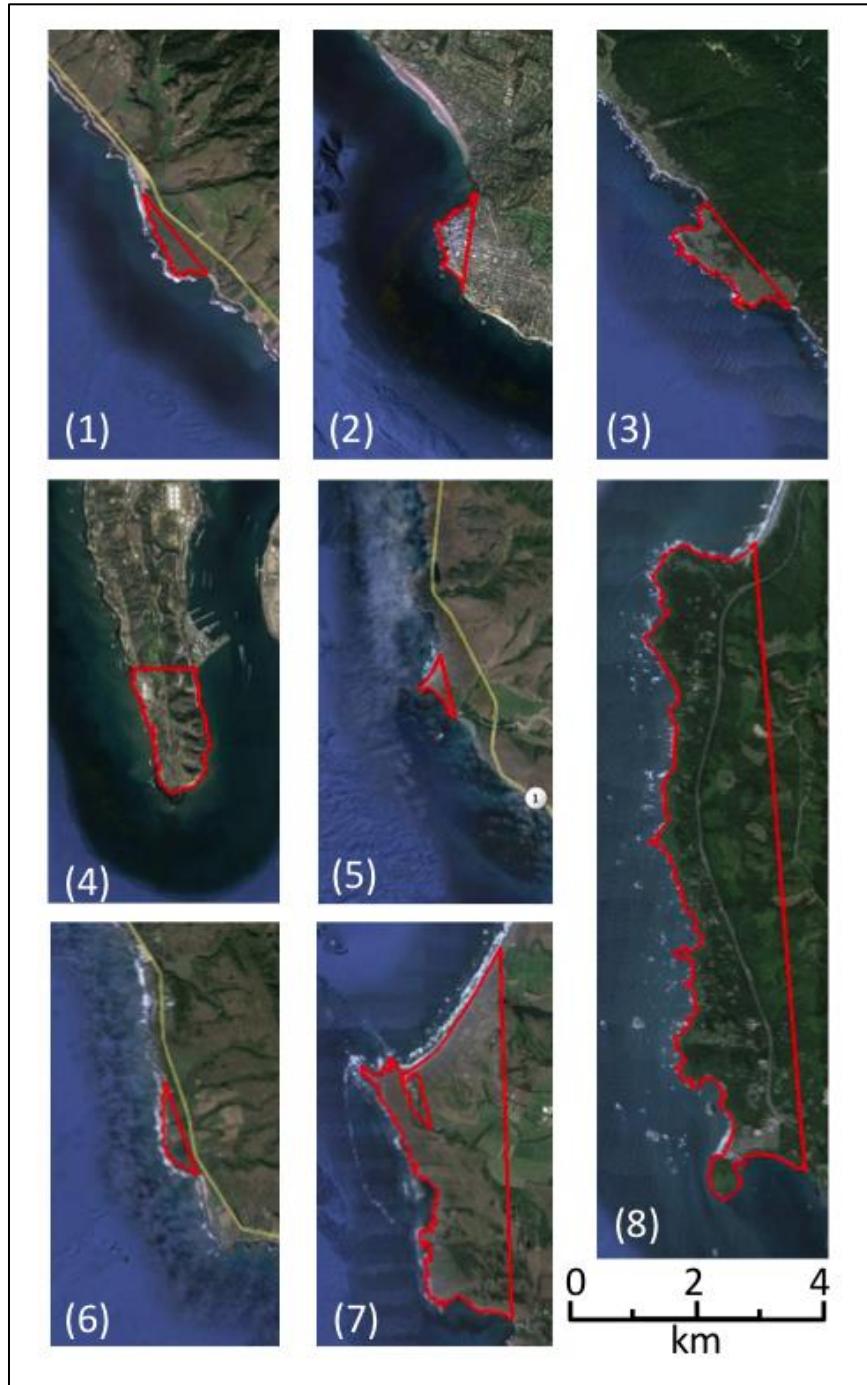


Figure 2.9. Representative headlands for each class. 1) Point El Jarro, 2) Point La Jolla, 3) Horseshoe Point, 4) Point Loma, 5) Point Sierra Nevada, 6) Bolsa Point, 7) Point Arena, and 8) Patrick’s Point/Trinidad Head. Red polygons delineate the headland extent as defined using remote-sensing imagery, geological maps, navigational charts, and shoreline characterization data.

as the analysis proceeded, many of the simplest parameters did not exert as much influence as were initially expected. For example, aspect ratio appears to be a characteristic of a headland that can affect an alongshore jet (Signell and Geyer, 1991) or sea stack-headland evolution (Limber and Murray, 2015). However, this parameter does not play a primary role in defining clusters – it had a low *F*-score, indicating that it had limited skill in differentiating between headlands (i.e., most headlands exhibit similar aspect ratios). The iterative sequence of removing parameters and rerunning the clustering and MDS analyses proved that the most distinct classes emerge when only the top three *F*-scoring parameters are used.

Based on the use of perimeter, bathymetric slope ratio, and apex angle, the headlands fell into eight distinctive clusters, with only one member of Type 4 (Point Loma), which could be considered an outlier – leaving just 7 classes: 4 classes of small headlands, 1 mid-size class and 2 classes of big headlands (one class with acute angles and the other with obtuse angles). The MDS plot (Figure 2.10) shows that Types 1, 3, 5, and 6 are similar, and distinction between classes may depend on which parameters are used in the analysis (Figure 2.6). Relative to that group of clusters, Types 7 and 8 are distinct (the two big headland classes), and also Types 2 and 4 are distinct (both characterized by acute angles and deep waters downstream of the headland).

The importance of the three primary parameters may be interpreted in terms of flow and wave processes. For example, the size of the headland is critical relative to the width of wave action, and the apex sharpness is important for flow separation and eddy generation. The change in bathymetry from one side of the headland to the other irrespective of the details of the headland can also be key to flow separation and offshore

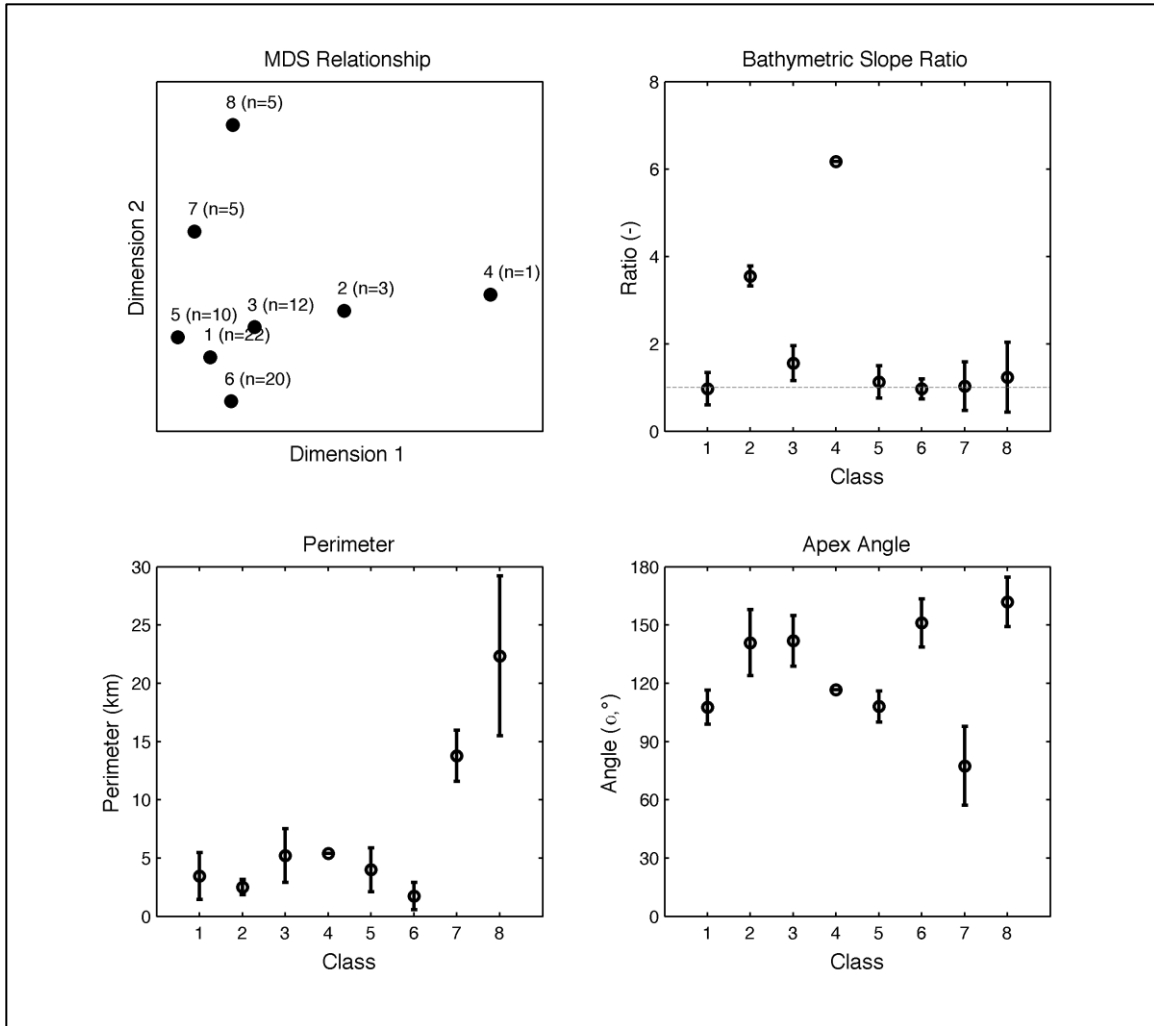


Figure 2.10. Multi-dimensional scaling (MDS) plot and the means of the three parameters responsible for cluster generation. The variability around each mean is one standard deviation. Top left: MDS relationship among the classes and size of class. Bottom left: Perimeter (km). Top right: Bathymetric slope ratio. The dotted line signifies a ratio of 1. Bottom right: Headland apex angle, α (degrees).

export of sediment: deep water downstream is more likely to yield an offshore loss of sand and a break in the continuity of longshore transport – this parameter emerges below as the most important in identifying headlands that align with littoral cell boundaries.

This first-of-its-kind classification does not come without areas for improvement to either the method or the data itself. For the headland classes, three revisions could be considered to enhance the results. First, whereas 78 headlands is a sizable number, the California coast is 1,800 km long and several potential entries to the database were excluded due to not satisfying the criteria detailed in Section 4. A different set of parameters to delineate headlands may produce a larger database. Second, offshore reefs and sea stacks were not included in the boundary of a headland due to lack of data. Some of these features, particularly the reefs, were likely resolved in the bathymetry, but the overall sizes of the headlands could be larger than when defined by the shoreline. Hence the size parameters (L , W , perimeter, and area) may be underestimated. Last, the bedrock geology offshore could have an additional control on the clusters or at least correlate with some of the geomorphic parameters. Stul et al. (2012) were able to incorporate geology more explicitly than this study, which suggests headlands and littoral cell boundaries may be better understood when the lithology and resistance to erosion are considered. Examining any or all of the preceding could test the efficacy of the current classifications.

2.6.2 Wave-Driven Transport Past Headlands

These headland classes provide a descriptive grouping of similar sizes, shapes, and shoreline complexities – classes determined by morphological similarity, without any

information on waves, or sediment transport. Given that the role of wave energy in circulation and sediment transport around headlands is critical (Davies, 1974; Hume et al., 2000; Pattiaratchi et al., 1987), a brief exploration of how waves interact with headlands was conducted to demonstrate an application of the headland classes. From wave data at 10 m on each of the three headland transects, the angle between waves and shore-normal was determined as a measure of longshore transport for the 78 headlands. Without determining power and without estimating the sediment flux (Kamphuis, 2010), it is possible to identify when longshore transport is continuous around the headland or when it is in opposite directions on either side of the headland, indicating a discontinuity in wave-driven transport past the headland. The transport for the 78 headlands was characterized for winter and summer mean and 95-percentile conditions as one of four possibilities: continuous upcoast, continuous downcoast, convergent, or divergent (Figure 2.11).

The results by headland class show that the geomorphically-based clusters translate well to wave-driven transport scenarios. Only headland Type 4 (Point Loma) is discontinuous under all conditions – likely to always block wave-driven transport. Headland Type 2 is also often divergent, with continuous transport occurring at times, but only downcoast. Type 8 is similar to Type 2, but transport is blocked less often (size seems less important than asymmetry). At Type 7 headlands, wave-driven transport is blocked more often, but upcoast transport can also occur in winter. At other headlands (the central grouping of clusters: 1, 3, 5 and 6), continuous transport past the headland is common for mean and 95-percentile conditions and both upcoast and downcoast

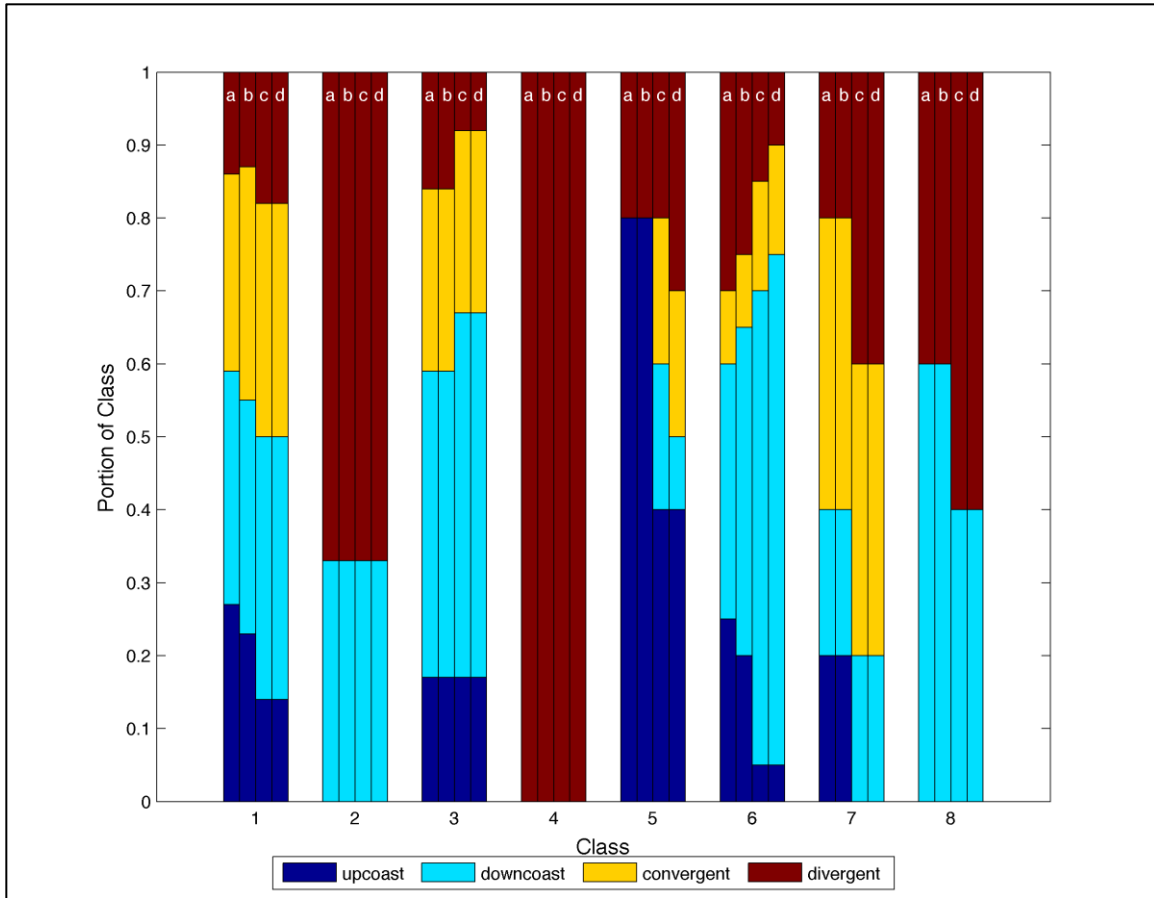


Figure 2.11. Portion of transport possibilities (upcoast, downcoast, convergent, and divergent) for each headland class under four wave conditions (a - winter, 95-percentile, b - winter, mean, c - summer, 95-percentile, and d - summer, mean). Each class size is normalized. Upcoast and downcoast transport is continuous around the headland, so that it will not block sediment transport, while convergent and divergent transport will not allow transport around the headland.

transport can occur. While 95-percentile conditions are most important because transport will occur during high-energy events, there are only small differences between incident directions for mean and high-energy conditions. There is seasonality for all types other than Types 2 and 4, as expected and consistent with the ideas put forward by van Rijn (2010). The seasonal shifts between continuous or blocked transport is supported by the work in Australia by Stul et al. (2012) and Goodwin et al. (2013), which suggest that headland transport can effectively turn ‘on’ or ‘off’ seasonally.

2.6.3 Littoral Cell Boundaries in California

The 27 headlands identified by Habel and Armstrong (1978) as littoral cell boundaries can be related to the headland classes to determine if certain geomorphic and/or bathymetric parameters may clarify a headland’s role in blocking sediment transport. Table 2.3 shows that all of the headlands of Type 4 and Type 2 are littoral cell boundaries and both are characterized by marked bathymetric slope ratios, with steep slopes and deep water downstream when flow is southward. Type 8 (biggest headlands) has 4 out of 5 headlands acting as boundaries and Type 7 has 3 out of 5 (big headlands, smaller than Type 8, but with acute apex). The other headland types (1, 3, 5, 6) have less than a third of their members acting as boundaries (Table 3). This is consistent with the analyses presented in Figure 2.11 where Types 2, 4, 7, and 8 typically experience being divergent or convergent for wave-driven transport. Based on these results, big headlands and headlands with deep water downstream (and acute apexes) are effective littoral cell boundaries. While those headland types are likely to act as littoral cell boundaries, the relationship between type and boundary is not entirely convincing. Fourteen of the 27

littoral cell boundary headlands fall into headland classes that are not typically boundaries. For example, one boundary falls into Type 5, which is characterized by small sizes and obtuse apices – headlands that may be easily enveloped and by-passed by alongshore currents.

sizes and obtuse apices – headlands that may be easily enveloped and by-passed by alongshore currents.

The seasonal wave power is shown alongside transport direction in Figure 2.12. Winter wave power is larger than in summer for almost all of the headlands, regardless of headland type. Seasonal variability in wave power and transport direction is evident with some headlands turning transport ‘on’ in winter conditions (e.g., Bolinas Point) while others become barriers to transport (e.g., Bruhel Point). Members of Type 6 headlands are the most seasonally variable of all the boundary headlands while those in Types 2, 3, 4, 7 are consistent across the seasons. The littoral cell boundary headlands can be sorted into two categories: those that do not change seasonally, and those that change seasonally. The 20 non-seasonal headlands include 9 headlands for which wave transport is continuous and in a consistent direction both winter and summer and 11 headlands for which wave transport is discontinuous. The wave-driven transport past the remaining 7 headlands changes seasonally, with 6 becoming a boundary seasonally and one Type 6 headland experiencing reversed transport seasonally.

The association of some littoral cell boundaries with headland classes that are not likely to block sediment transport may be explained by inadequacies in headland clustering, indexing of continuity of wave-driven transport past headlands, or definition of the boundaries of littoral cells. Inadequacy in headland clustering may be due to

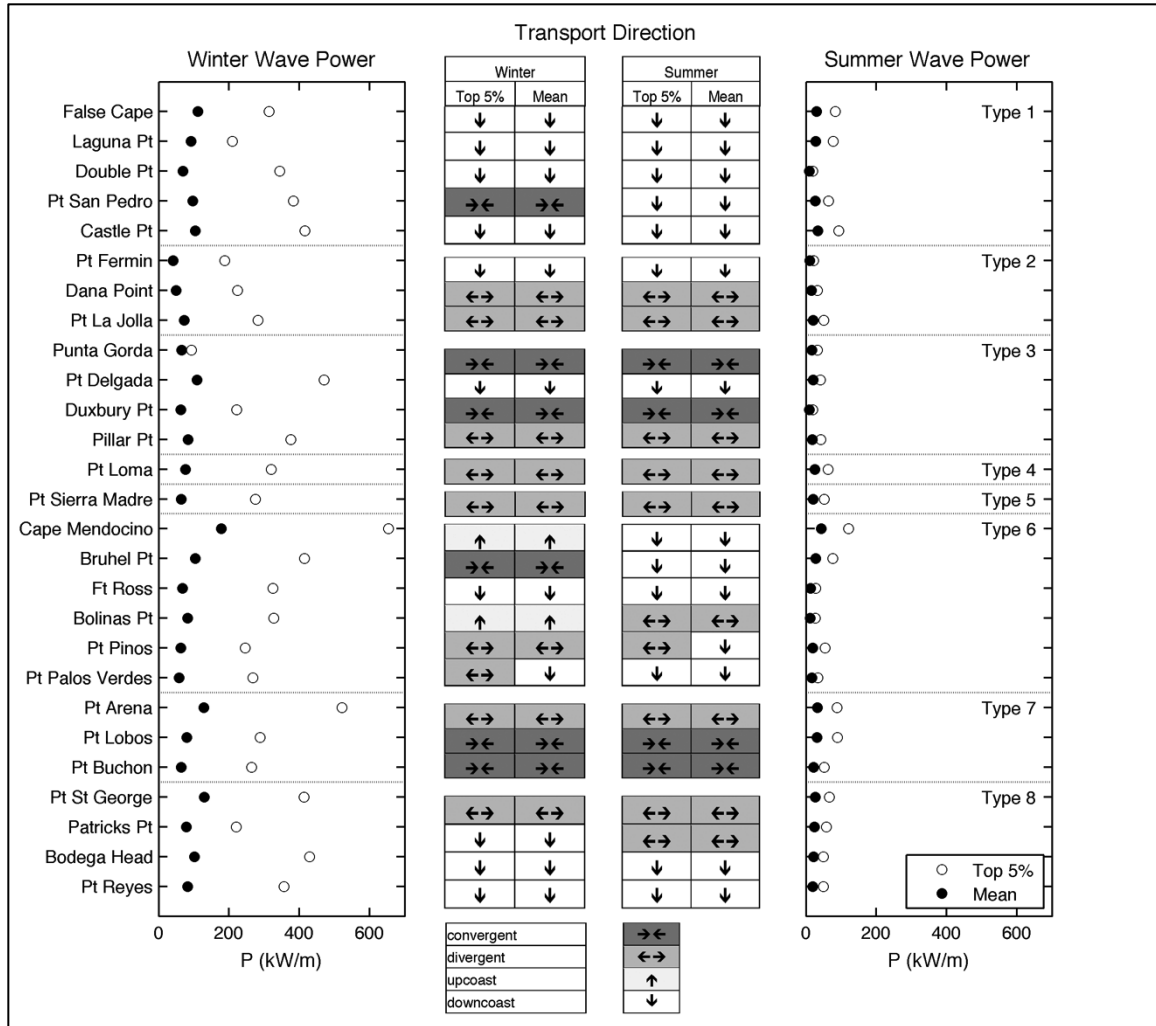


Figure 2.12. Average wave power (kW/m) and transport direction in winter and summer mean (solid dots) and 95-percentile (open dots) conditions for the 27 California headlands used to define the traditional California littoral cell boundaries. The headlands are grouped by class type. Winter conditions generate larger wave power than summer for all headlands. Convergent and divergent transport directions are considered barriers to alongshore transport and can produce *permanent* boundaries (e.g., Types 4 and 7). Seasonal shifts in transport direction produce *seasonal* boundaries (e.g., some headlands in Type 6). See Table 2.3 for portion of littoral cell boundary headlands within a class.

omission of a key morphological factor or problems with the clustering approach. This seems unlikely given the routine use of *K*-means clustering and the comprehensive initial list of parameters. The second possibility is that a simple wave-direction analysis does not properly capture the likelihood of continuous/blocked transport. High-resolution numerical modeling in a subsequent analysis could elucidate this point. Notwithstanding inadequacies in clustering or indexing of transport, the findings suggest significant inadequacies in the definition of littoral cell boundaries – specifically those that align with small/mid-sized headlands without acute apexes or deep water downstream (i.e., Types 1, 3, 5, 6).

The conclusions above show that a better definition of littoral cell boundary is required and a recognition that while some boundaries may be close to perfect obstacles, others are weak and variable with significant leakage. Stul et al. (2012) described littoral cells as tiered according to primary, secondary, and tertiary levels along the coast of Western Australia with sediment exchange possible among the lower levels. California's littoral cells as defined by Habel and Armstrong (1978) do not contain subcells, but Patsch and Griggs (2007) expanded some of the cells to create compound cells (e.g., Santa Monica). Other cells defined by Habel and Armstrong (1978) are in such close proximity that the divisions could be arbitrary, such as near the mouth of the San Francisco Bay where the Bolinas Bay and San Francisco cells are adjacent to each other. Further, the method used by Habel and Armstrong (1978) to delineate the boundaries was not explicitly described, so the factors they used are ambiguous. This contrasts with the bathymetry, topography, remote sensing imagery, historic coastal change, shoreline position, sediment information, dunes, and geological maps that were compiled by Stul et

al. (2012) to create the Western Australia boundaries. Redefining littoral cell boundaries for California is beyond the scope of this paper, but clearly a need for the region.

2.7 Conclusion

California headlands were grouped into eight classes that represent distinct headland types in terms of geomorphic and bathymetric parameters. Headland perimeter, apex sharpness, and bathymetric slope ratio were found to exert the most control on classifying the 78 headlands along the California coast. Hindcast wave data were used to investigate the likelihood of continuous sediment transport around the headland and determine the efficacy of the headland as a littoral cell boundary. Headlands characterized by large size, deep water downstream and acute apex angles were shown to result in low likelihood of wave-driven transport past the headland. Most of these headlands aligned with littoral cell boundaries. However, many littoral cell boundaries aligned with headlands that did not fall into these classes, raising questions about the efficacy of these headlands in blocking alongshore transport. Based on these findings, the traditional California littoral cell boundaries are questionable and an in-depth analysis is needed.

2.8 References

- Baptista, P., Cunha, T.R., Gama, C., Bernardes, C., 2012. A new and practical method to obtain grain size measurements in sandy shores based on digital image acquisition and processing. *Sedimentary Geology* 282, 294-306.
- Bastos, A.C., Kenyon, N.H., Collins, M., 2002. Sedimentary processes, bedforms and facies, associated with a coastal, headland: Portland Bill, Southern UK. *Marine Geology* 187, 235-258.
- Berthot, A., Pattiaratchi, C., 2006. Field measurements of the three-dimensional current structure in the vicinity of a headland-associated linear sandbank. *Continental Shelf Research* 26, 295-317.
- Black, K., Oldman, J., Hume, T., 2005. Dynamics of a 3-dimensional, baroclinic, headland eddy. *New Zealand Journal of Marine and Freshwater Research* 39, 91-120.
- Buscombe, D., Rubin, D.M., Lacy, J.R., Storlazzi, C.D., Hatcher, G., Chezar, H., Wyland, R., Sherwood, C.R., 2014. Autonomous bed-sediment imaging-systems for revealing temporal variability of grain size. *Limnology and Oceanography-Methods* 12, 390-406.
- Buscombe, D., Rubin, D.M., Warrick, J.A., 2010. A universal approximation of grain size from images of noncohesive sediment. *Journal of Geophysical Research* 115.
- Davies, P.A., Dakin, J.M., Falconer, R.A., 1995. Eddy Formation Behind a Coastal Headland. *Journal of Coastal Research* 11, 154-167.
- Deines, K.L., 1999. Backscatter Estimation Using Broadband Acoustic Doppler Current Profilers. RD Instruments Application Note FSA-008, 1-5.
- Denniss, T., Middleton, J.H., Manasseh, R., 1995. Recirculation in the Lee of Complicated Headlands - A Case-Study of Bass-Point. *Journal of Geophysical Research-Oceans* 100, 16087-16101.
- Emery, W.J., Thomson, R.E., 2001. *Data Analysis Methods in Physical Oceanography*. Elsevier, New York.
- Everts, C.H., Eldon, C.D., 2005. Sand Capture In Southern California Submarine Canyons. *Shore and Beach* 73, 3-12.
- Freeland, H., 1990. The Flow of a Coastal Current Past a Blunt Headland. *Atmosphere-Ocean* 28, 288-302.
- George, D.A., Hill, P.S., 2008. Wave climate, sediment supply and the depth of the sand-mud transition: A global survey. *Marine Geology* 254, 121-128.
- George, D.A., Largier, J.L., Storlazzi, C.D., Barnard, P.L., 2015. Classification of rocky headlands in California with relevance to littoral cell boundary delineation *Marine Geology* 369, 137-152.
- Goodwin, I.D., Freeman, R., Blackmore, K., 2013. An insight into headland sand bypassing and wave climate. variability from shoreface bathymetric change at Byron Bay, New South Wales, Australia. *Marine Geology* 341, 29-45.
- Goring, D.G., Nikora, V.I., 2002. Despiking acoustic Doppler velocimeter data. *Journal of Hydraulic Engineering-Asce* 128, 117-126.
- Guillou, N., Chapalain, G., 2011. Effects of waves on the initiation of headland-associated sandbanks. *Continental Shelf Research* 31, 1202-1213.

Habel, J.S., Armstrong, G.A., 1978. Assessment and Atlas of Shoreline Erosion Along the California Coast. State of California, Department of Navigation and Ocean Development, Sacramento, CA, p. 277.

Hickey, B.M., 1992. Circulation over the Santa-Monica San-Pedro Basin and Shelf. *Progress in Oceanography* 30, 37-115.

Hickey, B.M., Dobbins, E.L., Allen, S.E., 2003. Local and remote forcing of currents and temperature in the central Southern California Bight. *Journal of Geophysical Research-Oceans* 108.

Holdaway, G.P., Thorne, P.D., Flatt, D., Jones, S.E., Prandle, D., 1999. Comparison between ADCP and transmissometer measurements of suspended sediment concentration. *Continental Shelf Research* 19, 421-441.

Hume, T.M., Oldman, J.W., Black, K.P., 2000. Sediment facies and pathways of sand transport about a large deep water headland, Cape Rodney, New Zealand. *New Zealand Journal of Marine and Freshwater Research* 34, 695-717.

Inman, D.L., 1986. Southern California Coastal Processes Data Summary.

Klinger, B., 1993. Gyre Formation at a Corner by Rotating Barotropic Coastal Flows along a Slope. *Dynamics of Atmospheres and Oceans* 19, 27-63.

Knur, R.T., Kim, Y.C., 1999. Historical sediment budget analysis along the Malibu coastline, Sand Rights '99- Bringing Back the Beaches. ASCE, Ventura, CA, p. 292.

Larson, M., Hoan, L., Hanson, H., 2010. Direct Formula to Compute Wave Height and Angle at Incipient Breaking. *Journal of Waterway, Port, Coastal, and Ocean Engineering* 136, 119-122.

Leidersdorf, C.B., Hollar, R.C., Woodell, G., 1994. Human Intervention with the Beaches of Santa Monica Bay, California Shore and Beach 62, 29-38.

Limber, P.W., Patsch, K.B., Griggs, G.B., 2008. Coastal sediment budgets and the littoral cutoff diameter: A grain size threshold for quantifying active sediment inputs. *Journal of Coastal Research* 24, 122-133.

MacCready, P., Pawlak, G., 2001. Stratified flow along a corrugated slope: Separation drag and wave drag. *Journal of Physical Oceanography* 31, 2824-2839.

Madsen, O.S., 1994. Spectral wave-current bottom boundary layer flows, *Coastal Engineering 1994*, 24th International Conference Coastal Engineering Research Council, pp. 384-398.

Magaldi, M.G., Ozgokmen, T.M., Griffa, A., Chassignet, E.P., Iskandarani, M., Peters, H., 2008. Turbulent flow regimes behind a coastal cape in a stratified and rotating environment. *Ocean Modelling* 25, 65-82.

Nickols, K.J., Gaylord, B., Largier, J.L., 2012. The coastal boundary layer: predictable current structure decreases alongshore transport and alters scales of dispersal. *Marine Ecology Progress Series* 464, 17-35.

Noble, M.A., Rosenberger, K.J., Hamilton, P., Xu, J.P., 2009. Coastal ocean transport patterns in the central Southern California Bight. *Earth Science in the Urban Ocean: the Southern California Continental Borderland* 454, 193-226.

Orme, A.R., 1991. The Malibu coast – a contribution to the city-wide wastewater management study, p. 50.

Patsch, K., Griggs, G., 2007. Development of Sand Budgets for California's Major Littoral Cells. Institute of Marine Sciences, University of California, Santa Cruz, p. 115.

Pentney, R.M., Dickson, M.E., 2012. Digital Grain Size Analysis of a Mixed Sand and Gravel Beach. *Journal of Coastal Research* 28, 196-201.

Pingree, R.D., 1978. Formation Of Shambles And Other Banks By Tidal Stirring Of Seas. *Journal of the Marine Biological Association of the United Kingdom* 58, 211-226.

Reid, J.A., Reid, J.M., Jenkins, C.J., Zimmermann, M., Williams, S.J., Field, M.E., 2006. usSEABED: Pacific Coast (California, Oregon, Washington) Offshore Surficial-sediment Data Release.

Roughan, M., Mace, A.J., Largier, J.L., Morgan, S.G., Fisher, J.L., Carter, M.L., 2005. Subsurface recirculation and larval retention in the lee of a small headland: A variation on the upwelling shadow theme. *Journal of Geophysical Research-Oceans* 110.

Short, A.D., 1999. *Handbook of beach and shoreface morphodynamics*. John Wiley, New York.

Signell, R.P., Geyer, W.R., 1991. Transient Eddy Formation around Headlands. *Journal of Geophysical Research-Oceans* 96, 2561-2575.

Soulsby, R., 1997. *Dynamics of Marine Sands: A Manual for Practical Applications*. Thomas Telford, London.

Stewart, S.R., 2014. Tropical Cyclone Report. Hurricane Simon (EP192014), in: National Hurricane Center, N. (Ed.), p. 18.

Storlazzi, C.D., Jaffe, B.E., 2008. The relative contribution of processes driving variability in flow, shear, and turbidity over a fringing coral reef: West Maui, Hawaii. *Estuarine Coastal and Shelf Science* 77, 549-564.

Stul, T., Gozzard, J., Eliot, I., Eliot, M., 2012. Coastal Sediment Cells between Cape Naturaliste and the Moore River, Western Australia in: Transport, W.A.D.o. (Ed.). Damara WA Pty Ltd and Geological Survey of Western Australia, Fremantle, WA, Australia, p. 44.

Thorne, P.D., Vincent, C.E., Hardcastle, P.J., Rehman, S., Pearson, N., 1991. Measuring Suspended Sediment Concentrations Using Acoustic Backscatter Devices. *Marine Geology* 98, 7-16.

USACE, 1984. Shore Protection Manual, in: U. S. Army Corps of Engineers, C.E.R.C. (Ed.). Department of the Army, Waterways Experiment Station, Corps of Engineers, Vicksburg, p. 656.

van Rijn, L.C., 2010. Coastal erosion control based on the concept of sediment cells. *CONSCIENCE, Deltares, The Netherlands*, p. 80.

Verron, J., Davies, P., Dakin, J., 1991. Quasigeostrophic Flow Past a Cape in a Homogeneous Fluid. *Fluid Dynamics Research* 7, 1-21.

Xu, J.P., Noble, M.A., 2009. Variability of the Southern California wave climate and implications for sediment transport. *Earth Science in the Urban Ocean: the Southern California Continental Borderland* 454, 171-191.

2.9 Appendix 1

Classified Headland Database with Key Geomorphic Clustering Parameters
Italicized Headland Name Indicates Littoral Cell Boundary (Habel and Armstrong, 1978)

Headland Id	Headland	Headland Class	Perimeter (km)	Apex Sharpness (α , $^{\circ}$)	Bathymetric Slope Ratio
1	<i>Pt. St. George</i>	8	18.27	164.8	0.624
2	<i>Trinidad Head/Patricks Point</i>	8	20.27	172.4	1.086
3	<i>False Cape</i>	1	1.76	114.9	1.146
4	<i>Cape Mendocino</i>	6	2.11	136.0	0.663
5	<i>Punta Gorda</i>	3	6.49	142.6	0.970
6	<i>Pt. Delgada</i>	3	6.93	147.7	1.074
7	Cape Vizcaino	1	3.75	111.2	1.216
8	<i>Bruhel Pt</i>	6	3.98	155.4	0.673
9	<i>Laguna Pt</i>	1	2.30	101.4	0.767
10	<i>Pt Arena</i>	7	16.21	54.9	0.649
11	Havens Neck	1	2.70	100.6	0.611
12	Black Pt	5	4.94	82.6	1.083
13	Horseshoe Pt	3	5.61	143.7	1.381
14	Salt Pt	1	4.64	96.4	0.578
15	<i>Fort Ross</i>	6	1.71	139.3	0.962
16	Goat Rock	6	0.85	146.6	0.774
17	<i>Bodega Head</i>	8	16.01	174.1	1.570
18	<i>Pt Reyes</i>	8	23.60	143.7	2.418
19	<i>Double Pt</i>	1	2.39	117.1	1.196
20	<i>Bolinas Pt</i>	6	1.60	137.5	1.067
21	<i>Duxbury Pt</i>	3	3.16	128.2	1.355
22	Rocky Pt	1	1.06	99.6	0.108
23	Pt Bonita	5	4.79	81.6	0.349
24	Mussel Rock	6	1.19	167.4	0.932
25	Mori Pt	6	0.59	149.1	0.942
26	Rockaway	6	0.84	145.5	0.998
27	<i>Pt San Pedro</i>	1	2.89	97.4	0.467
28	<i>Pillar Pt</i>	3	3.06	125.2	2.087
29	Bolsa Pt	6	2.45	153.6	0.861
30	Pigeon Pt	5	2.59	76.5	1.354
31	Franklin Pt	3	4.11	167.5	1.500
32	Ano Nuevo	1	7.33	110.6	0.783
33	El Jarro Pt	1	2.28	109.2	1.014
34	Pt Santa Cruz	5	2.44	53.4	2.346
35	Cabrillo Pt	6	0.70	143.2	1.270

36	Lovers Pt	6	0.58	155.3	1.143
37	<i>Pt Pinos</i>	6	4.34	147.5	0.965
38	Pt Joe	6	1.49	150.9	0.674
39	Cypress Pt/Pescadero Pt	3	10.20	129.2	1.258
40	Monterey Peninsula	8	33.59	154.4	0.441
41	<i>Pt Lobos</i>	7	13.75	56.1	1.877
42	Yankee Pt	1	3.15	112.9	0.730
43	<i>Castle Pt</i>	1	2.46	105.5	1.220
44	Hurricane Pt	1	3.41	123.9	1.067
45	Pt Sur	3	4.48	137.7	2.061
46	Cooper/Pfeiffer Pt	1	8.37	126.0	0.452
47	Gamboa Pt	5	0.93	72.8	0.838
48	Lopez Pt	6	1.62	171.8	1.386
49	Salmon Cone	6	0.66	138.9	0.766
50	Ragged Pt	3	2.37	128.9	1.406
51	<i>Pt Sierra Nevada</i>	5	1.51	73.8	0.909
52	Pt Piedras Blancas	6	3.86	163.5	0.690
53	San Simeon Pt	1	3.05	100.4	1.227
54	Estero Pt	1	2.49	99.9	1.600
55	Cayucos Pt	1	2.40	107.0	1.225
56	Morro Rock	6	2.27	174.1	0.965
57	<i>Pt Buchon</i>	7	10.51	88.0	0.512
58	Pt San Luis	3	7.70	146.5	2.011
59	Pt Sal	1	6.75	108.2	1.023
60	Purisma Pt	1	1.63	107.7	0.899
61	Pt Penderales	5	2.23	57.6	0.990
62	Pt Arguello	7	13.08	97.7	0.816
63	Pt Conception	5	1.98	74.6	0.637
64	Government Pt	1	2.55	108.0	1.141
65	Coal Oil Pt/Goleta Pt	1	6.82	93.7	1.465
66	Santa Barbara Pt	3	5.16	159.6	2.091
67	Rincon Pt	1	1.88	117.2	1.410
68	Pitas Pt	3	3.29	145.0	1.533
69	Pt Mugu	6	0.63	153.8	1.087
70	Pt Dume	7	15.29	90.4	1.298
71	<i>Palos Verdes Pt</i>	6	1.50	128.8	1.135
72	Pt Vicente	5	0.95	88.0	0.938
73	Long Pt	6	1.80	162.3	1.406
74	<i>Pt Fermin</i>	2	3.00	159.1	3.376
75	Abalone Pt	5	1.43	57.4	0.857

76	<i>Dana Pt</i>	2	1.75	138.0	3.468
77	<i>Pt La Jolla</i>	2	2.71	125.5	3.818
78	<i>Pt Loma</i>	4	5.41	116.6	6.173

2.10 Appendix 2: Making Headland Classes From A Geospatial Mash-Up

2.10.1 A Headland-sized Knowledge Gap

Rocky headlands are prominent coastal morphological features that may focus wave energy, shed eddies, deflect or block alongshore currents and sediment transport, or create down-current retention zones (e.g., Davies et al., 1995; Alaei et al., 2004; Winant, 2006). Presently, we make assumptions about the relationships between sediment flux and sediment reservoirs, which are important when analyzing sand mining in the Bay or beach nourishment on the outer coast. Whereas extensive studies of nearshore physical processes have resulted in a good understanding of alongshore and cross-shore transport at beaches, flow and sediment transport along rocky shores and around headlands remains poorly understood.

Research gaps and societal needs prompted us to explore how headlands affect circulation and transport rates of sediment or biota. Unlike other physical marine features that have existing classification structures (e.g., beaches [Wright and Short, 1984 and Scott et al., 2011], coral reefs [Freeman et al., 2012], and submarine canyons [Harris and Whitney, 2011]), headlands are not systematically categorized. Developing a classification for headlands will open new avenues for research, both in explaining these headland types (e.g., geological framework or rock types) and in determining the effect of different headland types on flow, sediment transport, and associated geomorphology and ecology. This article describes how we used GIS to create a database of headland shape, size, complexity, and nearshore bathymetry to categorize different types of headlands

along the California coast. George et al., 2015, provides a more complete description of our study and findings.

2.10.2 Headlands Along the Ocean, Headlands in the Bay

The planform details of headlands are identifiable from satellite imagery, maps, and geodatabases that include digitized shorelines. Headlands are frequently associated with cliff-backed shorelines, which comprise approximately 80% of the ocean's coasts (Emery and Kuhn, 1982). Inside San Francisco Bay, shown in Figure 2.13, some headlands create dynamic locations for navigation and habitats – e.g., Point San Pablo, Point Richmond, and Coyote Point. Other in-bay headlands are well known to the surfing, kayaking, and sailing communities for their turbulence – e.g., Fort Point at the Golden Gate, Yellow Bluff in Richardson Bay, and Point Blunt on Angel Island.

This study spanned the 1,800-km outer California coast, which comprises a variety of beaches and geological features: approximately 28% pocket beaches, 32% sandy beaches, and 39% rocky shoreline (Scholar and Griggs, 1998). Headlands are associated with all the coastline types with particular prominence in creating pocket beaches and defining rocky shorelines. We identified 78 outer-coast headlands using USGS geological maps, remote-sensing imagery, NOAA navigational charts, and shoreline characterization geospatial databases from the California Coastal Sediment Management Workgroup (CSMW). Several potential entries were excluded for not satisfying these criteria; adjustments to them may increase the number of headlands in the database. For the present, we chose to bypass the Bay to maintain the ocean focus of the study.

We developed the following selection process for headlands: 1) identify a perturbation in the coastline in the remotely-sensed imagery; 2) confirm a named headland in the navigational charts; 3) cross-confirm with similar geology units in the geological maps; and 4) identify similarities in shoreline characterization in the CSMW geospatial database (Figure 2.14). Criterion #2 preferentially selects headlands that are substantial in relative size, with the smallest headland 2 hectares in area. At each headland a baseline was obtained by creating the straight coastline that would exist without that headland.

2.10.3 GIS for Geometry and Bathymetry

From the geospatial database, we extracted several geometric parameters using a variety of ESRI tools and third-party extensions (XTools Pro and ET Geowizards) (Figure 2.15). These parameters quantify the size, symmetry, and complexity of each headland and its relationship to the general trend of the coastline. For some parameters, it was appropriate to take an “upcoast” (‘up’) and a “downcoast” (‘dn’) measurement. A few examples of these parameters include: 1) “perimeter length of a headland” derived by subtracting the baseline length (L) from the overall perimeter of each headland polygon, 2) “apex angle,” defined as the angle of the ocean-facing front of a headland, determined by summing the up and down angles between the cross-headland transect and along-headland transects (α_{up} and α_{dn} , respectively) and 3) “bathymetric slope” described in more detail below. Additional parameters were derived from these measured parameters, including aspect ratio (headland width/length), and rugosity (baseline length/perimeter length).

The underwater expression of a headland was determined by extracting bathymetry from merged topographic and bathymetric digital elevation model (DEM) of the California Seafloor Mapping Program and California Shoreline Mapping Project, a joint study by the California Ocean Protection Council, USGS, and NOAA. This database is enormous – on the scale of 2 terrabytes – with the high-resolution acoustic surveys in LAS v1.2 format and DEM data in ERDAS IMG format (1,500 m x 1,500 m tiles). The full project area includes four production blocks spanning approximately 16,000 km² and 17 counties. NOAA did not generate contours, however, which led us to develop an efficient contouring protocol. We only required data along five transects for each of the 78 headlands, shown in Figure 2.16. Three transects perpendicular to the headland and a shore-normal reference transect on either side of the headland, where the shoreline is approximately straight and aligns with the baseline of the headland. Rather than generate bathymetry contours for the entire dataset, we built three models to cull through the database's 8,040 tiles and generated contours only in the relevant tiles. An abbreviated description of the process is: 1) using a transect, identify relevant DEM tiles; 2) create contours at 0, 5, 10, 15, 20, 25, 30, 40, 50, and 75 m NAVD88 within those tiles; 3) find intersections of the transects with the contours; 4) in the case of multiple intersections (caused by artifacts in the contouring process or offshore linear bars), average the distances to reduce to single intersections for each contour (for alongshore bars and shoals, the first intersection was used); 5) calculate the distance between the shoreline and each contour. Outside of GIS, we derived a suite of ratios and bathymetric slopes from these distances for further analysis in conjunction with the geometric values described earlier.

2.10.4 Conclusion

From merged shoreline and bathymetric headlands parameters, we used cluster analysis to group features in a way that maximizes the difference between the groups and minimizes the difference within a group. Several of the basic parameters (e.g., size, shape, shoreline complexity) suggested clusters, but ultimately three parameters – perimeter length, bathymetric slope ratio, and apex angle – were found to jointly classify the headlands into eight groups. For more details about the cluster analysis and conclusions, see George et al. (2015). A similar approach to classifying headlands inside San Francisco Bay eventually would be possible, because the California Ocean Protection Council, USGS, and NOAA consortium is mapping the bathymetry to the same high resolution as was done on the outer coast through the California Seafloor Mapping Program.

2.10.5 References

- Alaee, M.J., Ivey, G., Pattiaratchi, C., 2004. Secondary circulation induced by flow curvature and Coriolis effects around headlands and islands. *Ocean Dynamics* 54, 27-38.
- California Sediment Management Workgroup Shoreline Characterization Database (<http://www.dbw.ca.gov/csmw/SpatialData.aspx>)
- California Seafloor Mapping Program and California Shoreline Mapping Project (<http://walrus.wr.usgs.gov/mapping/csmp/index.html>)
- Davies, P.A., Dakin, J.M., Falconer, R.A., 1995. Eddy Formation Behind A Coastal Headland. *Journal of Coastal Research* 11, 154-167.
- Emery, K.O., Kuhn, G.G., 1982. Sea Cliffs: Their processes, profiles and classification. *Geological Society of America Bulletin* 93, 644-654.
- Freeman, L.A., Miller, A.J., Norris, R.D., Smith, J.E., 2012. Classification of remote Pacific coral reefs by physical oceanographic environment. *Journal of Geophysical Research-Oceans* 117, C02007, doi:10.1029/2011JC007099.
- George, D.A., Largier, J.L., Storlazzi, C.D., Barnard P.L., 2015. Classification of rocky headlands in California with relevance to littoral cell boundary delineation. *Marine Geology* 369, 137-152.

- Harris, P.T., Whiteway, T., 2011. Global distribution of large submarine canyons: Geomorphic differences between active and passive continental margins. *Marine Geology* 285, 69-86.
- Scholar, D.C., Griggs, G.B, 1998. Pocket Beaches of California: Sediment Transport Along a Rocky Coastline. California's Coastal Natural Hazards. University of Southern California Sea Grant Program.
- Scott, T., Masselink, G., Russell, P., 2011. Morphodynamic characteristics and classification of beaches in England and Wales. *Marine Geology* 286, 1-20.
- Winant, C.D., 2006. Three-dimensional wind-driven coastal circulation past a headland. *Journal of Physical Oceanography* 36, 1430-1438.
- Wright, L.D., Short, A., 1984. Morphodynamic variability of surf zones and beaches - a synthesis. *Marine Geology* 56, 93-118.

2.10.6 Appendix 2 Figures



Figure 2.13. Aerial image of San Francisco Bay region showing flow and sediment transport patterns around selected headlands. The headlands vary in size and shape from Yellow Bluff (flat, small) to Fort Point and Pt. San Pablo (sharp, large). Satellite photograph in natural color from NASA Operational Land Imager (OLI) on Landsat 8 on April 16, 2013 (<http://earthobservatory.nasa.gov/IOTD/view.php?id=81238>).

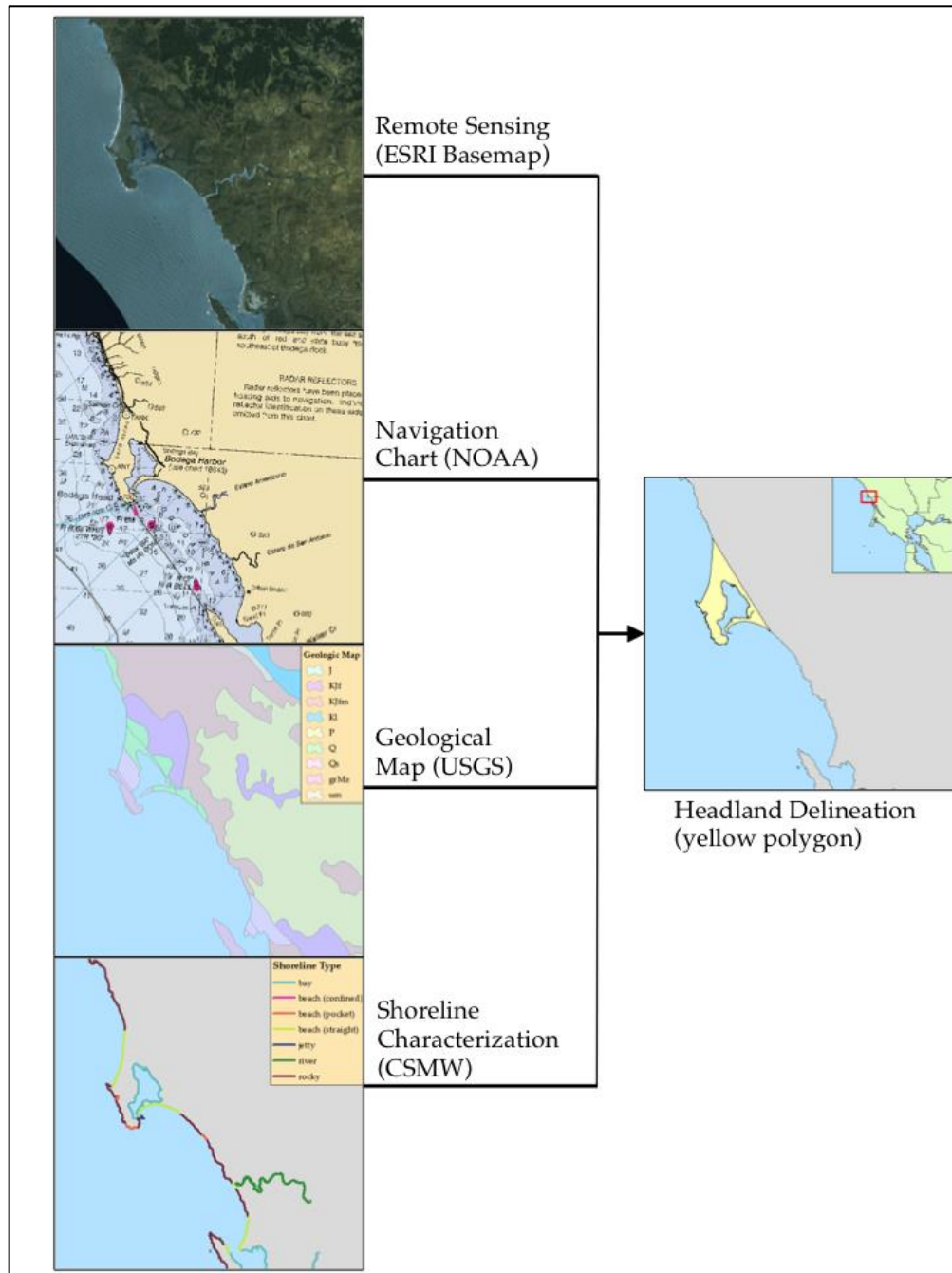


Figure 2.14. Selection process for identifying a headland in ArcGIS using four sources of information, including layers from the National Atmospheric and Oceanic Administration (NOAA), United States Geological Survey (USGS), and the California Sediment Management Workgroup (CSMW). The example is Bodega Head on the Sonoma County coastline north of San Francisco. Using these layers, 78 headlands were selected between Pt. St. George (Crescent City) and Pt. Loma (San Diego). No headlands were identified inside San Francisco Bay because of the outer-coast focus of the study.

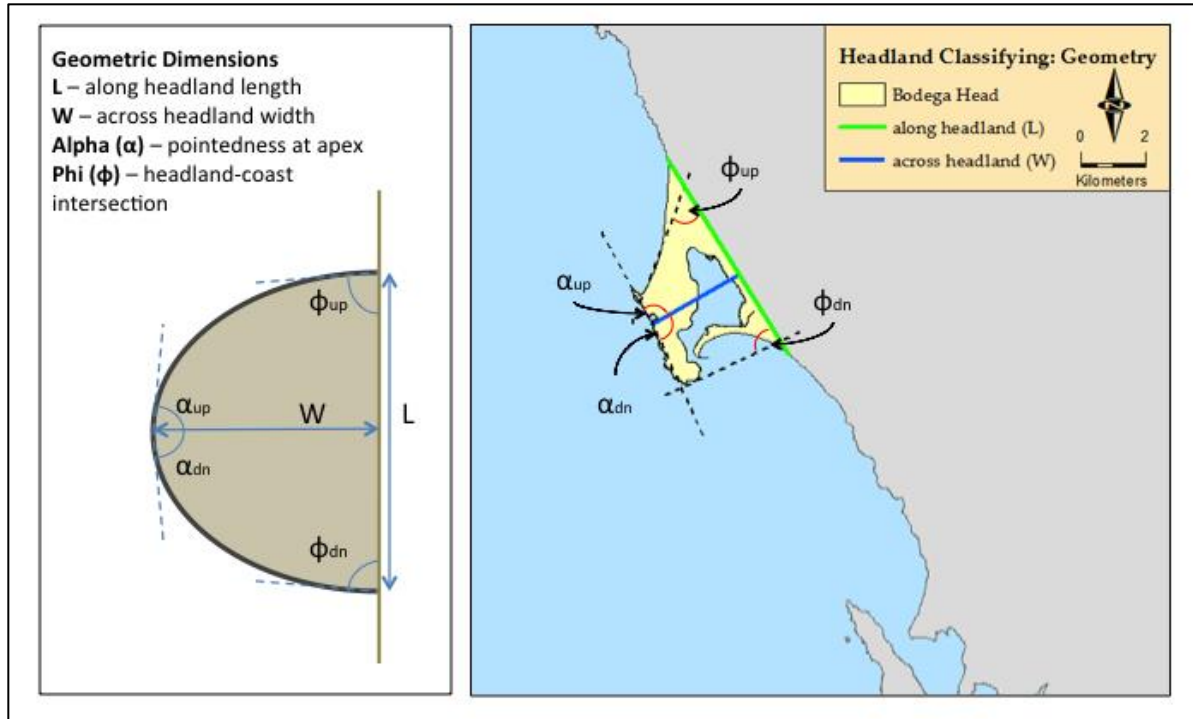


Figure 2.15. Schematic and Bodega Head example of geometric parameters gathered in ArcGIS to generate the database for classification of California headlands. Various tools were used to automate the calculations of length, angles, and size (perimeter and area). The difference between up and down angles emerged as an additional metric of the asymmetry of a headland (ϕ) and the pointedness of the apex angle (α).

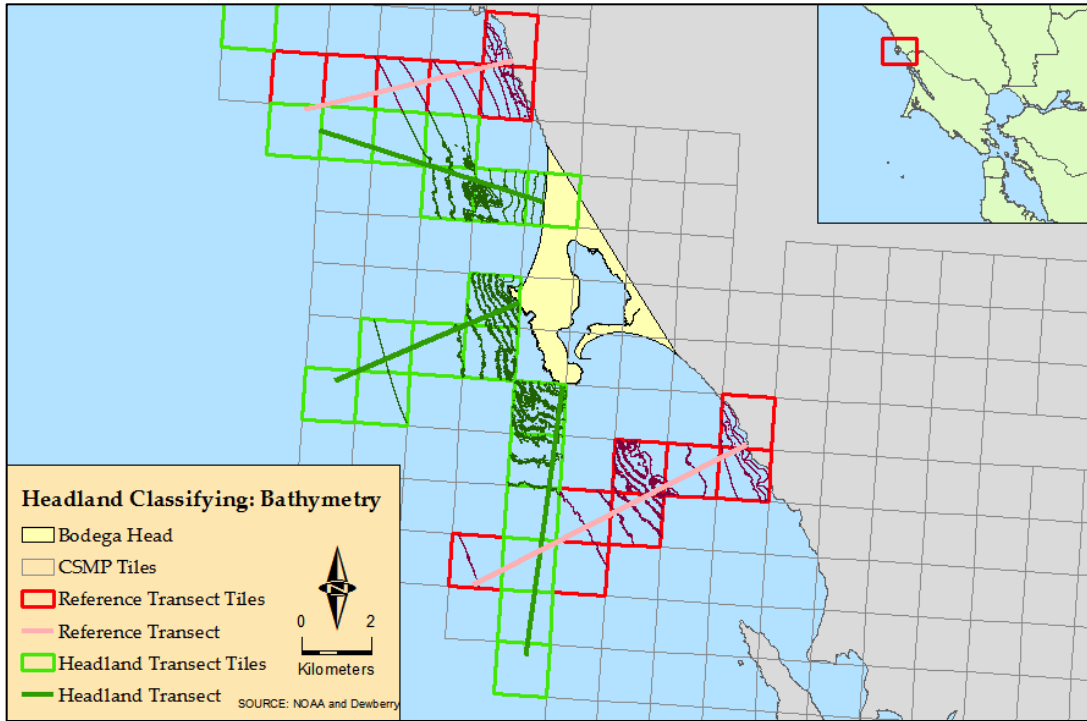


Figure 2.16. Bathymetry extraction at Bodega Head from the merged California Seafloor Mapping Program and California Shoreline Mapping Project database. Distance to specific contour depths was determined by identifying which raster tiles intersected the transects and generating contours prior to distance calculations.

**Chapter 3 – Sediment Flux around Rocky Headlands:
An Example of Sand Transport at Pt. Dume,
California**

3.1 Introduction and Background

Rocky headlands are known to influence coastal flows and alongshore movement of suspended materials. For example, van Rijn (2010) notes that headlands can act as: (1) convergence points for wave energy; (2) obstructions to, or points of convergence for, alongshore tide- and wind-induced currents; (3) protrusions to generate nearshore recirculation zones ; (4) obstructions to littoral drift; (5) fixation points for seaward rip currents promoting offshore transport; and, (6) fixation points for spit formation and shoals originating from headland erosion. In the case of the latter three characteristics, littoral cell boundaries, at least as they have been defined historically, commonly align with headlands where spatially prescribed features of the flow are thought to prevent sediment transport around the point or cape feature (Habel and Armstrong, 1978; Stul et al., 2012; van Rijn, 2010). That said, a conundrum exists regarding whether such boundaries are as effective as discussed by George et al. (2015) and for which particle sizes (Limber et al., 2008).

3.1.1 Hydrodynamics at Headlands

The hydrodynamics associated with headlands are important for characterizing sediment transport, in particular how eddies, wakes, and jets can convey suspended material. Black et al. (2005) listed factors that may influence eddy growth, size, shape, and decay including complexity of coastline and bathymetry, bottom friction, unsteadiness of flow, horizontal tidal excursion, tidal current direction, and horizontal eddy viscosity. Magaldi et al. (2008) identified two key differences between headland wakes and island wakes: the presence of the lateral coastline up/downstream of the

obstacle and the importance of a shallow sloping bottom boundary. The coastline exerts friction on the alongshore flow, therefore increasing the Reynolds number (Verron et al., 1991). In addition, the shelf and potential for nearshore stratification alter fluid dynamics (e.g., potential vorticity, baroclinic instabilities) as well as formation of lee waves (Freeland, 1990; Klinger, 1993; MacCready and Pawlak, 2001). Many studies have opted to examine flow and sediment transport through numerical modeling, although more often in a theoretical sense than location-based. Three such studies examined how different parameters affect flow: aspect ratio of the headland length/width, drag, and far-field tidal flow velocity (Signell and Geyer, 1991); friction, velocity, and geometry (Davies et al., 1995); and, the interaction of wave and current boundary layers and the resulting reduction of current intensity from wave-induced roughness (Guillou and Chapalain, 2011).

Tides and their interaction with geomorphology have received the majority of attention for producing headland flow but this neglects the role of waves and wave-current interactions. Waves cause sediment transport through several mechanisms, such as exhibiting asymmetrical orbital velocities beneath the crest and trough of a breaking wave that entrain sediment and drive it in the onshore direction (Soulsby, 1997). Any sediment that is suspended diffuses through the wave boundary layer and deposits depending on grain size or degree of flocculation for fine sediment. Because wave energy is focused at headlands, longshore transport becomes an important element to determine sediment pathways. Short (1999) illustrated sand bypassing a headland theoretically as a multi-stage process with longshore transport from waves being the driver. As Goodwin et al. (2013) observed, an estimated 80% of longshore transport and headland bypassing

along the New South Wales of Australia occurs in water depths less than 4 m; similar shallow water transport has been suggested in the Santa Barbara region of California based on years of beach profile observations (D. Hoover, USGS, pers. comm.). The lack of attention on waves for alongshore sediment flux provides an opportunity to deepen understanding headland sediment transport pathways.

3.1.2 Conceptual Sediment Transport Pathways

The combination of waves and tidally-driven currents forces sediment flux along a shoreline. As summarized in Soulsby (1997), the phase speed and wavelength of waves are modified by currents to cause wave refraction and the interaction of the wave and current boundary layers enhances the steady and oscillatory components of bed shear stress; other important elements include non-linear interactions between waves and currents. However, these two primary drivers have several possible behaviors when interacting with headlands. Summarizing the findings of the mentioned modeling studies, the four likely current patterns for transport around a headland are (A) flow separates from nearshore; (B) flow separates and forms a headland eddy; (C) flow separates and reattaches downstream of the headland; and (D) flow remains attached (Figure 3.1). Similar possibilities are expected for flow in the opposite direction due to tidal reversal, although the flow is not necessarily symmetrical due to geomorphic asymmetry commonly found in headlands and asymmetry in regional shelf-wide circulation. For wave-driven transport, the flow is related to the dominant wave direction being (E) balanced across the headland or (F) oblique and dominated in one direction. For the flow-specific scenarios, scenario (A) results in export of nearshore sediment offshore as the

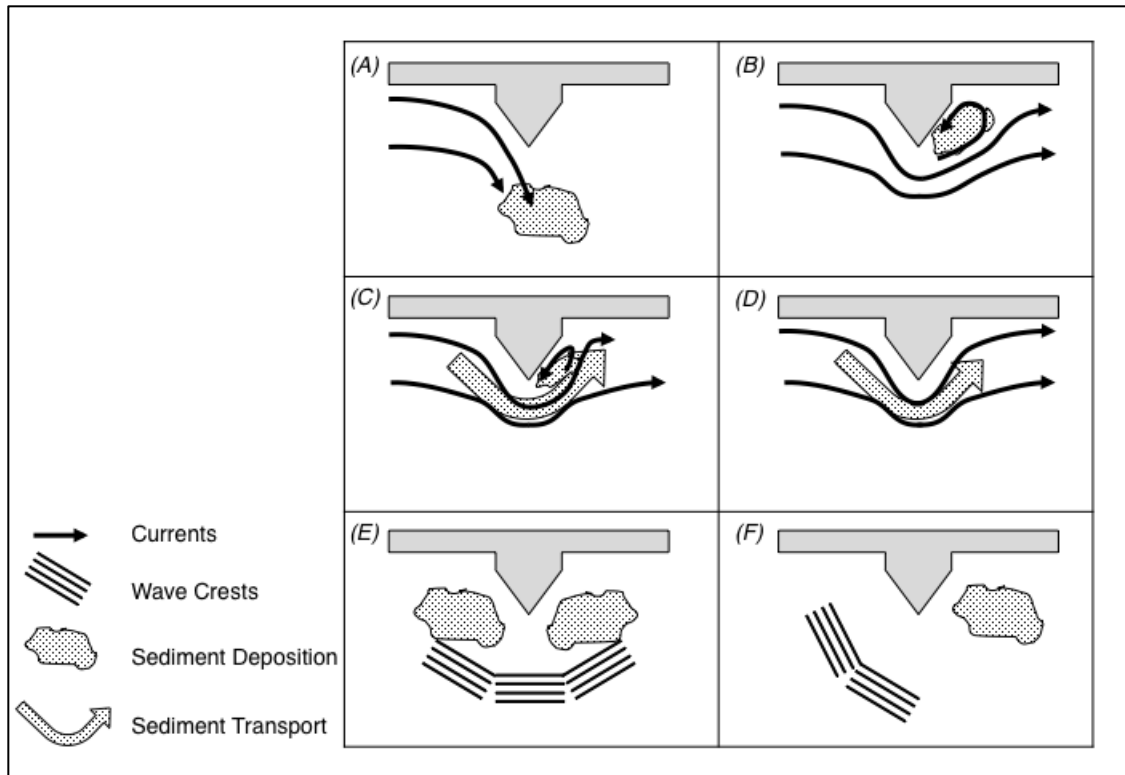


Figure 3.1. Flow and wave-driven transport possibilities around a headland: (A) flow separates from nearshore with export of sediment offshore; (B) flow separates and forms a headland eddy with a downstream deposition zone; (C) flow separates and reattaches downstream of the headland with near-continuous sediment transport and potential for a small deposition zone; (D) flow remains attached with continuous transport past the headland; (E) waves are balanced across the headland with headland adjacent sand banks; and (F) waves are oblique and dominated in one direction that create a downdrift deposition zone.

flow carries suspended loads into deeper waters, scenario (B) creates a large downstream zone which may not receive coarse sediment but in which finer sediment may accrete due to weaker currents in the eddy, scenario (C) generates a near-continuous sediment transport but potential for accretion or deposition in a zone immediately adjacent to the apex of the headland in the eddy, and scenario (D) produces a continuous non-interrupted transport of particles past the headland. For the wave-driven scenarios, scenario (E) results in headland adjacent sand banks by balancing the bed shear stresses on opposing sides of the apex that decrease with distance from shore and the apex (Guillou and Chapalain, 2011), and (F) produces a downdrift accumulation zone where asymmetrical bed shear stresses propel the sediment toward the protected side of the apex that causes suspended loads to deposit. Each of these scenarios will show distinctive flow directions or wave parameters in observational records as detailed in Table 3.1.

3.1.3 Study Motivation

Because of the risks of fieldwork, the circulation at only a few headlands has been investigated specifically to understand sediment transport and those studies have focused on sandbanks rather than alongshore flux. At Portland Bill, U.K., Bastos et al. (2002) found that the “tidal stirring concept” is part of generating and maintaining linear sandbanks associated with a headland. Tidal stirring was first described by Pingree (1978) as tidally-produced residual eddies that are altered by the Coriolis effect, pressure gradient forces and inertia. Bastos et al. (2002) presented conceptual models of bed shear stress in two zones: an inner convergence zone with subsequent transport toward the headland and an outer zone where subsequent transport was away from the headland.

Table 3.1. Concepts for Headland Circulation and Sediment Flux

Scenario	Flow or Wave Characterization	Sediment Response	Observational Criteria
A	Separation and jet	Offshore export	Accelerated flow along one side of headland and at apex in same direction with negligible counter flow on opposite side; convergence zones possible at apex
B	Separation and eddy	Downstream deposition	Flow follows shape of headland from one side and across apex where separation occurs; counter flow along opposite side
C	Separation and reattachment	Near-continuous sediment transport and small downstream deposition zone	Flow follows shape of headland from one side, across apex, and approaches downstream coastline; counter flow immediately adjacent to opposing side
D	Attached	Continuous transport around headland	Flow follows shape of headland from one side, across apex, and along opposite side
E	Balanced	Headland adjacent sandbanks	Wave parameters (H_s , T_p) are similar on opposite sides, θ_{dom} varies due to refraction
F	Oblique and direction dominated	Downdrift deposition	Wave parameters on exposed side are larger (H_s) and longer (T_p), θ_{dom} varies due to refraction

Transient eddies through the tidal phases were observed to exchange sand between a sandbank and offshore around Cape Levillain, Australia (Berthot and Pattiaratchi, 2006a). Even in wave-dominated locations, tidal signals of flow, and consequently potential for transport, are noticeable, such as at Cape Rodney, New Zealand, where the sediment type on the bed coarsens substantially at the apex of the headland compared to the sandbank deposits off-apex (Hume et al., 2000).

Taking the existing knowledge together, the basic assumption is that a combination of longshore and tidal currents moves sediment mobilized by breaking waves at a headland. The research aim of this study was to examine how sediment flux can vary spatially and temporally around a rocky headland on a wave-dominated coastline. The specific research objectives addressed were: (1) to examine potential sediment transport at a rocky headland under different oceanographic and meteorological conditions (e.g., spring and neap tidal cycles and local or basin-wide storm waves); (2) to contrast conditions and resultant transport on opposite sides of the headland; and (3) to assess the likelihood of the headland to be a barrier to transport.

3.2 Study Site

Several criteria were used to select an appropriate field location for a generalized study of sediment flux around a headland. The desired headland needed to be nearly symmetrical to minimize geomorphological influences and imitate the design of theoretical numerical models, have published suspected transport rates from prior work, and preferentially be a sandy system as muddy systems at headlands are not as common globally. Pt. Dume, Malibu, California, satisfied these criteria with the added benefit of

being at the center of a decades-old conundrum about its effectiveness as a barrier within the Santa Monica Littoral Cell.

Pt. Dume is the largest headland inside Santa Monica Bay (Figure 3.2), a sub-bay of the Southern California Bight. The geology and geomorphology of the Pt. Dume headland region is unique with a headland-submarine canyon complex. George et al. (2015) defined the nearly symmetrical triangular-shaped Pt. Dume to be 12 km long (west-east alongshore axis) and 4 km in amplitude (north-south cross-shore axis). The entire headland lies south of the Malibu Coast Fault and is comprised of a mix of Holocene, Pleistocene and Tertiary era rock and alluvial deposits. The apex is predominantly sandstone. The head of Dume Submarine Canyon lies immediately offshore, within 1 km of the headland.

Generally, mean and subtidal circulation in the Bight is poleward, driven by the Southern California Eddy and Southern California Countercurrent, both offshoots of the equatorward flowing California Current System (Hickey, 1992; Noble et al., 2009). Within Santa Monica Bay however, Hickey et al. (2003) describe a clockwise gyre. The shelf in Santa Monica Bay is 30-40 km long with a maximum cross-shelf width of <20 km. Internal tides that transition to tidal bores were documented by Noble et al. (2009) as the near-bed flow travels across the shelf. The Bight and Santa Monica Bay are sheltered from Pacific wave energy out of the northwest by Pt. Conception 160 km west of Pt. Dume; the Channel Islands also block much of the westerly swell. Xu and Noble (2009) described the wave climate inside the Bight as moderate with winter storm waves from the west although long-period ($T_p > 15$ s) swell enters from the south and southwest primarily during summer and autumn. In their analysis of 23 years of hourly buoy data in

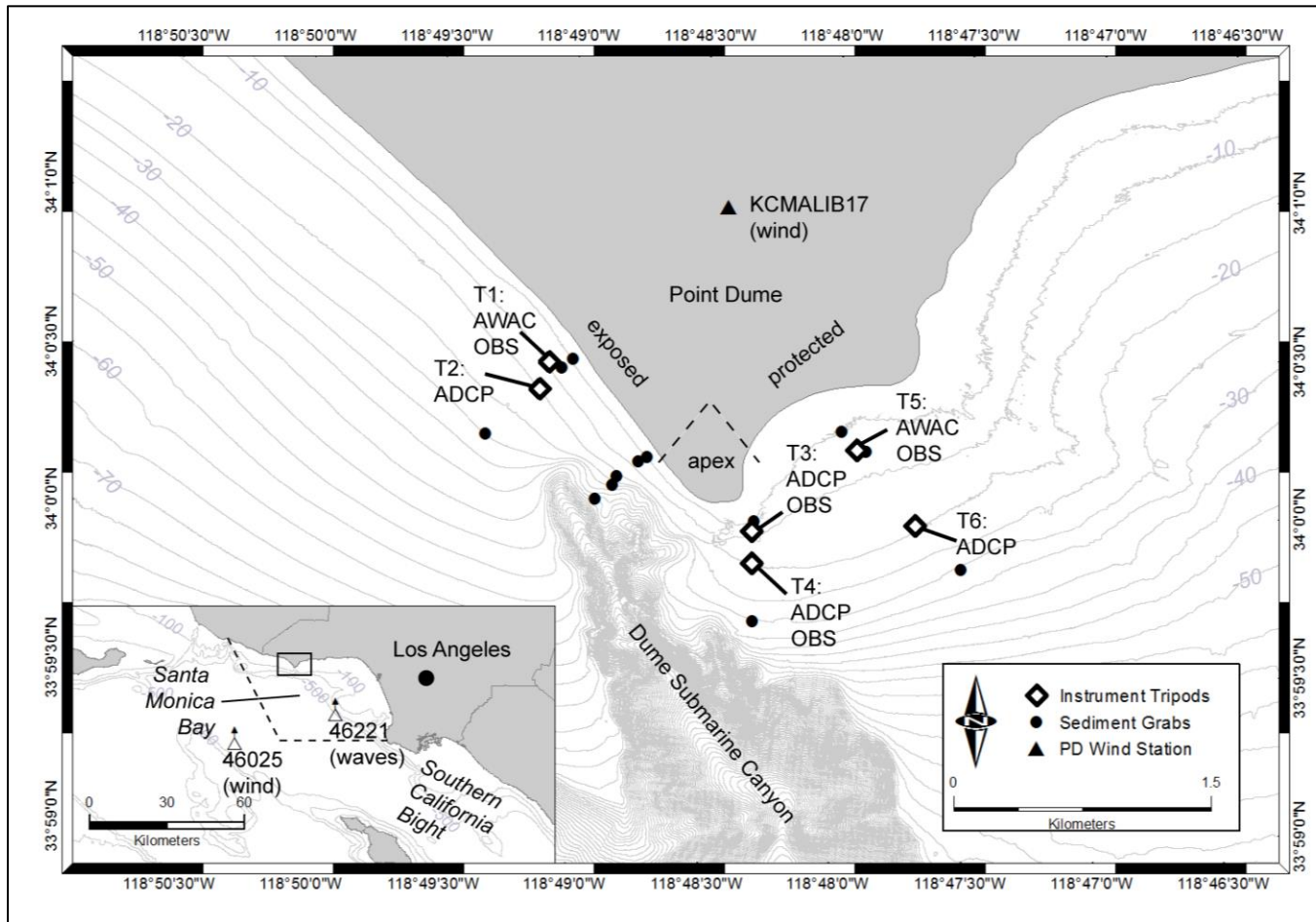


Figure 3.2. Site map of Point Dume, Malibu, California, with instrument tripod and sediment grab locations. Instruments were deployed from 21 September to 6 December 2014. Data from the NDBC buoys (inset) and the Weather Underground weather station (KCMALIB17) were downloaded over the same time frames as the deployment for regional wind and wave conditions. Bathymetry is from NOAA in 5 m contour intervals, with the Dume Submarine Canyon indicated.

the Santa Monica Basin, Xu and Noble (2009) calculated a significant wave height (H_s) mean of 1.3 m and 1.1 m for winter and summer, respectively; the 95th percentile in winter increases to 2.3 m and 1.6 m in the summer. Because of the predominant wave direction, net sand transport has traditionally been hypothesized to be to the east and south along the curving shore of Santa Monica Bay (Leidersdorf et al., 1994).

Santa Monica Bay and its littoral cell periodically receive attention from sediment researchers. Habel and Armstrong (1978) produced the first explicit boundaries of the Santa Monica Littoral Cell terminating at Pt. Dume and the adjacent Dume Submarine Canyon. Leidersdorf et al. (1994) presented a sharp contrast between the narrow unnourished beaches along the northern shore and the heavily altered central and southern shorelines of the bay. A key point in that analysis was the assumption that sediment moved around Pt. Dume in an eastward direction. Patsch and Griggs (2007) estimated a total sand supply of 569,000 m³/yr moving in the system, of which 402,000 m³ (71%) is from beach nourishment actions. They also identified that natural sand supply from rivers and bluffs has been reduced by 13% from dams and coastal armoring projects. This last study also expanded the littoral cell to 91 km in length by extending the boundary to the west, which incorporated Pt. Dume as a subcell within the overall system. Some researchers have attempted to quantify how the point-canyon complex affects alongshore transport of sand, with estimates ranging from 10% to 90% of sediment bypassing the headland and being lost in the canyon (Inman, 1986; Knur and Kim, 1999; Orme, 1991).

3.3 Methods

The observational elements of this study were developed to address the theoretical objectives on a localized scale. The design of the study examined spatial and temporal variability through three questions based on the study objectives: (1) Are there differences in sediment transport under different oceanographic conditions or meteorological conditions? (2) Are there discernable differences in the forcing conditions on either side and across the apex of the headland and if so, are there subsequent differences in sediment transport? (3) If those differences exist, are they substantial enough to disrupt transport around the apex of the headland and cause the headland to be a barrier to littoral drift?

3.3.1 Field Data Collection

The field program sampling design was informed by methods for the study of marine sediment dynamics described by Soulsby (1997), by prior research at headlands in Australia (Berthot and Pattiaratchi, 2006a), the United Kingdom (Bastos et al., 2002) and California (Roughan, Mace, et al., 2005), and by recent work on the “coastal boundary layer” that exists immediately beyond the surf zone (Nickols et al., 2012). Data were collected on the meteorologic and oceanographic forcing and resulting local hydrodynamics (tides, waves, and currents), composition of the bed, and suspended sediment transport. Fieldwork was conducted from the end of summer to the beginning of winter conditions (19 September 2014 – 6 December 2014) to capture a diversity of wave, current, and storm conditions.

3.3.1.1 Instrumentation

The headland was divided into three zones (wave-exposed, apex, and protected) and instrument packages were deployed at six locations along three transects normal to the shoreline (Figure 3.2, Table 3.2) to measure tides, waves, currents, and suspended sediment. Four Teledyne RDI Acoustic Doppler Current Profilers (ADCP) and two Nortek Acoustic Wave And Currents (AWAC) were programmed to measure the three-dimensional components of current velocity (U , V , W , m/s) every 5 min. The AWACs also measured wave parameters of significant wave height (H_s , m), dominant period (T_p , s) and wave direction (θ_{dom}) every 60 min in 5 min bursts. Four Aquatec 210-TY loggers with Seapoint 880- μ m optical backscatter sensors (OBS) were deployed at the three shallow stations and at the deep station at the headland apex; these instruments sampled the level of backscatter return every 5 min in 30 s bursts.

3.3.1.2 Bed Sediment Collection

To characterize the seabed in shallower depths adjacent to instrument locations and closer to the apex of the headland, 17 grab samples were collected during the deployment along four shore-normal transects using a Van Veen sampler (Figure 3.2). Approximately 500 g of sample was collected from each station and bagged for grain size analysis.

3.3.1.3 Additional Data Sources

The Santa Monica Bay NDBC buoy #46221 (Coastal Data Information Program, CDIP station #028) is approximately 23 km southeast of Pt. Dume at a depth of 363 m. Hourly observations of wave height, period, and direction were acquired from 18

Table 3.2. Instrument Datasets

Location	Longitude	Latitude	Depth (m)	Measurements	Instruments
<i>Deployed for Study</i>					
T1	-118.818150	34.00768	8	Currents, waves Turbidity	AWAC (1000 kHz) OBS
T2	-118.818710	34.00624	15	Currents	ADCP (1200 kHz)
T3	-118.805200	33.99892	11	Currents Turbidity	ADCP (1200 kHz) OBS
T4	-118.805154	33.99725	16	Currents Turbidity	ADCP (1200 kHz) OBS
T5	-118.798630	34.00328	10	Currents, waves Turbidity	AWAC (1000 kHz) OBS
T6	-118.794850	33.99937	17	Currents	ADCP (300 kHz)
<i>National Data Buoy Center, NOAA</i>					
B1 (#46221)	-118.633	33.855	363	Waves	Waverider Buoy
B2 (#46025)	-119.053	33.749	5 m above sealevel	Wind	Advance Modular Payload System (AMPS) (1 Hz)
<i>Weather Underground</i>					
PD Wind (KCAMALIB17)	-118.807	34.016	65 m above sealevel	Wind	Davis Vantage Vue

September – 6 December 2014. Wind data were downloaded from the Santa Monica Basin NDBC buoy #46025 (35 km southwest of Pt. Dume at a depth of 935 m) and the closest Weather Underground station on Point Dume, KCAMALIB17; wind speed and direction were acquired over the same time frame although the data were in different resolutions (NDBC buoy – hourly, Weather Underground station – 5 min). Bed sediment grain sizes were extracted from the usSEABED database (Reid et al., 2006) at nine locations in the study area.

3.3.2 Data Processing

The time series of wave, current, and suspended sediment data, and the seafloor sediment samples were processed to determine alongshore flux under different forcing conditions. Specifically, background meteorological and oceanographic conditions were characterized from the waves and currents and specific deviating events (i.e., local storms) identified. The processed data were packaged into inshore and offshore bands based on the spatial array of the instruments, which had been deployed in a design to address the regional variability of hydrodynamics and suspended sediment response. This treatment of the data for space and time was intended to analyze the perturbation of sediment transport around the headland and assess the potential for sediment blocking.

3.3.2.1 Wind and Waves

The terrestrial Pt. Dume wind record required hourly subsampling and interpolation to align with the offshore buoy wind record and other measured parameters (tides, waves, currents, and turbidity). The wave data from the two AWACs (T1 and T5) were initially processed by instrument software to convert raw acoustic returns to time

series of data. The output time series were despiked using a phase-space method with a cubic polynomial to interpolate across removed points (Goring and Nikora, 2002). The cleaned significant wave height (H_s , m) and dominant period (T_p , s) were used to calculate wave power (P , kW/m) according to

$$P = \frac{1}{8} \rho g H_s^2 \sqrt{gh} \quad (3.1)$$

where ρ (kg/m³) is water density, h is water depth (m), and g is gravity (m/s²). The potential velocities for wave-driven longshore currents (V_L , m/s) were calculated using the Larson et al. (2010) method for direct computation of the incipient breaking wave properties of wave height (H_b) and angle (θ_b) and applying them to the USACE (1984) equation

$$V_L = 20.7 m \sqrt{g H_b} \sin(2\theta_b) \quad (3.2)$$

where m is the bed slope. In addition, wave-driven alongshore sediment transport, Q_c (m³/yr), was also possible to be calculated using the CERC equation (USACE, 1984)

$$Q_c = 2.2 \times 10^6 \frac{H_b^{5/2}}{\gamma_b^{1/2}} \sin(2\theta_b) \quad (3.3)$$

where $\gamma_b = H_b/h_b$.

3.3.2.2 Currents

Similar to the wave data, current data from the ADCPs (T2-T4 and T6) and AWACs (T1 and T5) were processed initially with instrument software to convert raw acoustic returns to time series of data. The data were then rotated to true north and subsampled to obtain hourly data using a cubic spline function. The near-surface bins were removed by applying an echo intensity threshold of 60%, determined through an iterative process (M. Robart, BML, pers. comm.), below which data quality degraded due

to bubbles and side-lobe reflection off the air-water interface. The bottom bin that corresponded to 1 meter above the bed (mab) was isolated as the near-bottom layer. The thickness of the near-bottom layer varied between 0.25 m (T2, T3, T4, T6) and 0.5 m (T1, T5). Following the guidance of Emery and Thomson (2001), the data were filtered at frequencies of 6 hr (0.1667 cph) and 33 hr (0.0303 cph) to separate subtidal (low-passed), tidal/diurnal (band-passed) and high-frequency variability. Alongshore and cross-shore directions were determined based on the bathymetric contours and shoreline orientation: positive alongshore velocity was oriented 130° at T1 and T2, 90° at T3 and T4 and 60° at T5 and T6 (and positive cross-shore velocities at 40°, 0°, and -30°, respectively).

3.3.2.3 *Bed Shear Stress*

The total shear stress (τ_{total} , N/m²) on the bed is a non-linear combination of wave-derived shear stress (τ_w , N/m²) and current-derived shear stress (τ_{cur} , N/m²). Total shear stress could only be calculated at stations T1 and T5 where wave data were collected in addition to currents. A routine following Madsen (1994) was used to calculate all three shear stresses that utilized time series of current velocity (U , m/s) and direction (θ_c , rad), a reference height for U (z_0 , m), H_s , T_p , wave direction (θ_w , rad), h , temperature (T , °C), salinity (S , psu), seabed mean sediment grain size (D_{50} , m), and seabed sediment grain density (ρ_{sed} , kg/m³). The process determines bed roughness (assuming a Nikuradse roughness of two times D_{50}), the angle between θ_c and θ_w , near-bottom orbital velocity, and angular wave frequency to calculate the friction velocity for currents, waves, and combined waves-currents. Shear stresses were then calculated by multiplying friction velocity by the density of the seawater for a final output of τ .

3.3.2.4 *Bed Sediment*

Sediment samples were washed twice with distilled water and then dried for 48 hr at 30°C. Grain size analyses were conducted using photogrammetric methods developed by Buscombe et al. (2010), where multiple images of the dried sediment are processed with Matlab algorithms. This technique has been employed successfully (through high significant correlations with sieving methods) for coastal environments in California and the United Kingdom (Buscombe et al., 2014), Portugal (Baptista et al., 2012) and New Zealand (Pentney and Dickson, 2012). Five photographs were taken for each sample with the sediment stirred between pictures because grain size can vary within a single sample. Sediment grain size statistics generated by the algorithm (mean, standard deviation, as well as the 5th, 16th, 25th, 75th, 84th, 90th, and 95th percentiles) for the five photographs were averaged to produce a distribution at each station.

3.3.2.5 *Turbidity and Flux*

The OBS data (T1, T3, T4, and T5) were downloaded and despiked following the same methods as for the wave records to remove obvious erroneous data points. Gaps from the despiking were filled using a cubic spline and the cleaned time series were subsampled to hourly averages to align with the wave and current data. The data at T3 were unusable due to biofouling on the optical window within a week of deployment. To develop turbidity measurements to T2 (where no OBS instrument was deployed) and T3 data from T4 was manipulated using the method detailed by Deines (1999) as both ADCPs had the same frequency as T4. This is a two-step process that first calculates relative backscatter, S_v , to correct the acoustic backscatter data for signal spreading with

distance from the transducers and for absorption by the water and then develops a regression relationship to the optical backscatter data to apply to other locations. Successful examples of this method include Holdaway et al. (1999), Thorne et al. (1991), and Storlazzi and Jaffe (2008). The regression at T4 had an $R^2=0.30$, which is considered acceptable for this method although not a particularly robust correlation. Acoustic suspended sediment concentration (SSC) was estimated at T2 and T3 using the T4 regression relationship; acoustic SSC was calculated at T1 and T5 using the OBS and backscatter measurements at those stations. No turbidity or acoustic SSC time series are available at T6 because no OBS was deployed at this station and the ADCP used a different frequency than the other moorings. Total cumulative suspended sediment flux consisting of both along and cross-shore components (\overline{SSF}_{total}) was calculated by combining instantaneous flow velocities and acoustic SSC values in the following process:

$$\overline{SSF}_{total} = \sum_{t=1}^{1,771} \left(\overline{Acoustic\ SSC} \times \overline{Flow}_{along} + \overline{Acoustic\ SSC} \times \overline{Flow}_{cross} \right) \quad (3.4)$$

3.3.3 Data Analysis

Several analyses were designed to best utilize the data for addressing the research questions. To analyze for differences in sediment transport under different oceanographic conditions or meteorological conditions, events were isolated in the hydrodynamic (waves and tide) records and the subsequent sediment flux tallied at the inshore and offshore stations. Dividing the sediment volume by the duration normalized the relative impact of each event for a per day sediment transport rate. To determine if there were

differences on either side and across the apex of the headland, the flow directions and sediment flux at the inshore and offshore stations within the three geographic regions (exposed, apex, protected) were characterized by percent of time of alongshore currents and by sediment flux. Regional patterns of flow and transport were then used to assess which scenario or scenarios describe the sediment pathways according to the criteria presented in Section 1. The final analysis used the sediment pathways qualitatively to assess if the headland is a barrier to littoral drift.

3.4 Results

3.4.1 Tide and Wave Event Determination

Regional average wave conditions over the collection period were $H_s = 1.03 \text{ m} \pm 0.31$, $T_p = 12.0 \text{ s} \pm 2.8$, and $\theta_w = 244^\circ \pm 30$ with wind speed of $3.26 \text{ m/s} \pm 1.99$ and direction of $226^\circ \pm 92$; the largest tidal range through the semi-diurnal mixed tide cycle was 2.21 m (Table 3.3). Specific time periods were identified to investigate sediment transport under different physical forcings (Figure 3.3). In addition to the data collected, storm analysis reports from NOAA were used to isolate five distinct segments of time: spring tides, neap tides, a hurricane swell event in early October from Hurricane Simon, a large swell event associated with a distant North Pacific Aleutian low pressure system in late October, and a winter storm in late November (Table 3.3). The tidal segments were picked from periods of extremely low wave activity in early November to minimize the influence of waves on flow and sediment transport. Hurricane Simon was a category 4 hurricane that officially lasted 1-7 October 2014 off the west coast of Mexico eventually

Table 3.3. Events During Deployment

Event	Start (2014, local time)	End (2014, local time)	Duration (d)	H_s^1 (m)	T_p^1 (s)	θ_{dom}^1 (°)	Tidal Range ² (m)	Wind Speed ³ (m/s)	Wind Direction ³ (°)
Full Record	9/21, 0:00	12/3, 18:00	73.75	1.03±0.31/2.23	12.0±2.8/20.0	244±30/338	2.21	3.26±1.99/12.3	226±92/-
Spring Tides	11/5, 17:00	11/8, 17:00	3.00	0.66±0.09/0.91	13.0±2.3/20.0	234±30/289	2.21	3.07±1.46/6.2	267±103/-
Neap Tides	11/11, 9:00	11/14, 9:00	3.00	0.77±0.08/1.02	13.0±1.5/16.7	252±11/282	1.38	2.81±1.51/7.2	260±45/-
Hurricane Simon	10/7, 10:00	10/9, 2:00	1.67	1.14±0.17/1.53	12.0±2.1/16.7	172±20/209	2.05	2.00±1.16/4.0	200±100/-
Winter Storm	11/20, 0:00	11/22, 0:00	3.00	1.54±0.23/2.23	11.1±2.1/14.3	266±6/282	2.16	4.53±2.03/8.9	249±99/-
Aleutian Low	10/25, 12:00	10/29, 0:00	3.50	1.28±0.26/1.86	11.8±2.1/15.4	253±30/285	1.88	3.10±2.18/8.6	250±62/-

1 – Mean ±1 Std. Dev /Maximum at Station B1

2 – Range at Station T2

3 – Mean/Maximum at Station B2

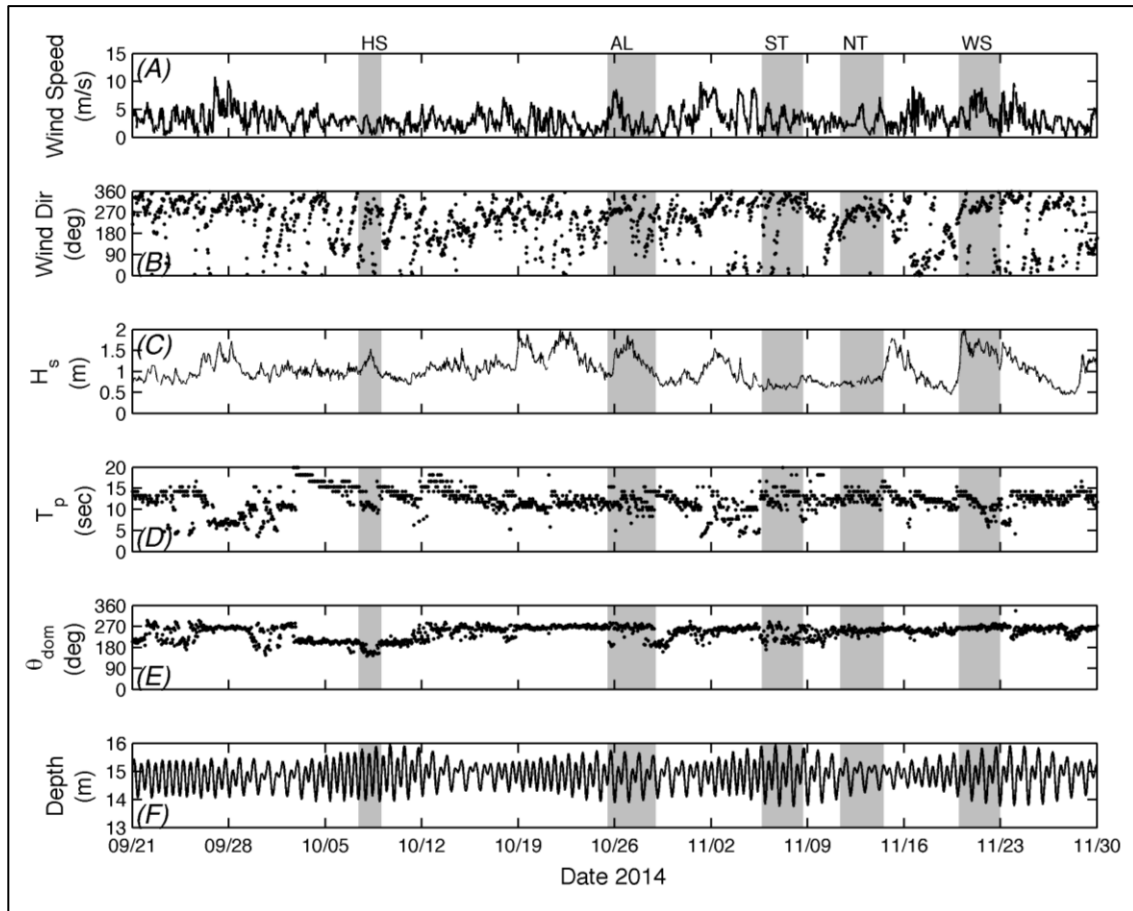


Figure 3.3. Regional conditions during the deployment of the instruments for wind speed and direction at B2 (A, B), wave height, period, and direction at B1 (C, D, E), and tide at T2 (F). Specific events are noted (Hurricane Simon – HS, Aleutian low – AL, spring tide – ST, neap tide – NT, and winter storm – WS). The hurricane is identified by the change in wave direction to mostly south and the increase in wave height. The Aleutian low event and winter storm are mostly evident in the wave height and wind speed. The tidal events were selected when wave height was the smallest of the record.

making landfall as a tropical storm in Baja California Sur, Mexico (Stewart, 2014). Waves from the south began arriving in the southern California region 2 October and lasted for approximately eight days, although the largest waves lasted for less than two days. For the Aleutian low event, NOAA charts from the Pacific Wind Wave Analysis (wave height contours and select surface winds) and Pacific Surface Analysis Preliminary (high and low pressure areas identified from sea level pressure, winds, and other variables, <http://nomads.ncdc.noaa.gov/ncep/charts>) showed a large low pressure system with sea level atmospheric pressure of 985 mb and H_s of more than 8 m off the California coast on 24 October. The waves struck Santa Monica Bay from the west on 25 October and lasted slightly more than three days. The same NOAA charts showed a series of winter storms arriving in southern California in late November that caused approximately six days of enhanced wave activity from the west, although only the first three days were selected to isolate the first storm for analysis.

3.4.2 Wind

The wind magnitude and direction at the two wind stations reflect their offshore (B2) and coastal (PD Wind) positions. B2 was more dynamic with velocities exceeding 4 m/s and few occurrences of no wind (Table 3.3). This contrasts with PD Wind, which showed daily cycles of increased afternoon wind that rapidly builds to 2-4 m/s but then ceased in the evenings. The diurnal wind frequencies at both stations showed the cyclical sea-breeze pattern of onshore-offshore winds common in coastal environments. The fastest and most sustained velocities at both stations occurred during the winter storm, exceeding 5 m/s at B2 and 2.5 m/s at PD Wind. Even though wind blew from all

directions for the duration of the study period, the principal axis of the diurnal winds showed B2 is dominated from the west and PD Wind is along a southwest-northeast alignment.

3.4.3 Wave Climate

The wave climate was characterized by H_s , T_p , θ_w , and P from the Santa Monica Bay buoy (B1) and the two AWACs located on the exposed (T1) and protected (T5) sides of the headland (Table 3.4). Wave activity was largest at the buoy where H_s exceeded 2 m and T_p reached 20 s while the lowest overall wave activity was recorded at the protected side of the headland. The wave direction was fairly consistent by station with the buoy mostly from the west, the exposed side from the southwest, and the protected side from south-southwest. During Hurricane Simon, waves at the buoy came from the south and south-southeast, making this event the most noticeable deviation from typical conditions. Wave period lengthened to 15-20 s during the first part of the hurricane and there were two discernable peaks in wave height that can be associated with wave direction. The larger of the peaks occurred approximately three-quarters through the event when waves came from the south-southeast. During the Aleutian low event, wave height increased noticeably with accompanying increases in wave period for all stations. A similar pattern was observed during the winter storm with some of the largest wave heights of the record measured at all three stations (Figure 3.3 and Figure 3.8).

The majority of wave power, P , at the buoy originated from the west and exceeded 2×10^4 W/m approximately 10% of the time (Figure 3.4). A small event of low P ($< 2 \times 10^4$ W/m) came from mostly the southwest during Hurricane Simon with

Table 3.4. Wave Observations and Longshore Current Calculation

Station	Parameter	Range	Mean \pm 1 Std. Dev
B1	H_s (m)	0.44-2.23	1.03 \pm 0.31
	T_p (s)	3.12-20.00	12.00 \pm 2.8
	θ_{dom} ($^\circ$)	72 $^\circ$ -338 $^\circ$	244 $^\circ$ \pm 30
	P ($\times 10^4$ W/m)	0.18-6.96	1.33 \pm 8.3
T1	H_s (m)	0.41-1.65	0.84 \pm 0.22
	T_p (s)	4.02-17.83	12.74 \pm 2.40
	θ_{dom} ($^\circ$)	175 $^\circ$ -257 $^\circ$	222 $^\circ$ \pm 14
	P ($\times 10^4$ W/m)	0.19-3.03	0.85 \pm 0.45
	V_L (m/s)		1.90
T5	H_s (m)	0.27-1.87	0.62 \pm 0.18
	T_p (s)	5.00-18.40	13.32 \pm 1.69
	θ_{dom} ($^\circ$)	146 $^\circ$ -220 $^\circ$	198 $^\circ$ \pm 9.0
	P ($\times 10^4$ W/m)	0.09-4.35	0.53 \pm 0.37
	V_L (m/s)		0.73

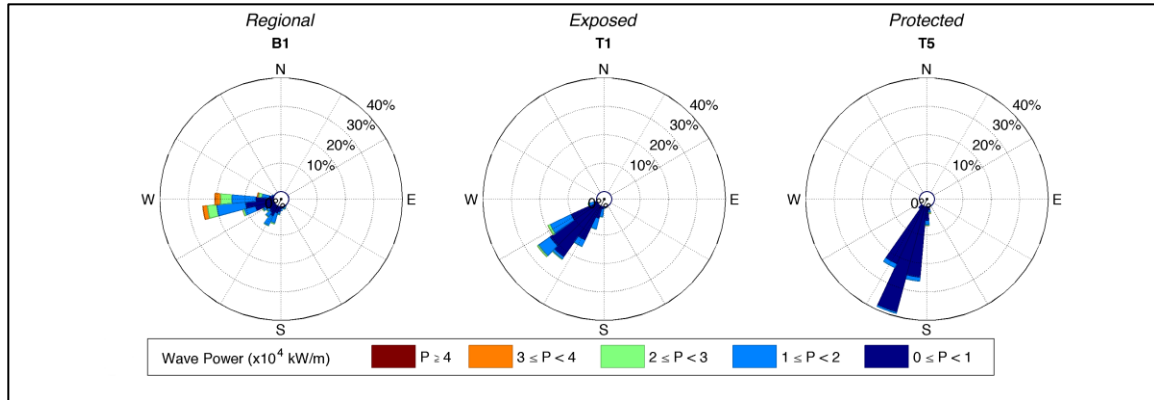


Figure 3.4. Hourly wave power for the 74 days of the study. Data for B1 (regional) were downloaded from NOAA online sources; data at T1 (exposed) and T5 (protected) were from deployed AWACs. Wave power is largest at B1 and comes primarily from the west. Closer to land, wave power at T1 is larger with more of a southwest origin than T5.

approximately one day of energy originating from the south-southeast towards the end of hurricane swell. Wave power at the buoy peaked during the winter storm at more than 6×10^4 W/m. On the exposed side of the headland, P was contained in the southwest sector and did not exceed 3×10^4 W/m. The largest peak occurred during the Aleutian low with observable increases during the hurricane and winter storm (Figure 3.8a). The protected side of the headland showed the smallest amount of P , never exceeding 2×10^4 W/m and contained entirely in the south-southwest sector. The wave events produced less pronounced deviations in P from typical conditions on the protected side with one exception. During the hurricane, P spiked briefly for less than a day coincident with a shift swell direction to south-southeast at the buoy (Figure 3.8b).

The calculated potential velocity for wave-driven longshore currents (V_L) showed the large difference between the exposed and protected sides of the headland. On the exposed side, $V_L = 1.90$ m/s and on the protected side, $V_L = 0.73$ m/s. An important note about these velocities is that they were not recorded but rather provide a guide of what could occur given the variation in wave conditions on either side of the headland.

3.4.4 Near-bottom Currents

The currents 1 mab at the six stations over the duration of the deployment show markedly different patterns if the data came from the exposed, apex, or protected transects and inshore or offshore moorings. The mean and maximum speeds, and mean vector directions for near-bottom currents are shown in Table 3.5. Current roses for the full record at each station show that the exposed transect moorings (T1 and T2) flowed almost exclusively to the southeast, the inshore protected mooring (T5) flowed

Table 3.5. Near-bottom Current Velocities and Turbidity

Station	Currents			Acoustic SSC (kg/m ³)	
	Parameter	Mean ±1 Std. Dev	Maximum ¹	Range	Mean ±1 Std. Dev
T1	Speed (m/s)	0.08±0.05	0.32	3.76-5.81	4.60±0.26
	Direction (°) ²	174°±83	-		
T2	Speed (m/s)	0.07±0.04	0.29	0-1.39	0.66±0.24
	Direction (°)	184°±83	-		
T3	Speed (m/s)	0.13±0.09	0.65	0-2.55	1.13±0.41
	Direction (°)	153°±81	-		
T4	Speed (m/s)	0.13±0.09	0.66	0-2.48	0.96±0.39
	Direction (°)	205°±83	-		
T5	Speed (m/s)	0.08±0.04	0.26	1.99-3.95	3.11±0.26
	Direction (°)	194°±67	-		
T6	Speed (m/s)	0.13±0.08	0.57	-	-
	Direction (°)	176°±96	-		

1 – Current direction showed all 360°

2 – Current flowing towards

exclusively to the southwest and the offshore protected mooring (T6) on a north-south axis, with most of the flow to the south (Figure 3.5). The off-apex transects showed dominant flow toward the apex with the inshore stations more clearly demonstrating this pattern than the offshore moorings. The flow patterns on the apex transect were bi-modal with eastward and southwestward modes inshore (T3) and westward and southeastward modes offshore (T4). The fastest speeds occurred along the apex transect moorings, exceeding 0.2 m/s approximately 20% of the time.

The unfiltered alongshore and cross-shore velocities displayed a complicated near-bottom circulation pattern around the headland. The exposed inshore (T1) and protected inshore (T5) stations flowed toward the apex with the velocities on the exposed side consistently faster (Figure 3.6). The exposed offshore (T2) was coupled with the inshore station on the same transect but the same is not true on the protected transect – the offshore station was substantially faster than the inshore one and showed a strong cross-shore flow. When the occurrence of the flow by direction was tallied, the dominant apexward flow was confirmed as the exposed side stations showed 74-76% toward the point and the protected stations showed 64-79% (Table 3.6). Flow across the apex was more balanced in either direction although the inshore station showed more inward flow (43%) than the offshore station (43%).

3.4.5 Sediment: Bed Distribution and Suspension

The overall bed sediment distribution was coarse sand to the west of the point and in shallow water depths with fining to the east and towards deeper water (Figure 3.7). Sediment grain size immediately around the headland was sand-dominated, even at the

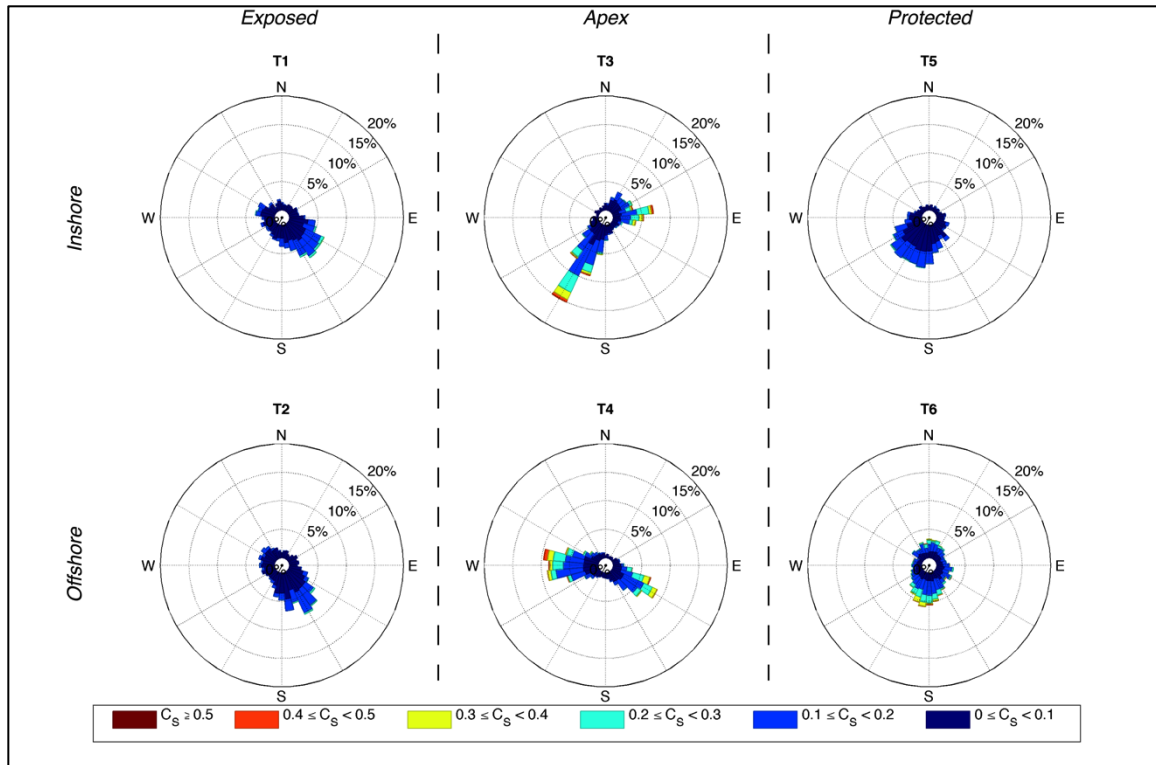


Figure 3.5. Hourly unfiltered near-bottom current velocities from the deployed current meters (ADCPs at T2, T3, T4, and T6; AWACs at T1 and T5). Dominant flow on the exposed side (T1 and T2) is to the southeast and on the protected side (T5) to the southwest and south (T6). Flow is fastest and switches direction across the apex (T3 and T4).

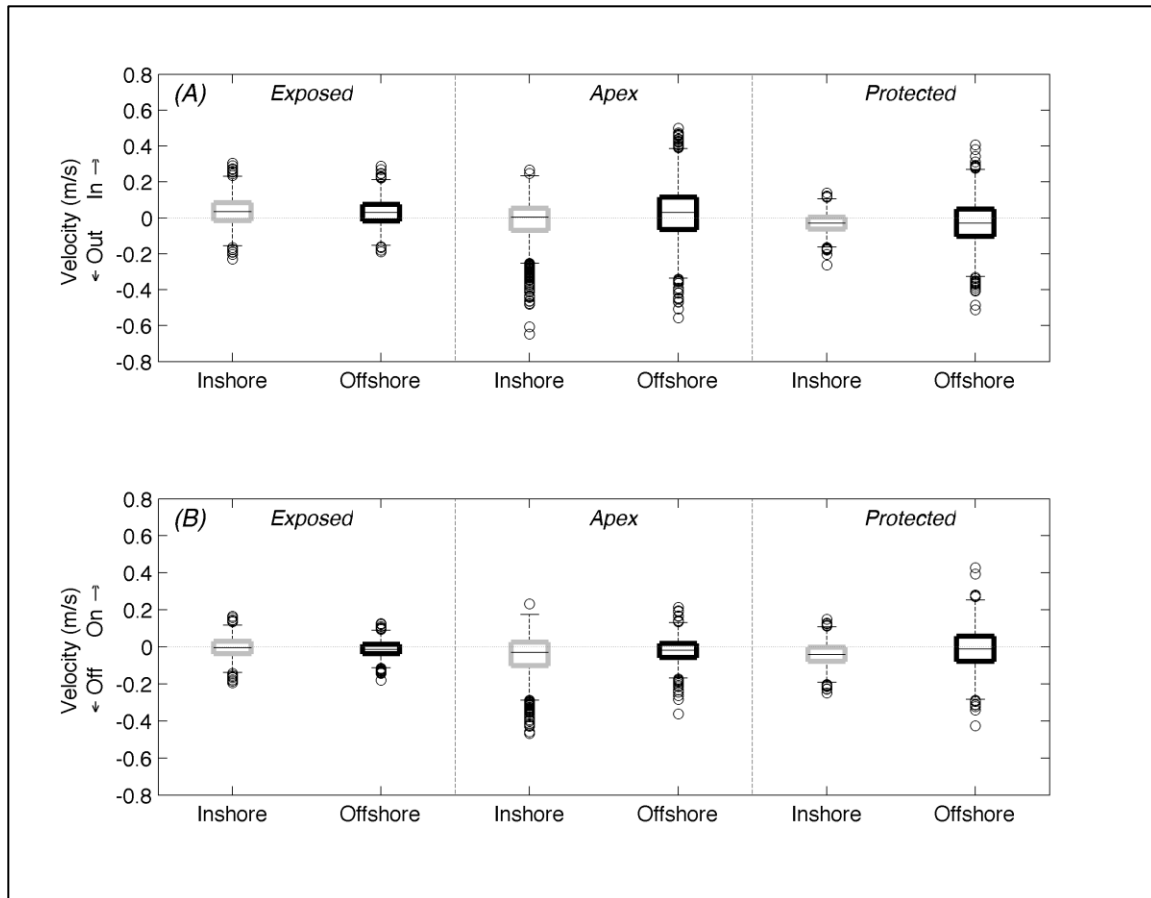


Figure 3.6. Alongshore (A) and cross-shore (B) current velocities for the current meters divided into exposed, apex, and protected transects and by inshore (gray boxes) and offshore (black boxes) stations. On each box, the black line is the median, the edges of the box are the 25th and 75th percentiles, the whiskers extend to the most extreme data points not considered outliers, and outliers are plotted individually as circles.

Table 3.6. Alongshore and Cross-shore Current Occurrence

Station	Alongshore Occurrence (%) ¹		Cross-shore Occurrence (%) ²	
	In	Out	Onshore	Offshore
T1	74	26	67	33
T2	76	24	62	38
T3	53	47	42	58
T4	43	57	48	52
T5	21	79	80	20
T6	36	64	67	33

1 – In and Out defined as crossing the apex into or out of Santa Monica Bay

2 – Onshore and Offshore defined as shoreward or oceanward flow direction

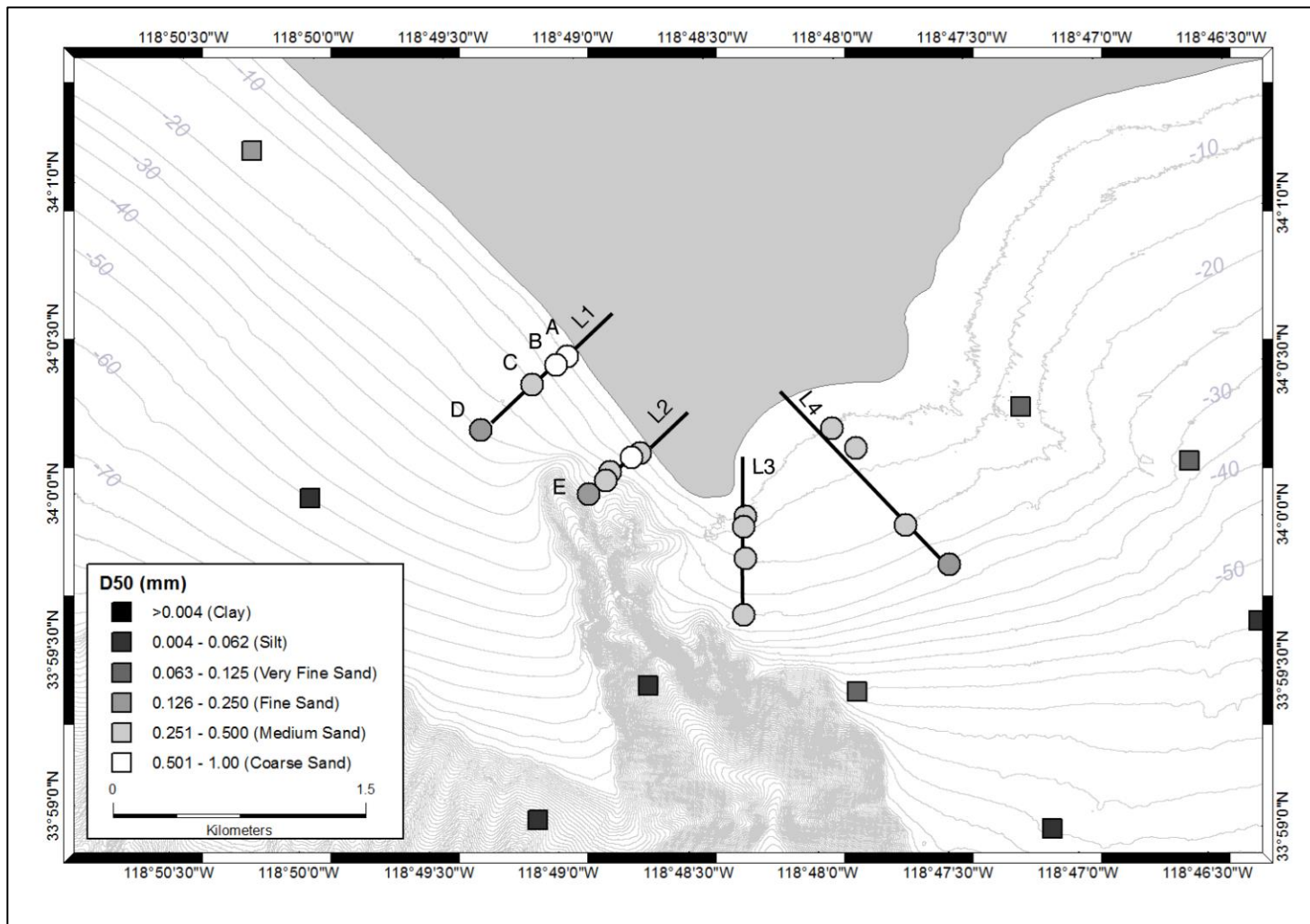


Figure 3.7. Surface sediment grain size, D_{50} , from this study (circles along 'L' transects) and the usSEABED database (squares).

station located in the head of Dume Canyon (Table 3.7). Around the apex, D_{50} ranged from 0.196-0.572 mm with spatial patterns in the cross-shore and east-west directions. Three of the four shallow (5 and 8 m) stations on the exposed side of the headland were coarse sand with $D_{50} > 0.500$ mm (L1A, L1B, and L2B). This contrasted with the medium sand at the equivalent depths on the protected side and at the apex (L3A, L3B, L4A, and L4B). Sediment farther offshore and in the canyon became considerably finer to muddy sand or sandy mud. Below 15 m, grain size was finer across all transects as a shift to medium sand occurred on the exposed side. On transects L1 and L4 (the two farthest from the apex) at 25 m, the bed sediment decreased in size to fine sand with $D_{50} < 0.250$ mm. The finest sample of the 17 grabs was in the head of the canyon with $D_{50} = 0.196 \pm 0.01$ mm. The usSEABED samples farther from the headland that are deeper and to the east show $D_{50} < 0.125$ mm or finer (Reid et al., 2006).

At the off-apex inshore sites, the amount of wave-driven shear stress dominated over that due to currents. The stronger connection between τ_{total} and the waves became apparent when tripling of τ_{total} was observed during the hurricane, Aleutian low and winter storm events compared to low wave periods on the exposed side, regardless of alongshore current velocities (Figure 3.8a). This same station experienced consistently larger τ_{total} than on the protected side even though the current velocities were comparable between the stations. Underwater video of the seafloor taken during deployment and recovery of the instruments on the exposed side confirmed that the bed is in near constant motion from surface waves even during the low wave energy periods that allowed diving. The largest spike in τ_{total} on the protected side occurred during the hurricane when wave direction shifted temporarily to impact the coastline directly without much refraction

Table 3.7. Surface Sediment Grabs

Station	Longitude (°W)	Latitude (°N)	Depth (m)	$D_{50} \pm 1$ Std. Dev (mm)
L1A	-118.81666	34.00783	5	0.512±0.050
L1B (T1)	-118.81735	34.00736	8	0.572±0.056
L1C (T2)	-118.81886	34.00628	15	0.383±0.013
L1D	-118.82215	34.00383	25	0.244±0.025
L2A	-118.81189	34.00275	5	0.443±0.028
L2B	-118.81243	34.00249	8	0.507±0.030
L2C	-118.81378	34.00171	18	0.378±0.016
L2D	-118.81405	34.00122	26	0.294±0.010
L2E	-118.81515	34.00049	45	0.196±0.005
L3A	-118.80506	33.99945	7	0.449±0.018
L3B (T3)	-118.80512	33.99890	11	0.379±0.012
L3C (T4)	-118.80501	33.99719	16	0.326±0.039
L3D	-118.80502	33.99416	25	0.299±0.041
L4A	-118.79958	34.00423	5	0.319±0.021
L4B (T5)	-118.79802	34.00320	10	0.290±0.006
L4C (T6)	-118.79476	33.99914	17	0.288±0.014
L4D	-118.79193	33.99705	26	0.232±0.015

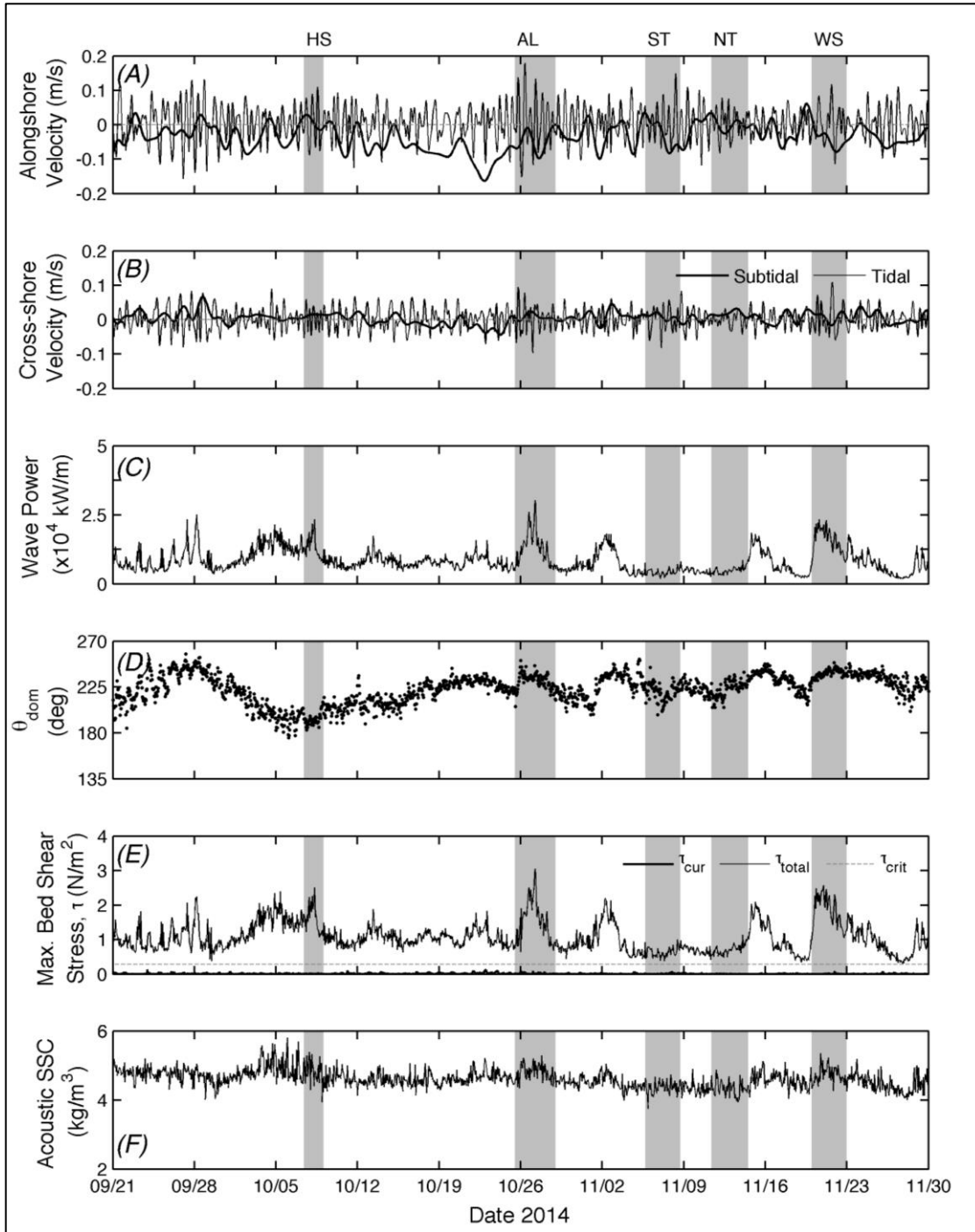


Figure 3.8a. Near-bottom alongshore (A) and cross-shore currents (B), wave power (C) and direction (D), maximum bed shear stress (τ_{total} , E), and acoustic SSC (F) at the inshore exposed station (T1). See Figure 3.3 for event identifications. For τ_{total} , current- (τ_{cur}) and wave-driven (τ_w) shear stress are combined with the threshold of motion (τ_{crit}) indicated as the dashed line for the specific grain size collected on the bed at each station.

(Figure 3.8b). The other large wave events caused less pronounced increases in τ_{total} on the protected side. In terms of potential sediment suspension, τ_{total} remained above the threshold of motion as determined for the grain sizes collected from the bed at both inshore stations.

The hourly fluctuations throughout the acoustic SSC time series were expected from the dissipation of wave energy in the surf zone. The shear stresses and different D_{50} caused distinctive responses at the off-apex inshore sites. The lower bound of acoustic SSC on the exposed side was close to the upper bound on the protected side (Table 3.5). The time series on the exposed side showed clearer increases in SSC associated with large wave events than on the protected side (Figure 3.8a, b). Spatially around the headland, acoustic SSC showed higher values at the inshore stations than offshore and lowest overall at the apex (Figure 3.10). The inshore exposed station showed the highest turbidity among all the stations with a mean of 4.60 kg/m^3 with a large drop to a mean of 0.66 kg/m^3 at the offshore station. This gradient was steeper than that on the apex transect where the means and ranges were similar for both stations (Table 3.5). No gradient could be determined without an accompanying offshore station on the protected transect. Total cumulative suspended sediment flux (SSF_{total}) showed similar patterns with the highest values at the inshore stations compared to the offshore and the inshore exposed station the largest overall SSF_{total} (Figure 3.10, Table 3.8). SSF_{total} at the inshore apex station was roughly one-third of the other two inshore stations. Both exposed stations and the apex offshore station showed flux to the east-southeast while the flux was to the southwest at the remaining moorings.

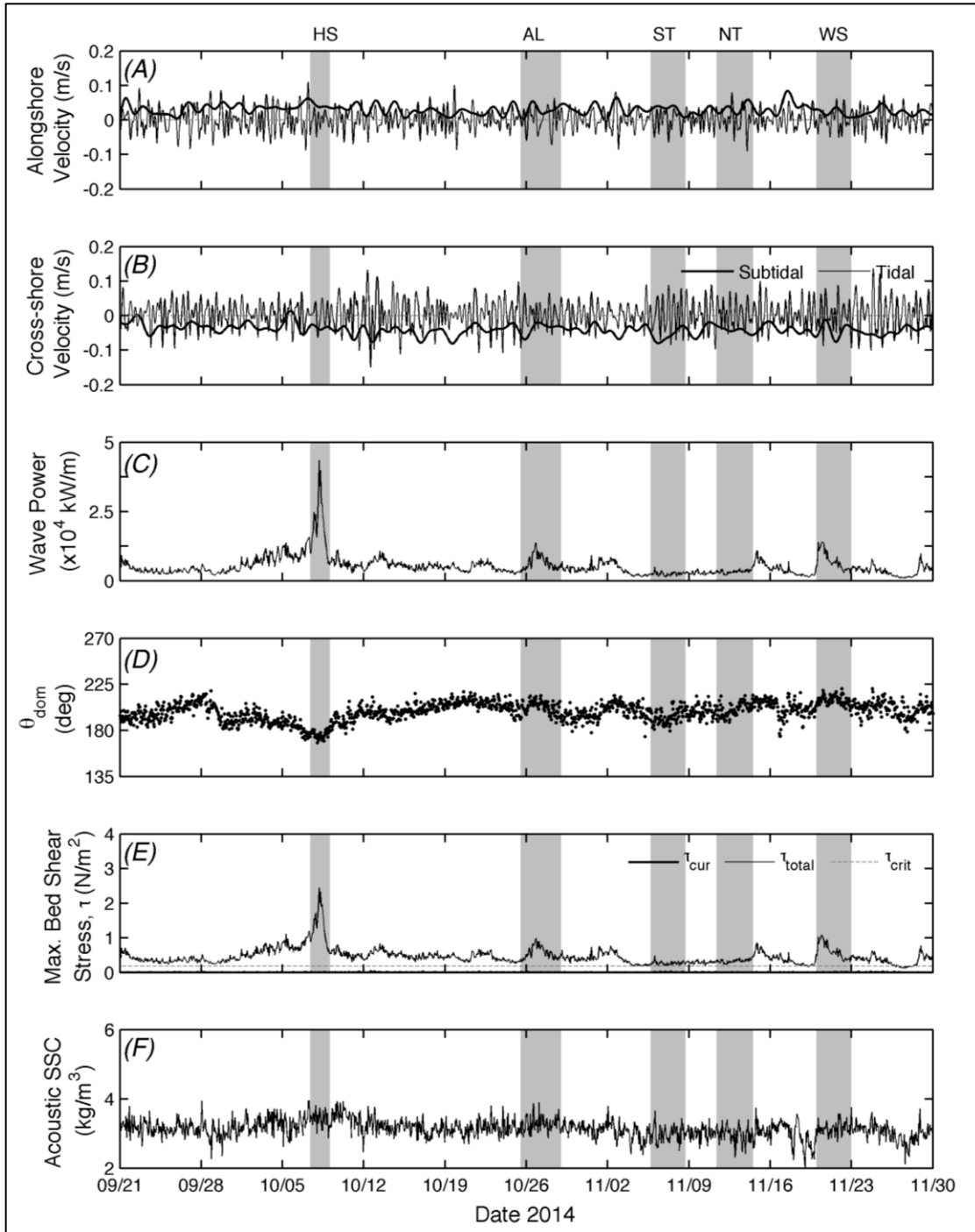


Figure 3.8b. Near-bottom alongshore (A) and cross-shore currents (B), wave power (C) and direction (D), maximum bed shear stress (τ_{total} , E), and acoustic SSC (F) at the inshore protected station (T5).

3.4.6 Synthesis of Results: Sediment Flux around Pt. Dume

While the results of waves, currents, suspended sediment, and seafloor sediment grain size provided an overall characterization of conditions at Pt. Dume, SSF_{total} and daily rates of transport at the three inshore stations extracted from the time series were the most useful to directly address the research questions (Table 3.8); SSF_{total} was not available for all three offshore stations. The average per day sediment transport rates for different oceanographic and meteorological conditions showed that the Aleutian low and winter storm events are larger than the hurricane (4.0-4.3 vs. 3.1 kg/m²/d). However, each event demonstrated spatial variability that reflected the origin of the event itself. The per day transport on the exposed side of the headland was largest for the Aleutian low and smallest for the hurricane (6.7 and 1.7 kg/m²/d, respectively). This contrasted with the transport rates on the protected side of the headland where the hurricane and Aleutian low were the largest and winter storm smaller (4.5 and 3.7 kg/m²/d, respectively). Across the apex, which showed the lowest values of the three regions, the hurricane and winter storm were the largest and the Aleutian low, the smallest (3.0-3.1 and 1.6 kg/m²/d, respectively). The transport decreased across the apex compared to either side of the headland for the winter storm and Aleutian low but was larger than the exposed side during the hurricane. The direction of flux during the events was also spatially variable with the protected side ranging from 203°-231°, the apex from 156°-273°, and the exposed side from 98°-205°. Flux was consistently toward the apex on the protected side for all events and headed onshore on the exposed side from west-originating events (winter storm and Aleutian low). The apex showed flux from the protected side toward

Table 3.8. Cumulative Sediment Transport, SSF_{total} , (kg/m^2) at Inshore Stations, 1 mab

	Regional Mean	Exposed			Apex			Protected		
Cumulative Total ¹	n/a	293			113			282		
<i>Events</i>	Per day ¹	Event Total	Per day ¹	Direction	Event Total	Per day ¹	Direction	Event Total	Per day ¹	Direction
Hurricane	3.1±1.4	2.85	1.7	205°	5.1	3.1	156°	7.49	4.5	231°
Aleutian low	4.3±2.6	20.1	6.7	98°	4.8	1.6	208°	13.4	4.5	217°
Winter storm	4.0±1.2	15.9	5.3	101°	9.0	3.0	273°	11.1	3.7	203°

1 – For duration, see Table 3.3

the exposed side for the winter storm, whereas it was reversed during the hurricane and offshore for the Aleutian low.

3.5 Discussion

3.5.1 Near-bottom Flow and Sediment Flux

The near-bottom circulation pattern around Pt. Dume can be characterized as mostly consistent apex-ward flow from either side with reversing flow direction at the apex (Table 3.6); all flows are affected by wave-driven currents. Because the flow at the apex switches tidally and the off-apex flow generally does not, convergence zones develop on either side of the headland. The alongshore flow on the exposed side most likely separates whereas on the protected side, a back eddy forms. The two modes of flow can be identified as Scenarios A and B in Figure 3.1 based on the time series of flow at the six stations (Figure 3.9). Scenario A behavior, which occurred 42% of the time, arises when flow alongshore is “in” (to the east for this headland) on the exposed side, “out” (to the west) on the protected side and across the apex. Scenario B behavior, which occurred 41% of the time, transpires as flow alongshore is “in” on the exposed side and across the apex but “out” on the protected side; the inshore and offshore stations on the protected side also show flow directions indicative of parts of an eddy. The flow patterns are mixed between A and B for the remaining 17% of the time and never indicate flow moving in the same alongshore direction (in or out) for all stations, thus eliminating Scenarios C and D. In addition to the flow, the dominant wave direction is from the southwestern quadrant that limits wave-driven flow to be directionally constrained

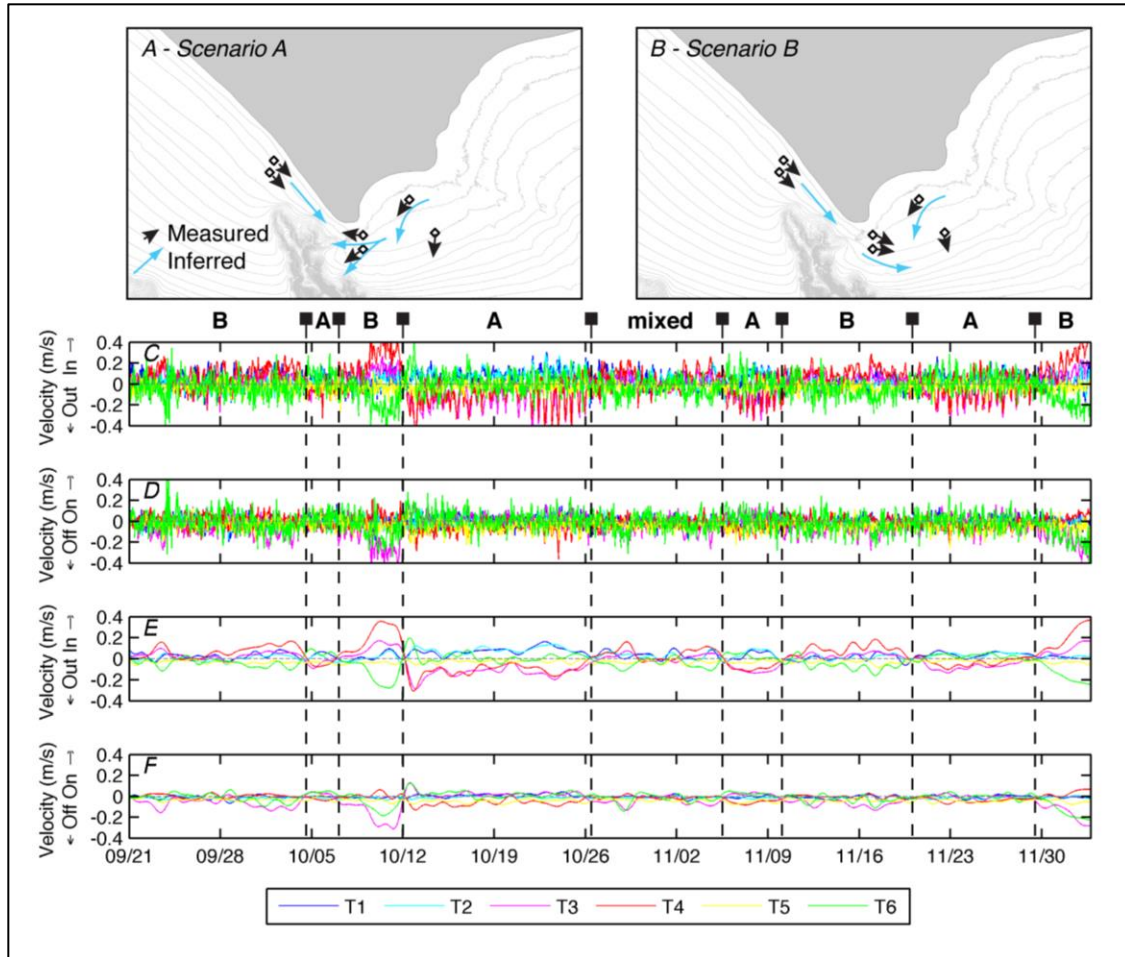


Figure 3.9. Near-bed circulation in space (*A, B*) and through time (*C-F*) to identify flow scenarios presented in Figure 3.1. In *A* and *B*, the black arrows represent measured direction of flow and blue are inferred currents for each scenario. Unfiltered time series of alongshore (*C*) and cross-shore (*D*) flow show tidal pulsing during the two scenarios. Subtidally filtered time series of alongshore (*E*) and cross-shore (*F*) flow allow sharper identification of the scenarios. The longevity of scenario type (*A* or *B*) is indicated by the zones between the dashed vertical lines.

similar to Scenario F (unbalanced wave exposure). The regional geography prevents swell originating from the east, which removes Scenario E as a possibility. Together, the flow and wave combination matches a blend of Scenarios A, B and F.

The blend of Scenarios A/B and F create a complex hydrodynamic regime from which sediment transport and deposition patterns can be expected to be equally complicated; the presence of a submarine canyon plays an obfuscating role. The theorized sediment pathways are transport offshore at the apex (from the exposed side), deposition on the protected side, and no sediment transiting across the apex. The bed sediment D_{50} seems to support this expectation by being coarse along the probable route of an offshore jet on the exposed side and finer under the eddy on the protected side. The spatial pattern in SSF_{total} at the inshore stations reaffirms the theorized pathways by showing a two-thirds decrease between the apex station and either of the exposed or protected stations (Figure 3.10). This type of pattern in the sediment transport is slightly similar to that observed at Cape Rodney in New Zealand where sediment transport pathways differed on different sides of the headland (Hume et al., 2000). The canyon may be altering the sediment supply by allowing removal of sediment (Everts and Eldon, 2005) in transit toward the apex from the exposed side, although the flux direction at the apex offshore station aligns with the probable jet direction (Figure 3.11).

Despite the canyon, the separation of flux in magnitude and direction suggests three regions for sediment transport around a headland that falls into Scenarios A/B and F. The zone on the exposed side is the most energetic from waves, which leads to high turbidity and flux (Table 3.8). The central zone at the apex is transitional where tidal currents have intensified but decreased sediment availability causes flux that is almost

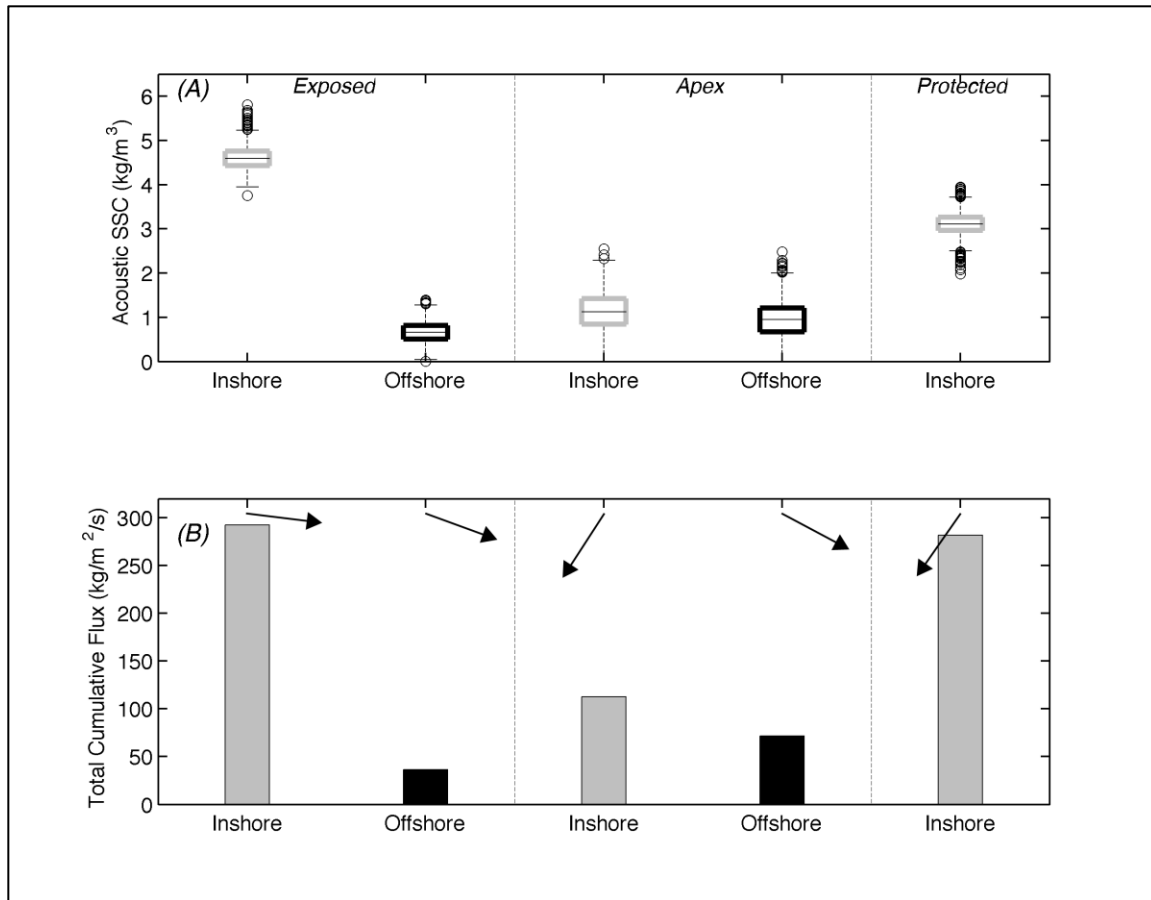


Figure 3.10. (A) Acoustic SSC divided into exposed, apex, and protected transects and by inshore (gray boxes) and offshore (black boxes) stations. On each box, the black line is the median, the edges of the box are the 25th and 75th percentiles, the whiskers extend to the most extreme data points not considered outliers, and outliers are plotted individually as circles. (B) Cumulative total suspended sediment flux (columns) by inshore (gray) and offshore (black) stations with direction of mean flux (arrows).

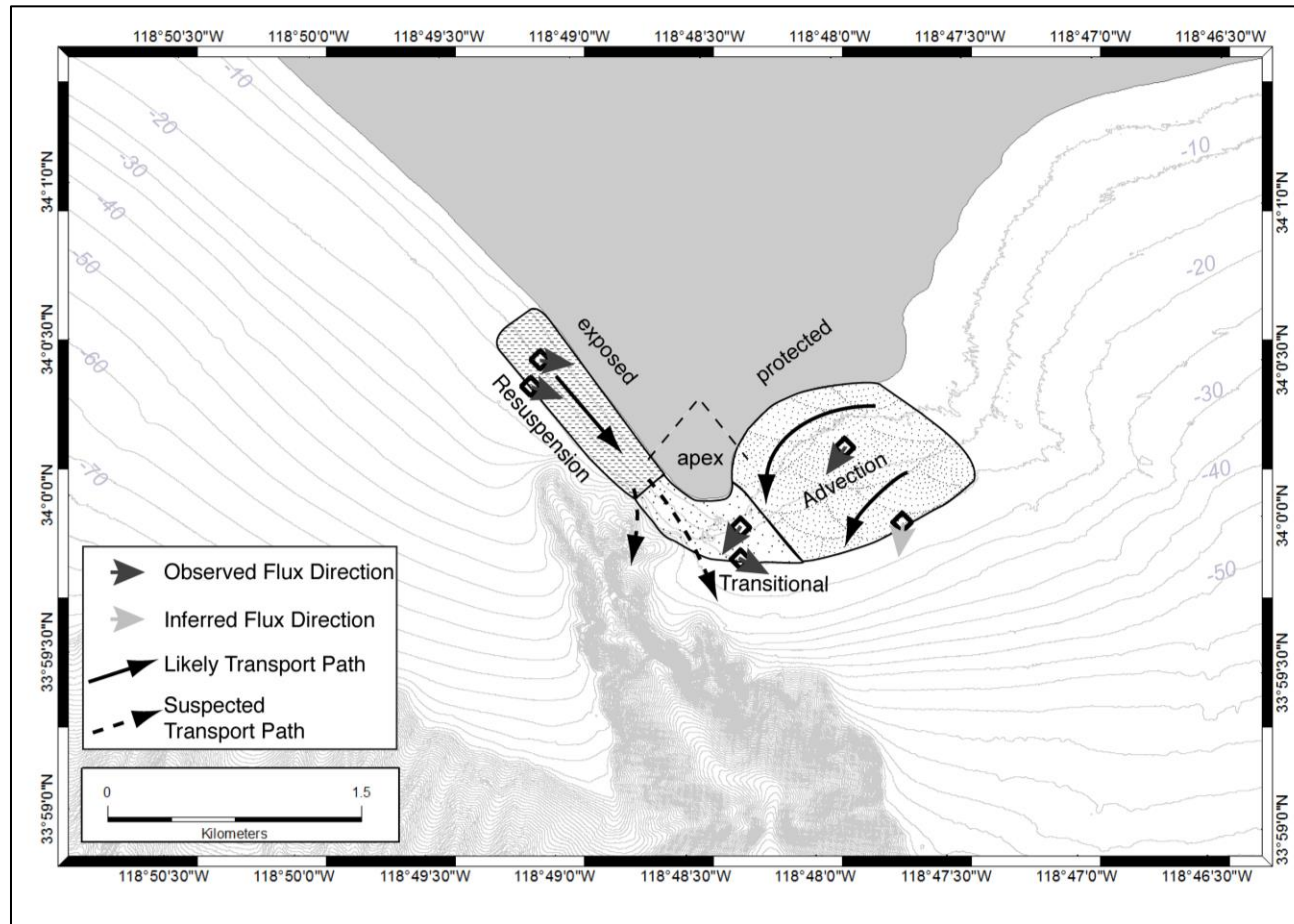


Figure 3.11. Conceptual model of sediment transport pathways around the tip of Pt. Dume with resuspension, transitional, and advection regions. Transport is complicated by the head of the canyon off the exposed side of the headland. Sediment traveling alongshore on the exposed side would likely be ejected at the apex following Scenario A whereas on the protected side, an eddy and dominant wave direction allows deposition following Scenarios B and F (Figure 3.1).

one-third that of the other regions. The protected zone experiences a decrease in both wave and tidal energy but the finer bed sediment is more readily advected, resulting in an increase in flux compared to the transitional zone. Regions of differing sediment transport around a headland have been postulated for Cape Rodney, NZ (Hume et al., 2000), Portland Bill, UK (Bastos et al., 2002), and inferred from hydrodynamics at Bass Point, Australia (Denniss et al., 1995) lending support to the conceptual model for Pt. Dume and hydrodynamically-similar headlands.

Underpinning these zones is the variation in longshore currents and wave-driven transport across the surfzone. Transport in all of the regions is connected to the grain size with fining in the offshore direction as bed shear stress decreases. Although focused on the sand fractions at Pt. Dume, this is similar in theory to the dynamics governing the sand-mud transition. As George and Hill (2008) detailed in a global dataset of sand-mud transitions, the depth of the transition, which indicates a shift in energetics, can be correlated to H_s . The magnitude of the currents and subsequent transport is largest on the exposed side before bed friction and coastal geometry have deformed the waves. Refraction around the headland reduces the energy available for generating the requisite shear stresses to resuspend bed sediment. The spatial variation in τ_{total} and response in turbidity is easily seen between the exposed and protected sides (Figure 3.12). The τ_{total} and acoustic SSC relationship is more correlated on the exposed side with $R^2=0.26$ ($p<0.01$ for $n=1,771$) compared to the protected side with $R^2=0.17$ ($p<0.01$ for $n=1,771$), although neither are particularly strong. Even so, resuspension is likely the dominant process on the exposed side with larger waves and longshore current whereas advection is likely to dominate on the protected side. The spatial differences are clearer when large

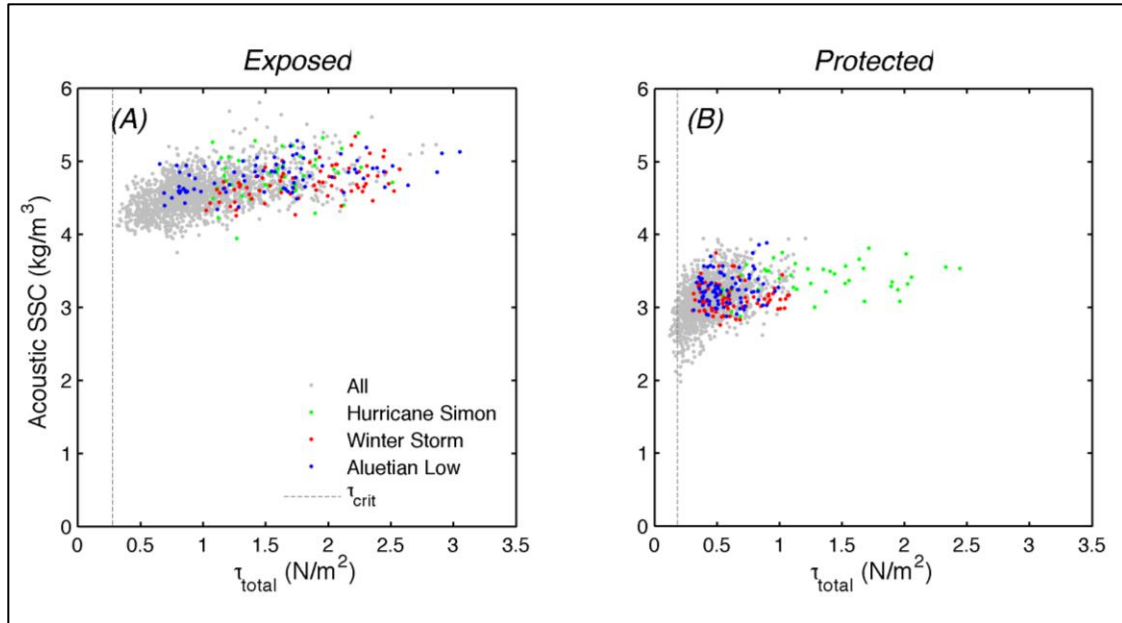


Figure 3.12. Relationship between τ_{total} and acoustic SSC on the exposed (A) and protected (B) sides of the headland with large wave events highlighted and the threshold of motion (τ_{crit}) indicated as the dashed line for the specific grain size collected on the bed at each station. On the exposed side, acoustic SSC increases when τ_{total} increases whereas on the protected side, there is not a clear relationship.

wave events are isolated. For example, during the Aluetian low event, the exposed side shows a better correlation ($R^2=0.20$, $p<0.01$ for $n = 85$) and higher total flux (20.1 kg/m²/s) than on the protected side where the correlation is insignificant ($R^2=0.02$, $p=0.17$ for $n = 85$) and total flux is lower (13.4 kg/m²/s). When the wave direction shifted during the hurricane, total flux was more than twice as large on the more protected side compared to the exposed side (Table 3.8).

3.5.2 Headland as a Barrier to Littoral Drift

Because of its size, Dume Submarine Canyon, and the regional geography, Pt. Dume was initially described as the terminal point for the Santa Monica Littoral Cell (Habel and Armstrong, 1978). As mentioned earlier, subsequent studies by Inman (1986), Orme (1991), and Knur and Kim (1999) attempted to quantify how the point-canyon complex affects alongshore transport of sand, with estimates of 10-90% of sediment bypassing the headland and being lost in the canyon. After Patsch and Griggs (2007) conducted a review of existing studies to create a sediment budget for the littoral cell, a new perspective emerged that described the headland as an internal boundary between two sub-cells. The current study partially supports that contention. If the circulation patterns follow Scenario A/B plus F, jets would shunt certain grain sizes offshore at the headland apex but the canyon removes most of the larger grain (e.g., sand) fractions. This creates a sorting effect, where the fine grain sediment (e.g., mud) that remains in suspension may transit around Pt. Dume, while the coarser sediment is trapped offshore.

From a narrow definition of a littoral cell that only considers sand, Pt. Dume is a significant barrier. However, if the full distribution of sediment grain sizes in the area is

considered, Pt. Dume is only a partial, coarse-grain preferential barrier. The concept of sorting sediment grain sizes within a littoral cell was explored by Limber et al. (2008) using a littoral cell cutoff grain size diameter, or the minimum sand grain size found on the beaches of a cell. The idea that a headland could shift between barrier types aligns with Scenario B (a large downstream zone that may not receive coarse sediment, but in which finer sediment may accrete due to weaker currents) and Scenario F (unbalanced wave exposure) in that shifting meteorological and oceanographic conditions can disrupt the typical pathways. The flow separation and transitional zone at the apex indicate how and where the different grain sizes detach from each other.

Taking a further step on how the interaction of the headland shape and flow dynamics affects the littoral cell boundary, Pt. Dume may be a barrier to sediment transport on a seasonal basis. One example of this response can be found in Goodwin et al. (2013) who identified that when dominant wave direction at Cape Byron, Australia, shifted 20°, sediment transport changed significantly around the headland in both the longshore and cross-shore directions. Seasonal shifting was explored recently by George et al. (2015), who found that periodic shifts in wave energy determine the efficacy of a littoral cell boundary. In their classification, Pt. Dume was found to be a partial boundary due to a more energetic winter wave climate. A more canyon-specific study of the physical and geological processes at the head of the canyon under different conditions would help clarify the sediment pathways both spatially and temporally.

3.6 Conclusion

Sediment transport around rocky headlands was examined through a field experiment that tested conceptual models of sediment pathways that are dependent on flow and wave direction. Waves, currents, turbidity, and bed sediment gathered at the field location, Pt. Dume, California, revealed that transport is a blend of three of the conceptual models. Through wave and near-bottom current observations, the flow was characterized as most often directed towards the point from either side of the headland with flow separation at the apex. On the more exposed side of the headland, wave-driven longshore currents are stronger and bed shear stress is larger resulting in resuspension and high suspended sediment flux toward the apex. On the more protected side of the headland, finer bed sediment and lower velocities indicate a less dynamic region where advection plays a larger role in flux than resuspension. Sediment is unlikely to transit across the apex where despite the fastest velocities, sediment supply is limited by probable ejection of sand from the exposed side. The transport of any sediment around the headland depends on the grain size by separating into either deposition zones on the shelf or into Dume Submarine Canyon (sand) or alongshore and offshore transport (mud). From this study, Pt. Dume is a mixed barrier to sediment, which suggests it is a partial littoral cell boundary. Other headlands with similar morphologies or hydrodynamics could be investigated with the conceptual models to better characterize natural barriers to littoral drift.

3.7 References

- Alaee, M.J., Ivey, G., Pattiaratchi, C., 2004. Secondary circulation induced by flow curvature and Coriolis effects around headlands and islands. *Ocean Dynamics* 54, 27-38.
- Backstrom, J.T., Jackson, D.W.T., Cooper, J.A.G., 2009. Mesoscale shoreface morphodynamics on a high-energy regressive coast. *Continental Shelf Research* 29, 1361-1372.
- Baptista, P., Cunha, T.R., Gama, C., Bernardes, C., 2012. A new and practical method to obtain grain size measurements in sandy shores based on digital image acquisition and processing. *Sedimentary Geology* 282, 294-306.
- Barnard, P.L., Hansen, J.E., Erikson, L.H., 2012. Synthesis Study of an Erosion Hot Spot, Ocean Beach, California. *Journal of Coastal Research* 28, 903-922.
- Bastos, A.C., Kenyon, N.H., Collins, M., 2002. Sedimentary processes, bedforms and facies, associated with a coastal, headland: Portland Bill, Southern UK. *Marine Geology* 187, 235-258.
- Berthot, A., Pattiaratchi, C., 2006. Field measurements of the three-dimensional current structure in the vicinity of a headland-associated linear sandbank. *Continental Shelf Research* 26, 295-317.
- Best, T.C., Griggs, G.B., 1991. The Santa-Cruz Littoral Cell - Difficulties in Quantifying a Coastal Sediment Budget.
- Black, K., Oldman, J., Hume, T., 2005. Dynamics of a 3-dimensional, baroclinic, headland eddy. *New Zealand Journal of Marine and Freshwater Research* 39, 91-120.
- Booij, N., Ris, R.C., Holthuijsen, L.H., 1999. A third-generation wave model for coastal regions - 1. Model description and validation. *Journal of Geophysical Research-Oceans* 104, 7649-7666.
- Buscombe, D., Rubin, D.M., Lacy, J.R., Storlazzi, C.D., Hatcher, G., Chezar, H., Wyland, R., Sherwood, C.R., 2014. Autonomous bed-sediment imaging-systems for revealing temporal variability of grain size. *Limnology and Oceanography-Methods* 12, 390-406.
- Buscombe, D., Rubin, D.M., Warrick, J.A., 2010. A universal approximation of grain size from images of noncohesive sediment. *Journal of Geophysical Research* 115.
- Camus, P., Mendez, F.J., Medina, R., Cofino, A.S., 2011. Analysis of clustering and selection algorithms for the study of multivariate wave climate. *Coastal Engineering* 58, 453-462.
- CGS, 2002. California Geomorphic Provinces. California Geological Survey, California Department of Conservation, p. Note 36.
- CGS, 2006. California Geological Map, Map Series 57 ed. California Geological Survey, California Department of Conservation.
- Chadwick, D.B., Largier, J.L., 1999. Tidal exchange at the bay-ocean boundary. *Journal of Geophysical Research-Oceans* 104, 29901-29924.
- Collen, J.D., Gardner, J.P.A., Garton, D.W., 2009. Application of the littoral cell concept to managing a protected atoll: Palmyra Atoll National Wildlife Refuge. *Ocean & Coastal Management* 52, 628-635.

Cooper, N.J., Pontee, N.I., 2006. Appraisal and evolution of the littoral 'sediment cell' concept in applied coastal management: Experiences from England and Wales. *Ocean & Coastal Management* 49, 498-510.

Covault, J.A., Normark, W.R., Romans, B.W., Graham, S.A., 2007. Highstand fans in the California borderland: The overlooked deep-water depositional systems. *Geology* 35, 783-786.

CSMW, 2010. California Beach Erosion Assessment Survey. Coastal Sediment Management Workgroup, Sacramento, CA, p. 72.

Dai, Z.J., Liu, J.T., Lei, Y.P., Zhang, X.L., 2010. Patterns of Sediment Transport Pathways on a Headland Bay Beach-Nanwan Beach, South China: A Case Study. *Journal of Coastal Research* 26, 1096-1103.

Davies, J.L., 1974. The coastal sediment compartment. *Australian Geographical Studies* 12, 139-151.

Davies, P.A., Dakin, J.M., Falconer, R.A., 1995. Eddy Formation Behind a Coastal Headland. *Journal of Coastal Research* 11, 154-167.

de Castilhos, J.A., Gre, J.C.R., 2006. Beach morphodynamics and sediment transport along the northern coast of Santa Catarina, Brazil. *Journal of Coastal Research*, 1756-1761.

Deines, K.L., 1999. Backscatter Estimation Using Broadband Acoustic Doppler Current Profilers. RD Instruments Application Note FSA-008, 1-5.

Denniss, T., Middleton, J.H., Manasseh, R., 1995. Recirculation in the Lee of Complicated Headlands - A Case-Study of Bass-Point. *Journal of Geophysical Research-Oceans* 100, 16087-16101.

Drake, P.T., McManus, M.A., Storlazzi, C.D., 2005. Local wind forcing of the Monterey Bay area inner shelf. *Continental Shelf Research* 25, 397-417.

Emery, K.O., Kuhn, G.G., 1982. Sea cliffs: Their processes, profiles, and classification. *Geological Society of America Bulletin* 93, 644-654.

Emery, W.J., Thomson, R.E., 2001. *Data Analysis Methods in Physical Oceanography*. Elsevier, New York.

Erikson, L.H., Storlazzi, C.D., Golden, N.E., 2014. Modeling Wave and Seabed Energetics on the California Continental Shelf. Pamphlet to accompany data set., in: Survey, U.S.G. (Ed.), Santa Cruz, California.

Erikson, L.H., Wright, S.A., Elias, E., Hanes, D.M., Schoellhamer, D.H., Largier, J., 2013. The use of modeling and suspended sediment concentration measurements for quantifying net suspended sediment transport through a large tidally dominated inlet. *Marine Geology* 345, 96-112.

ESRI, 2013. *ArcGIS Desktop: Release 10.1* Environmental Systems Resource Institute, Redlands, CA.

Everts, C.H., Eldon, C.D., 2000. Beach-Retention Structures and Wide Sandy Beaches in Southern California. *Shore and Beach* 68, 11-22.

Everts, C.H., Eldon, C.D., 2005. Sand Capture In Southern California Submarine Canyons. *Shore and Beach* 73, 3-12.

Freeland, H., 1990. The Flow of a Coastal Current Past a Blunt Headland. *Atmosphere-Ocean* 28, 288-302.

Freeman, L.A., Miller, A.J., Norris, R.D., Smith, J.E., 2012. Classification of remote Pacific coral reefs by physical oceanographic environment. *Journal of Geophysical Research-Oceans* 117.

George, D.A., Hill, P.S., 2008. Wave climate, sediment supply and the depth of the sand-mud transition: A global survey. *Marine Geology* 254, 121-128.

George, D.A., Largier, J.L., Storlazzi, C.D., Barnard, P.L., 2015. Classification of rocky headlands in California with relevance to littoral cell boundary delineation. *Marine Geology* 369, 137-152.

Goodwin, I.D., Freeman, R., Blackmore, K., 2013. An insight into headland sand bypassing and wave climate variability from shoreface bathymetric change at Byron Bay, New South Wales, Australia. *Marine Geology* 341, 29-45.

Goring, D.G., Nikora, V.I., 2002. Despiking acoustic Doppler velocimeter data. *Journal of Hydraulic Engineering-Asce* 128, 117-126.

Grifman, P., Hart, J., Ladwig, J., Schulhof, M., 2012. DRAFT Sea Level Rise Vulnerability Study for the City of Los Angeles. University of Southern California Sea Grant Program, Los Angeles, CA, p. 87.

Guillou, N., Chapalain, G., 2011. Effects of waves on the initiation of headland-associated sandbanks. *Continental Shelf Research* 31, 1202-1213.

Habel, J.S., Armstrong, G.A., 1978. Assessment and Atlas of Shoreline Erosion Along the California Coast. State of California, Department of Navigation and Ocean Development, Sacramento, CA, p. 277.

Harris, P.T., Whiteway, T., 2011. Global distribution of large submarine canyons: Geomorphic differences between active and passive continental margins. *Marine Geology* 285, 69-86.

Hickey, B.M., 1992. Circulation over the Santa-Monica San-Pedro Basin and Shelf. *Progress in Oceanography* 30, 37-115.

Hickey, B.M., Dobbins, E.L., Allen, S.E., 2003. Local and remote forcing of currents and temperature in the central Southern California Bight. *Journal of Geophysical Research-Oceans* 108.

Holdaway, G.P., Thorne, P.D., Flatt, D., Jones, S.E., Prandle, D., 1999. Comparison between ADCP and transmissometer measurements of suspended sediment concentration. *Continental Shelf Research* 19, 421-441.

Holthuijsen, L.H., Booij, N., Ris, R.C., 1993. A spectral wave model for the coastal zone, *Proceedings of the 2nd International Symposium on Ocean Wave Measurement and Analysis*, New Orleans, pp. 630-641.

Hume, T.M., Oldman, J.W., Black, K.P., 2000. Sediment facies and pathways of sand transport about a large deep water headland, Cape Rodney, New Zealand. *New Zealand Journal of Marine and Freshwater Research* 34, 695-717.

Inman, D.L., 1986. Southern California Coastal Processes Data Summary.

Inman, D.L., Frautschy, J.D., 1966. Littoral processes and the development of shorelines, Coastal Engineering Special Conference. ASCE, pp. 511-536.

Jones, O.P., Simons, R.R., Jones, E.J.W., Harris, J.M., 2006. Influence of seabed slope and Coriolis effects on the development of sandbanks near headlands. *Journal of Geophysical Research-Oceans* 111.

- Kamphuis, J.W., 2010. Introduction to coastal engineering and management, 2nd Edition. World Scientific, Singapore.
- Kaplan, D.M., Halle, C., Paduan, J., Largier, J.L., 2009. Surface currents during anomalous upwelling seasons off central California. *Journal of Geophysical Research* 114.
- Klinger, B., 1993. Gyre Formation at a Corner by Rotating Barotropic Coastal Flows along a Slope. *Dynamics of Atmospheres and Oceans* 19, 27-63.
- Knur, R.T., Kim, Y.C., 1999. Historical sediment budget analysis along the Malibu coastline, Sand Rights '99- Bringing Back the Beaches. ASCE, Ventura, CA, p. 292.
- Kruskal, J.B., 1964. Multidimensional-Scaling by Optimizing Goodness of Fit to a Nonmetric Hypothesis. *Psychometrika* 29, 1-27.
- Kruskal, J.B., Wish, M., 1978. Multidimensional Scaling. SAGE Publications.
- Largier, J.L., Magnell, B.A., Winant, C.D., 1993. Subtidal Circulation over the Northern California Shelf. *Journal of Geophysical Research-Oceans* 98, 18147-18179.
- Larson, M., Hoan, L., Hanson, H., 2010. Direct Formula to Compute Wave Height and Angle at Incipient Breaking. *Journal of Waterway, Port, Coastal, and Ocean Engineering* 136, 119-122.
- Leidersdorf, C.B., Hollar, R.C., Woodell, G., 1994. Human Intervention with the Beaches of Santa Monica Bay, California Shore and Beach 62, 29-38.
- Limber, P.W., Murray, A.B., 2015. Sea stack formation and the role of abrasion on beach-mantled headlands. *Earth Surface Processes and Landforms* 40, 559-568.
- Limber, P.W., Patsch, K.B., Griggs, G.B., 2008. Coastal sediment budgets and the littoral cutoff diameter: A grain size threshold for quantifying active sediment inputs. *Journal of Coastal Research* 24, 122-133.
- Loureiro, C., Ferreira, O., Cooper, J.A.G., 2012. Geologically constrained morphological variability and boundary effects on embayed beaches. *Marine Geology* 329, 1-15.
- MacCready, P., Pawlak, G., 2001. Stratified flow along a corrugated slope: Separation drag and wave drag. *Journal of Physical Oceanography* 31, 2824-2839.
- MacQueen, J.B., 1967. Some Methods for Classification and Analysis of Multivariate Observations, 5th Berkeley Symposium on Mathematical Statistics and Probability. University of California Press, Berkeley, California, pp. 281-297.
- Madsen, O.S., 1994. Spectral wave-current bottom boundary layer flows, *Coastal Engineering* 1994, 24th International Conference Coastal Engineering Research Council, pp. 384-398.
- Magaldi, M.G., Oztokmen, T.M., Griffa, A., Chassignet, E.P., Iskandarani, M., Peters, H., 2008. Turbulent flow regimes behind a coastal cape in a stratified and rotating environment. *Ocean Modelling* 25, 65-82.
- Milliman, J.D., Farnsworth, K.L., 2011. River Discharge to the Coastal Ocean: A Global Synthesis. Cambridge University Press, New York.
- Mullenbach, B.L., Nittrouer, C.A., Puig, P., Orange, D.L., 2004. Sediment deposition in a modern submarine canyon: Eel Canyon, northern California. *Marine Geology* 211, 101-119.
- Neill, S.P., Scourse, J.D., 2009. The formation of headland/island sandbanks. *Continental Shelf Research* 29, 2167-2177.

Nickols, K.J., Gaylord, B., Largier, J.L., 2012. The coastal boundary layer: predictable current structure decreases alongshore transport and alters scales of dispersal. *Marine Ecology Progress Series* 464, 17-35.

Noble, M.A., Rosenberger, K.J., Hamilton, P., Xu, J.P., 2009. Coastal ocean transport patterns in the central Southern California Bight. *Earth Science in the Urban Ocean: the Southern California Continental Borderland* 454, 193-226.

OPC, 2013. State Of California Sea-Level Rise Guidance Ocean Protection Council, Sacramento, CA, p. 13.

Orme, A.R., 1991. The Malibu coast – a contribution to the city-wide wastewater management study, p. 50.

OST, 2011. South Coast California MPA Monitoring Plan. MPA Monitoring Enterprise, California Ocean Science Trust, Oakland, CA.

Patsch, K., Griggs, G., 2006. Littoral Cells, Sand Budgets, and Beaches: Understanding California's Shoreline, Institute of Marine Sciences, University of California, Santa Cruz, p. 40.

Patsch, K., Griggs, G., 2007. Development of Sand Budgets for California's Major Littoral Cells. Institute of Marine Sciences, University of California, Santa Cruz, p. 115.

Pattiaratchi, C., James, A., Collins, M., 1987. Island wakes and headland eddies: A comparison between remotely sensed data and laboratory experiments. *Journal of Geophysical Research: Oceans* 92, 783-794.

Pentney, R.M., Dickson, M.E., 2012. Digital Grain Size Analysis of a Mixed Sand and Gravel Beach. *Journal of Coastal Research* 28, 196-201.

Perg, L.A., Anderson, R.S., Finkel, R.C., 2003. Use of cosmogenic radionuclides as a sediment tracer in the Santa Cruz littoral cell, California, United States. *Geology* 31, 299-302.

Pingree, R.D., 1978. Formation Of Shambles And Other Banks By Tidal Stirring Of Seas. *Journal of the Marine Biological Association of the United Kingdom* 58, 211-226.

Reid, J.A., Reid, J.M., Jenkins, C.J., Zimmermann, M., Williams, S.J., Field, M.E., 2006. usSEABED: Pacific Coast (California, Oregon, Washington) Offshore Surficial-sediment Data Release.

Ris, R.C., Holthuijsen, L.H., Booij, N., 1999. A third-generation wave model for coastal regions - 2. Verification. *Journal of Geophysical Research-Oceans* 104, 7667-7681.

Rosati, J.D., 2005. Concepts in sediment budgets. *Journal of Coastal Research* 21, 307-322.

Roughan, M., Mace, A.J., Largier, J.L., Morgan, S.G., Fisher, J.L., Carter, M.L., 2005. Subsurface recirculation and larval retention in the lee of a small headland: A variation on the upwelling shadow theme. *Journal of Geophysical Research-Oceans* 110.

Sallenger, A.H., Krabill, W., Brock, J., Swift, R., Manizade, S., Stockdon, H., 2002. Sea-cliff erosion as a function of beach changes and extreme wave runup during the 1997-1998 El Nino. *Marine Geology* 187, 279-297.

SANDAG, 2009. Coastal Regional Sediment Management Plan for the San Diego Region. Prepared by Moffatt and Nichol, Everest International Consultants and SIAC. San Diego Association of Governments, p. 220.

Sanderson, P.G., Eliot, I., 1999. Compartmentalisation of beachface sediments along the southwestern coast of Australia. *Marine Geology* 162, 145-164.

Scholar, D.C., Griggs, G.B., 1997. Pocket Beaches of California: Sediment Transport Along a Rocky Coastline, Proceedings of California's Coastal Natural Hazards. University of Southern California Sea Grant Program, Santa Barbara, pp. 65-75.

Scott, T., Masselink, G., Russell, P., 2011. Morphodynamic characteristics and classification of beaches in England and Wales. *Marine Geology* 286, 1-20.

Short, A.D., 1999. Handbook of beach and shoreface morphodynamics. John Wiley, New York.

Signell, R.P., Geyer, W.R., 1991. Transient Eddy Formation around Headlands. *Journal of Geophysical Research-Oceans* 96, 2561-2575.

Silva, R., Baquerizo, A., Losada, M.A., Mendoza, E., 2010. Hydrodynamics of a headland-bay beach-Nearshore current circulation. *Coastal Engineering* 57, 160-175.

Slagel, M.J., Griggs, G.B., 2008. Cumulative losses of sand to the California coast by dam impoundment. *Journal of Coastal Research* 24.

Soulsby, R., 1997. Dynamics of Marine Sands: A Manual for Practical Applications. Thomas Telford, London.

Stewart, S.R., 2014. Tropical Cyclone Report. Hurricane Simon (EP192014), in: National Hurricane Center, N. (Ed.), p. 18.

Storlazzi, C.D., Field, M.E., 2000. Sediment distribution and transport along a rocky, embayed coast: Monterey Peninsula and Carmel Bay, California. *Marine Geology* 170, 289-316.

Storlazzi, C.D., Jaffe, B.E., 2008. The relative contribution of processes driving variability in flow, shear, and turbidity over a fringing coral reef: West Maui, Hawaii. *Estuarine Coastal and Shelf Science* 77, 549-564.

Storlazzi, C.D., Reid, J.A., 2010. The influence of El Nino-Southern Oscillation (ENSO) cycles on wave-driven sea-floor sediment mobility along the central California continental margin. *Continental Shelf Research* 30, 1582-1599.

Stuiver, C., 2013. Coastal evolution of soft cliff coasts: headland formation and evolution on the Southwest Isle of Wight, *Engineering and the Environment*. University of Southampton, p. 277.

Stul, T., Gozzard, J., Eliot, I., Eliot, M., 2012. Coastal Sediment Cells between Cape Naturaliste and the Moore River, Western Australia in: Transport, W.A.D.o. (Ed.). Damara WA Pty Ltd and Geological Survey of Western Australia, Fremantle, WA, Australia, p. 44.

Thorne, P.D., Vincent, C.E., Hardcastle, P.J., Rehman, S., Pearson, N., 1991. Measuring Suspended Sediment Concentrations Using Acoustic Backscatter Devices. *Marine Geology* 98, 7-16.

USACE, 1984. Shore Protection Manual, in: U. S. Army Corps of Engineers, C.E.R.C. (Ed.). Department of the Army, Waterways Experiment Station, Corps of Engineers, Vicksburg, p. 656.

van Rijn, L.C., 2010. Coastal erosion control based on the concept of sediment cells. *CONSCIENCE*, Deltares, The Netherlands, p. 80.

Verron, J., Davies, P., Dakin, J., 1991. Quasigeostrophic Flow Past a Cape in a Homogeneous Fluid. *Fluid Dynamics Research* 7, 1-21.

Winant, C.D., 2006. Three-dimensional wind-driven coastal circulation past a headland. *Journal of Physical Oceanography* 36, 1430-1438.

- Wingfield, D.K., Storlazzi, C.D., 2007. Spatial and temporal variability in oceanographic and meteorologic forcing along Central California and its implications on nearshore processes. *Journal of Marine Systems* 68.
- Wright, L., Short, A., 1984. Morphodynamic Variability of Surf Zones and Beaches - A Synthesis. *Marine Geology* 56, 93-118.
- Xu, J.P., Noble, M.A., 2009. Variability of the Southern California wave climate and implications for sediment transport. *Earth Science in the Urban Ocean: the Southern California Continental Borderland* 454, 171-191.
- Young, A.P., Ashford, S.A., 2006. Application of airborne LIDAR for seacliff volumetric change and beach-sediment budget contributions. *Journal of Coastal Research* 22, 307-318.

**Chapter 4 – Modeling Sediment Bypassing around
Idealized Rocky Headlands**

4.1 Introduction

Sediment transport around rocky headlands is less understood in terms of dynamics and mechanisms than other coastal environs, such as at beaches or near engineered structures. Suppositions related to wave focusing at headlands have provided an underpinning of littoral processes, including shoreline position evolution and embayed beach dynamics (Backstrom et al., 2009; Dai et al., 2010; Silva et al., 2010). However, research explicitly investigating how such perturbations manifest themselves is either location-based (Roughan, Terrill, et al., 2005; Warner and MacCready, 2009) or in theorized numerical model schemes that are not always reflective of natural systems (Magaldi et al., 2008; Signell and Geyer, 1991). Previous headland studies focused on separation of tidal or mean flows instead of the effect of waves on alongshore transport. The lack of attention on wave-driven processes is in contrast to conceptual models of sediment bypassing headland processes (Short, 1999). This gap is compelling to address because improvements can be made to understanding littoral cells, including coupling mechanisms between the shelf and shore (including headlands) and sediment budgets, a problem raised by Inman and Masters (1994). In addition, sediment bypassing as a control on river mouth morphology, analogous to headlands in terms of physical perturbation to alongshore transport, was recently characterized by Nienhuis et al. (2016) which indicates the attention being given to bypassing. Lastly, prudent sediment management as part of climate change adaptation strategies (King et al., 2016) requires advancement in knowledge regarding alongshore sediment transport.

This study investigates how wave-forcing and other physical processes, headland geomorphology, sediment grain size, and substrate composition affect alongshore sediment flux using a process-based numerical model. Two framing questions are posed: (1) What are the controlling morphological and oceanographic parameters on sediment of varying sizes bypassing a headland? and (2) How do those parameters interact to enable or prevent bypassing? The paper is organized to begin with a brief review of prior modeling efforts, concepts of littoral cells, and factors that may affect sediment bypassing. The next section details the numerical modeling approach and analysis, including the exploration of the dynamic nature of sediment bypassing through systematic adjustments of morphological, oceanographic, and sedimentological factors. The modeling results are presented in three sections: (1) overview of circulation patterns and sediment transport volumes around the headlands, (2) findings from analysis of the individual factors, and (3) alongshore variation of forcing terms on a transect around each headland. The paper concludes with a discussion about the most important factors, the mechanisms for sediment bypassing, and a generalized transport concept based on the modeling results.

4.2 Background

4.2.1 Modeling Flow and Flux around Headlands

To date, modeling has emphasized tidal flow past headlands using generic idealized Gaussian headland designs to address questions of hydrodynamics and sediment accretion. Signell and Geyer (1991) described the three key dimensionless parameters for flow separation and eddy formation as the aspect ratio of a headland, the depth/drag ratio

across the length of headland, and the ratio of flow velocity to flow frequency across the length of headland. The absence of waves has been common as seen in Alae et al. (2004); Berthot and Pattiaratchi (2006b); Davies et al. (1995); Park and Wang (2000). Guillou and Chapalain (2011) introduced waves into their modeling effort to investigate sandbanks near symmetrical headlands while Jones et al. (2006) explored the role of Coriolis in deposition patterns near the apex of a conical headland. Other studies manipulated the idealized Gaussian design by varying the nearshore slope (Jones et al., 2006; Magaldi et al., 2008), or the size, tidal excursion across the headland length, or sharpness of a headland (Warner and MacCready, 2009). These, and similar, efforts, have relied on theoretical headlands without testing their models against specific or categorized classes of headlands.

Where sediment movement was examined in the studies above, it was in the context of headland-associated sand banks (Berthot and Pattiaratchi, 2006b; Guillou and Chapalain, 2011; Jones et al., 2006). While flux was deduced from morphological change to the bed, none of the studies connected variously shaped headlands to different deposition zones. The question of how headlands affect wave-driven transport in the alongshore direction remains unanswered, which leaves a gap in understanding littoral drift, sand bypassing, and flux of biological or contaminant material.

4.2.2 Headlands as Barriers to Sediment Flux

Headlands are expected to inhibit alongshore sediment flux and may act as barriers to entirely block flux. In general terms, van Rijn (2010) suggests the most important characteristics of headlands to be: (1) convergence points for wave energy; (2) obstructions to alongshore tide- and wind-induced currents; (3) protrusions to generate

nearshore re-circulation zones ; (4) obstructions to littoral drift; (5) fixation points for seaward rip currents promoting offshore transport; and, (6) fixation points for spit formation and shoals originating from headland erosion. Where sediment does not pass a headland, the promontory is typically used as a terminal end to a littoral cell. A littoral cell is defined as an alongshore region in which sand is retained and recirculated without alongshore export (Rosati, 2005). Examples can be found in California (Inman and Frautschy, 1966; Patsch and Griggs, 2006), Australia (Stul et al., 2012), and the United Kingdom (<http://www.scopac.org.uk/sediment-transport-update.html>). Davies (1974) questioned the arbitrary drawing of boundaries and suggested anchoring littoral cells to headlands or at the very least, extensive sections of rocky coast. He also noted that headlands may be filtering sediment grain sizes, a concept Limber et al. (2008) expanded upon by suggesting smaller sediment grain sizes be included in the sediment budgets of California littoral cells.

The temporal aspect of flux is important to consider as one of the defining elements of a boundary. Under time-varying conditions, a headland may block sediment at one time and allow bypassing when occasional or anomalous events occur. Recognizing that the coastal environment is dynamic, van Rijn (2010) referred to absolute and partial boundaries to denote headlands that never allow bypassing and those that may under favorable conditions. Leakage of sediment would be expected across more porous boundaries with connectivity between smaller adjacent littoral cells (termed “open” by Davies (1974)) allowing alongshore exchange (Figure 4.1). “Closed” cells would be anchored at headlands that act as complete barriers to sediment.

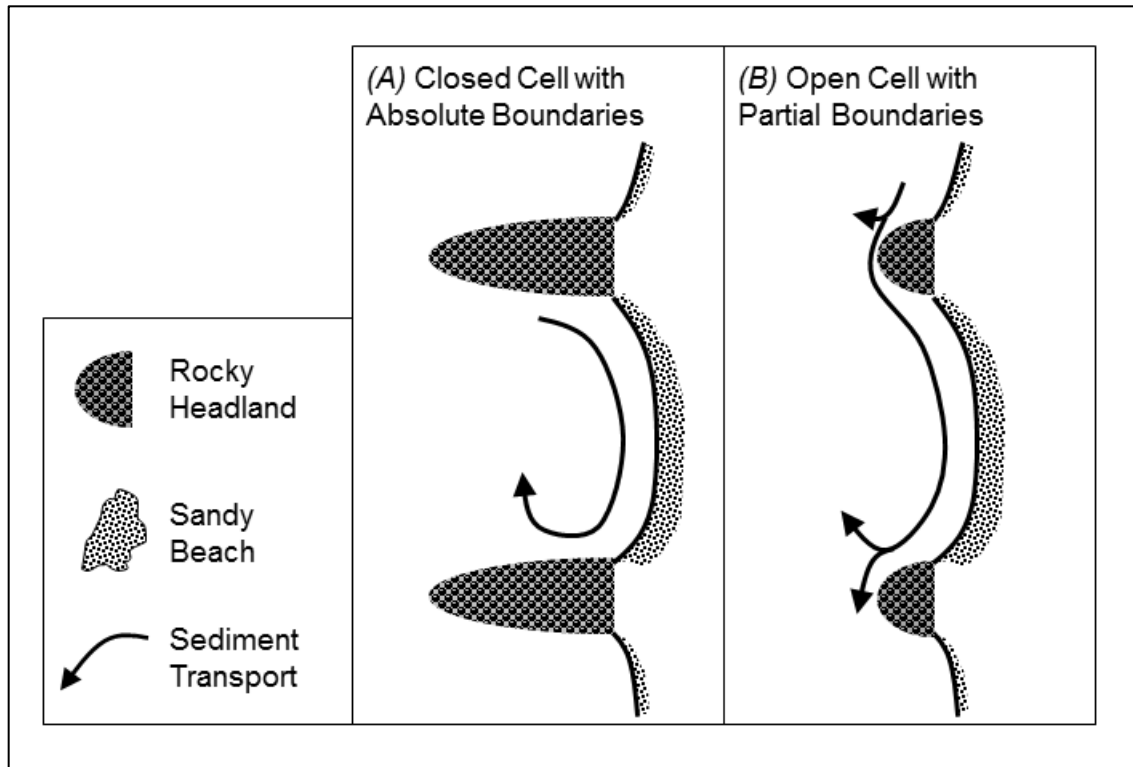


Figure 4.1. Conceptual littoral cell types and associated boundaries based on Davies (1974) and van Rijn (2010). (A) A closed cell that does not allow sediment to escape to adjoining cells with absolute boundaries. (B) An open cell from which some sediment may be exchanged with adjoining cells, defined by partial boundaries.

In reality, no headland is expected to be an absolute boundary to all sediment. As a result, the conundrum is better outlined as how often does bypassing occur, for what grain sizes, and how much volume is transported. Despite the clear conceptual models of Davies (1974) and van Rijn (2010), the balance between headland geomorphology and coastal processes that cause sediment bypassing remains opaque. With rocky headlands, there are an infinite number of combinations using wave climates, tidal ranges, geomorphology, geology, bathymetry, sediment (volumes and grain sizes), submerged aquatic vegetation, and substrates, such as hard rock reefs. Sediment flux around headlands becomes ever more important to quantify with climate change expected to cause shifts in wave climates and alongshore sediment transport (Adams et al., 2011). Littoral cell boundaries at headlands could evolve as wave energy and incident angles fluctuate resulting in substantial changes to beaches and shoreline geomorphology.

4.2.3 Factors That Affect Sediment Bypassing a Headland

The theoretical, numerical modeling, and field observational studies mentioned above provide a large suite of parameters thought to play a role in nearshore processes that influence sediment bypassing. The parameters can be organized into three categories of factors: morphology, oceanography, and sedimentology (Table 4.1). Morphology encapsulates the physical form of a headland, bathymetry surrounding the headland, and offshore physical environment. Oceanography relates to the wave and current forcing terms that drive processes that subsequently cause movement of water and sediment. Sedimentology captures the sediment grain size parameters, substrate composition, and

Table 4.1. Factors Influencing Sediment Bypassing a Headland

Factor	Parameter ¹	Spectrum			
Morphology	Headland Size	Small ³	Medium ³	Large ³	
	Headland Shape	Pointed ³	Curved	Blocky ³	
	Headland Symmetry	Upstream Skew	Balanced ³	Downstream Skew	
	Aspect Ratio	Length >> Width	Length = Width	Length << Width	
	Nearshore Shelf Width	Narrow	Medium ³	Wide	
	Adjacent Slope	Upstream Deeper	Balanced ³	Downstream Deeper	
	Headland-Beach Intersection	Acute	Right	Oblique	
	Shoreline Rugosity	Smooth ³	Mixed	Rugged	
	Offshore Apex	Ocean ³	Submerged Reef	Island	
	Oceanography	Wave Size	Small ³	Medium	Large ³
		Wave Period	Short ³	Medium	Long ³
		Deep Water Wave Angle	Direct (e.g., 270) ³	Middle (e.g., 315)	Oblique (e.g., 345) ³
		Tidal Range	Micromareal	Mesomareal ³	Macromareal
		Regional Current Speed	None ³	Slow ³	Fast
Regional Current Direction		Heading ³	Across	Following	
Sediment	Wind Speed	None	Slow ³	Fast	
	Wind Direction	Onshore	Alongshore ³	Offshore	
	Coriolis	Equator	Mid-latitudes ³	Pole	
	Sediment Type	Muds	Sands ³	Pebbles	
	Sediment Size (e.g., sand)	Fine ³	Fine-Medium ³	Medium ³	
	Substrate	Sandy ³	Mixed	Reef ³	
	Sediment Source ²	Fluvial	Cliff Erosion	Marine ³	

1 – bold-face indicates parameter tested in current study

2 – “spectrum” does not apply to describe range of sediment sources

3 – variability of parameter in current study where applicable; aspect ratio and headland-beach intersection dependent on headland size and shape.

source of the sediment. The parameters in Table 4.1 create a matrix of testable permutations to analyze the sensitivity of bypassing to particular combinations.

For this modeling study, a subset of parameters was chosen within each factor category expected to have the strongest influence on bypassing as a first-order multivariate analysis. Six questions were constructed to test the dependence of bypassing on the selected factors.

1. Morphology (oceanography and sediment factors held constant to compare different headland shapes and sizes):

- a. How does headland morphology affect alongshore flow?
- b. How does headland morphology affect sediment deposition amounts and patterns?

2. Oceanography (morphology and sediment factors held constant to compare different oceanographic conditions):

- a. How do ocean conditions (tides, wave height, wave period, wave direction, and regional current) influence sediment flux around headlands?

3. Sedimentology (morphology and oceanography factors held constant to compare different sediment sizes and bed types):

- a. How do differently sized sand fractions respond to identical morphological and oceanographic conditions?
- b. How does bed sediment availability at a headland influence sediment flux around that headland?

4. Overall Bypassing (integrating all factors):

a. What characteristics of morphology and oceanography lead to bypassing at a headland for which grain sizes?

The influence of morphology, oceanography, and sediment factors were tested by quantitative metrics described in the following section.

4.3 Methods

4.3.1 Headland Morphology

George et al. (2015) classified 78 headlands along California into eight groups by geomorphic and bathymetric parameters: size (perimeter), sharpness (angle of headland apex), and bathymetric slope ratios between opposite sides of a headland. This dataset was used to design four representative headlands based on the mean perimeter and apex angle for each class (Figure 4.2). Headland types 1 (small size, medium point), 6 (small size, broad point), 7 (medium size, sharp point), and 8 (large size, broad point) were selected to symbolize the biggest differences among the eight classes and to represent classes of headlands that have been previously treated as littoral cell boundaries, which implies no sediment bypassing. Bathymetric slope ratios were also important in differentiating the classes but were not explored here.

4.3.2 Numerical Models

The experimental design involved systematically investigating sediment transport of three different grain size scenarios when forced by different oceanographic conditions at the four headlands. In total, 120 simulations were performed exploring the influence of

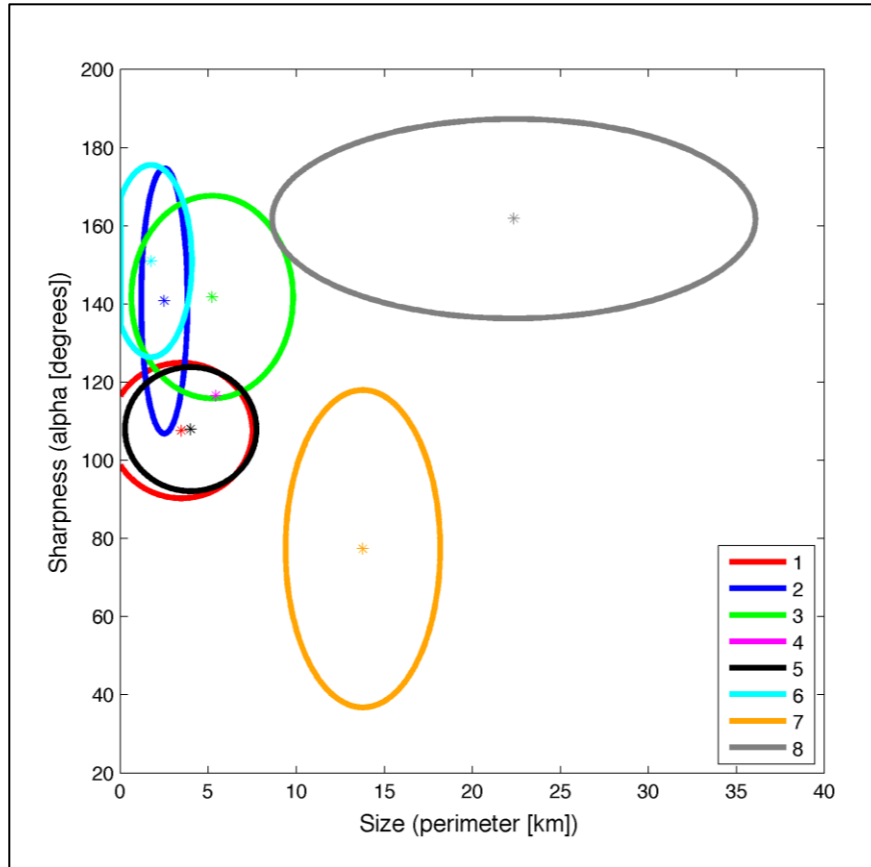


Figure 4.2. Size and sharpness of the eight headland classes developed by George et al. (2015). Four idealized headlands were developed for modeling using the dimensions of T1, T6, T7, and T8.

tides, wave conditions, regional currents, grain sizes, and bed sediment supply adjacent to the headlands on alongshore sediment flux (Table 4.2). Sediment transport was modeled with a process-based numerical hydrodynamic and sediment transport model, Delft3D (D3D). The FLOW segment of the model solves the equations of motion, conservation of water, and conservation of sediment at each time step on a staggered Arakawa-C grid (Lesser et al., 2004; Stelling, 1984). The model uses hydrostatic and Boussinesq assumptions to solve the unsteady shallow-water problems in 2-dimensional horizontal (2DH) or 3-dimensional mode. For waves, D3D was coupled with the spectral wave model Simulating WAVes Nearshore (SWAN) that models the propagation of deep ocean waves into shallower waters nearshore. SWAN simulates the transformation of wave action density using the action balance equation (Booij et al., 1999; Holthuijsen et al., 1993; Ris et al., 1999). Sediment transport and deposition of non-cohesive sand was computed in the FLOW portion of the coupled model using the TRANSPOR2004 transport equations (Lesser et al., 2004). D3D separates the sediment transport into suspended and bed-load components (van Rijn, 2007a, b, c), with the suspended fraction calculated by the advection-diffusion equation and the bed-load represented by sand particles in the wave boundary layer in close contact with the bed (Elias and Hansen, 2013).

4.3.3 Model Input

4.3.3.1 Model Grids and Bathymetry

Three rectangular grids were used to maximize computational efficiency and best represent the physical processes. The largest was SWAN1 at 11 x 30 km using 50 m grid

Table 4.2. Numerical Model Simulations for Each Headland Type and Grain Size

Description	Hydrodynamics					Substrate		
	Tides	Waves				Currents	Sandy	Reef
		LD	LO	MD	MO			
Baseline	X						X	
Sandy Bed	X	X	X	X	X		X	
Reefed Headland	X		X	X	X			X
Regional Current	X			X	X	X		X

L = Least Wave Power, M = Most Wave Power, D = Direct Wave Angle, O = Oblique Wave Angle

cells for regional wave computations (Figure 4.3a). The hydrodynamic and sediment transport grid (FLOW) was 11 x 26 km using 25 m grid cells. SWAN1 passed wave information (significant wave height H_s , peak period T_p , and dominant direction θ_{dom}) to the outer boundaries of SWAN2, a nested 6 x 15 km grid with 25 m grid cells centered on the apex of the headlands. The dimensions of the four headland designs are in Table 4.3 and plan views in Figure 4.3b, c, e, and f. The bathymetry for the models was similar across headland designs to allow for direct comparison of processes and results. An underwater slope of 2% was established from 0 to -180 m across 9 km while a slope of 0.4% from 0 to +4 m across 1 km represented the beach above the waterline (Figure 4.3d). Each headland was given an elevation of +15 m rising straight from the beach as a vertical cliff at the shoreline. A shoaling zone approximately 1 km wide was built adjacent to the headland sloping from 0 to 20 m that wrapped around the headland and smoothly connected to bathymetry upstream and downstream of the headland. The larger headlands (T7 and T8) protruded farther from shore than T1 and T6.

4.3.3.2 *Oceanographic Forcing Terms*

Three types of forcing were considered: tides, waves, and regional currents. Inputs were developed based on observations from the wave-dominated coastline of California to emphasize sediment flux due to wave action. According to the tidal regime classification of Hayes (1979), California is a lower mesotidal (1-2 m) environment, which is observed on roughly 26% of the world's coastlines. The wave climate, however, is quite dynamic due to direct exposure to the Pacific Ocean along the bulk of the state. Average and top 95% H_s along California reside in the upper 25% of global wave conditions (see Appendix A.1).

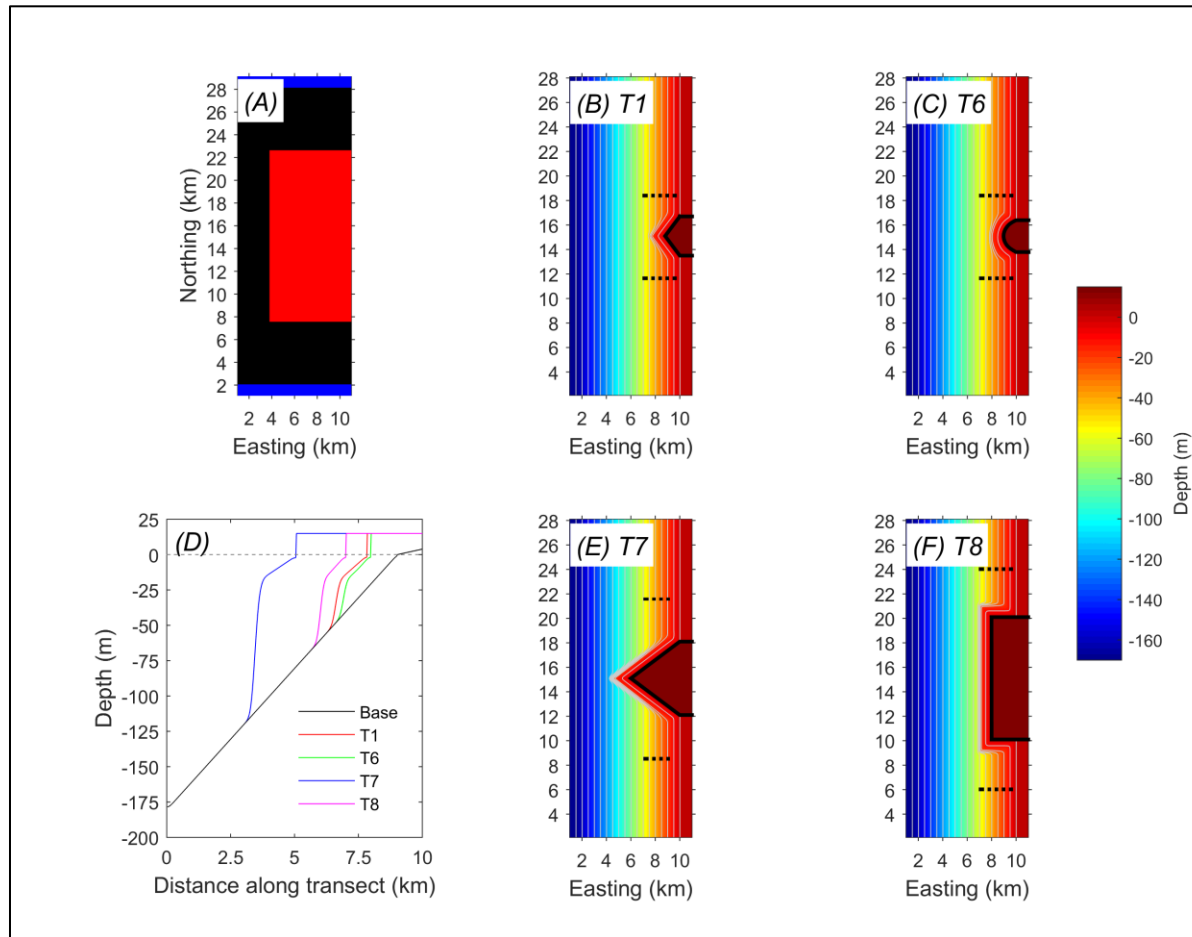


Figure 4.3. Grids, bathymetry, and cross-shore profiles used in modeling study. (A) Computational grids for SWAN1 (blue), FLOW (black), and SWAN2 (red). Bathymetry and plan view of headlands shown with the headland noted by black line, 2.5-km long cross-shore transects at the headland shoulders as dashed lines, and contours at 10 m intervals for T1 (B), T6 (C), T7 (E), and T8 (F). (D) Cross-shore profiles at the apex of the headlands showing the protrusion into the flow field compared to the base line located away from the headland.

Table 4.3. Design of Idealized Headlands based on George et al. (2015) (G2015)
Classification

Headland Class	Description (size, apex)	Occurrence of Class in G2015	Alongshore Length (m) ¹	Cross-shore Distance (m) ^{1,2}	Apex Angle (deg)
T1	Small, medium	28%	3,200	1,200	107°
T6	Small, broad	26%	2,600	1,100	151°
T7	Medium, sharp	6%	6,200	2,900	77°
T8	Large, broad	6%	10,000	2,000	180°

1 – for headland only, not adjacent surfzone

2 – measured from beach-headland intersection point

To develop a representative semi-diurnal mixed tide, astronomic tidal constituents were extracted from the NOAA tide gage at Port San Luis, California (PSLC1 – 9412110, 35° 10.1' N, 120°45.2' W, Table 4.4). Following the methods of Lesser (2009) and Hansen et al. (2013) for reducing a complex tide to a representative simplified tide for computational efficiency, an artificial diurnal constituent termed C_1 with amplitude (amp) and phase (ϕ) was calculated using observed constituents K_1 and O_1 according to

$$C_{1amp} = \sqrt{2K_1O_1} \quad (4.1)$$

$$\phi_{C_1} = \frac{\phi_{K_1} + \phi_{O_1}}{2} \quad (4.2)$$

The combination of semi-diurnal M_2 and diurnal C_1 produces a mixed, semi-diurnal tide that can represent tidal effects along a region similar to the US West Coast. This artificial diurnal tide has a period twice that of the semi-diurnal M_2 tide, so that there is no spring-neap variability.

Wave conditions were developed from a modeled wave climate for California (Erikson et al., 2014). This climate is based on 32 years (1980-2011) of wave data over the outer shelf that propagated to the nearshore using SWAN. Mean and 95-percentile summer and winter values for H_s , T_p , and θ_{dom} calculated by Erikson et al. (2014) informed the four wave climates created for modeling in this study. Wave conditions represent low and high energy flux and direct and oblique incident wave angles (Table 4.5).

A steady regional current speed of 0.10 m/s was selected based on observed subtidal surface and near-bed velocities in the Southern California Bight (Noble et al., 2009) and along the coast of northern California (Largier et al., 1993). A uniform north-

Table 4.4. Major Tidal Constituents at Port San Luis, California and Calculated C1

Constituent	Amplitude (m)	Phase (deg)
M2	0.50	296°
S2	0.15	30°
N2	0.12	28°
K1	0.36	15°
O1	0.23	14°
C1*	0.41	91°

* - see Equation (4.1) and Equation (4.2) in the text

Table 4.5. Wave Conditions for Forcing Numerical Models

		Wave Power Parameters	
		Least	Most
Incident Wave Angle	Direct	$H_s = 2$ m $T_p = 10$ s $\theta_{dom} = 270^\circ$	$H_s = 7$ m $T_p = 16$ s $\theta_{dom} = 270^\circ$
	Oblique	$H_s = 2$ m $T_p = 10$ s $\theta_{dom} = 345^\circ$	$H_s = 7$ m $T_p = 16$ s $\theta_{dom} = 345^\circ$

to-south flow was chosen to be parallel to the shore and isobaths on the northern and southern boundaries.

4.3.3.3 *Sediment*

Sediment transport processes vary in response to source areas of sediment and sediment size. In one set of scenarios, a uniformly distributed sediment bed 50 m thick was used similar to that observed at Pt. Dume, California, which allowed for sediment resuspension at the headland to contribute to flux. In another set of scenarios, the nearshore (~1 km wide) immediately adjacent to the headland was devoid of sediment as is the case with a rocky reef zone (similar to Bodega Head, California) and the flux past the headland was due to upstream sources alone. Three sediment grain sizes were selected to bracket the majority of sands observed on Californian beaches: 125, 250, and 500 μm . The lowest value corresponds to the most common littoral cutoff diameter (LCD) that is the smallest sediment typically retained in a littoral cell (Limber et al., 2008). The middle value is based on observations by Barnard et al. (2013) at Ocean Beach, San Francisco, California, who determined 250 μm was representative of the beach and ebb-tidal delta at the Golden Gate. The upper boundary is based on the large expanses of medium sand of approximately 500 μm observed on the wave-exposed side of Pt. Dume, Malibu, California (George et al. (2016). The thresholds of motion for the grain sizes as determined by critical shear stress (τ_{crit}) were calculated to be 0.178, 0.195, and 0.259 N/m^2 , respectively, following the method described by Soulsby (1997). No sediment entered through the model boundaries in a suspended or bedload form, although sediment can be exported out of the model domain.

4.3.4 Modeling Approach

Field validation and calibration of model settings for this headland study were not possible. However, various D3D hydrodynamic and sediment transport models have been field validated in environments and under conditions similar to those simulated in the current study, including at Ocean Beach and the mouth of San Francisco Bay (Barnard et al., 2013; Erikson et al., 2013), the Elwha River Delta (Gelfenbaum et al., 2015), the mouth of the Columbia River (Elias et al., 2012), nearshore sand dredge pits north of Miami (Benedet and List, 2008), and fringing reefs in Hawaii (Hoeke et al., 2013). Most relevant is a field-calibrated D3D modeling effort on sand bypassing seven headlands in Brazil (Vieira da Silva et al., 2016). These studies were consulted for guidance to develop initial operational settings that were then refined using sensitivity analyses, if necessary.

The modeling approach was to compare across the model scenarios, incorporating physical processes while maximizing computational efficiency. Three open boundaries were set on the western, northern, and southern extents of all the model domains. In the FLOW portion, the western boundary was forced by the representative tide in all models and the northern and southern boundaries were either Neumann boundaries (for tides and waves only) or the southward 0.1 m/s current. The deep-water waves propagated across the large SWAN1 model boundaries and the transformed waves then propagated across the small SWAN2 model boundaries. The flow and wave models were coupled every 30 min during which relevant information was passed between them, including water levels, current velocities, and wave forces. The FLOW portion was run in 2DH while SWAN was 2D (the only option available). Through sensitivity analysis, the Bijker (1967) formulation for wave-current interaction was selected, which is a robust approach for

coastal, sandy systems (Deltares, 2014). The formulation first treats suspended and bedload transport separately in the direction of flow and then calculates transport due to wave asymmetry and bed slope according to Bailard (1981). The transport vectors are a combination of the suspended and bedload terms. Other numerical parameter settings for model operation included water temperature of 15° C, salinity of 31 ppt, water density of 1025 kg/m³, uniform wind speed of 0.1 m/s from the north, viscosity of 2 m²/s, diffusivity of 10 m²/s, and Chezy value of 65 m^{1/2}/s for roughness, with the last three determined by sensitivity analyses of the model for these three grain sizes and bed slopes. Because the goal of the modeling did not include investigating morphological change to the seafloor specifically, bed updating to affect the hydrodynamics was suppressed. All model results were examined after a 24-hr model spin-up period was completed. The simulations stabilized hydrodynamically and showed negligible variability in velocities and water levels. Sediment transport and deposition time series began after the spin-up period.

4.3.4.1 Uncertainty in Modeling

Predictions of geomorphology and sediment transport contain many uncertainties. Haff (1996) categorized seven sources of uncertainty for geomorphic modeling as model imperfection, omission of important processes, lack of knowledge of initial conditions, sensitivity to initial conditions, unresolved heterogeneity, occurrence of external forcing, and inapplicability of the factor of safety concept. The limitations for this modeling effort fall into three of these categories. The first is model imperfection in terms of design and operation. Computational effort was considered when determining the minimum size cell that allowed the expected coastal processes to be represented in a time step that permitted

fast simulation times. The decision to pursue a 2DH model, also for computational considerations, removed the potential for vertical structure and upwelling, processes that have been observed at other headlands (Warner and MacCready, 2009), as well as wave-driven undertow circulation. The omission of important processes, the second category, includes exclusion of wind variability (e.g., wind opposing the wave field), multiple sediment grain size interactions that may affect bed armoring (Reed et al., 1999), and near-bed hydrodynamic effects from bathymetric changes due to sediment deposition. The last two processes were not employed in the modeling to retain the focus on water column transport of suspended sand, although both processes would be expected to reduce the volumes of sediment mobilized during the simulations. The third category is sensitivity to initial conditions, which received some attention through the adjustment of the bed type from sandy to reef, but also could have been addressed through additional models built from the list in Table 4.1. Initial equilibrium bed morphology could have been generated through preliminary modeling but, because the small-scale near-bed hydrodynamic processes were not the focus of this study, a simple initial bed was chosen to investigate the research questions.

4.3.5 Analysis Approach

Several types of model output were used to characterize the results including 1) spatial patterns of velocity, bed shear stress, and sediment deposition, 2) cumulative total sediment volume through 2.5 km long cross-shore transects located near the northern and southern intersections of the beach and headland, hereafter called the headland shoulders, and at the apex of the headland, and 3) observations of instantaneous data related to

forcing terms and sediment transport along a transect 400 m offshore that roughly followed the core of the fastest alongshore velocities on the upstream side of a headland.

An analytical framework was developed to address the six questions targeting the factors (see Section 2.3). The following series of dimensionless relationships were constructed to quantify the sensitivity of bypassing to the test parameters. For these equations, L = least wave power, M = most wave power, D = direct waves, O = oblique waves, and C = regional current.

4.3.5.1 Morphology

The morphology test compared the effect of the headland shape and size on topographic steering of flow and sediment deposition under the same oceanographic forcing using the same sediment composition. To test the headland effect on flow, the total area where $U > 0.5$ m/s in the model domain was normalized by the total available area. The threshold of 0.5 m/s was chosen based on Shields parameter calculations in which 0.49 m/s was found to mobilize the coarsest modeled grain size. The ratio between two different headlands ($M_{factor1}$) indicated which headland causes a larger effect on flow by enhancing velocities for the same forcing condition (4.3) where $M_{factor1} > 1$ indicated headland1 has a larger effect on flow, $M_{factor1} = 1$ indicated headlands have equal effect on flow, and $M_{factor1} < 1$ indicated headland2 has a larger effect on flow.

$$M_{factor1} = \frac{\left(\frac{\sum \text{area } U > 0.5 \text{ ms}^{-1}}{\text{available area}} \right)_{\text{headland1}}}{\left(\frac{\sum \text{area } U > 0.5 \text{ ms}^{-1}}{\text{available area}} \right)_{\text{headland2}}} \quad (4.3)$$

For the two sediment-based morphology tests, a threshold > 0.1 m of deposition was chosen through sensitivity analysis. The total deposited volume and area of

deposition was calculated in a region extending 250 m to 2,750 m from the shoreline and alongshore from $\frac{1}{4}$ headland width upstream of the headland to $\frac{1}{4}$ headland width downstream of the headland. The 250 m value is chosen to exclude most of the surfzone (70% of waves breaking inshore of this line on the upstream side of the headlands for the large wave power and oblique wave angle conditions). Alongshore extent was determined through sensitivity analysis. This region was selected to focus on the headland zone within the overall model domain by minimizing the beach processes on the calculation.

For the first test of the headland effect on sediment transport, the ratio between volume deposited off two different headlands ($M_{factor2}$) indicated which headland causes a larger effect on deposition for the same forcing condition, as given in Equation (4.4), where $M_{factor2} > 1$ indicated headland1 has a larger effect on volume deposited, $M_{factor2} = 1$ indicated headlands have equal effect on volume deposited, and $M_{factor2} < 1$ indicated headland2 has a larger effect on volume deposited.

$$M_{factor2} = \frac{(\text{volume deposited})_{headland1}}{(\text{volume deposited})_{headland2}} \quad (4.4)$$

For the second test on the headland effect on sediment transport, the ratio between area of deposition off two different headlands ($M_{factor3}$) indicated which headland causes a larger effect on area of deposition for the same forcing condition, as given in Equation (4.5), where $M_{factor3} > 1$ indicated headland1 supported a larger area of deposition, $M_{factor3} = 1$ indicated headlands have equal effect on area of deposition, and $M_{factor3} < 1$ indicated headland2 has a larger effect on area of deposition.

$$M_{factor3} = \frac{(\text{area of deposition})_{headland1}}{(\text{area of deposition})_{headland2}} \quad (4.5)$$

4.3.5.2 Oceanography

The oceanography test compared the effect of different oceanographic forcing on sediment deposition for a headland using the same sediment composition. To test the different oceanographic forcing, the difference in cumulative sediment volume transported through the two transects on the headland shoulders (Δvolume) was calculated to index sediment bypassing for the grain sizes under each forcing scenario. Testing how the different ocean conditions (wave height, wave period, wave direction, and regional current) influence sediment bypassing around the same headland utilized three relationships. The first factor, $O_{factor1}$, compared the bypassing between the direct and oblique waves, as given in Equation (4.6), where $O_{factor1} < 1$ indicated more bypassing under oblique waves, $O_{factor1} = 1$ indicated equal bypassing for the two wave angles, and $O_{factor1} > 1$ indicated more bypassing by direct waves.

$$O_{factor1} = \frac{\Delta\text{volume}_{MD}}{\Delta\text{volume}_{MO}} \quad (4.6)$$

The second factor, $O_{factor2}$ compared the bypassing between the least-power and most-power wave conditions, as given in Equation (4.7), where $O_{factor2} < 1$ indicated more bypassing under the most-power waves, $O_{factor2} = 1$ indicated equal bypassing for the two wave power values, and $O_{factor2} > 1$ indicated more bypassing under the least-power waves.

$$O_{factor2} = \frac{\Delta\text{volume}_{LO}}{\Delta\text{volume}_{MO}} \quad (4.7)$$

The third factor, $O_{factor3}$ compared the bypassing between oblique waves with the addition of a regional current and oblique waves only, as given in Equation (4.8), where

$O_{factor3} < 1$ indicated more bypassing without the current, $O_{factor3} = 1$ indicated the current had no effect, and $O_{factor3} > 1$ indicated more bypassing with the current.

$$O_{factor3} = \frac{\Delta\text{volume}_{MO+C}}{\Delta\text{volume}_{MO}} \quad (4.8)$$

4.3.5.3 Sedimentology

The sedimentology test compared the effect of different sediment grain sizes and sediment availability on sediment deposition for a headland under the same oceanographic forcing. The test for how different sized sand fractions respond to identical morphological and oceanographic conditions is related primarily to particle settling velocity and total bed shear stress. Using the same results generated for Equation (4.4), $S_{factor1a}$ and $S_{factor1b}$ describe the ratio of volume deposited between different grain sizes for a given headland, as given by Equation (4.9), where $S_{factor1a} > 1$ indicated that a larger volume of fine sand is deposited than fine-medium sand and $S_{factor1b} > 1$ indicated that a larger volume of medium sand is deposited than fine-medium sand.

$$S_{factor1a} = \frac{(\text{volume deposited})_{125\mu m}}{(\text{volume deposited})_{250\mu m}} \quad (4.9)$$

$$S_{factor1b} = \frac{(\text{volume deposited})_{500\mu m}}{(\text{volume deposited})_{250\mu m}}$$

Similarly, the results calculated for Equation (4.5) were used to determine $S_{factor2a}$, and $S_{factor2b}$ based on the ratio of area of deposition between different grain sizes, as given by Equation (4.10), where $S_{factor2a} > 1$ indicated that fine sand is deposited over a larger area than fine-medium sand and $S_{factor2b} > 1$ indicated that medium sand is deposited over a larger area than fine-medium sand .

$$S_{factor\ 2a} = \frac{(\text{area of deposition})_{125\ \mu m}}{(\text{area of deposition})_{250\ \mu m}} \quad (4.10)$$

$$S_{factor\ 2b} = \frac{(\text{area of deposition})_{500\ \mu m}}{(\text{area of deposition})_{250\ \mu m}}$$

To test the effect on bypassing from sediment availability adjacent to a headland, the ratio $S_{factor3}$ between the volume deposited for a sandy bed and for a reefed headland (4.11) was developed using the results generated for (4.4) where $S_{factor3} < 1$ indicated the reefed headland caused larger volumes of deposition, $S_{factor3} = 1$ indicated the two substrates caused equal volumes of deposition, and $S_{factor3} > 1$ indicated the sandy bed caused larger volumes of deposition.

$$S_{factor\ 3} = \frac{(\text{volume deposited})_{MO\ sandy\ bed}}{(\text{volume deposited})_{MO\ reefed\ headland}} \quad (4.11)$$

Similarly, the results calculated for Equation (4.5) were used to determine $S_{factor4}$, the ratio of area of deposition between the headland substrate types, as given by Equation (4.12), where $S_{factor4} < 1$ indicated the reefed headland caused deposition over a larger area, $S_{factor4} = 1$ indicated the substrates caused deposition over equal areas, and $S_{factor4} > 1$ indicated the sandy bed caused deposition over a larger area.

$$S_{factor\ 4} = \frac{(\text{area of deposition})_{MO\ sandy\ bed}}{(\text{area of deposition})_{MO\ reefed\ headland}} \quad (4.12)$$

4.3.5.4 Overall Bypassing

To investigate the cumulative morphological, oceanographic, and sedimentological influences on sediment bypassing a headland, the ratio of total sediment volume transported through the northern (or updrift) and southern (or downdrift) shoulder transects, $\beta_{headland}$, was calculated as

$$\beta_{\text{headland}} = \frac{\text{volume}_{\text{downdrift}}}{\text{volume}_{\text{updrift}}}, \text{ where } \beta_{\text{headland}} = \begin{cases} > 1 & \text{bed eroded} \\ = 1 & \text{unconstrained} \\ 0-1 & \text{constrained} \\ = 0 & \text{blocked} \\ < 0 & \text{opposed pathways} \end{cases} \quad (4.13)$$

The categories used in (4.13) are graphically depicted in Figure 4.4 and defined as the following:

- Bed eroded – sediment flux is larger across the downdrift shoulder, indicating bed erosion in front of the headland is supplying sediment
- Unconstrained – sediment flux is continuous and uninterrupted by the headland
- Constrained – sediment flux is reduced between the updrift and downdrift shoulders by the headland
- Blocked – sediment flux from the updrift to downdrift shoulder is prevented by the headland
- Opposed Pathways – bypassing does not occur due to divergent (convergent) flow at the shoulders that direct sediment away (toward) the headland apex with no sediment being transported past the headland.

4.3.5.5 Forcing Terms

Model output from D3D and SWAN includes basic hydrodynamic parameters such as water levels, velocities, bed shear stresses, and wave characteristics (H_s , T_p , θ_{dom} , and L). Whereas the current data were sufficient to characterize flow, the wave characteristics were used to calculate two more informative parameters regarding wave forcing. Wave power, P (W/m), can be used to describe the overall energy flux available from waves to mobilize sediment and is calculated as

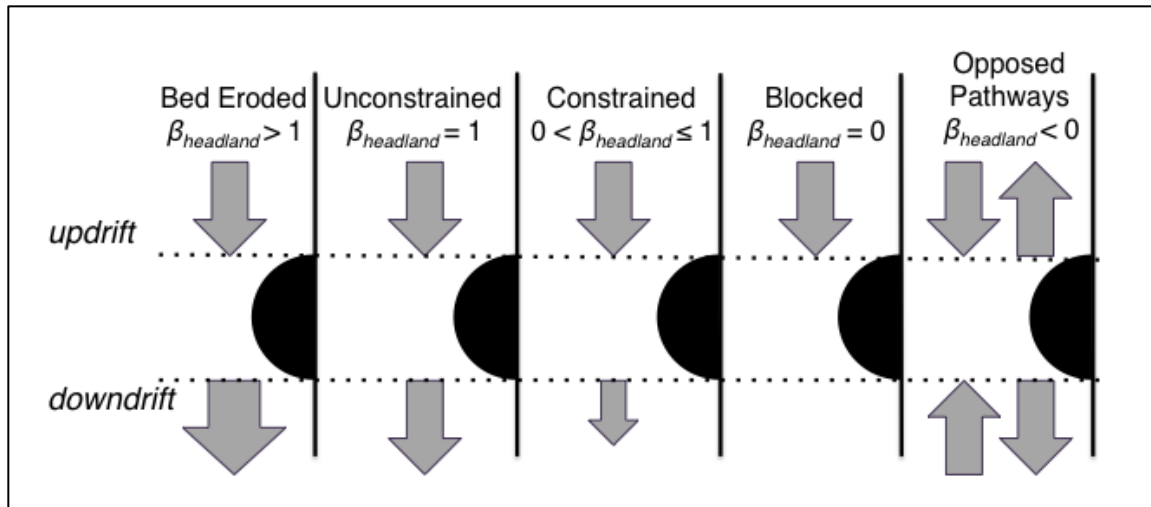


Figure 4.4. Schematic depicting categories of $\beta_{headland}$ as defined in Equation (4.13).

$$P = E \frac{C}{2} = \frac{1}{8} \rho g H_s^2 \frac{C}{2} = \frac{1}{16} \rho g H_s^2 C \quad (4.14)$$

where ρ is water density, g is gravity, and C is velocity of propagation in deep water, (Kamphuis, 2010). Part of this power is available to force alongshore flow, and this is known as the alongshore radiation stress S_{xy} given as

$$S_{xy} = EnC \cos(\alpha_s) \left(\frac{\sin(\alpha_s)}{C} \right) = En \sin(2\alpha_s) \quad (4.15)$$

where n is the energy flux parameter defined as $n = \frac{1}{2} \left[1 + \frac{2kd}{\sinh 2kd} \right]$ with k as the wave number and d as water depth, and α_s is the angle of waves relative to the shore, with 90° indicating shore-normal waves (Dean and Dalrymple, 2002).

4.4 Results

The modeling results are presented in three sections. The first provides a general overview based on patterns of flow and sediment transport volumes. The second section addresses the overarching research questions by describing the findings from analysis of the factors. The third section provides understanding of the patterns and factors through analysis of forcing terms and the sediment response along a transect for a subset of simulations.

4.4.1 General Current and Deposition Patterns

The “tides only” baseline simulations showed the slowest currents (< 0.10 m/s) throughout the domain without any distinguishing flow patterns by the headland, so this scenario will not be further presented. When waves were added, the direction of flow was

determined primarily by the incident wave angle, whereas the velocity was related to wave size and period (Figure 4.5). The two least-energy wave conditions caused localized currents < 1 m/s, but in different areas depending on the wave angle. Direct waves enhanced velocities at headland shoulders, particularly for the broad headlands where jets develop at 45° to the shoreline. This contrasted with the oblique waves, which caused southward currents at the beaches moving at approximately 1 m/s upstream of the headlands. The two most-energy wave conditions produced substantially faster currents that extended across larger portions of the model domain. The patterns are similar between least and most energy direct waves with distinct jets separating at the headland shoulders, but the currents exceed 2 m/s on the sides of the headlands under the most energy conditions. This contrasts with the circulation patterns from oblique waves, which varied by headland. The flow around the small/medium headland (T1) remained connected from the updrift to downdrift sides. Disruption of the flow and formation of an offshore rip current occurred at the upstream headland shoulder for the small/broad (T6), medium/sharp (T7), and large/broad (T8) headlands. The angle of the rip current axis to the shore was roughly 90° , 75° , and 45° , respectively. On the downstream side of T7 and T8, eddies formed with flow reversed toward the apex.

Sediment flux volumes were sensitive to grain size with decreasing amounts as the sediment size increased (Figure 4.6). Total volume for the transects at the two headland shoulders showed the smallest amounts of sediment transport occurred during the two least-power wave conditions, regardless of wave angle. These volumes were 1-3 magnitudes smaller than that transported during the most-power wave conditions. The influence of the wave angle was more evident during the most-power wave conditions

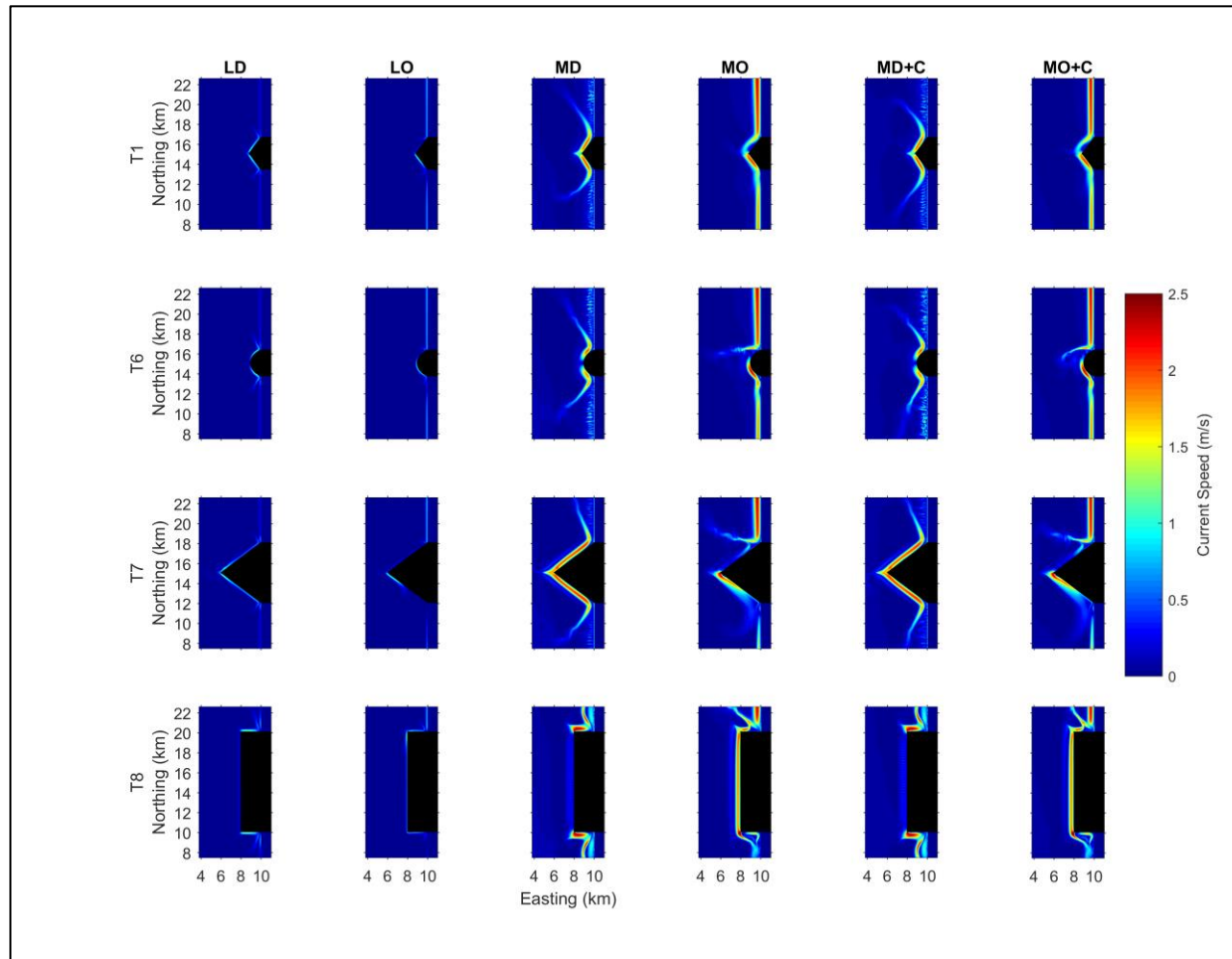


Figure 4.5. Model results of current speed for waves only and for waves with a regional current forcing during the fastest velocity timestep where L = least wave power, M = most wave power, D = direct wave angle, O = oblique wave angle, and C = regional current.

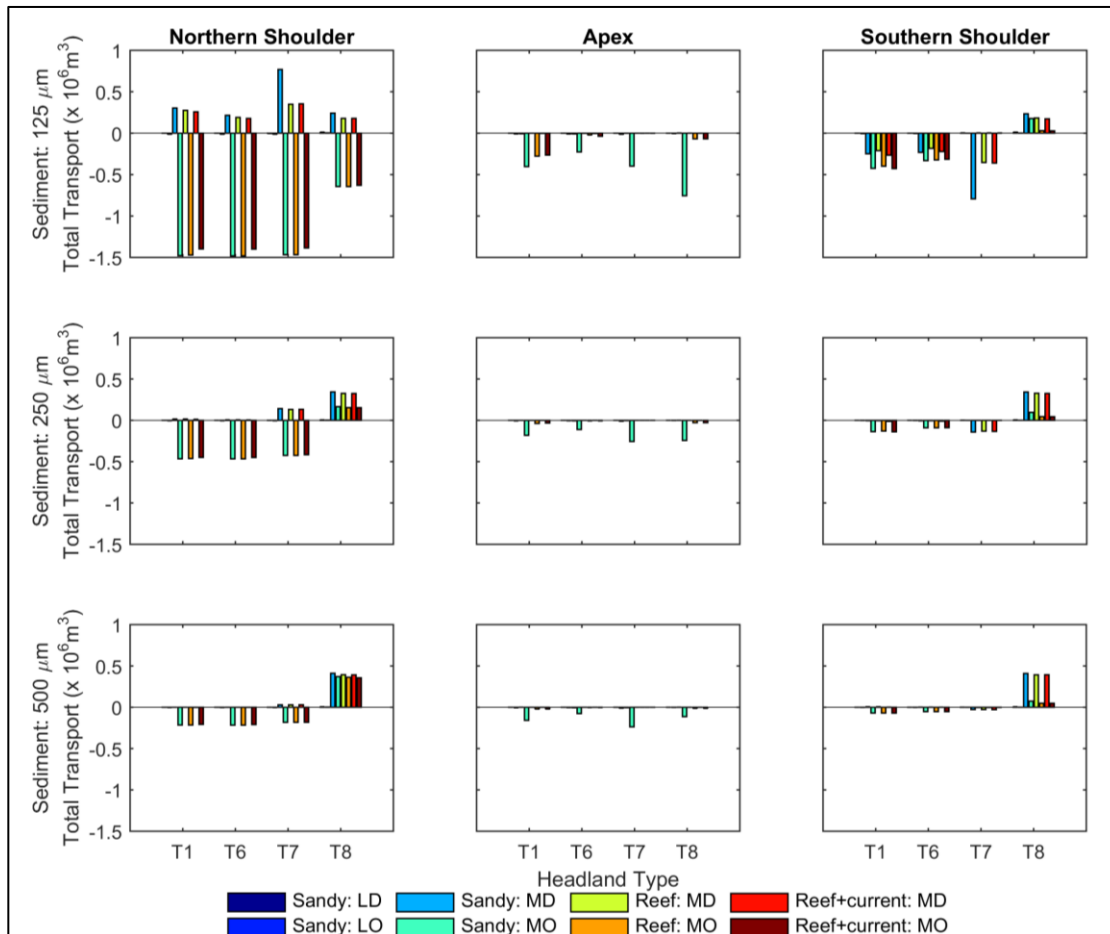


Figure 4.6. Cumulative total transport of the three grain sizes through a 2.5 km long cross-shore transect on the northern and southern headland shoulders and through a transect at the headland apex. Results from the baseline simulation were excluded, as sediment transport volumes were negligible. Positive transport is northward.

with the flow of sediment from the updrift to downdrift sides under the oblique angle and away from the headlands under the direct angle. The deposition zones aligned with where the high velocity jets decelerated and sediment settled from suspension (Appendix A.3). The only headland that appeared to allow sediment bypassing in a continuous stream was T1 under oblique waves and for the fine sand class only; all others showed discontinuous sediment transport between the updrift to downdrift sides of the headland.

Graphical results of bed shear stress and deposition patterns can be found in Appendices A.2 and A.3, respectively.

4.4.2 Analysis of Key Factors

4.4.2.1 Morphology

The tests for morphology focused on how the size and shape of the headlands affected the topographic steering of flow and sediment deposition patterns. Visual inspection of spatial patterns found that the direct wave angle conditions generated nearly symmetrical configurations of either flow or sediment deposition, prompting a focus on oblique waves for testing the effect of morphology on sediment transport past headlands (Figure 4.5).

Ratios for $M_{factor1}$ (flow patterns) under the least-power wave conditions showed wide variability among the headlands (Table 4.6) with only T1 and T8 near unity. Headland T1 caused 2.5 times more area of enhanced velocity than T6 but only 0.57 of the area of T7, whereas T6 caused smaller areas than T7 and T8 by 0.23 and 0.38, respectively. Headland T7 generated 1.7 times more area than T8 for the same wave condition. The variability was greatly reduced under the most-power wave conditions with T1-T6 and T6-T7 just slightly above unity whereas T1 caused 1.2 times more area

Table 4.6. Ratios* for $M_{factor1}$ (see Equation (4.3))

Oblique Angle		Least-Power Waves			
		T1	T6	T7	T8
Most-Power Waves	T1		2.50	0.57	0.96
	T6	1.08		0.23	0.38
	T7	1.20	1.11		1.68
	T8	0.75	0.69	0.62	

* - Upper-right portion of matrix gives ratios for least-power wave relationships and the low-left portion of matrix gives ratios for most-power wave relationships.

than T7. On the opposite side, T8 was consistent in causing approximately 0.70 times of the area of the other three headlands. Taking the two wave conditions together, $M_{factor1}$ suggested that blocky headlands cause more disruption than pointed ones and large headlands cause more disruption than small ones. The two sediment related morphology factors focused on the volume deposited and the area of deposition. Ratios for $M_{factor2}$ (volume deposited) were similar across the three grain sizes with T1 and T6 causing the least and T8 causing the most deposition when the headlands were compared to each other (Table 4.7a). The ratios for $M_{factor3}$ (area of deposition) showed that T7 and T8 caused more than 40% more deposition than either T1 or T6 (Table 4.7b). Taken together, these two factors showed that larger headlands caused more deposition over larger areas than the smaller headlands, regardless of the shape.

4.4.2.2 Oceanography

The three oceanography factors focused on how changing wave power, wave angle, and the presence of a regional current influence the sediment bypassing between the headland shoulders (Table 4.8). The ratios for $O_{factor1}$ (different wave angles) were near 0 for T1, T6 and T7, which indicated that direct waves prevent sediment from transiting across the headland, regardless of grain size. However, $O_{factor1}$ for T8 showed non-zero values (0.54, 5.98, and 2.50 for fine, fine-medium, and medium grain sizes, respectively). The direct waves on the large blocky headland allowed flux through the headland shoulder transects with coarser material more mobile than fine sand. The ratios for $O_{factor2}$ (different wave power) were near 0 for all headlands and grain sizes, showing that minimal sediment was mobilized during low wave power conditions. The last oceanography factor, $O_{factor3}$ (addition of regional current to large oblique waves), ranged

Table 4.7. Ratios for $M_{factor2}$ as given by Equation (4.4) – upper panel – for $M_{factor3}$ as given by Equation (4.5) – lower panel.

		Volume Deposited			
		T1	T6	T7	T8
Fine Sand	T1				
	T6	1.13			
	T7	0.73	0.65		
	T8	0.49	0.44	0.68	
Fine-Medium Sand	T1				
	T6	1.31			
	T7	0.72	0.55		
	T8	0.56	0.43	0.78	
Medium Sand	T1				
	T6	1.41			
	T7	0.69	0.49		
	T8	0.58	0.41	0.83	

		Area of Deposition			
		T1	T6	T7	T8
Fine Sand	T1				
	T6	1.44			
	T7	0.87	0.60		
	T8	0.58	0.40	0.66	
Fine-Medium Sand	T1				
	T6	1.12			
	T7	0.57	0.51		
	T8	0.36	0.33	0.64	
Medium Sand	T1				
	T6	1.39			
	T7	0.63	0.45		
	T8	0.40	0.28	0.62	

Table 4.8. Ratios for all $O_{factors}$

		$O_{factor1}$	$O_{factor2}$	$O_{factor3}$
	See:	(4.6)	(4.7)	(4.8)
Fine Sand	T1	0.06	0.02	0.90
	T6	0.01	0.01	0.94
	T7	0.00	0.01	0.94
	T8	0.54	0.00	0.97
Fine-Medium Sand	T1	0.04	0.02	0.93
	T6	0.00	0.02	0.96
	T7	0.00	0.01	0.98
	T8	5.98	0.01	1.00
Medium Sand	T1	0.03	0.03	0.94
	T6	0.00	0.03	0.96
	T7	0.01	0.02	0.99
	T8	2.50	0.00	0.98

from 0.9-1.0 for the headlands across all grain sizes. The near unity values indicated that the current did not enhance transport substantially compared to solely wave-driven transport. Most-power waves from an oblique angle is the most effective scenario for bypassing.

4.4.2.3 Sediment

The first set of sediment factors used the volume deposited and the area of deposition to test the effect on transport from grain size ($S_{factor1}$ and $S_{factor2}$, respectively). Ratios for $S_{factor1a}$ (deposition of fine sand vs. fine-medium sand) were approximately double ranging from 1.73 to 2.01, whereas for $S_{factor1b}$ (deposition of medium sand vs. fine-medium sand) the ratios ranged 0.81 to 0.87 indicating less mobility for medium sand (Table 4.9a). It is important to consider that the deposition of fine sand was larger due to more being in transport. When the ratios for the headlands were averaged and converted to percentages, 85% more fine sand is deposited than fine-medium and 18% more fine-medium is deposited than medium sand. The two blocky headlands (T6 and T8) caused more deposition of fine sand than the pointed headlands but all four headlands caused similar deposition for the two coarser grain sizes. The ratios for $S_{factor2a}$ (deposition of fine sand vs. fine-medium sand) ranged from 2.12 to 3.37, whereas for $S_{factor2b}$ (deposition of medium sand vs. fine-medium sand) the ratios ranged 0.65 to 0.82. The widespread range for $S_{factor2a}$ was due to bimodal grouping of the small headlands (T1 and T6) on the upper half of the range and the larger headlands on the lower half. Averages showed 158% more deposition for fine sand than fine-medium and 26% more deposition for fine-medium than medium sand. Viewing both factors together revealed that 1) the ratio between fine sand mobility and fine-medium sand mobility was 2-3 times

Table 4.9. Ratios for (a) $S_{factor1}$ and $S_{factor2}$ and (b) $S_{factor3}$ and $S_{factor4}$.

(a)	Grain Size Comparison			
	$S_{factor1}$		$S_{factor2}$	
See:	(4.9)a	(4.9)b	(4.10)a	(4.10)b
T1	1.73	0.84	3.37	0.82
T6	2.01	0.78	2.61	0.65
T7	1.70	0.87	2.21	0.73
T8	1.96	0.81	2.12	0.75
Mean	1.85±0.16	0.82±0.04	2.58±0.57	0.74±0.07

(b)	Substrate Comparison		
		$S_{factor3}$	$S_{factor4}$
See:	(4.11)	(4.12)	
Fine Sand	T1	1.44	1.27
	T6	1.62	1.42
	T7	1.25	1.32
	T8	2.24	1.61
	Mean	1.64±0.43	1.41±0.15
Fine-Medium Sand	T1	1.80	2.24
	T6	2.21	2.27
	T7	1.32	1.57
	T8	2.78	1.84
	Mean	2.03±0.62	1.98±0.34
Medium Sand	T1	2.02	2.56
	T6	2.51	3.04
	T7	1.53	1.90
	T8	2.86	1.88
	Mean	2.23±0.58	2.34±0.56

larger than the ratio between fine-medium sand mobility and medium sand mobility; and 2) the blocky headlands caused more deposition while the small headlands caused more deposition of fine sand.

The second set of sediment factors used the volume deposited and the area of deposition to test the effect on transport from differing bed conditions adjacent to the headland ($S_{factor3}$ and $S_{factor4}$, respectively) (Table 4.9b). The ranges of ratios for $S_{factor3}$ varied by grain size with 1.25-2.24 for fine sand, 1.32-2.78 for fine-medium sand, and 1.53-2.86 for medium sand. T7 showed the smallest and T8 the largest ratios consistently for all grain sizes. Flux was larger from sandy beds than reefed headlands although it also increased with the size of the sediment. The ranges of ratios for $S_{factor4}$ varied differently than those for $S_{factor3}$ with 1.27-1.61 for fine sand, 1.57-2.27 for fine-medium sand, and 1.88-3.04 for medium sand. While there was more deposition from a sandy bed than a reefed headland, no discernable pattern related to the morphology of the headlands was identifiable. From this second set of sediment factors, flux was observed to be higher from sandy beds, but the localized effects of sediment transport and the alongshore littoral drift were not able to be separated.

4.4.2.4 Overall Bypassing

The ratio of the sediment transport volumes through the northern and southern cross-shore transects ($\beta_{headland}$) showed the influence of the headland morphologies for the varying grain sizes, bed type, and wave/current conditions on sediment bypassing (Figure 4.7). The most consistent observation for $\beta_{headland}$ related to direct waves, which led to opposing pathways for fine and fine-medium sand at headlands T1, T6, and T7. Headland T1 constrained sediment flux for oblique wave conditions for all grain sizes and bed

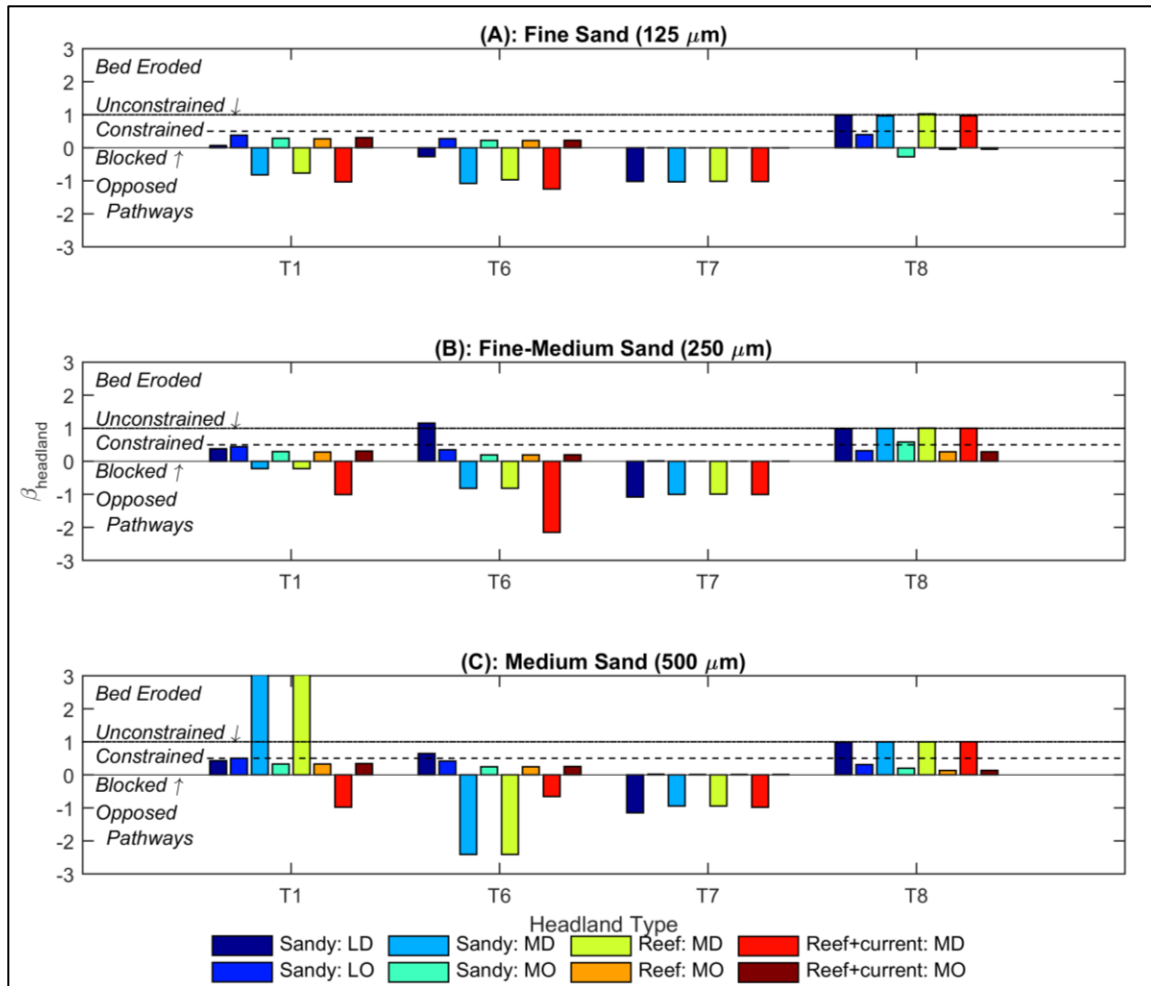


Figure 4.7. Sediment bypassing ratios between northern and southern shoulders for (A) fine sand (125 μm), (B) fine-medium sand (250 μm), and (C) medium sand (500 μm) under variable forcing conditions and substrates (Table 4.2). The no-wave scenario was not included as sediment transport volumes were negligible. The dashed line indicates $\beta_{\text{headland}} = 0.5$ as a division inside the “constrained” zone. See Equation (4.13) for definitions of β_{headland} categories.

types; for medium sand, the bed eroded under direct waves except when the regional current caused opposed pathways. Headland T6 showed similar patterns as T1 for fine and fine-medium sand, although $\beta_{headland}$ was twice as large for opposed pathways for fine-medium sand. Medium sand at T6 was constrained 75% more when the regional current was added to the large direct wave conditions. Headland T7 consistently blocked the transport across grain sizes and bed types for both wave directions. Headland T8 was the only headland to show unconstrained conditions when transport was equal on either side of the morphological feature, which occurred for all grain sizes and bed types under direct waves. Under oblique waves, transport was constrained consistently by T8 for the larger grain sizes and blocked for the fine sand. The T8 observations may be an artifact of the transects being placed farther from the headland shoulders and therefore incorporating more beach processes than the other headlands.

4.4.3 Forcing Terms and Sediment Response

Using the results from the analysis of the factors, the reefed headland under the most-power waves from the oblique angle without a regional current was selected for investigation into how the forcing terms affect sediment bypassing. The water level, current, wave, and sediment observations extracted from the alongshore transect 400 m offshore revealed sharp differences among the morphologies as described below.

4.4.3.1 Headland T1 – small size, medium point

This transect was approximately 4,500 m long with the parameters varying across the entire transect (Figure 4.8a). The water level set up less than 0.15 m against the northern shoulder of the headland and decreased across the remainder of the headland. Current velocities, U , were southerly and fastest (2 m/s) upstream of the northern

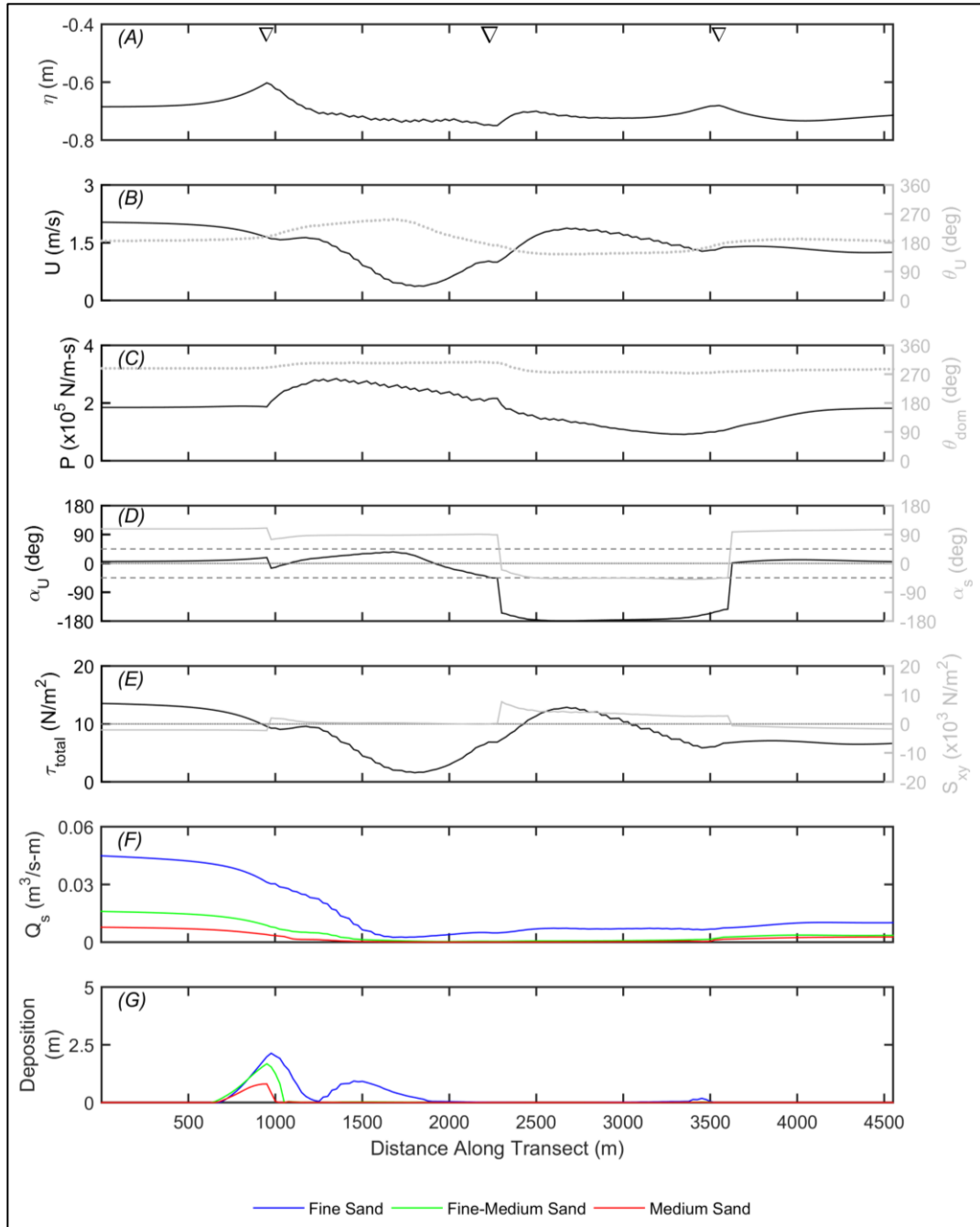


Figure 4.8 (a) Model observations for headland T1 with adjacent rocky reef from an alongshore transect 400 m offshore that ran $\frac{1}{4}$ the length of the headland upstream to downstream during the time step of fastest velocity. The headland apex is marked by the large triangle in the center and the headland shoulders as the two smaller triangles in panel A. The dashed lines in panel D indicate 45° and -45° . Parameters shown are (A) water level, (B) current speed and direction (180° = southward), (C) wave power and wave direction (270° = from west), (D) current and wave angle relative to the shoreline (0° = current or wave shore parallel; 90° = shore-normal), (E) total bed shear stress from combined waves and currents, and radiation stress from waves, (F) total sediment flux for fine (blue), fine-medium (green) and medium (red) sand, and (G) total sediment deposition (same colors).

shoulder but slowed to less than 0.5 m/s and redirected to the southwest-west along the northern face of the headland; at the apex and south, velocities increased to approximately 1 m/s and re-established a southerly flow. Wave power, P , was constant at 2.0×10^5 N/m-s upstream of the northern shoulder and peaked at approximately 3.0×10^5 N/m-s on the shoulder. Wave power then decreased across the northern face of the headland and hit a nadir of less than 1.0×10^5 N/m-s on the southern face; downstream of the headland, P returned to 2.0×10^5 N/m-s. Wave direction was fairly consistent from the west at 270° , indicating a refraction from the input oblique angle of 345° . However, the incident angles of the current (α_U) and waves (α_s) (the angle of either adjusted to be relative to the shore instead of true north) revealed distinctive alongshore segments: updrift/downdrift of the headland showed $\alpha_U=0^\circ$ (alongshore current towards the south) and $\alpha_s=90^\circ$ (shore-normal waves), on the northern face the flow angle α_U varied between -45° and 45° and wave angle $\alpha_s=75^\circ$, whereas on the southern face the flow angle $\alpha_U=180^\circ$ (reversed alongshore current) and the wave angle is between 0° and 180° , which is not real. The shear stress exerted on the bed by the combined waves and current, τ_{total} tracked the pattern of U , with consistent bed stress upstream of the headland, decreased τ_{total} on the northern face, and increased τ_{total} on the southern face and unchanging but reduced values downstream of the headland. The alongshore radiation stress by the waves with respect to the shoreline, S_{xy} , followed the relative angle closely by switching direction when α_s shifted from $>90^\circ$ to $<90^\circ$. For example, between 90° and 180° , S_{xy} is negative (southward) and between 0° and -90° , S_{xy} is positive (northward); when $\alpha_s = 90^\circ$, $S_{xy} = 0$. The sediment response to the spatially varying hydrodynamics was captured in the suspended sediment flux, Q_s , which decreases as flow decreases, representing a flux

convergence that results in deposition height on north side of the headland. Fine sand transport was more than 2 times the flux of the next larger grain size. This sediment fraction remained in suspension along the entire transect representing continuous transport, although it approached zero along the northern face at the same location as the slowest U and lowest τ_{total} before increasing. This contrasted with flux of the other two sediment sizes that decreased to 0 along the northern face and remained so until the southern shoulder of the headland. Accompanying the flux variability were accumulations of sediment on the northern side of the headland where U slowed, τ_{total} decreased, and Q_s began to decline. Deposits of fine sand were the largest (peak of 2.5 m) and medium sand the smallest (peak of 0.5 m).

4.4.3.2 Headland T6 – small size, broad point

This transect was approximately 5,500 m long (Figure 4.8b). The water level set up approximately 0.10 m against the northern shoulder of the headland and decreased by 0.20 across the northern face; it increased on the southern shoulder by 0.10 but remained lower on the downstream side than the upstream one. Current velocities, U , were southerly and fastest (2 m/s) upstream of the northern shoulder but slowed to near 0 m/s and alternated in direction between south and west along the northern face of the headland; at the apex and downstream, velocities increased to approximately 1 m/s and re-established a southerly flow. Wave power, P , was constant at 1.5×10^5 N/m-s upstream of the northern shoulder, increased to approximately 3.0×10^5 N/m-s on the shoulder and stayed elevated almost the length of the headland before returning to 1.5×10^5 N/m-s on the downstream side. Similar to T1, wave direction was fairly consistent from the west at 270° . The incident angles of the current (α_U) and waves (α_s) showed three alongshore

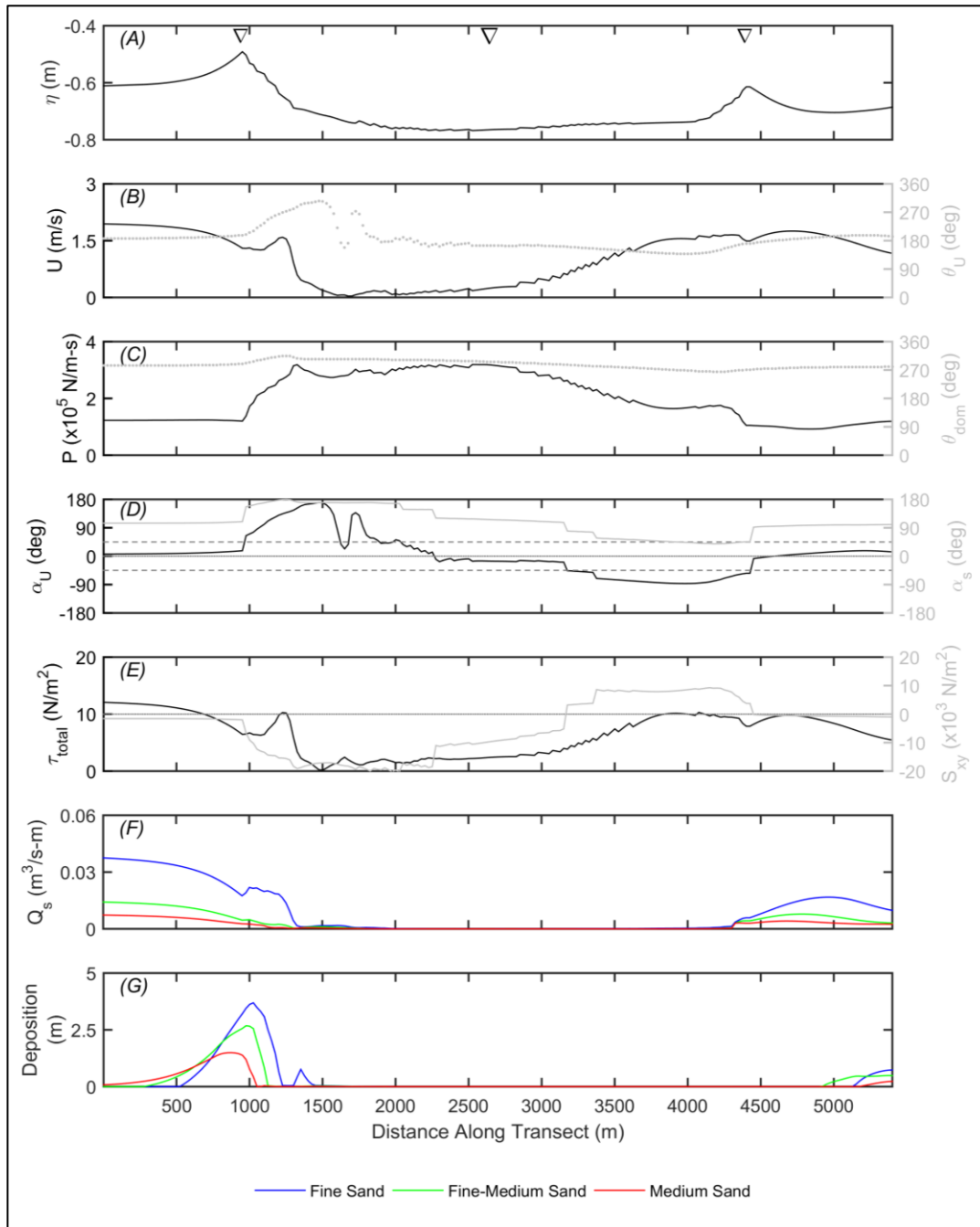


Figure 4.8(b) Same as (a) for T6.

segments with the upstream and downstream sections at $\alpha_U=0^\circ$ and $\alpha_s=90^\circ$ while the middle section exhibited a gradual shift in α_s from 180° to 45° and in α_U from 180° to -90° . The shear stress, τ_{total} followed similar trends as U , although τ_{total} remained above 0 where U was nearly zero, due to waves. Radiation stress, S_{xy} , changed direction where the relative angle shifted at the shoulders and apex; it was large ($-20,000 \text{ N/m}^2$) on the northern face and gradually shifted to be positive on the southern face past the apex. Fine sand flux was again more than 2 times that of the next larger grain size on the upstream side but then decreased to 0 across the face of the headland for all sediment. Transport increased again starting at the southern shoulder at rates half as large as the upstream side. Similar to T1, the accumulation of sediment on the northern side of the headland coincided where U slowed, τ_{total} decreased, and Q_s began to decline with deposits of fine sand more than 3 m over a smaller area and deposits of medium sand less than 2 m over a larger area.

4.4.3.3 Headland T7 – medium size, sharp point

This transect was longer than 10,000 m and showed contrasting zones upstream and downstream of the apex (Figure 4.8c). The water level set up approximately 0.10 m against the northern shoulder of the headland and rapidly decreased by 0.30 across the first 1,000 m of the northern face. It then increased gradually towards the apex before dropping 0.20 m at the apex and remaining constant. Current velocities rapidly decreased from 2 m/s to near 0 on the upstream side of the apex, accelerated to 2 m/s at the apex and then slowed to near 0 m/s at the end of the transect. Current direction changed from south to north along the northern face; at the apex and along the south face, direction re-established a southerly flow before a brief segment of northerly flow at the southern

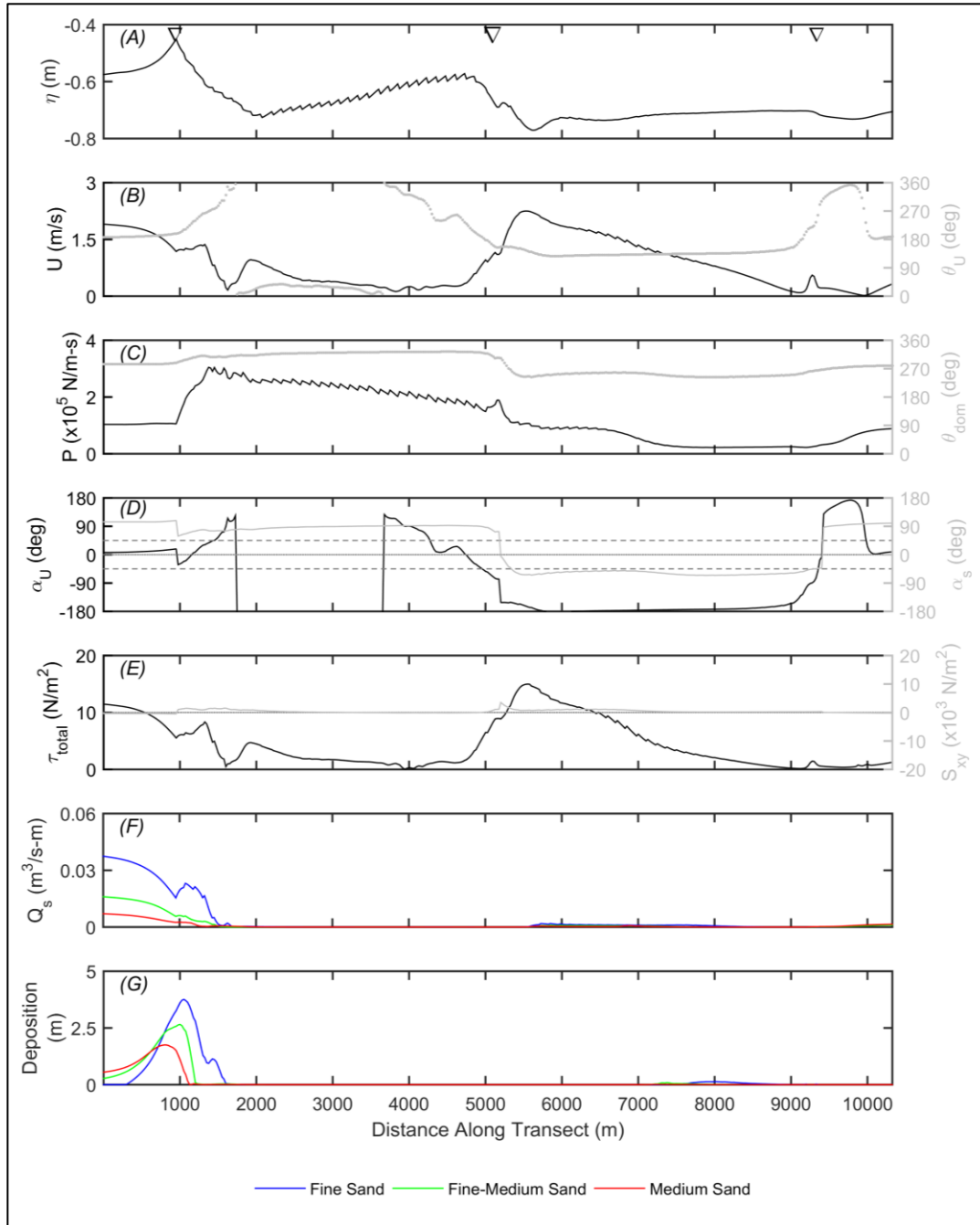


Figure 4.8(c) Same as (a) for T7.

shoulder. Wave power almost doubled from 1.0×10^5 N/m-s to 3.0×10^5 N/m-s across the northern shoulder and gradually decreased to near 0 on the southern face; P remained lower downstream. Wave direction was bimodal at 315° on the northern half of the headland and from the west at 270° on the southern half. The incident angle of the current reflected the flow reversals with α_U changing between 0° , -180° and 90° along the transect. In contrast, α_s was a contrast across the apex with the northern half at 90° and the southern half at -45° before returning to 90° south of the shoulder. Shear stress was lower on the north face and higher on the south face, with τ_{total} approaching 0 as U decreased south of the headland. Radiation stress, S_{xy} , was weak and showed the least variability of all the headlands. The S_{xy} increased over a short segment at the apex but returned to near 0 as α_s switched between 90° and -45° . The sediment response was flux of fine sand more than 2 times that of the next larger grain size on the upstream side to the northern shoulder followed by a decrease to 0 for the remainder of the transect for all sediment. Sediment accumulated on the northern side of the headland where Q_s began to decline with deposits of fine sand more than 3 m over a smaller area and deposits of medium sand approximately 2 m over a larger area.

4.4.3.4 Headland T8 – large size, broad point

This transect was 18,000 m long with most of the variability in parameters on the northern and southern faces of the headland (Figure 4.8d). The water level set up was the largest of the headlands with approximately 0.30 m against the northern shoulder of the headland followed by a 0.35 m decrease across northern face. It then remained constant across the western face of the headland and increased 0.10 m downstream of the southern shoulder. Current velocities were around 1 m/s but varied in direction and magnitude

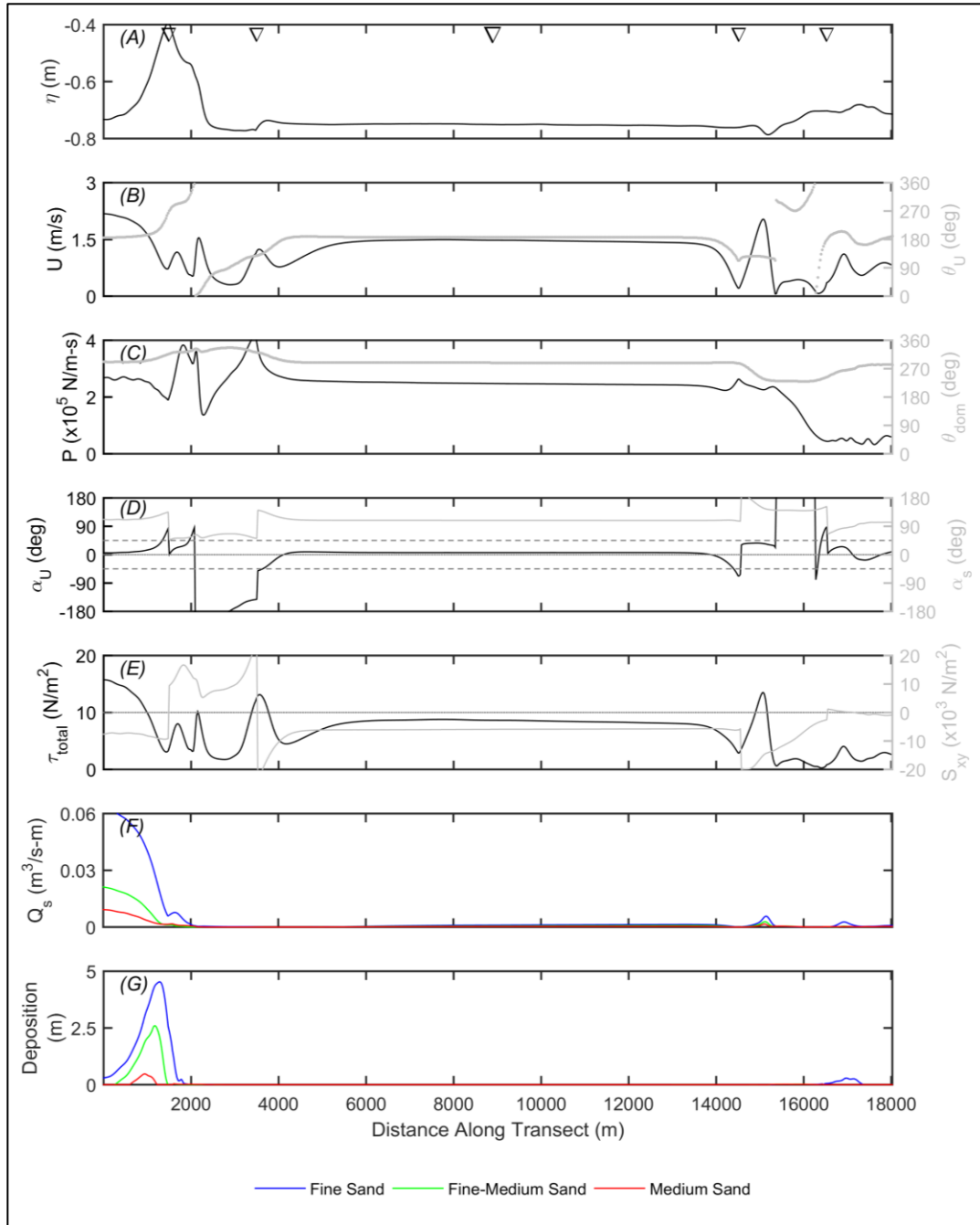


Figure 4.8(d) Same as (a) for T8 with additional markers for the corners of the headland noted in (A).

along the northern shoulder and uniform at 1 m/s across the western face; a similar flow feature (changing direction and magnitude along the transect) occurred on the southern face and a 0.5 m/s southward flow was observed downstream of the headland. The pattern on the southern corner was east and west then north and south as the transect cut through reversing flow on the downstream side of the headland. Wave power varied between 2.0×10^5 N/m-s and 4.0×10^5 N/m-s across the northern shoulder and was 3.0×10^5 N/m-s across the western face, similar to values north of the headland. On the southern face, wave power decreased to 0.5×10^5 N/m-s in the wave shadow. Wave direction was from the west at 270° for most of the headland with a 2,000 m long section of northwesterly swell on the northern face and of southwesterly swell on the southern face. Small-scale flow features are evident in the reversing direction of the current on the northern and southern faces. The incident wave angle, α_s , changed from 90° to 45° along the northern face and from 90° to 135° along the southern face; along the western face α_s was consistent at 90° . High stress locations were observed on the northern face where U varied strongly. However, stress was uniform across the western face. A peak was seen in τ_{total} on the southern shoulder but approached zero downstream of the headland, in the wave shadow. Radiation stresses, S_{xy} , were the largest of all the headlands with maxima of positive and negative $20,000$ N/m². on the north face and zero radiation stress in the wave shadow downstream of the headland. All of the sediment flux upstream of the northern face was blocked at the shoulder where deposition of fine sand was 4.5 m, fine-medium sand 2.5 m and medium sand 0.3 m. No sediment was transported along the western face although on the southern face minimal amounts of fine sand were observed in suspension and deposited on the bed.

4.5 Discussion

The spatial patterns of circulation, wave energy, sediment flux, and deposition revealed that morphology, wave angle, and sediment availability are key factors in sediment bypassing potential. The sediment grain size showed variable responses for identical conditions with fine sand the most mobile and medium sand less sensitive to the various factors that were tested. The physical forcings on the alongshore transect for the four headlands showed markedly different patterns for currents, wave power, and sediment flux that will be examined below. This section concludes with a description of limitations and improvements associated with the numerical modeling for future work.

4.5.1 Factors Affecting Sediment Bypassing

Generalizing the findings from the analysis of the factors leads to the following characterizations about the morphological and oceanographic parameters that control sediment of varying sizes bypassing a headland:

- Morphology – The set of $M_{factors}$ that were used to test size and shape of the headland showed that size is a more important parameter than shape based on the larger headlands of T7 and T8 causing more widespread disruption to flow and deposition of sediment; within the two size groups (large and small), the blockier headlands of T6 and T8 also cause more disruption than their pointed companions. This suggests that large headlands in general will be more effective at preventing sediment bypassing although a small blocky headland may also constrain bypassing.
- Oceanography – The set of $O_{factors}$ that were used to test wave angle and wave power identified that large waves at an oblique angle generated 1-2 magnitudes

more sediment flux than small waves at an oblique angle or large waves at a direct angle; the addition of a relatively slow (< 0.1 m/s) regional current did not markedly enhance flux. While oblique incident waves are known to cause higher transport (Ashton and Murray, 2006a, b), the factor analysis indicated that low and high energy conditions must be coupled with the wave angle to offer a more complete understanding of bypassing potential. The high-energy oblique conditions were selected for more in-depth analysis because they produced a more dynamic response in the models that was independent of the headland morphology.

- Sedimentology – The relationships testing sediment grain size were less informative to address the question of sediment bypassing as common knowledge of sediment dynamics already informs that finer sediment is more mobile. However, the sediment availability based on the substrate type (sandy bed vs. reefed headland) showed that distinguishing between alongshore littoral drift and localized resuspension processes is important.

4.5.2 Specifying Sediment Bypassing Potential

The $\beta_{headland}$ findings (Figure 4.7) provided a guide to generalize how sediment volume, grain size, wave conditions, and morphology combine to determine a sediment bypassing (Figure 4.9). Interpreting the $\beta_{headland}$ results leads to the following characterization of bypassing potential for the four headlands modeled in this study, although applying the descriptions to headlands found in nature would be a beneficial cross-check:

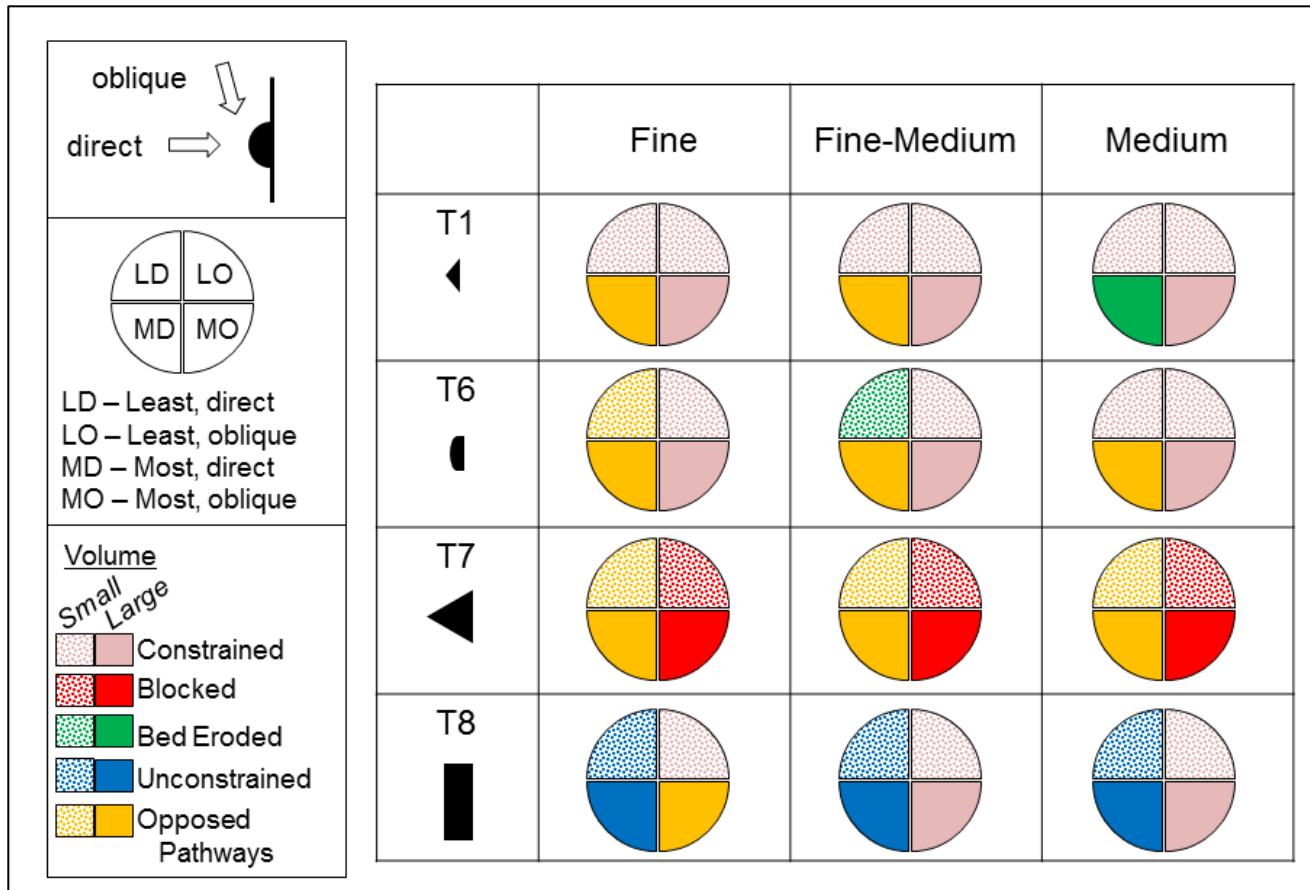


Figure 4.9. Summary of sediment bypassing a headland based on $\beta_{headland}$ for all grain sizes. See Equation (4.13) for definitions of $\beta_{headland}$ categories.

T1 headlands: constrain sediment, allows connected flow but sediment grain size is partitioned and more fine sediment is transported around apex than other sizes.

T6 headlands: constrain sediment, with decreasing efficacy as sediment grain size increases, due to fine sediment being ejected by high velocity cross-shore flow (see Figure 4.5).

T7 headlands: full block to sediment, causes deposition of littoral drift sediment on upstream face of headland by disrupting the flow and ejecting fluid in cross-shore direction.

T8 headlands: because of size, localized processes important (i.e., at corners of headland) where sediment can accrete and be mobilized with shifts in wave angle. Other segments of headland function similar to straight coastline although transport is more likely to be supply-limited rather than transport-limited due to protuberance into deeper waters outside of surfzone width.

These headland depictions improve upon the purely geomorphic descriptions of headland types presented in George et al. (2015) by adding coastal processes to the characterizations. The enhancement of the earlier descriptions allows for a more critical assessment of littoral cell boundaries in California associated with headlands, which is beyond the scope of this study. Those boundaries, initially designated by Habel and Armstrong (1978), are likely to be less robust as modern techniques are proving that boundaries are dynamic by nature. This modeling effort demonstrates that littoral cell boundaries associated with headlands can indeed exist but more processes related to

sediment bypassing should be considered with the expectation that changing conditions may temporarily erode or reinforce the efficacy of a boundary.

4.5.3 Mechanisms for Sediment Bypassing

The second question addressed in this modeling study explores how the parameters interact to enable or prevent bypassing. The observations along the shore-parallel transect identified patterns in the forcing terms and sediment responses for the large oblique wave conditions, all of which were sensitive to morphology. For example, water level set up on the northern shoulder occurred for all the headlands but was the least on T1. Headland T1 was also the only headland to allow flow to stay connected around the entire promontory and not produce a cross-shore jet (rip current). In contrast, the water level set up is the highest for T8 but also drops the most, setting up the steepest pressure gradient and, as seen in the spatial velocity fields, which stalls the alongshore flow and creates the widest and strongest cross-shore jet observed. All of the headlands showed a decrease in wave power on the downstream side of the apex (representing a wave shadow), but P was more consistent across T1 than the others. The current and wave power disruptions of alongshore current are so complete for headlands T6, T7, and T8 that they block sediment flux along the transect. This suite of observations reframes the question to what permits a smaller, pointed headland to allow sediment bypassing while a larger, broad headland impedes bypassing.

As Ashton and Murray (2006a) and many others have described, wave angle relative to the shoreline is a primary cause for alongshore sediment flux. The refraction of waves and the accompanying energy around a headland accentuates the morphological differences, as was introduced in (4.14) and (4.15). The equation for alongshore wave

power in the breaking wave zone, P_{ab} , which drives sediment transport through wave-generated momentum, is given as

$$P_{ab} = \frac{1}{16} \frac{\rho g^{3/2}}{\gamma_{sb}^{5/2}} H_b^{5/2} \sin(2\alpha_b) \quad (4.16)$$

where ρ is water density, g is gravity, γ_{sb} is the breaker index for significant waves, H_b is the breaking wave height, and α_b is the incident wave angle at breaking (Kamphuis, 2010). Of these, α_b is responsive to the different headland morphologies by changing with the various shorelines, as seen in panel D of Figure 4.8. If all other terms are held constant, $\sin(2\alpha_b)$ provides a guide about the amount of P_{ab} expected at the four modeled headlands by scaling the remaining terms between 0 (no transport) and ± 1 (maximum transport). From this calculation, the more pointed headlands (T1 and T7) will experience nearly maximum transport compared to only 50% of maximum for the broader T6 and no transport for the large, broad headland (T8) under direct waves (Table 4.10). When waves shift to be oblique, α_b shifts accordingly and transport ranges from medium (T8) to medium-high (T7) to maximum (T1 and T6). The two wave angles and Equation (4.16) suggest that at least 50% of maximum transport should be expected for any headland when α_b falls within the following 60° ranges, if there is enough energy from the waves to generate and maintain resuspension: 15-75° and 105-165°.

In the models, the north-south aligned beach upstream and downstream of each headland creates an angle of 165° to the oblique waves, generating transport at 50% of maximum potential. When the wave-driven current that is carrying the sediment intercepts the headlands and is deflected (T6, T7, T8) or wraps around (T1), sediment is transport away. For T1, enough energy remains to sustain transport of fine sand, as seen

Table 4.10. Incident Waves on Northern Faces of Headlands by Wave Angle.

Headland Class	Headland Shoreline Angle (from north)	Direct Wave (270°)		Oblique Wave (345°)	
		α_b	$\sin(2\alpha_b)^*$	α_b	$\sin(2\alpha_b)^*$
T1	217°	53°	0.96	128°	-0.97
T6	195°	75°	0.50	150°	-0.87
T7	231°	39°	0.98	114°	-0.74
T8	90° (north)	180°	0.00	255°	0.50
	180° (west)	90°	0.00	165°	-0.50

* - scales P_{ab} in Equation (4.16) as 0 = no transport, ± 1 = maximum transport

in Figure 4.8a, although it is reduced in concentration. For the other headlands, the offshore diversion of the flow transports the sediment offshore where waves and currents are weaker and the sediment falls out of suspension. This wave-current interaction can therefore partition sediment grain sizes as well as alter the volume of sediment in transit.

The initiation of motion for cohesionless sand particles has long been understood to be a function of size, particle-to-particle contact forces, and fluid forces (Shields, 1936). In the case of particle transport around the modeled headlands, the spatial variability in fluid forces due to morphology appears to sort the sediment according to size with finer sediment being more mobile over larger expanses. Coarser sediment, which requires larger τ_{total} to maintain active transport, will be removed from suspension and accrete in areas where τ_{total} decreases rapidly. For the modeled headlands, this occurs fairly consistently near the headland shoulders where deposits of medium sand were observed.

If these mechanisms are considered as a unified system, sediment bypassing can be envisioned as a multi-stage process, similar to that generally postulated by Short (1999) and proposed around a headland on the southern side of the mouth of San Francisco Bay (Battalio, 2014). The process would be a balance between small trickles of sediment under very frequent but energetically minimal conditions and sudden mass movements of sediment under very infrequent extremely large energy events. The model results from the current study suggest that grain sizes will respond differently to these large events with coarser material possibly flowing in opposite directions as finer sand. The concept of redirected sediment pathways with changed conditions agree with

findings in Australia around Cape Byron (Goodwin et al., 2013) and in Brazil around a collection of seven headlands (Vieira da Silva et al., 2016).

4.5.4 Generalized Sediment Bypassing

When using a single transect, changes in flow strength may be due to cross-shore meandering of the alongshore flow and thus transect data may not always accurately represent the system. In this study, a disparity emerged between the reduction of flux observed in alongshore transect and the cumulative flux values observed through the cross-shore transects on the shoulders used to determine $\beta_{headland}$. The mechanisms as discussed in the previous section may not necessarily be restricted to the width of the alongshore transect, but because $\beta_{headland}$ amalgamates through the offshore jets and accounts for reversing flows and eddies, a sediment bypassing schematic was developed based on Figure 4.9.

To illustrate the summation of the different mechanisms interacting, the sediment pathways and deposition zones were generalized for the headlands using two wave angles (direct and oblique) and two broadly defined grain sizes (fine and coarse) based on the model results (Figure 4.10). Similar to the findings of Guillou and Chapalain (2011), sand banks of fine material are expected off the apex for direct waves when the headland is triangular or small with respect to the surfzone width (or both). This corresponds with T1, T6 and T7. A large broad-faced headland (T8) is likely to produce deposits immediately adjacent to the headland shoulders. In all cases, coarser material is transported shoreward where it is deposited near the headland shoulders. Accumulation is seen in the eddy zones formed by oblique wave angles, which is contrary to the conceptualization about deposition in eddy zones by

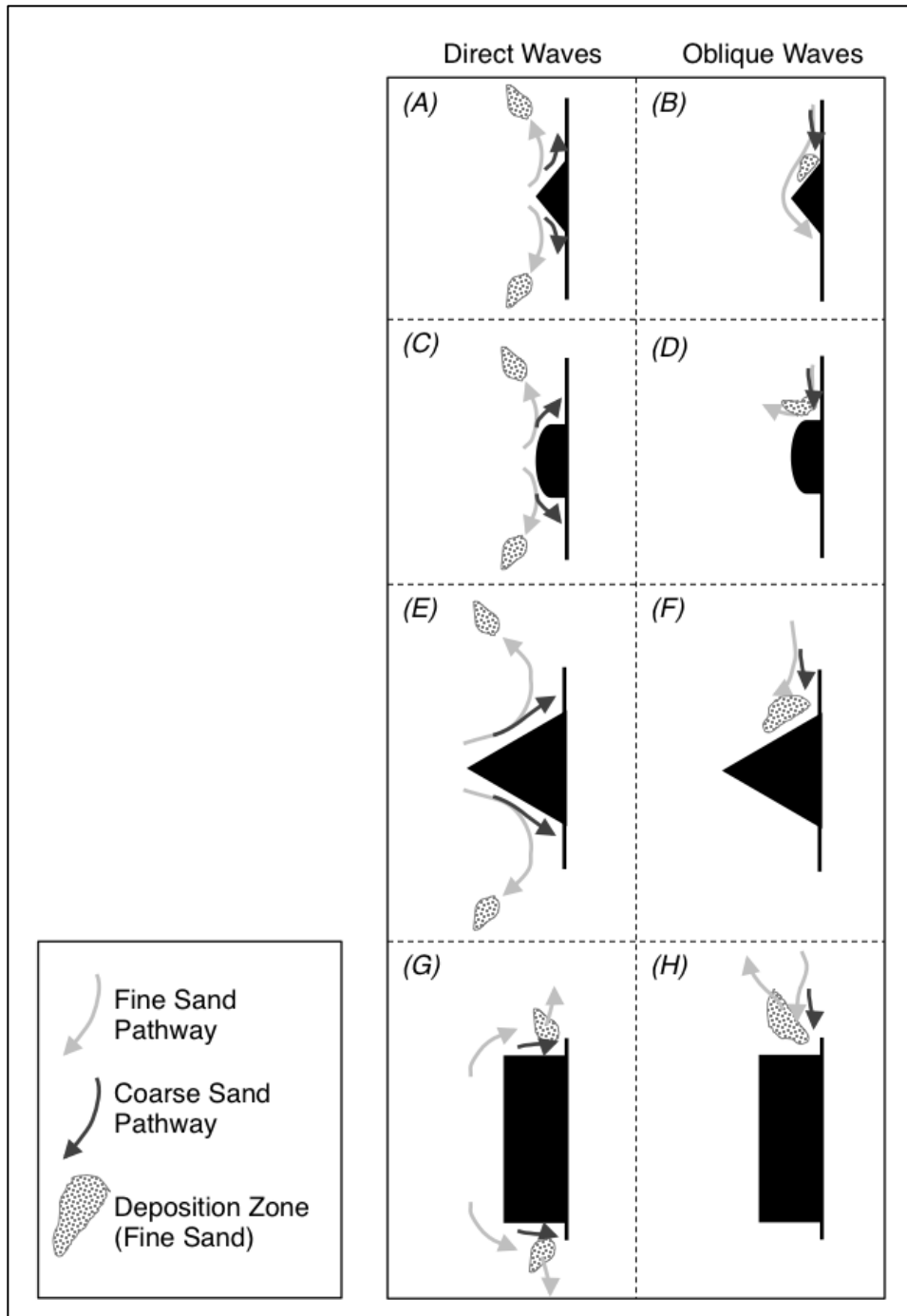


Figure 4.10. Conceptual sediment pathways and deposition zones for fine and coarse sediment under direct (A, C, E, G) and oblique (B, D, F, H) wave angles for the four generalized headlands.

Guillou and Chapalain (2011). The pathways realign to be alongshore when the wave angle shifts to be oblique but the morphology of the headland affects the fate of the sediment. In addition, the scale of the conditions generating the eddies should be considered: extreme events on a $< 5\%$ frequency are likely to be strong enough to both mobilize and advect sediment away from the headland. Based on the 5% frequency event modeled in this study, transport of fine sediment occurs around small, pointed headlands (T1) but not large ones (T7 and T8), which create offshore deposition zones on the upstream sides of the headlands. Coarse material is generally prevented from rounding any of the headlands. The partitioning according to sediment grain size is expected because the interaction between wave angles and morphology creates spatial variability of bed shear stresses. As mentioned earlier, these accumulation zones may be re-worked when low-frequency, energy events redistribute bed deposits and temporarily alter sediment pathways.

4.5.5 Model Improvements

Refinements to numerical modeling efforts are possible. Improvements range from incorporating modifications described in Section 4.3.4.1 to expanding the hydrodynamic forcing conditions (i.e., additional wave angles or faster regional currents) and the range of sediment grain sizes (i.e., mud and gravel fractions). One approach for modeling redesign could be to use the matrix in Table 4.1 for a sensitivity analysis by applying Markov-chain Monte Carlo methods in which a random selection of variables are chosen to simulate in a numerical model (Markov, 1906; Metropolis et al., 1953). The effect of bed slope, a classifying element used by George et al. (2015), could also be investigated to understand the influence of the subaqueous morphology. As this first-

order modeling effort concludes, many opportunities remain for expansion and inclusion of additional parameters in future modeling studies.

4.6 Conclusion

A numerical modeling study using Delft-3D and SWAN was undertaken with the overarching goal to better understand sediment bypassing around rocky headlands. Four morphologically distinct headlands were designed based on headlands commonly observed in California and tests were performed using oceanographic forces (tides, waves, and regional currents), three grain sizes (fine, fine-medium, and medium sand), and two bed types (sandy bed and reefed headland). The results from the 120 simulations revealed that the headland morphology, wave angle, and sediment grain size determine the transport and fate of sediment around the protuberances. An analysis of morphologic, oceanographic, and sedimentologic factors identified large oblique waves over a reefed headland as the most informative conditions of the model scenarios. The four headlands divided morphologically first by size and then by shape. Oblique incident wave angles propelled sediment alongshore whereas direct wave angles prevented sediment crossing the apex of any headland for most grain sizes. Finer sediment was more mobile than coarser sand classes and was deposited over larger areas on high velocity flows that form at the upstream headland shoulders under oblique waves. Large pointed and large blocky headlands emerged as the most likely barriers to sediment bypassing, although pointed headlands were more effective than broad ones. The dominant mechanism of transport was wave-forced transport, which depends on the relative angle between the waves and the shoreline, which changes by headland.

4.7 References

- Adams, P.N., Inman, D.L., Lovering, J.L., 2011. Effects of climate change and wave direction on longshore sediment transport patterns in Southern California. *Climatic Change* 109, 211-228.
- Alaee, M.J., Ivey, G., Pattiaratchi, C., 2004. Secondary circulation induced by flow curvature and Coriolis effects around headlands and islands. *Ocean Dynamics* 54, 27-38.
- Ashton, A.D., Murray, A.B., 2006a. High-angle wave instability and emergent shoreline shapes: 1. Modeling of sand waves, flying spits, and capes. *Journal of Geophysical Research-Earth Surface* 111.
- Ashton, A.D., Murray, A.B., 2006b. High-angle wave instability and emergent shoreline shapes: 2. Wave climate analysis and comparisons to nature. *Journal of Geophysical Research-Earth Surface* 111.
- Backstrom, J.T., Jackson, D.W.T., Cooper, J.A.G., 2009. Mesoscale shoreface morphodynamics on a high-energy regressive coast. *Continental Shelf Research* 29, 1361-1372.
- Bailard, J.A., 1981. An Energetics Total Load Sediment Transport Model for Plane Sloping Beaches. *Journal of Geophysical Research* 86, 10938-10954.
- Baptista, P., Cunha, T.R., Gama, C., Bernardes, C., 2012. A new and practical method to obtain grain size measurements in sandy shores based on digital image acquisition and processing. *Sedimentary Geology* 282, 294-306.
- Barnard, P.L., Foxgrover, A.C., Elias, E.P.L., Erikson, L.H., Hein, J.R., McGann, M., Mizell, K., Rosenbauer, R.J., Swarzenski, P.W., Takesue, R.K., Wong, F.L., Woodrow, D.L., 2013. Integration of bed characteristics, geochemical tracers, current measurements, and numerical modeling for assessing the provenance of beach sand in the San Francisco Bay Coastal System. *Marine Geology* 345, 181-206.
- Barnard, P.L., Hansen, J.E., Erikson, L.H., 2012. Synthesis Study of an Erosion Hot Spot, Ocean Beach, California. *Journal of Coastal Research* 28, 903-922.
- Bastos, A.C., Kenyon, N.H., Collins, M., 2002. Sedimentary processes, bedforms and facies, associated with a coastal, headland: Portland Bill, Southern UK. *Marine Geology* 187, 235-258.
- Battalio, B., 2014. Littoral Processes Along The Pacific And Bay Shores Of San Francisco, California, USA. *Shore and Beach* 82, 3-21.
- Benedet, L., List, J.H., 2008. Evaluation of the physical process controlling beach changes adjacent to nearshore dredge pits. *Coastal Engineering* 55.
- Berthot, A., Pattiaratchi, C., 2006a. Field measurements of the three-dimensional current structure in the vicinity of a headland-associated linear sandbank. *Continental Shelf Research* 26, 295-317.
- Berthot, A., Pattiaratchi, C., 2006b. Mechanisms for the formation of headland-associated linear sandbanks. *Continental Shelf Research* 26, 987-1004.
- Best, T.C., Griggs, G.B., 1991. The Santa-Cruz Littoral Cell - Difficulties in Quantifying a Coastal Sediment Budget.
- Bijker, E.W., 1967. Some considerations about scales for coastal models with movable bed. Delft Hydraulics Laboratory, Delft, The Netherlands.
- Bin Ab Razak, M.S., 2015. Natural headland sand bypassing; towards identifying and modelling the mechanisms and processes. CRC Press/Balkema.

- Black, K., Oldman, J., Hume, T., 2005. Dynamics of a 3-dimensional, baroclinic, headland eddy. *New Zealand Journal of Marine and Freshwater Research* 39, 91-120.
- Booij, N., Ris, R.C., Holthuijsen, L.H., 1999. A third-generation wave model for coastal regions - 1. Model description and validation. *Journal of Geophysical Research-Oceans* 104, 7649-7666.
- Bowman, D., Guillen, J., Lopez, L., Pellegrino, V., 2009. Planview Geometry and morphological characteristics of pocket beaches on the Catalan coast (Spain). *Geomorphology* 108, 191-199.
- Bowman, D., Rosas, V., Pranzini, E., 2014. Pocket beaches of Elba Island (Italy) – Planview geometry, depth of closure and sediment dispersal. *Estuarine, Coastal and Shelf Science* 138, 37-46.
- Buscombe, D., Rubin, D.M., Lacy, J.R., Storlazzi, C.D., Hatcher, G., Chezar, H., Wyland, R., Sherwood, C.R., 2014. Autonomous bed-sediment imaging-systems for revealing temporal variability of grain size. *Limnology and Oceanography-Methods* 12, 390-406.
- Buscombe, D., Rubin, D.M., Warrick, J.A., 2010. A universal approximation of grain size from images of noncohesive sediment. *Journal of Geophysical Research* 115.
- Camus, P., Mendez, F.J., Medina, R., Cofino, A.S., 2011. Analysis of clustering and selection algorithms for the study of multivariate wave climate. *Coastal Engineering* 58, 453-462.
- CGS, 2002. California Geomorphic Provinces. California Geological Survey, California Department of Conservation, p. Note 36.
- CGS, 2006. California Geological Map, Map Series 57 ed. California Geological Survey, California Department of Conservation.
- Chadwick, D.B., Largier, J.L., 1999. Tidal exchange at the bay-ocean boundary. *Journal of Geophysical Research-Oceans* 104, 29901-29924.
- Chelli, A., Pappalardo, M., Llopis, I.A., Federici, P.R., 2010. The relative influence of lithology and weathering in shaping shore platforms along the coastline of the Gulf of La Spezia (NW Italy) as revealed by rock strength. *Geomorphology* 118, 93-104.
- Collen, J.D., Gardner, J.P.A., Garton, D.W., 2009. Application of the littoral cell concept to managing a protected atoll: Palmyra Atoll National Wildlife Refuge. *Ocean & Coastal Management* 52, 628-635.
- Cooper, N.J., Pontee, N.I., 2006. Appraisal and evolution of the littoral 'sediment cell' concept in applied coastal management: Experiences from England and Wales. *Ocean & Coastal Management* 49, 498-510.
- Covault, J.A., Normark, W.R., Romans, B.W., Graham, S.A., 2007. Highstand fans in the California borderland: The overlooked deep-water depositional systems. *Geology* 35, 783-786.
- CSMW, 2010. California Beach Erosion Assessment Survey. Coastal Sediment Management Workgroup, Sacramento, CA, p. 72.
- da Silva, G.M., Mousavi, S.M.S., Jose, F., 2012. Wave-driven sediment transport and beach-dune dynamics in a headland bay beach. *Marine Geology* 323, 29-46.
- Dai, Z.J., Liu, J.T., Lei, Y.P., Zhang, X.L., 2010. Patterns of Sediment Transport Pathways on a Headland Bay Beach-Nanwan Beach, South China: A Case Study. *Journal of Coastal Research* 26, 1096-1103.

- Davies, J.L., 1974. The coastal sediment compartment. *Australian Geographical Studies* 12, 139-151.
- Davies, P.A., Dakin, J.M., Falconer, R.A., 1995. Eddy Formation Behind a Coastal Headland. *Journal of Coastal Research* 11, 154-167.
- de Castilhos, J.A., Gre, J.C.R., 2006. Beach morphodynamics and sediment transport along the northern coast of Santa Catarina, Brazil. *Journal of Coastal Research*, 1756-1761.
- Dean, R.G., Dalrymple, R.A., 2002. *Coastal Processes with Engineering Applications*. Cambridge University Press, Cambridge, UK.
- Deines, K.L., 1999. Backscatter Estimation Using Broadband Acoustic Doppler Current Profilers. RD Instruments Application Note FSA-008, 1-5.
- Deltares, 2014. *Delft3D-FLOW User Manual*, Delft, The Netherlands.
- Denniss, T., Middleton, J.H., Manasseh, R., 1995. Recirculation in the Lee of Complicated Headlands - A Case-Study of Bass-Point. *Journal of Geophysical Research-Oceans* 100, 16087-16101.
- Drake, P.T., McManus, M.A., Storlazzi, C.D., 2005. Local wind forcing of the Monterey Bay area inner shelf. *Continental Shelf Research* 25, 397-417.
- Elias, E.P.L., Gelfenbaum, G., Van der Westhuysen, A.J., 2012. Validation of a coupled wave-flow model in a high-energy setting: The mouth of the Columbia River. *Journal of Geophysical Research-Oceans* 117, 21.
- Elias, E.P.L., Hansen, J.E., 2013. Understanding processes controlling sediment transports at the mouth of a highly energetic inlet system (San Francisco Bay, CA). *Marine Geology* 345, 207-220.
- Emery, K.O., Kuhn, G.G., 1982. Sea cliffs: Their processes, profiles, and classification. *Geological Society of America Bulletin* 93, 644-654.
- Emery, W.J., Thomson, R.E., 2001. *Data Analysis Methods in Physical Oceanography*. Elsevier, New York.
- Erikson, L.H., Storlazzi, C.D., Golden, N.E., 2014. Modeling Wave and Seabed Energetics on the California Continental Shelf. Pamphlet to accompany data set., in: Survey, U.S.G. (Ed.), Santa Cruz, California.
- Erikson, L.H., Wright, S.A., Elias, E., Hanes, D.M., Schoellhamer, D.H., Largier, J., 2013. The use of modeling and suspended sediment concentration measurements for quantifying net suspended sediment transport through a large tidally dominated inlet. *Marine Geology* 345, 96-112.
- ESRI, 2013. *ArcGIS Desktop: Release 10.1* Environmental Systems Resource Institute, Redlands, CA.
- Everts, C.H., Eldon, C.D., 2000. Beach-Retention Structures and Wide Sandy Beaches in Southern California. *Shore and Beach* 68, 11-22.
- Everts, C.H., Eldon, C.D., 2005. Sand Capture In Southern California Submarine Canyons. *Shore and Beach* 73, 3-12.
- Freeland, H., 1990. The Flow of a Coastal Current Past a Blunt Headland. *Atmosphere-Ocean* 28, 288-302.
- Freeman, L.A., Miller, A.J., Norris, R.D., Smith, J.E., 2012. Classification of remote Pacific coral reefs by physical oceanographic environment. *Journal of Geophysical Research-Oceans* 117.

Gelfenbaum, G., Stevens, A.W., Miller, I., Warrick, J.A., Ogston, A.S., Eidam, E., 2015. Large-scale dam removal on the Elwha River, Washington, USA: Coastal geomorphic change. *Geomorphology* 246, 649-668.

George, D.A., Hill, P.S., 2008. Wave climate, sediment supply and the depth of the sand-mud transition: A global survey. *Marine Geology* 254, 121-128.

George, D.A., Largier, J.L., Storlazzi, C.D., Barnard, P.L., 2015. Classification of rocky headlands in California with relevance to littoral cell boundary delineation. *Marine Geology* 369, 137-152.

George, D.A., Largier, J.L., Storlazzi, C.D., Robart, M.J., Gaylord, B.P., 2016. Sediment flux around rocky headlands: an example of sand transport at Pt. Dume, California.

Goodwin, I.D., Freeman, R., Blackmore, K., 2013. An insight into headland sand bypassing and wave climate variability from shoreface bathymetric change at Byron Bay, New South Wales, Australia. *Marine Geology* 341, 29-45.

Goring, D.G., Nikora, V.I., 2002. Despiking acoustic Doppler velocimeter data. *Journal of Hydraulic Engineering-Asce* 128, 117-126.

Grifman, P., Hart, J., Ladwig, J., Schulhof, M., 2012. DRAFT Sea Level Rise Vulnerability Study for the City of Los Angeles. University of Southern California Sea Grant Program, Los Angeles, CA, p. 87.

Guillou, N., Chapalain, G., 2011. Effects of waves on the initiation of headland-associated sandbanks. *Continental Shelf Research* 31, 1202-1213.

Habel, J.S., Armstrong, G.A., 1978. Assessment and Atlas of Shoreline Erosion Along the California Coast. State of California, Department of Navigation and Ocean Development, Sacramento, CA, p. 277.

Haff, P.K., 1996. Limitations on predictive modeling in geomorphology. *Scientific Nature of Geomorphology*, 337-358.

Hansen, J.E., Elias, E., Barnard, P.L., 2013. Changes in surfzone morphodynamics driven by multi-decadal contraction of a large ebb-tidal delta. *Marine Geology* 345, 221-234.

Harris, P.T., Whiteway, T., 2011. Global distribution of large submarine canyons: Geomorphic differences between active and passive continental margins. *Marine Geology* 285, 69-86.

Hayes, M.O., 1979. Barrier island morphology as a function of wave and tide regime, in: Leatherman, S.P. (Ed.), *Barrier islands from the Gulf of St. Lawrence to the Gulf of Mexico*. Academic Press, New York, NY, pp. 1-29.

Hickey, B.M., 1992. Circulation over the Santa-Monica San-Pedro Basin and Shelf. *Progress in Oceanography* 30, 37-115.

Hickey, B.M., Dobbins, E.L., Allen, S.E., 2003. Local and remote forcing of currents and temperature in the central Southern California Bight. *Journal of Geophysical Research-Oceans* 108.

Hoeke, R.K., Storlazzi, C.D., Ridd, P.V., 2013. Drivers of circulation in a fringing coral reef embayment: A wave-flow coupled numerical modeling study of Hanalei Bay, Hawaii. *Continental Shelf Research* 58, 79-95.

Holdaway, G.P., Thorne, P.D., Flatt, D., Jones, S.E., Prandle, D., 1999. Comparison between ADCP and transmissometer measurements of suspended sediment concentration. *Continental Shelf Research* 19, 421-441.

- Holthuijsen, L.H., Booij, N., Ris, R.C., 1993. A spectral wave model for the coastal zone, Proceedings of the 2nd International Symposium on Ocean Wave Measurement and Analysis,, New Orleans, pp. 630-641.
- Hume, T.M., Oldman, J.W., Black, K.P., 2000. Sediment facies and pathways of sand transport about a large deep water headland, Cape Rodney, New Zealand. *New Zealand Journal of Marine and Freshwater Research* 34, 695-717.
- Inman, D.L., 1986. Southern California Coastal Processes Data Summary.
- Inman, D.L., Frautschy, J.D., 1966. Littoral processes and the development of shorelines, Coastal Engineering Special Conference. ASCE, pp. 511-536.
- Inman, D.L., Masters, P.M., 1994. Status of Research on the Nearshore. *Shore and Beach* 62, 11-20.
- Jones, O.P., Simons, R.R., Jones, E.J.W., Harris, J.M., 2006. Influence of seabed slope and Coriolis effects on the development of sandbanks near headlands. *Journal of Geophysical Research-Oceans* 111.
- Kamphuis, J.W., 2010. Introduction to coastal engineering and management, 2nd Edition. World Scientific, Singapore.
- Kaplan, D.M., Halle, C., Paduan, J., Largier, J.L., 2009. Surface currents during anomalous upwelling seasons off central California. *Journal of Geophysical Research* 114.
- King, P.G., McGregor, A.R., Whittet, J.D., 2016. Can California coastal managers plan for sea-level rise in a cost-effective way? *Journal of Environmental Planning and Management* 59, 98-119.
- Klinger, B., 1993. Gyre Formation at a Corner by Rotating Barotropic Coastal Flows along a Slope. *Dynamics of Atmospheres and Oceans* 19, 27-63.
- Knur, R.T., Kim, Y.C., 1999. Historical sediment budget analysis along the Malibu coastline, Sand Rights '99- Bringing Back the Beaches. ASCE, Ventura, CA, p. 292.
- Komar, P.D., 2010. Shoreline Evolution and Management of Hawke's Bay, New Zealand: Tectonics, Coastal Processes, and Human Impacts. *Journal of Coastal Research* 26, 143-156.
- Kruskal, J.B., 1964. Multidimensional-Scaling by Optimizing Goodness of Fit to a Nonmetric Hypothesis. *Psychometrika* 29, 1-27.
- Kruskal, J.B., Wish, M., 1978. Multidimensional Scaling. SAGE Publications.
- Largier, J.L., Magnell, B.A., Winant, C.D., 1993. Subtidal Circulation over the Northern California Shelf. *Journal of Geophysical Research-Oceans* 98, 18147-18179.
- Larson, M., Hoan, L., Hanson, H., 2010. Direct Formula to Compute Wave Height and Angle at Incipient Breaking. *Journal of Waterway, Port, Coastal, and Ocean Engineering* 136, 119-122.
- Leidersdorf, C.B., Hollar, R.C., Woodell, G., 1994. Human Intervention with the Beaches of Santa Monica Bay, California *Shore and Beach* 62, 29-38.
- Lesser, G.R., 2009. An Approach to Medium-term Coastal Morphological Modeling. Delft University of Technology, Delft, The Netherlands, p. 238.
- Lesser, G.R., Roelvink, J.A., van Kester, J., Stelling, G.S., 2004. Development and validation of a three-dimensional morphological model. *Coastal Engineering* 51, 883-915.
- Limber, P.W., Murray, A.B., 2015. Sea stack formation and the role of abrasion on beach-mantled headlands. *Earth Surface Processes and Landforms* 40, 559-568.

Limber, P.W., Patsch, K.B., Griggs, G.B., 2008. Coastal sediment budgets and the littoral cutoff diameter: A grain size threshold for quantifying active sediment inputs. *Journal of Coastal Research* 24, 122-133.

Loureiro, C., Ferreira, O., Cooper, J.A.G., 2012. Geologically constrained morphological variability and boundary effects on embayed beaches. *Marine Geology* 329, 1-15.

MacCready, P., Pawlak, G., 2001. Stratified flow along a corrugated slope: Separation drag and wave drag. *Journal of Physical Oceanography* 31, 2824-2839.

MacQueen, J.B., 1967. Some Methods for Classification and Analysis of Multivariate Observations, 5th Berkeley Symposium on Mathematical Statistics and Probability. University of California Press, Berkeley, California, pp. 281-297.

Madsen, O.S., 1994. Spectral wave-current bottom boundary layer flows, Coastal Engineering 1994, 24th International Conference Coastal Engineering Research Council, pp. 384-398.

Magaldi, M.G., Ozgokmen, T.M., Griffa, A., Chassignet, E.P., Iskandarani, M., Peters, H., 2008. Turbulent flow regimes behind a coastal cape in a stratified and rotating environment. *Ocean Modelling* 25, 65-82.

Markov, A.A., 1906. Rasprostranenie zakona bol'shikh chisel na velichiny, zavisyaschie drug ot druga. *Izvestiya Fiziko-matematicheskogo obschestva pri Kazanskom universitete*, 135–156.

Metropolis, N., Rosenbluth, A.W., Rosenbluth, M.N., Teller, A.H., Teller, E., 1953. Equation of State Calculations by Fast Computing Machines. *The Journal of Chemical Physics* 21, 1087-1092.

Milliman, J.D., Farnsworth, K.L., 2011. *River Discharge to the Coastal Ocean: A Global Synthesis*. Cambridge University Press, New York.

Mullenbach, B.L., Nittrouer, C.A., Puig, P., Orange, D.L., 2004. Sediment deposition in a modern submarine canyon: Eel Canyon, northern California. *Marine Geology* 211, 101-119.

Neill, S.P., Scourse, J.D., 2009. The formation of headland/island sandbanks. *Continental Shelf Research* 29, 2167-2177.

Nickols, K.J., Gaylord, B., Largier, J.L., 2012. The coastal boundary layer: predictable current structure decreases alongshore transport and alters scales of dispersal. *Marine Ecology Progress Series* 464, 17-35.

Nienhuis, J.H., Ashton, A.D., Nardin, W., Fagherazzi, S., Giosan, L., 2016. Alongshore sediment bypassing as a control on river mouth morphodynamics. *Journal of Geophysical Research: Earth Surface* 121, 664-683.

Noble, M.A., Rosenberger, K.J., Hamilton, P., Xu, J.P., 2009. Coastal ocean transport patterns in the central Southern California Bight. *Earth Science in the Urban Ocean: the Southern California Continental Borderland* 454, 193-226.

OPC, 2013. *State Of California Sea-Level Rise Guidance* Ocean Protection Council, Sacramento, CA, p. 13.

Orme, A.R., 1991. The Malibu coast – a contribution to the city-wide wastewater management study, p. 50.

OST, 2011. *South Coast California MPA Monitoring Plan*. MPA Monitoring Enterprise, California Ocean Science Trust, Oakland, CA.

Park, M.-J., Wang, D.-P., 2000. Tidal Vorticity around a Coastal Promontory. *Journal of Oceanography* 56, 261-273.

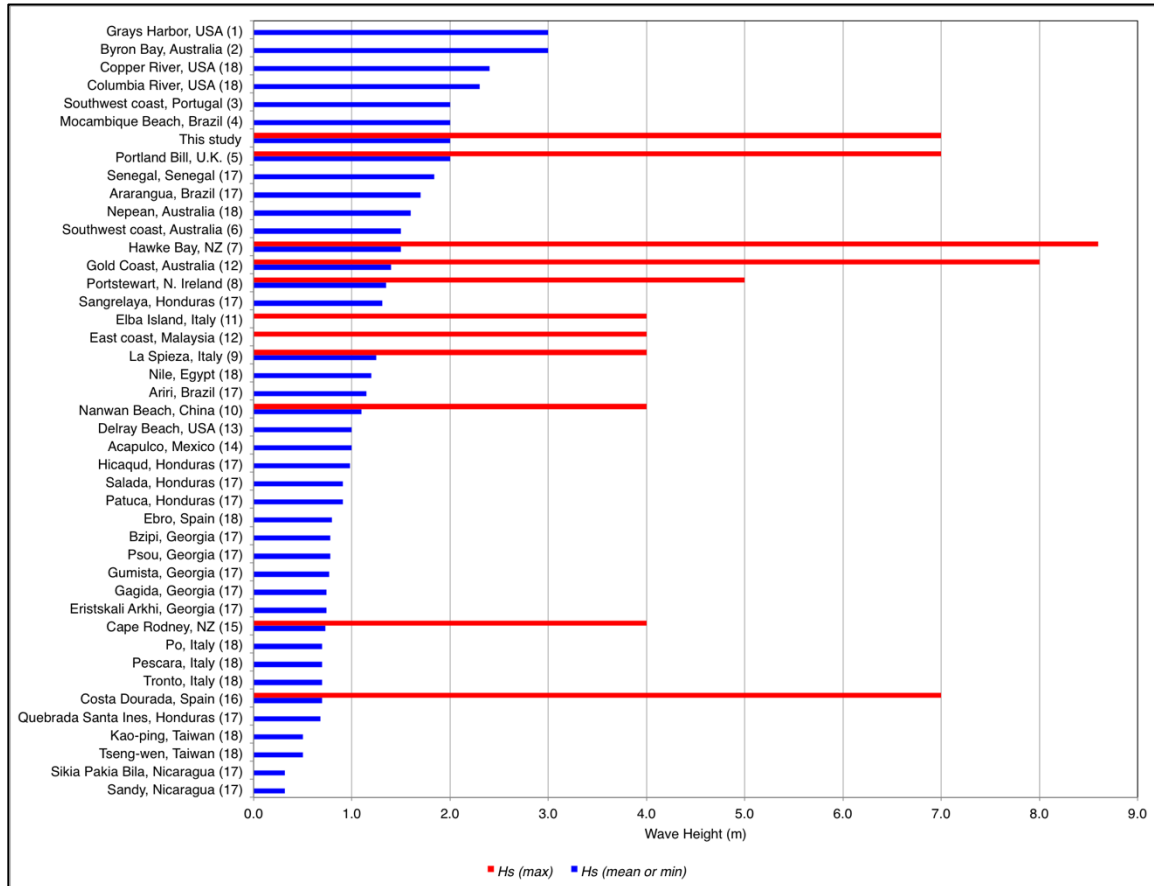
- Patsch, K., Griggs, G., 2006. Littoral Cells, Sand Budgets, and Beaches: Understanding California's Shoreline, Institute of Marine Sciences, University of California, Santa Cruz, p. 40.
- Patsch, K., Griggs, G., 2007. Development of Sand Budgets for California's Major Littoral Cells. Institute of Marine Sciences, University of California, Santa Cruz, p. 115.
- Pattiaratchi, C., James, A., Collins, M., 1987. Island wakes and headland eddies: A comparison between remotely sensed data and laboratory experiments. *Journal of Geophysical Research: Oceans* 92, 783-794.
- Pentney, R.M., Dickson, M.E., 2012. Digital Grain Size Analysis of a Mixed Sand and Gravel Beach. *Journal of Coastal Research* 28, 196-201.
- Perg, L.A., Anderson, R.S., Finkel, R.C., 2003. Use of cosmogenic radionuclides as a sediment tracer in the Santa Cruz littoral cell, California, United States. *Geology* 31, 299-302.
- Pingree, R.D., 1978. FORMATION OF SHAMBLES AND OTHER BANKS BY TIDAL STIRRING OF SEAS. *Journal of the Marine Biological Association of the United Kingdom* 58, 211-226.
- Reed, C.W., Niedoroda, A.W., Swift, D.J.P., 1999. Modeling sediment entrainment and transport processes limited by bed armoring. *Marine Geology* 154, 143-154.
- Reid, J.A., Reid, J.M., Jenkins, C.J., Zimmermann, M., Williams, S.J., Field, M.E., 2006. usSEABED: Pacific Coast (California, Oregon, Washington) Offshore Surficial-sediment Data Release.
- Ris, R.C., Holthuijsen, L.H., Booij, N., 1999. A third-generation wave model for coastal regions - 2. Verification. *Journal of Geophysical Research-Oceans* 104, 7667-7681.
- Rosati, J.D., 2005. Concepts in sediment budgets. *Journal of Coastal Research* 21, 307-322.
- Roughan, M., Mace, A.J., Largier, J.L., Morgan, S.G., Fisher, J.L., Carter, M.L., 2005. Subsurface recirculation and larval retention in the lee of a small headland: A variation on the upwelling shadow theme. *Journal of Geophysical Research-Oceans* 110.
- Roughan, M., Terrill, E.J., Largier, J.L., Otero, M.P., 2005. Observations of divergence and upwelling around Point Loma, California. *Journal of Geophysical Research-Oceans* 110.
- Ruggiero, P., Walstra, D.J.R., Gelfenbaum, G., van Ormondt, M., 2009. Seasonal-scale nearshore morphological evolution: Field observations and numerical modeling. *Coastal Engineering* 56, 1153-1172.
- Sallenger, A.H., Krabill, W., Brock, J., Swift, R., Manizade, S., Stockdon, H., 2002. Sea-cliff erosion as a function of beach changes and extreme wave runup during the 1997-1998 El Nino. *Marine Geology* 187, 279-297.
- SANDAG, 2009. Coastal Regional Sediment Management Plan for the San Diego Region. Prepared by Moffatt and Nichol, Everest International Consultants and SIAC. San Diego Association of Governments, p. 220.
- Sanderson, P.G., Eliot, I., 1999. Compartmentalisation of beachface sediments along the southwestern coast of Australia. *Marine Geology* 162, 145-164.
- Scholar, D.C., Griggs, G.B., 1997. Pocket Beaches of California: Sediment Transport Along a Rocky Coastline, Proceedings of California's Coastal Natural Hazards. University of Southern California Sea Grant Program, Santa Barbara, pp. 65-75.

- Scott, T., Masselink, G., Russell, P., 2011. Morphodynamic characteristics and classification of beaches in England and Wales. *Marine Geology* 286, 1-20.
- Shields, A., 1936. Anwendung der Aehnlichkeitsmechanik und der Turbulenzforschung auf die Geschiebebewegung, Preußische Versuchsanstalt für Wasserbau, Berlin.
- Short, A.D., 1999. Handbook of beach and shoreface morphodynamics. John Wiley, New York.
- Signell, R.P., Geyer, W.R., 1991. Transient Eddy Formation around Headlands. *Journal of Geophysical Research-Oceans* 96, 2561-2575.
- Silva, R., Baquerizo, A., Losada, M.A., Mendoza, E., 2010. Hydrodynamics of a headland-bay beach-Nearshore current circulation. *Coastal Engineering* 57, 160-175.
- Slagel, M.J., Griggs, G.B., 2008. Cumulative losses of sand to the California coast by dam impoundment. *Journal of Coastal Research* 24.
- Soulsby, R., 1997. Dynamics of Marine Sands: A Manual for Practical Applications. Thomas Telford, London.
- Stelling, G.S., 1984. On the construction of computational methods for shallow water flow problems, Faculty of Applied Sciences. Delft University of Technology, Delft, The Netherlands.
- Stewart, S.R., 2014. Tropical Cyclone Report. Hurricane Simon (EP192014), in: National Hurricane Center, N. (Ed.), p. 18.
- Storlazzi, C.D., Field, M.E., 2000. Sediment distribution and transport along a rocky, embayed coast: Monterey Peninsula and Carmel Bay, California. *Marine Geology* 170, 289-316.
- Storlazzi, C.D., Jaffe, B.E., 2008. The relative contribution of processes driving variability in flow, shear, and turbidity over a fringing coral reef: West Maui, Hawaii. *Estuarine Coastal and Shelf Science* 77, 549-564.
- Storlazzi, C.D., Reid, J.A., 2010. The influence of El Nino-Southern Oscillation (ENSO) cycles on wave-driven sea-floor sediment mobility along the central California continental margin. *Continental Shelf Research* 30, 1582-1599.
- Stuiver, C., 2013. Coastal evolution of soft cliff coasts: headland formation and evolution on the Southwest Isle of Wight, Engineering and the Environment. University of Southampton, p. 277.
- Stul, T., Gozzard, J., Eliot, I., Eliot, M., 2012. Coastal Sediment Cells between Cape Naturaliste and the Moore River, Western Australia in: Transport, W.A.D.o. (Ed.). Damara WA Pty Ltd and Geological Survey of Western Australia, Fremantle, WA, Australia, p. 44.
- Thorne, P.D., Vincent, C.E., Hardcastle, P.J., Rehman, S., Pearson, N., 1991. MEASURING SUSPENDED SEDIMENT CONCENTRATIONS USING ACOUSTIC BACKSCATTER DEVICES. *Marine Geology* 98, 7-16.
- USACE, 1984. Shore Protection Manual, in: U. S. Army Corps of Engineers, C.E.R.C. (Ed.). Department of the Army, Waterways Experiment Station, Corps of Engineers, Vicksburg, p. 656.
- van Rijn, L.C., 2007a. Unified View of Sediment Transport by Currents and Waves. I: Initiation of Motion, Bed Roughness, and Bed-Load Transport. *Journal of Hydraulic Engineering* 133, 649-667.
- van Rijn, L.C., 2007b. Unified View of Sediment Transport by Currents and Waves. II: Suspended Transport. *Journal of Hydraulic Engineering* 133, 668-689.

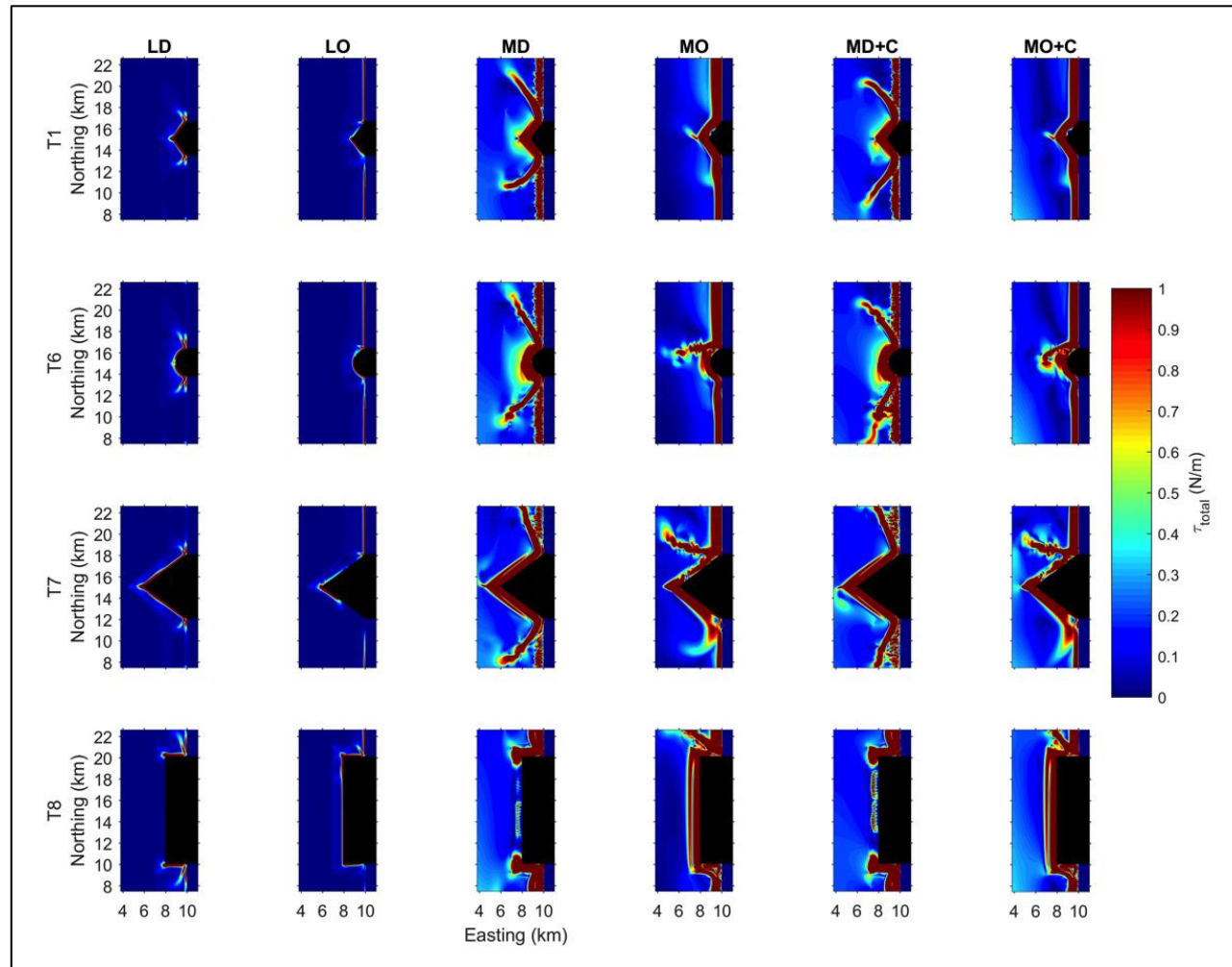
- van Rijn, L.C., 2007c. Unified View of Sediment Transport by Currents and Waves. III: Graded Beds. *Journal of Hydraulic Engineering* 133, 761-775.
- van Rijn, L.C., 2010. Coastal erosion control based on the concept of sediment cells. *CONSCIENCE*, Deltares, The Netherlands, p. 80.
- Verron, J., Davies, P., Dakin, J., 1991. Quasigeostrophic Flow Past a Cape in a Homogeneous Fluid. *Fluid Dynamics Research* 7, 1-21.
- Vieira da Silva, G., Toldo, E.E., H. da F. Klein, A., Short, A.D., Woodroffe, C.D., 2016. Headland sand bypassing - Quantification of net sediment transport in embayed beaches, Santa Catarina Island North Shore, Southern Brazil. *Marine Geology* 379, 13-27.
- Warner, S.J., MacCready, P., 2009. Dissecting the Pressure Field in Tidal Flow past a Headland: When Is Form Drag "Real"? *Journal of Physical Oceanography* 39, 2971-2984.
- Winant, C.D., 2006. Three-dimensional wind-driven coastal circulation past a headland. *Journal of Physical Oceanography* 36, 1430-1438.
- Wingfield, D.K., Storlazzi, C.D., 2007. Spatial and temporal variability in oceanographic and meteorologic forcing along Central California and its implications on nearshore processes. *Journal of Marine Systems* 68.
- Wright, L., Short, A., 1984. Morphodynamic Variability of Surf Zones and Beaches - A Synthesis. *Marine Geology* 56, 93-118.
- Xu, J.P., Noble, M.A., 2009. Variability of the Southern California wave climate and implications for sediment transport. *Earth Science in the Urban Ocean: the Southern California Continental Borderland* 454, 171-191.
- Young, A.P., Ashford, S.A., 2006. Application of airborne LIDAR for seacliff volumetric change and beach-sediment budget contributions. *Journal of Coastal Research* 22, 307-318.

4.8 Appendices

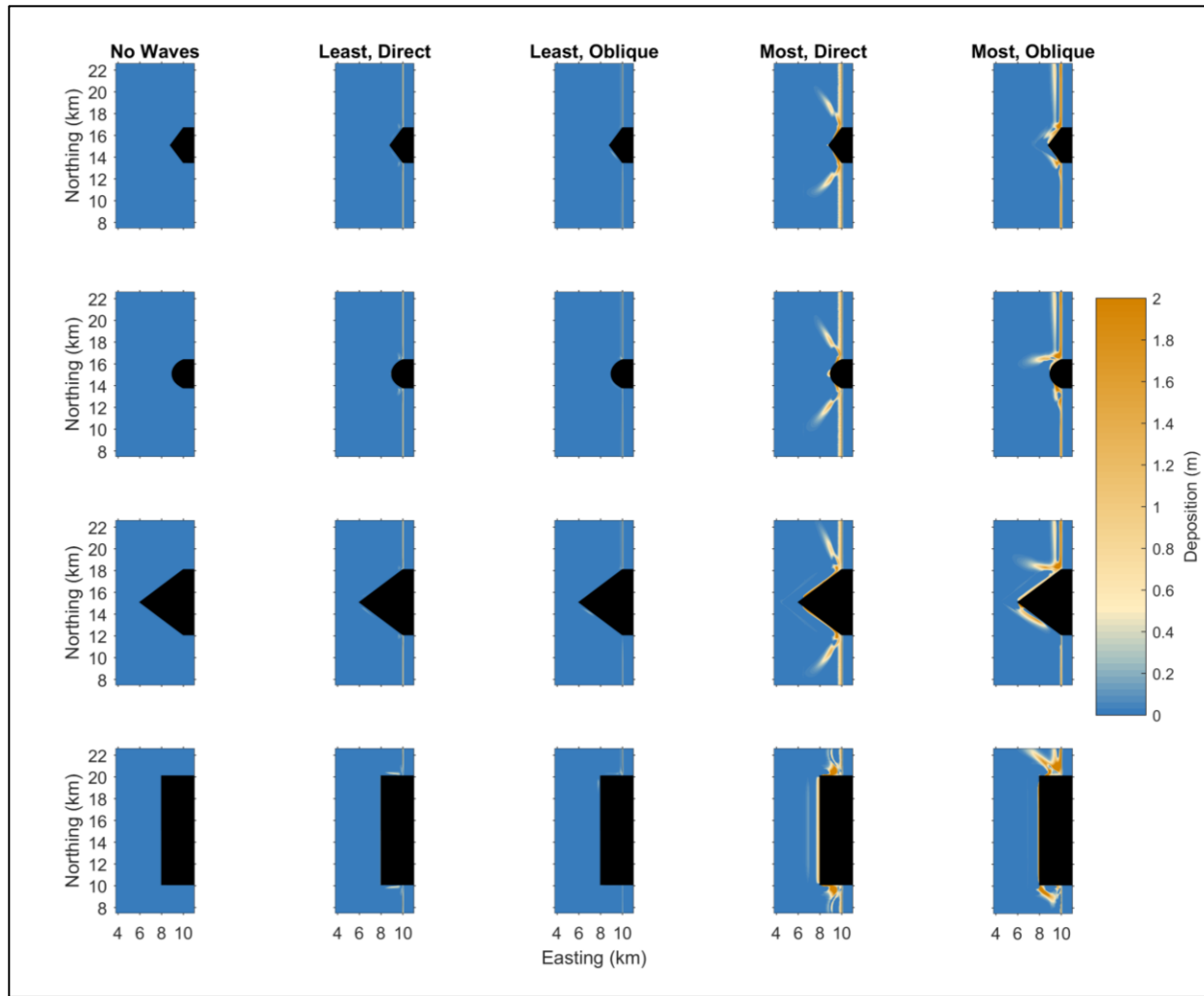
A. Appendices



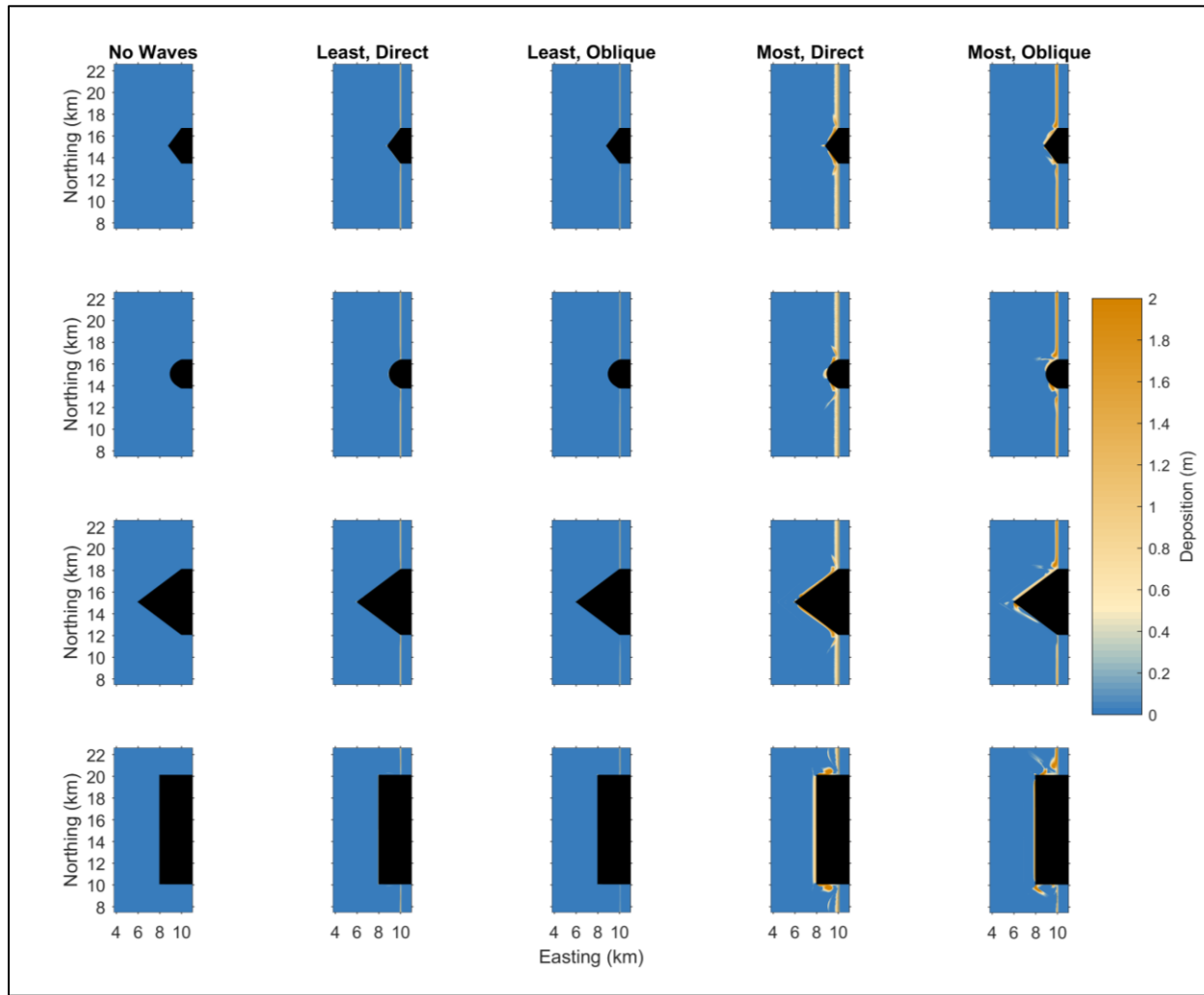
A.1. World wave conditions (H_s) from published field studies and observational records, and the model input for this study. Published data comes from the following sources: (1) Ruggiero et al. (2009); (2) Goodwin et al. (2013); (3) Loureiro et al. (2012); (4) da Silva et al. (2012); (5) Bastos et al. (2002); (6) Sanderson and Eliot (1999); (7) Komar (2010); (8) Backstrom et al. (2009); (9) Chelli et al. (2010); (10) Dai et al. (2010); (11) Bowman et al. (2014); (12) Bin Ab Razak (2015); (13) Benedet and List (2008); (14) Silva et al. (2010); (15) Hume et al. (2000); (16) Bowman et al. (2009); (17) Nienhuis et al. (2016); and (18) George and Hill (2008).



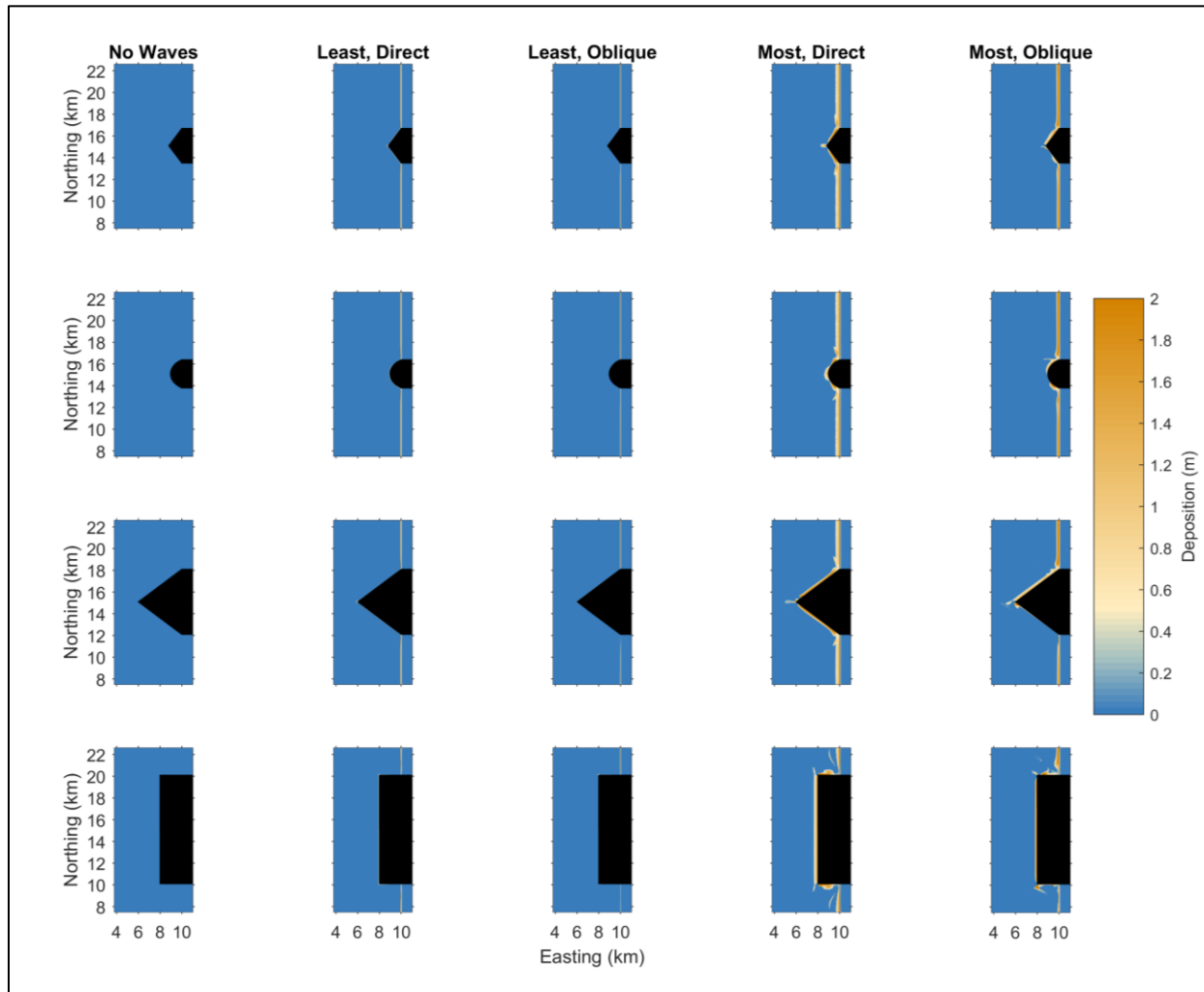
A.2. Model results of bed shear stress for waves only and for waves with a regional current forcing during the fastest velocity timestep where L = least wave power, M = most wave power, D = direct wave angle, O = oblique wave angle, and C = regional current.



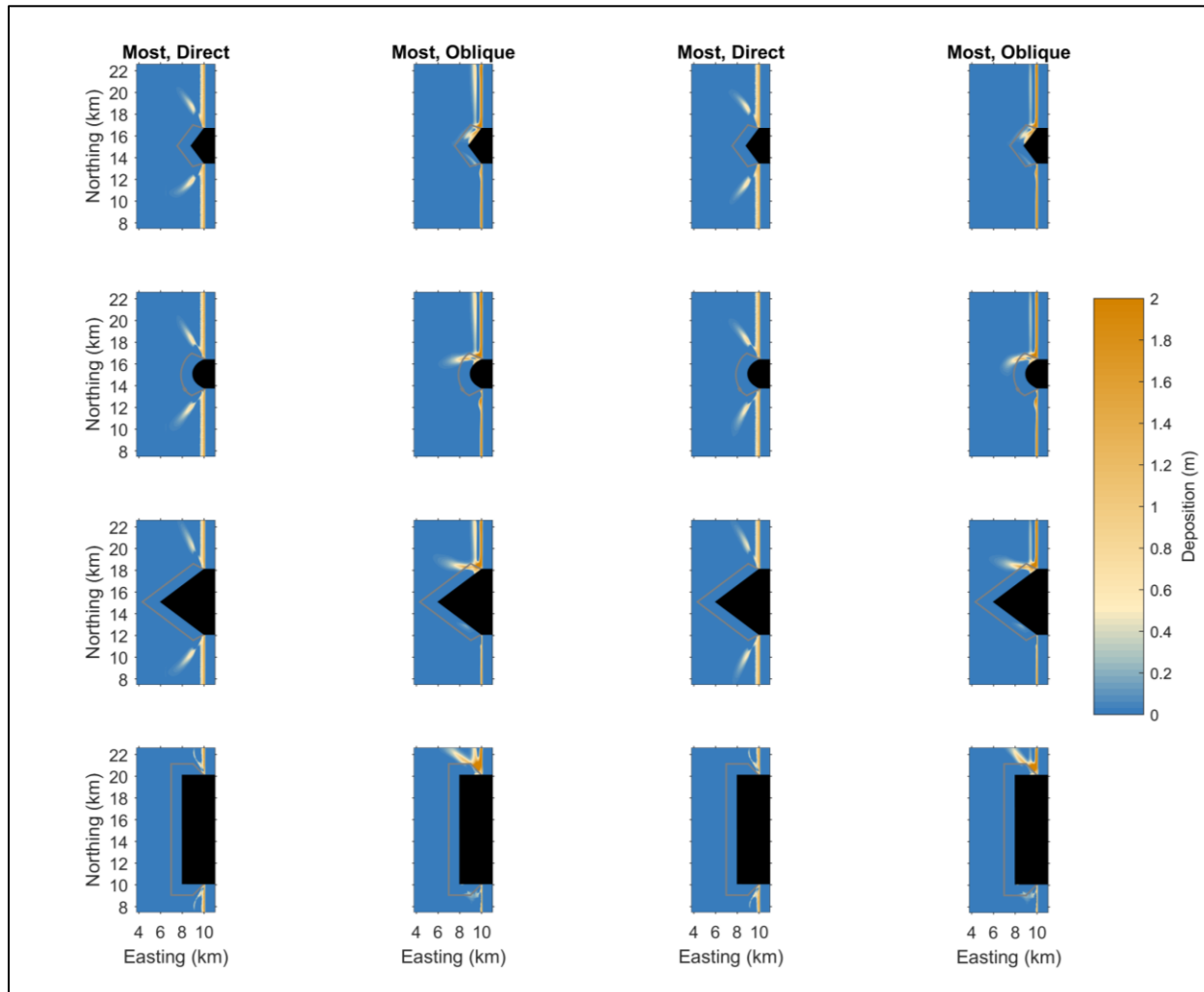
A.3. Deposition patterns for (a) fine sand in baseline and waves only conditions for a sandy bed.



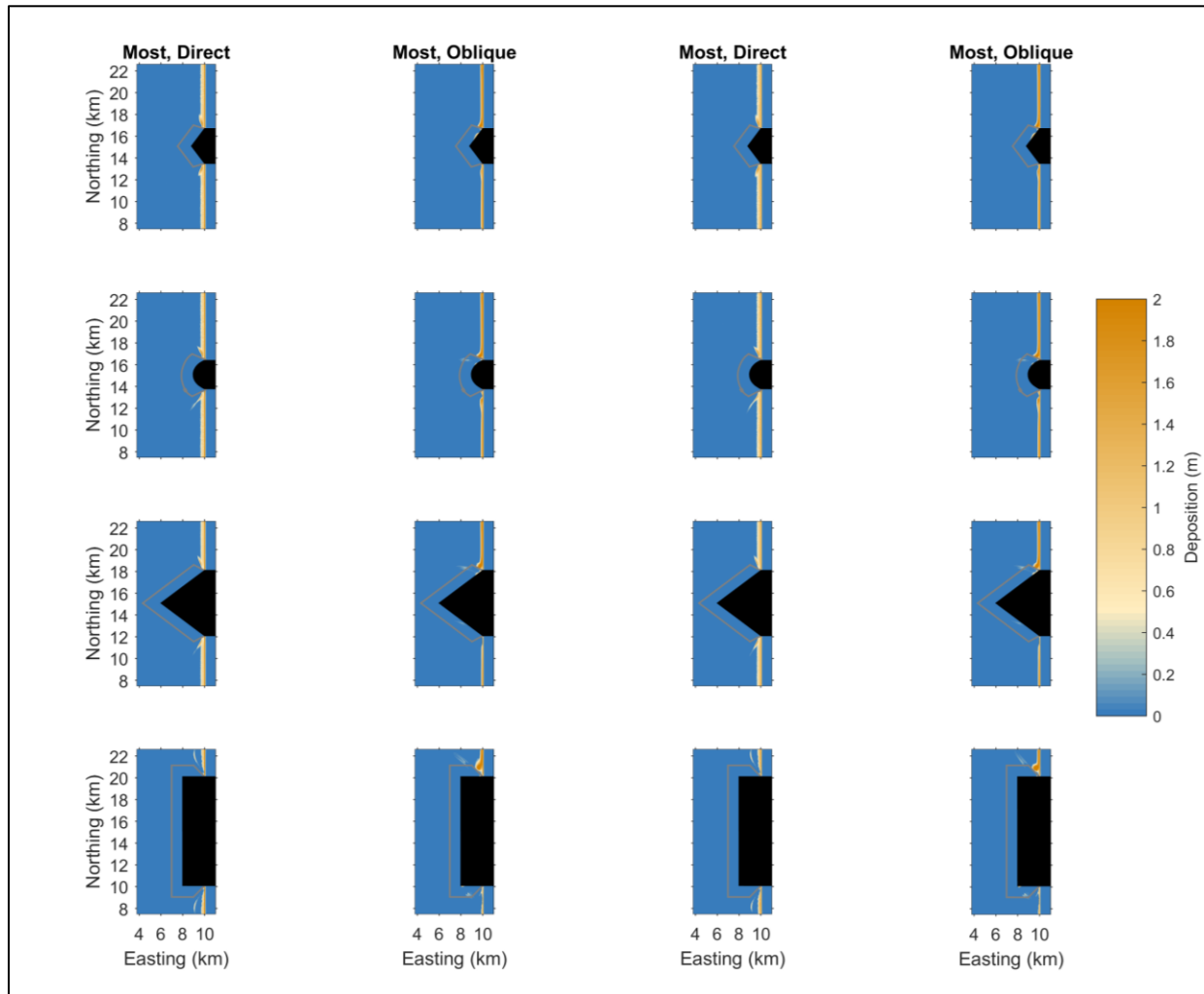
A.3. Deposition patterns for (b) medium-fine sand in baseline and waves only conditions for a sandy bed.



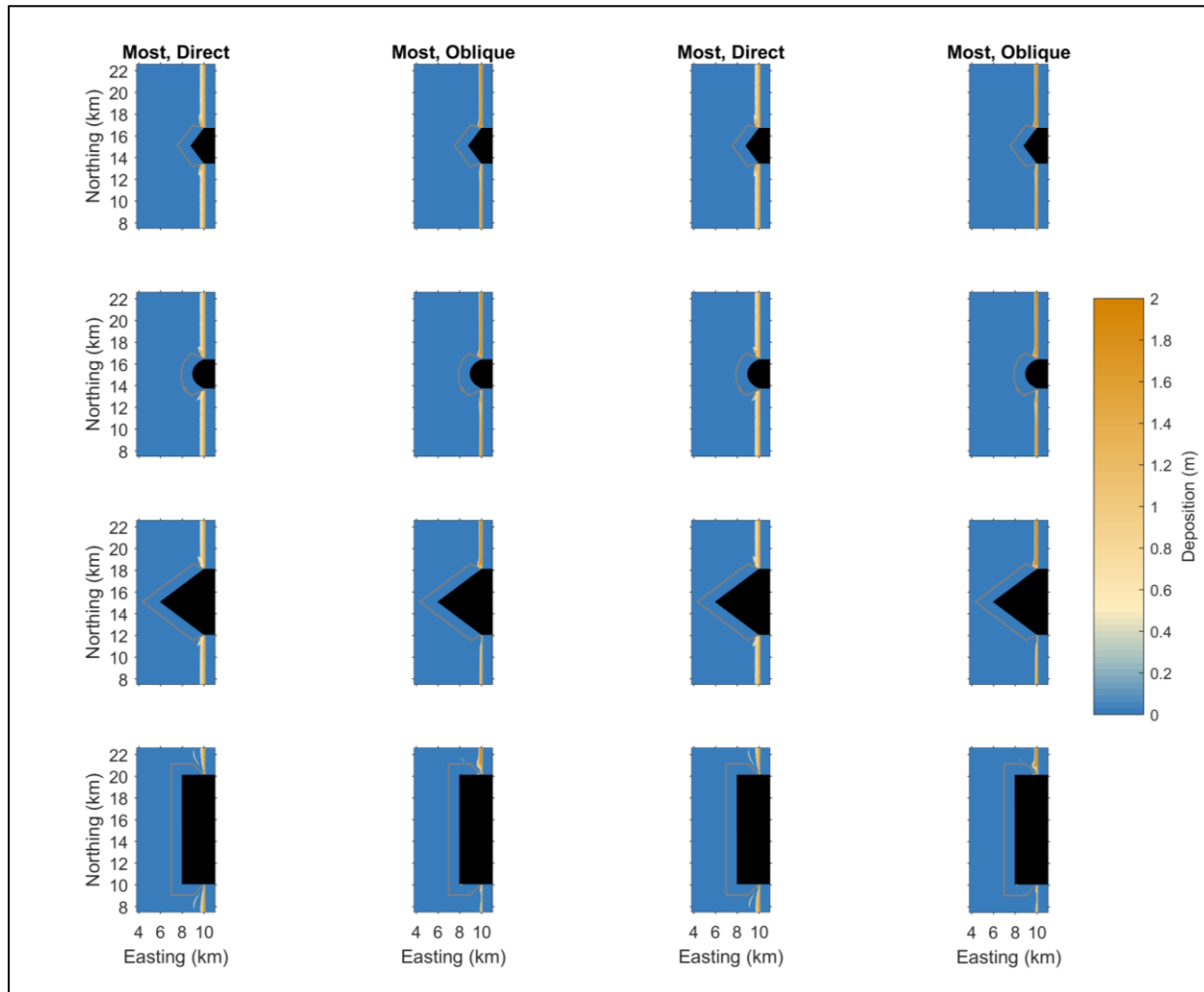
A.3. Deposition patterns for (c) medium sand in baseline and waves only conditions for a sandy bed.



A.3. Deposition patterns for (d) fine sand in waves only and with the addition of a regional current for a reefed headland. The reef zone is noted as the gray outlined region adjacent to the headland.



A.3. Deposition patterns for (e) medium-fine sand in waves only and with the addition of a regional current for a reefed headland. The reef zone is noted as the gray outlined region adjacent to the headland.



A.3. Deposition patterns for (f) medium sand in waves only and with the addition of a regional current for a reefed headland. The reef zone is noted as the gray outlined region adjacent to the headland.